FACULTY OF ENGINEERING AND ARCHITECTURE

CFD modelling of electric vehicle fire suppression:

Avoiding flame spread using sprinklers in a well-ventilated underground parking

Nienke Degraeve
Student number: 01911011

Supervisors: Dr.ir. Georgios Marakos, Prof.dr.ir. Bart Merci

Master's dissertation submitted in order to obtain the degree of Master of Science in Fire Safety Engineering

Academic year 2025 - 2026

Updated version after final feedback

GHENT UNIVERSITY

(blanco page)

Abstract

This study investigates the effectiveness of water-based sprinkler systems in mitigating fire spread from electric vehicle (EV) battery thermal runaway events in an underground parking garage (9.5 m × 16 m) using Fire Dynamics Simulator (FDS v6.9.1). A series of three-dimensional CFD simulations were conducted to evaluate how different sprinkler configurations influence heat release rate (HRR) and fire propagation between an initiating EV and two adjacent vehicles.

The study is contextualized by a thorough literature review on lithium-ion battery chemistry, the mechanics of thermal runaway (TR) and the characteristics of an EV fire. This theoretical foundation was used to establish a worst-case scenario for simulation, specifically selecting a 100% State of Charge (SOC) to reflect the highest potential for fire intensity and rapid fire growth. While the literature identifies significant risks regarding toxic gas emissions (such as hydrogen fluoride) and vapor cloud explosions (VCE), these phenomena were intentionally excluded from the numerical scope. This decision was made because these hazards are either not the primary drivers of vehicle-to-vehicle fire spread or cannot be modeled with sufficient accuracy within the constraints of FDS, which is a low-Mach-number solver.

10 cm computational grid, validated through sensitivity analysis, was used to balance accuracy and computational cost. Seven sprinkler scenarios were tested, varying activation (temperature), orientation, and discharge intensity.

Results show that an unconstrained fire scenario produces a peak HRR exceeding 18 MW due to multi-vehicle involvement. Sprinkler systems significantly reduce fire severity and stop or limit the fire spread, achieving up to an 82% reduction in peak HRR for standard ceiling-mounted systems (6.7 L/min) and up to 93% for high-intensity configurations. Although the FDS model shows that high-velocity jet flames are more buoyancy-dominated than in reality due to the neglect of pressure-driven expansion, the model successfully captures the critical interaction between water application and thermal exposure. These high-velocity jet flames, however, are only marginally affected by sprinkler discharge in the simulations; they are not the primary driver of vehicle-to-vehicle fire spread. Instead, fire propagation is driven by sustained thermal exposure leading to window failure and ignition of interior combustibles.

The results demonstrate that water-based sprinkler systems are effective in limiting large-scale EV fire propagation in enclosed parking structures, despite their inability to suppress thermal runaway at the battery cell level.

Keywords:

EV, thermal runaway, sprinklers, flame spread (between cars), (well-ventilated) underground parkings, FDS

AI Statement:

For this thesis, artificial intelligence tools ChatGPT (free version) and Google NotebookLM were used as supporting tools for language editing and text polishing.

The initial versions of all written content were independently produced by the author and subsequently improved with the assistance of these tools in terms of clarity, grammar, and structure.

The Python scripts used in this work were primarily developed through a conceptual approach, written by the author and then implemented in ChatGTP and further coded with support from AI-assisted suggestions.

The FDS input files were fully written by the author with feedback of the supervisors, however, NotebookLM was at times used as a supplementary tool to facilitate faster interpretation and consultation of the FDS-SM Manuals.

All literature sources were identified independently by the author. NotebookLM was only used in some cases to assist in the initial screening of relevance within available references and to create audiobooks to understand the topic better in a more relaxed way. The final selection of sources was made by the author without AI assistance.

All analysis, interpretation of results, and conclusions drawn from the FDS simulations are entirely based on the author’s own work and feedback of the supervisors, without any AI-generated analysis or interpretation support.

Acknowledgements

I would like to thank my supervisors, Bart Merci and Georgios Maragkos, for their extensive and valuable feedback, as well as their continuous guidance in steering this work in the right direction and for the enthusiasm they have shown for the subject itself.

I would also like to express my gratitude to everyone who showed interest in my research topic. Their engagement helped me to improve my ability to explain my work in a clear and comprehensive manner and encouraged me to critically reflect on and further develop my knowledge.

Table of content:

List of Tables

List of Figures

List of Formulas

List of Abbreviations

LIB	Lithium-ion Battery	LIF	Lithium Iron Phosphate
SEI	Solid Electrolyte Interphase	NMC	Lithium Nickel Manganese Cobalt
SOC	State Of Charge	NCA	Lithium Nickel Cobalt Aluminum Oxide
HF	Hydrogen Fluoride	TR	Thermal Runaway

ICEV	Internal combustion Engine Vehicle	BEV	Battery Electric Vehicle
THR	Total Heat Release	PHRR	Peak Heat Release Rate
VCE	Vapor Cloud Explosion	PHEV	Plug-in Hybrid Electric Vehicle
		REEV	Range-extended electric vehicle

Part 0: Introduction

Since the commercialization of the first lithium-ion battery by Sony in 1991, lithium-ion technology has enabled a new generation of high-energy storage applications.[1]Nearly two decades later, this advancement enabled companies such as Tesla to introduce some of the first commercially successful fully electric vehicles in 2008, powered by lithium-ion battery packs. Compared with conventional battery chemistries, lithium-ion batteries offer higher energy density and voltages exceeding 3 V per cell, enabling compact storage of large amounts of energy. As a result, EV adoption has increased rapidly. By 2024, approximately 1.4 million battery electric vehicles (BEVs) were newly registered in the European Union in a single year, contributing to a total fleet of nearly six million BEVs.[2] This exponential growth is driven by global efforts to reduce greenhouse gas emissions and dependence on fossil fuels. Yet, the same high-energy density that drives EV performance also creates unique safety risks. This research investigates the role of sprinklers in mitigating fire spread and assisting in suppression of EV battery fires in enclosed spaces by using FDS.

0.1) Thermal runaway fire risk

Despite their overall safety, lithium-ion batteries in EV's introduce a new fire hazard mechanism known as thermal runaway. This process is an auto-acceleratory, exothermic self-accelerating exothermic process in which the battery's internal temperature rises uncontrollably, ultimately leading to catastrophic failure almost always resulting in a heavy car fire.[3] The risk of vehicle fires caused by battery thermal runaway, however, is difficult to quantify accurately. Data on electric vehicle (EV) fire incidents are limited, and the exact ignition source of the reported data is often unknown. This makes it challenging to determine reliable fire probabilities. Additionally, comparing EV fire risk with that of internal combustion engine vehicles is complex, as EVs currently represent a smaller share of the vehicle fleet and typically have lower average age and mileage. Since fire risk is influenced by usage and ageing, direct comparisons may not fully reflect the true relative risk. But based on the limited sources, an estimation can be made for the amount of thermal runaway introduced fires each year in Europe.

According to the thesis *"Analysis of Electric Vehicle Fire Risk in Car Parks"*, the probability that a fully electric vehicle (EV) catches fire is:

$$P\_fire \text{ per } EV = 25/100\,000$$

[1] Veritasium. (2025, August 7). *The perfect battery material is dangerous* [Video]. YouTube. https://www.youtube.com/watch?v=AGglJehON5g
[2] Eurostat. (2026). Passenger cars in the EU. *Statistics Explained*. https://ec.europa.eu/eurostat/statistics-explained/SEPDF/cache/25886.pdf
[3] Ribière, P., Grugeon, S., Morcrette, M., Boyanov, S., Laruelle, S., & Marlair, G. (2011). Investigation on the fire-induced hazards of Li-ion battery cells by fire calorimetry. *Energy & Environmental Science*, *5*(1), 5271–5280. https://doi.org/10.1039/c1ee02218k

Assuming the average usage duration of an EV is 15 years, and the European EV fleet currently consists of 6 million vehicles, the expected number of EV fires per year can be estimated as:[4]

Annual EV fires = (6 000 000 x 0.00 025)/ 15 = 1 500 fires/year

From the paper *"Electric Vehicle Battery Charging Interference Intelligent Protection Device"*, fire types are classified, and if we assume only "fire during charging" events are caused by thermal runaway, the number of thermal runaway fires per year is:

1 500 x 0.23 = 345 thermal runaway fires/year

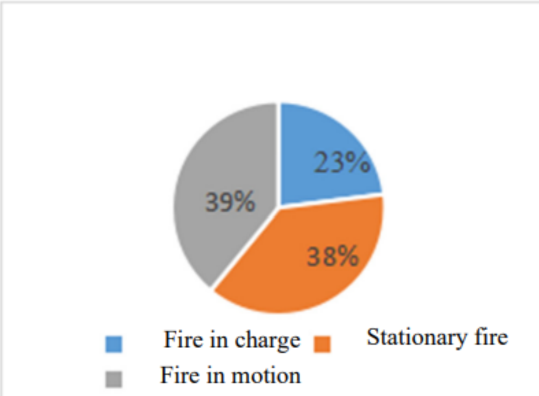

Figure 1: Analysis diagram of vehicle fire condition[5]

An alternative estimate can be done using the individual lithium-ion battery cell fire risk of:

P_fire risk = 1/10 000 000

A typical EV, however, contains 1 300 battery cells. This results in a probability that at least one cell in the EV catches fire:

P_EV fire = 1 - (1- 0.00 001)^1 300 = 0.013%

Using the same fleet of 6 million EVs over 15 years:

Annual EV fires = (6 000 000 x 0.00 013)/ 15 = 52 thermal runaway *fires/year*

However, currently, EVs represent only 2.5% of Europe's fleet. If all vehicles become fully electric, the number of thermal runaway fires would scale approximately by factor 40. Thus, this projected an annual thermal runaway amount of fires of 2 080 till 13 800 fire/year. Even if only 1% of these fires cause large-scale fire spread, this represents a considerable risk with potentially multi-million-euro damages per fire.

[4] Eurostat. (2026). Passenger cars in the EU. *Statistics Explained*. https://ec.europa.eu/eurostat/statistics-explained/SEPDF/cache/25886.pdf
[5] Xie, L., & Liu, B. (2022). Electric vehicle battery charging interference intelligent protection device. *Journal of Physics Conference Series*, *2310*(1), 012046. https://doi.org/10.1088/1742-6596/2310/1/012046

Moreover, thermal runaway introduced EV fires differ significantly from conventional ICEV in terms of fire dynamics. (See 1.7) Thermal runaway can cause a rapid increase in HRR, leading to faster fire growth and earlier PHRR. This rapid development increases the likelihood of fire spread to adjacent vehicles, which can occur within 3–4 minutes.[6] In enclosed environments such as underground car parks, this creates a significant hazard, as fire services may arrive after the fire has already intensified. Additionally, EV battery fires can produce jet flames, toxic gases, and prolonged burning due to internal energy release, making suppression more challenging.

0.2) Sprinklers to prevent severe damage

Fire safety in car parks is one of the key design topics. With the increasing number of EVs, such enclosed or half-open environments in often urban places are expected to contain a higher concentration of charged vehicles. Charging systems range from 3.7 kW slow chargers to ultra-rapid chargers exceeding 150 kW, increasing battery state of charge and potentially increasing thermal runaway severity.[7] (See 1.4) Water-based sprinkler systems are widely used as a primary fire protection measure in enclosed spaces. However, their effectiveness in suppressing EV fires, particularly those involving battery thermal runaway, is not yet fully understood.

Experimental fire testing is costly, complex, and difficult to control. Therefore, Computational Fluid Dynamics (CFD) provides a powerful and efficient method to simulate EV fire scenarios, analyze fire development, and evaluate sprinkler performance under controlled conditions. CFD simulations allow detailed investigation of heat release rate, temperature distribution, sprinkler activation timing, and suppression effectiveness.

0.2) Research theme

This research aims to design a representative EV fire development caused by thermal runaway in FDS to numerically investigate the effectiveness of water-based sprinkler systems in suppressing or limiting fire spread of electric vehicle fires in enclosed environments using CFD. Given the rapid increase in EV adoption and the severe consequences of battery fires, this study contributes to improving fire safety design and risk mitigation strategies for enclosed environments containing electric vehicles.

This thesis focuses on fully electric vehicles (EVs); plug-in hybrid electric vehicles (PHEVs) and range-extended electric vehicles (REEVs) are excluded from the scope. The vehicle type considered is the passenger car; other electrically assisted means of transport, such as bicycles, scooters, trucks, and buses, are not taken into account.

Research question:

---

6 George, J. (2023). Analysis of electric vehicle fire risks in car parks. In The University of Edinburgh, *Master thesis submitted in the Erasmus+ Study Programme International Master of Science in Fire Safety Engineering*.

7 George, J. (2023). Analysis of electric vehicle fire risks in car parks. In The University of Edinburgh, *Master thesis submitted in the Erasmus+ Study Programme International Master of Science in Fire Safety Engineering*.

“How effective are different water-based sprinkler system configurations, designed in accordance with the minimum requirements of current European standards, in suppressing electric vehicle fires caused by thermal runaway in enclosed environments, as determined through CFD simulations?”

Sub questions:

- *What sprinkler configuration is most effective in preventing fire spread to neighbouring vehicles and enhancing fire suppression?*
- *Can sprinkler systems prevent fire spread to adjacent vehicles in an EV fire scenario?*
- *How catastrophic is an EV fire without sprinkler protection?*
- *To what extent can Fire Dynamics Simulator (FDS) realistically reproduce electric vehicle fire dynamics?*
- *What is the effect of varying jet velocity, temperature, and nozzle area on jet flame behaviour under constant heat release rate (HRR) conditions?*
- *How do sprinkler parameters like activation temperature, nozzle orientation, and flow rate affect fire suppression efficiency and fire spread in electric vehicle fires, particularly under jet flame conditions in enclosed environments?*

This research focuses on fundamental analysis of the interaction between water-based suppression systems and EV fires, with particular attention to the suppression of jet flames resulting from thermal runaway events. These jet flames represent a key characteristic that differentiates EV fires from conventional ICEV fires and pose unique challenges for fire suppression in enclosed environments. The primary objective is to prevent fire spread and validate the fire suppression.

The overall objective is to develop scientifically supported recommendations for sprinkler system design and configuration to improve fire control and suppression of EV fires in enclosed spaces. Specifically, this research seeks to enhance the understanding of the complex interaction between EV fires and sprinkler systems and to identify optimal water-based suppression system parameters required for effective fire control and mitigation in such scenarios.

0.3) Methodology

The research is structured into five sequential phases to systematically evaluate the effectiveness of water-based sprinkler systems in mitigating electric vehicle (EV) fires:

- **Part 1: Literature Review and Dataset Analysis.** The initial phase involves a focused literature review to identify the key challenges of EV fires, specifically defining the mechanisms of thermal runaway and examining the chemical composition of lithium-ion batteries. This phase concludes with a detailed analysis of an experimental dataset (based on Kang et al., 2023) used for the calibration and validation of the numerical model.

- **Part 2: FDS Model Development**. A computational model is developed using Computational Fluid Dynamics (CFD) in Fire Dynamics Simulator (FDS v6.9.1). The model is built gradually to manage complexity:
    1. Simulating a single-vehicle fire without jet flames to establish a baseline and working geometry.
    2. Conducting a parametric study of jet flames on non-combustible geometry to isolate the effects of velocity, temperature, and vent area.
    3. Integrating the full parking garage geometry, including neighboring vehicles and environmental constraints. This stage also explicitly addresses the limitations and assumptions of the modeling approach, such as the low-Mach-number solver, and compares the simulated HRR of a single car with a jet flame with the experimental dataset.
- **Part 3: Implementation of Sprinkler Scenarios.** Various sprinkler system configurations are incorporated into the model, varying parameters such as activation temperatures, orientations (ceiling- vs. wall-mounted), and flow rates to become 7 scenarios. These setups are compared against a free-burning reference case (baseline) to measure relative suppression effectiveness.
- **Part 4: Evaluation of the Scenario's Results**. The performance of each different configuration is evaluated based on the Heat Release Rate (HRR), water flow densities, sprinkler activation times, gas temperatures, and the thermal load on adjacent vehicles. A first conclusion for each scenario is made.
- **Part 5: Discussion and conclusion.** The study concludes by identifying the most effective setup and discussing the key findings regarding fire containment in enclosed parking environments.

Part 1: Literature study

1.1) Chemical process of a Lithium-ion battery

A lithium-ion battery operates through a reversible electrochemical reaction between an anode and cathode, separated by an electrolyte and a porous separator in the middle of the electrolyte, to prevent short circuiting.[8] During discharging, lithium ions (Li^+) migrate from the anode through the electrolyte and across the separator to the cathode, while electrons (e^-) are unable to pass through the separator. They travel through the external circuit to the cathode, thereby providing electrical energy.

Both electrode materials have layered structures made of strongly covalent bonded frameworks held together by weak van der Waals forces. This architecture allows lithium ions to move in and out of the spaces between the layers during charge and discharge. During discharge, Li^+ ions enter the cathode and cause a slight expansion of the material; during charging, an external power source drives the ions back out, allowing the layers to contract again. The reverse applies to the anode. This reversible inclusion process, known as intercalation, can occur repeatedly without significant structural degradation of the covalent framework, enabling a reversible reaction. During the first charge, however, roughly 5% of the lithium ions react with the electrolyte at the anode surface to form the Solid Electrolyte Interphase (SEI), slightly reducing the battery's initial capacity. On the other hand, this thin, protective layer stabilizes the electrode and remains permeable to lithium ions.

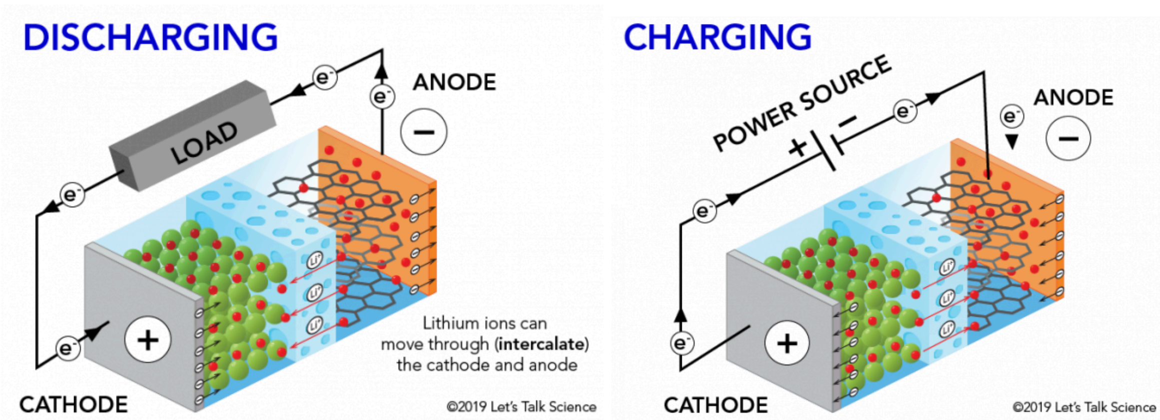

Figure 2: Lithium-ion battery proces[9]

A single Li-ion cell typically provides 3.3–3.7 V, and the total energy depends on voltage multiplied by capacity.

[8] Veritasium. (2025, August 7). *The perfect battery material is dangerous* [Video]. YouTube. https://www.youtube.com/watch?v=AGglJehON5g

[9] *How does a lithium-Ion battery work?* (2019, September 23). Let's Talk Science. https://letstalkscience.ca/educational-resources/stem-explained/how-does-a-lithium-ion-battery-work

The materials used for a lithium-ion battery are: a graphite anode and a cathode made from a lithium-containing metal oxide or phosphate, since elemental lithium is too reactive to use directly in its pure form. Common cathode materials include:[10]

- Lithium iron phosphate (LFP) ⇒ used in EVs
    - $FePO_4 + LiC_6 \rightleftharpoons C_6 + LiFePO_4$
- Lithium Manganese Oxide (LMO)
- Lithium Nickel Oxide (LNO)
- Lithium Nickel Manganese Cobalt (NMC) ⇒ used in EVs
    - $NiO_2 + LiC_6 \rightleftharpoons C_6 + LiNiO_2$
- Lithium Nickel Cobalt Aluminum Oxide (NCA) ⇒ used in EVs
    - $Mn_2O_4 + LiC_6 \rightleftharpoons C_6 + LiMn_2O_4$
- Lithium Cobalt Oxide (LCO) ⇒ typical in portable electronics
- Lithium titanate (LTO)
- Lithium Metal Polymer

The electrolyte is a non-aqueous solution of a lithium salt such as $LiPF_6$ in organic solvents and separators are generally made of a thermoplastic polyolefin, such as ethylene and propylene.

1.2) Mechanisms and Triggers of Thermal Runaway in Lithium-Ion Batteries

A thermal runaway is an auto-acceleratory, exothermic self-accelerating exothermic process in which the battery's internal temperature rises uncontrollably, ultimately leading to catastrophic failure.[11]

In an EV, if one battery cell enters thermal runaway, the intense heat it generates can quickly trigger the same reaction in neighboring cells. This self-accelerating exothermic process can spread through the entire battery module and, eventually, the whole pack within a brief time.

---

[10] Restuccia, F. (2025). A perspective on lithium-ion battery fire safety: from experiments to modelling approaches. *Journal of Physics Conference Series*, *3121*(1), 012048. https://doi.org/10.1088/1742-6596/3121/1/012048
[11] Ribière, P., Grugeon, S., Morcrette, M., Boyanov, S., Laruelle, S., & Marlair, G. (2011). Investigation on the fire-induced hazards of Li-ion battery cells by fire calorimetry. *Energy & Environmental Science*, *5*(1), 5271–5280. https://doi.org/10.1039/c1ee02218k

There are three main categories of triggers that can initiate a thermal runaway.[12]

1. Thermal impact: This includes external heat sources, such as fire (arson), or prolonged exposure to extremely high weather temperatures. Although low ambient temperatures do not directly trigger thermal runaway through heat, exposure to severe cold can induce internal cell damage (e.g., lithium plating), which can subsequently lead to thermal runaway during later charging.

2. Mechanical impact: Vehicle collisions or significant physical damage can compromise the battery structure. Even if no immediate failure occurs, this hidden damage can later trigger thermal runaway. In EV's currently on the market, battery packs are located in the bottom of the car and under the seats, between the wheel axles. This section is part of the high-strength safety cell, which protects both the passengers and the battery from mechanical shocks.

3. Electrical abuse: This may occur during overcharging, too fast charging, malfunctions or unapproved system elements in the charging infrastructure, or due to manufacturing defects.

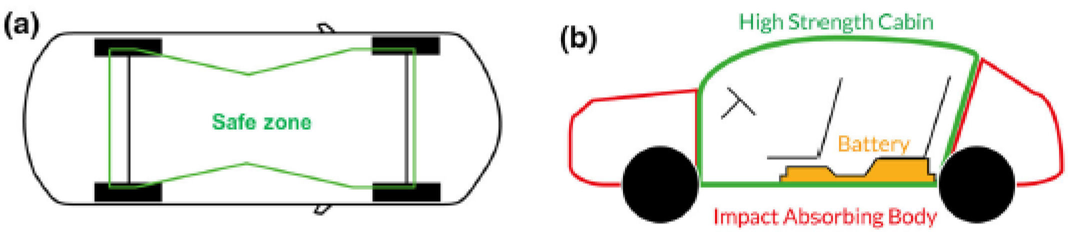

Figure 3: a) Safe zone of a car b) battery layout for a Nissan Leaf [13]

In the moments leading up to thermal runaway, several destabilizing processes begin reinforcing one another.[14] When the internal temperature rises into the range of approximately 80–130 °C, the solid electrolyte interphase (SEI) on the anode starts to decompose, exposing fresh reactive material and generating additional heat and gases. Under certain conditions, such as prior overcharging or uneven lithium deposition, lithium dendrites may already have formed inside the battery cell (their formation is not tied to a specific temperature).[15] These needle-like structures can pierce the separator and create internal short circuits.

---

[12] Sun, P., Huang, X., Research Centre for Fire Engineering, Hong Kong Polytechnic University, Bisschop, R., Department of Fire Research, RISE Research Institutes of Sweden, Niu, H., & Guangzhou Industrial Technology Research Institute, Chinese Academy of Sciences. (2020). A review of battery fires in electric vehicles. In *Fire Technology* (Vols. 56–56, pp. 1361–1410) [Journal-article]. Springer Science+Business Media, LLC. https://doi.org/10.1007/s10694-019-00944-3

[13] Sun, P., Huang, X., Research Centre for Fire Engineering, Hong Kong Polytechnic University, Bisschop, R., Department of Fire Research, RISE Research Institutes of Sweden, Niu, H., & Guangzhou Industrial Technology Research Institute, Chinese Academy of Sciences. (2020). A review of battery fires in electric vehicles. In *Fire Technology* (Vols. 56–56, pp. 1361–1410) [Journal-article]. Springer Science+Business Media, LLC. https://doi.org/10.1007/s10694-019-00944-3

[14] Ribière, P., Grugeon, S., Morcrette, M., Boyanov, S., Laruelle, S., & Marlair, G. (2011). Investigation on the fire-induced hazards of Li-ion battery cells by fire calorimetry. *Energy & Environmental Science*, *5*(1), 5271–5280. https://doi.org/10.1039/c1ee02218k

[15] Veritasium. (2025, August 7). *The perfect battery material is dangerous* [Video]. YouTube. https://www.youtube.com/watch?v=AGglJehON5g

As temperatures increase, the separator begins to shrink or deform at around 130 °C, which leads to internal short circuits as well and is associated regularly with a drop in voltage.[16] At the same time, the electrolyte reacts more vigorously with the electrodes and begins to vaporize, causing a rapid buildup of internal pressure. From experimental data, the safety vent typically opens between 170 °C and 195 °C to relieve this pressure and prevent an explosion. The cathode becomes thermally unstable and releases additional heat and, oxygen.

Together, these reactions form a rapidly accelerating feedback loop of heat generation. Once the system can no longer dissipate this energy, the cell enters full thermal runaway. Typically the point of no return exceeds roughly between 130°C and 250°C, depending partly on the State Of Charge (SOC) (See 1.4) and the chemistry of the battery.

1.3) Aging Effects of a Lithium-ion battery

As a lithium-ion battery undergoes repeated charge–discharge cycles, the SEI layer gradually grows.[17] The formation and continued growth of this layer consumes both lithium ions and electrolyte, reducing the amount of cyclable lithium and active electrolyte available within the battery. In addition, degradation processes lead to depletion of the anode material and a general loss of active material within the cell, resulting in a decrease in overall battery capacity. At the same time, the thicker SEI layer and the reduced amount of chemically reactive material can decrease the intensity of the reactions occurring during TR. Consequently, aged batteries may exhibit a lower HRR compared to new batteries. However, the influence of battery ageing on thermal runaway behaviour remains complex and may vary depending on the battery chemistry, ageing conditions, and state of health. Battery packs that have already experienced minor shocks, for example from a non-fatal collision, may have a damaged casing or wiring, which increases the risk of a TR.

1.4) Influence of State of Charge (SOC) on Lithium-Ion Battery Fire Behavior

Key fire characteristics such as fire growth rate, smoke toxicity, oxygen generation and explosion potential, are strongly dependent on the battery's state of charge (SOC). A lithium-ion battery at 100% SOC exhibits fundamentally different fire behavior compared to one at 0% SOC.[18]

---

16 Zhong, G., Mao, B., Wang, C., Jiang, L., Xu, K., Sun, J., & Wang, Q. (2018). Thermal runaway and fire behavior investigation of lithium ion batteries using modified cone calorimeter. *Journal of Thermal Analysis and Calorimetry*, *135*(5), 2879–2889. https://doi.org/10.1007/s10973-018-7599-7

17 Pastor, J. V., García, A., Monsalve-Serrano, J., & Golke, D. (2023). Analysis of the aging effects on the thermal runaway characteristics of Lithium-Ion cells through stepwise reactions. *Applied Thermal Engineering*, *230*, 120685. https://doi.org/10.1016/j.applthermaleng.2023.120685

18 Zhong, G., Mao, B., Wang, C., Jiang, L., Xu, K., Sun, J., & Wang, Q. (2018). Thermal runaway and fire behavior investigation of lithium ion batteries using modified cone calorimeter. *Journal of Thermal Analysis and Calorimetry*, *135*(5), 2879–2889. https://doi.org/10.1007/s10973-018-7599-7

Lithium-ion batteries contain two distinct energy sources: stored electrical energy and latent chemical energy within the cell materials.[19] At high SOC, both energy contributions are maximized and the battery is less thermal stable. A fully charged battery not only contains substantial electrical energy, but also has both the anode and cathode in chemically unstable, non-equilibrium states that strongly favor reactions. Consequently, oxygen generation from internal decomposition reactions is faster and more pronounced at higher SOC, contributing to increased fire intensity. In a fully charged battery, however, the reaction rates are so rapidly that the available oxygen, both internally generated and externally supplied, is insufficient to support complete combustion. This results in higher yields of toxic gases and a lower total energy released during a fire. However, a higher fire intensity and a higher peak heat release rate (HRR) is noticed, because the combustion heat is released over a very short time interval, producing an extremely intense but short-lived fire.[20] Furthermore, the temperature threshold for thermal runaway depends on both cathode chemistry and SOC, with higher SOC generally resulting in lower onset temperatures.[21] [22]

From a fire safety perspective, these effects have important implications for electric vehicles (EVs). Although the SOC at the moment of a fire remains unpredictable, battery fires are more likely to occur during charging, when SOC is high and thermal stability is reduced.[23]

1.5) Toxic gases

A key difference between electric vehicles and conventional combustion-engine vehicles is the composition and toxicity of gases released during a fire.[24] Lithium-ion battery (LIB) fires produce a distinct mixture of halogenated, asphyxiant, flammable, and carcinogenic compounds, including:[25]

- Hydrogen Fluoride (HF) – from decomposition of fluorine-containing components such as the electrolyte salt $LiPF_6$
- Hydrogen Chloride (HCl), Hydrogen Bromide (HBr), Hydrogen Cyanide (HCN)
- Carbon Monoxide (CO) – from incomplete combustion of battery organics and other vehicle materials

---

[19] Lyon, R. E., & Walters, R. N. (2016). *Energy release by rechargeable Lithium-Ion batteries in thermal runaway* (By Federal Aviation Administration; Technical Note DOT/FAA/TC-TN16/22; p. 26). Federal Aviation Administration. https://actlibrary.tc.faa.gov

[20] Zhong, G., Mao, B., Wang, C., Jiang, L., Xu, K., Sun, J., & Wang, Q. (2018). Thermal runaway and fire behavior investigation of lithium ion batteries using modified cone calorimeter. *Journal of Thermal Analysis and Calorimetry*, *135*(5), 2879–2889. https://doi.org/10.1007/s10973-018-7599-7

[21] Ribière, P., Grugeon, S., Morcrette, M., Boyanov, S., Laruelle, S., & Marlair, G. (2011b). Investigation on the fire-induced hazards of Li-ion battery cells by fire calorimetry. *Energy & Environmental Science*, *5*(1), 5271–5280. https://doi.org/10.1039/c1ee02218k

[22] Ditch, B., FM Global, Zeng, D., & FM Global. (2019). *Development of sprinkler protection guidance for lithium ion based energy storage systems*. FM Global. https://www.researchgate.net/publication/333653116

[23] Promat. (n.d.). FIRE PROTECTION SOLUTIONS FOR EV CHARGING ZONES IN CAR PARKS. In *WWW.PROMAT.COM* (pp. 3–4).

[24] Tohir, M. Z. M., & Martín-Gómez, C. (2025). Evaluating fire severity in electric vehicles and internal combustion engine vehicles: A statistical approach to heat release rates. *Fire Technology*, *61*(5), 2957–2998. https://doi.org/10.1007/s10694-025-01711-3

[25] Ribière, P., Grugeon, S., Morcrette, M., Boyanov, S., Laruelle, S., & Marlair, G. (2011a). Investigation on the fire-induced hazards of Li-ion battery cells by fire calorimetry. *Energy & Environmental Science*, *5*(1), 5271–5280. https://doi.org/10.1039/c1ee02218k

- Carbon Dioxide (CO_2)
- Nitrogen Oxides (NO, NO_2)
- Sulfur Dioxide (SO_2)
- Total Hydrocarbon Content (THC), sum of hydrogen- and carbon-containing organic compounds, from vaporized electrolyte solvents
- Volatile Organic Compounds (VOC), readily evaporating carbon-based chemicals
- Polycyclic Aromatic Hydrocarbons (PAHs), pose a known long-term health risk
- Particulate-bound metals, battery-specific elements such as Li, Ni, Co, and Mn (depending on cathode chemistry)

Among these, hydrogen fluoride (HF) is the most critical hazard. HF concentrations in EV fires are typically 10–60 times higher than in conventional vehicle fires, with reported releases of ~120–859 g in full-scale tests.[26] HF emissions depend on battery chemistry and state of charge (SOC): LFP cells often generate more HF than NMC cells, peak concentrations commonly occur at high SOC, and some tests show high cumulative HF even at low SOC.[27] Additional halogenated acids of HCl and HBr may be released in smaller amounts. LIB fires additionally release asphyxiant gases (CO, CO_2, HCN) at levels exceeding health limits.[28] CO production generally increases with SOC, and toxicity can be especially high during smoldering or non-ignited thermal runaway. Flammable hydrocarbons, VOC, soot-bound PAHs and metal species further increase health, fire, and explosion hazards.

Overall, battery chemistry and SOC influence the toxicity, flammability, and explosion risk of LIB fires, with hydrogen fluoride (HF) being the dominant toxic hazard, especially at higher SOC.

1.6) Explosion risk

During thermal runaway, lithium-ion batteries release flammable and toxic vent gases.[29] If these gases do not ignite immediately, they can accumulate and form a vapour cloud, which may result in a vapour cloud explosion (VCE) if ignition is delayed. This risk is significantly higher in confined spaces, such as car parks, where gas dispersion is limited. Although VCEs occur in only about 5% of EV fire incidents, they pose a serious hazard due to the potential for rapid fire spread, structural damage, and risks to occupants and firefighters. The likelihood of a VCE depends on factors such as battery state of charge (SOC), gas

[26] Hynynen, J., Willstrand, O., Blomqvist, P., & Andersson, P. (2023). Analysis of combustion gases from large-scale electric vehicle fire tests. *Fire Safety Journal*, *139*, 103829. https://doi.org/10.1016/j.firesaf.2023.103829
[27] Restuccia, F. (2025). A perspective on lithium-ion battery fire safety: from experiments to modelling approaches. *Journal of Physics Conference Series*, *3121*(1), 012048. https://doi.org/10.1088/1742-6596/3121/1/012048
[28] Hynynen, J., Willstrand, O., Blomqvist, P., & Andersson, P. (2023). Analysis of combustion gases from large-scale electric vehicle fire tests. *Fire Safety Journal*, *139*, 103829. https://doi.org/10.1016/j.firesaf.2023.103829
[29] George, J. (2023). Analysis of electric vehicle fire risks in car parks. In The University of Edinburgh, *Master thesis submitted in the Erasmus+ Study Programme International Master of Science in Fire Safety Engineering*.

composition, and the degree of confinement. Lower SOC levels (< 50%) produce a higher proportion of flammable gases, increasing the explosion risk.

However, in Fire Dynamics Simulator (FDS), modeling such explosions is not straightforward, and the results are often inaccurate because the model is not specifically designed for high-speed fluid dynamics.[30] The Mach number must remain below 0.3 (approximately 100 m/s), and the model simplifies the physics by neglecting compressibility effects. As a result, in the simulations of this report, it is assumed that the flammable gases ignite almost immediately and sufficiently ventilation in the parking environment prevents any significant pressure build-up.

1.7) Jet Flames, the main difference between ICEVs and EVs

The PHRR and THR of EVs and ICEVs are generally within the same order of magnitude.[31] The reason for this is that, confirmed by experimental tests, the primary driver of these values is the combustion of conventional car body materials rather than the battery pack itself. A more detailed table with the difference can be found in annex A.

The defining hazard of an EV fire is the manifestation of high-intensity jet flames, which are almost certain to occur during thermal runaway if the battery's SOC exceeds 50%.[32] [33] [34] These jet flames function as a "blowtorch," significantly accelerating fire spread to adjacent combustible components and neighboring vehicles. Furthermore, when thermal runaway is the root cause of a fire, the process may remain contained within the battery pack for an extended period, making it difficult to detect from the vehicle's exterior. Consequently, the first visible signs of fire are often sudden, violent jet flames. A key precursor to this phenomenon is the violent emission of white smoke, consisting of a mixture of electrolyte vapors: hydrogen, carbon monoxide, and alkanes from the battery. These gases accumulate beneath the vehicle and create a highly flammable environment. The length of jet flames typically ranges from 1.5 to 3 meters, depending on factors such as battery capacity, internal pressure, and vent nozzle geometry. Reported maximum height of jet flame is 0.31m - 0.96 m with peak jet velocities of 42.1 m/s.[35] [36] [37] Other sources write down velocities between

[30] FDS User Guide

[31] Kang, S., Kwon, M., Choi, J. Y., Sengkwan Choi, Fire Testing & Research Centre, Fire & Disaster Management Division, Korea Conformity Laboratories, Republic of Korea, Advanced Functional Nanohybrid Material Laboratory, Department of Chemistry, Dongkuk University, Republic of Korea, & School of the Built Environment, Ulster University, UK. (2023). Full-scale fire testing of battery electric vehicles [Journal-article]. *Applied Energy*, *332*, 120497. https://doi.org/10.1016/j.apenergy.2022.120497

[32] Zhao, C., Hu, W., Meng, D., Mi, W., Wang, X., & Wang, J. (2023). Full-scale experimental study of the characteristics of electric vehicle fires process and response measures. *Case Studies in Thermal Engineering*, *53*, 103889. https://doi.org/10.1016/j.csite.2023.103889

[33] Cui, Y., Liu, J., Cong, B., Han, X., & Yin, S. (2022). Characterization and assessment of fire evolution process of electric vehicles placed in parallel. *Process Safety and Environmental Protection*, *166*, 524–534. https://doi.org/10.1016/j.psep.2022.08.055

[34] George, J. (2023). Analysis of electric vehicle fire risks in car parks. In The University of Edinburgh, *Master thesis submitted in the Erasmus+ Study Programme International Master of Science in Fire Safety Engineering*.

[35] Cui, Y., Liu, J., Cong, B., Han, X., & Yin, S. (2022). Characterization and assessment of fire evolution process of electric vehicles placed in parallel. *Process Safety and Environmental Protection*, *166*, 524–534. https://doi.org/10.1016/j.psep.2022.08.055

[36] Mao, B., Zhao, C., Chen, H., et al., 2021. Experimental and modeling analysis of jet flow and fire dynamics of 18650-type lithium-ion battery. Appl. Energy 281, 116054.

[37] Zhou, Z., Zhou, X., Wang, D., et al., 2021. Experimental analysis of lengthwise/ transversal thermal characteristics and jet flow of large-format prismatic lithium-ion battery. Appl. Therm. Eng. 195, 117244.

16.6 m/s till 83.3 m/s.[38] The diameter of the pressure safety valve can have a broad range of dimensions going from 8 mm till 80 mm.[39] [40] [41] [42] The jet flames are intermittent rather than continuous, as gas generation within the battery is inherently unstable. Individual bursts typically last between 3 and 26 seconds, so the flame state of the BEV fire constantly switches between momentum and buoyancy control. The temperature of these flames can spike to peaks between 700 °C and 1100 °C within a fraction of a second, even while the battery pack itself remains at a much lower temperature (approx. 300 °C). The direction of these jet flames is governed by the location of safety valves and structural openings in the battery pack. Although most battery systems are designed with laterally positioned safety valves - resulting in predominantly sideways-directed jet flames - flames may also emerge from the front or rear of the battery pack. If this steel barrier between the batteries and the vehicle seating area remains intact, the jet flame is deflected and propagates along the underside and sides of the vehicle structure. If the barrier, however, becomes compromised due to cracks, openings, or the failure of rubber seals, the flame can penetrate into the seating area. This can rapidly ignite combustible interior materials, such as seat foam, significantly accelerating fire growth. Infrared imaging has further shown that jet flames may naturally split into two or three distinct clusters as gases are expelled through multiple vent openings.

Experimental findings reported in the study *Full-scale experimental study of the characteristics of electric vehicle fires process and response measures* by Chenxi Zhao et al. indicate that the first jet flame occurs approximately 17.1 seconds after visible flaming first appears due to a thermal runaway. In many cases, visible flames do not emerge immediately at the onset of thermal runaway. Instead, flammable gases accumulate until they encounter an ignition source, such as electrical sparks, triggering rapid ignition. This results in intense combustion and the sudden formation of (jet) flames or even an explosion once thermal runaway is fully established.

Figure 4: Jet flame release from an EV during a fire event[43]

[38] Jia, Z., Min, Y., Qin, P., Mei, W., Meng, X., Jin, K., Sun, J., & Wang, Q. (2023). Effect of safety valve types on the gas venting behavior and thermal runaway hazard severity of large-format prismatic lithium iron phosphate batteries. *Journal of Energy Chemistry*, *89*, 195–207. https://doi.org/10.1016/j.jechem.2023.09.052
[39] Jia, Z., Min, Y., Qin, P., Mei, W., Meng, X., Jin, K., Sun, J., & Wang, Q. (2023). Effect of safety valve types on the gas venting behavior and thermal runaway hazard severity of large-format prismatic lithium iron phosphate batteries. *Journal of Energy Chemistry*, *89*, 195–207. https://doi.org/10.1016/j.jechem.2023.09.052
[40] *Industrial VRLA Battery Safety Valve*. (n.d.). http://www.oursun-power.com/product-industrial-vrla-battery-safety-valve.html
[41] *Pressure relief valves for Lithium-Ion battery packs that are reclosable, with high flow-rate, for multi-use | Nifco*. (n.d.-b). Nifco. https://www.nifco.com/en/products/news/detail/kv9ihm0000000s2v.html
[42] George, J. (2023). Analysis of electric vehicle fire risks in car parks. In The University of Edinburgh, *Master thesis submitted in the Erasmus+ Study Programme International Master of Science in Fire Safety Engineering*.
[43] Zhao, C., Hu, W., Meng, D., Mi, W., Wang, X., & Wang, J. (2023b). Full-scale experimental study of the characteristics of electric vehicle fires process and response measures. *Case Studies in Thermal Engineering*, *53*, 103889. https://doi.org/10.1016/j.csite.2023.103889

1.8) The use of sprinklers to attack an EV fire

To sustain a fire, three elements must be present: oxygen, fuel, and an ignition source (heat). As discussed in the previous chapter, the decomposition of the cathode releases oxygen, which contributes to the availability of an oxidizer. The produced oxygen can be up to 30% of the oxygen rate for the battery fire.[44] Furthermore, thermal runaway itself is a strongly exothermic process, meaning it generates significant heat and effectively provides its own ignition source. The fuel consists of the remaining battery materials and the flammable gases produced during electrolyte vaporization. In addition, combustible components in the vehicle and oxygen from the surrounding environment can further support combustion. Yanfu Wang, et al. (2026) indicate that, in the absence of active suppression, an EV battery fire can escalate rapidly after visible smoke or flames are observed, with propagation potentially occurring within 3 to 5 minutes. [45]

1.8.1) Influence of Sprinklers on Fire Source

Water is chemically inert, but, with its high heat capacity, is one of the few extinguishing agents capable of effectively removing heat from a battery in thermal runaway and thus actively influencing the reaction.[46] By absorbing large amounts of energy, it can slow the progression of the self-accelerating exothermic process and reduce the likelihood of propagation to neighboring cells or modules. Moreover, the phase change of water into steam results in volumetric expansion, which can contribute to a localized inerting effect by reducing oxygen concentration near the fire source. However, water rarely stops the underlying processes completely. If even a single cell remains insufficiently cooled and the reaction continues, it may accelerate again once the cooling effect stops and can potentially re-ignite adjacent cells, even hours or days later. In addition, once a cell has entered thermal runaway, its internal structure is irreversibly damaged: the separator no longer functions, and the cathode has decomposed, making a return to its original stable, reversible operation impossible. Therefore, it is very important to handle the burned out or extinguished car with care.

When sprinklers are used on an EV, an additional challenge arises: battery packs are designed to be protected from rainwater and, as previously mentioned, from mechanical impacts.[47] This means that sprinklers located above the vehicle are generally unable to cool the battery pack directly. They will primarily cool the vehicle's exterior and any nearby combustible materials, which can help prevent fire spread, but they cannot meaningfully intervene in the thermal runaway process inside the battery. In simple terms, the presence of water only slows down the TR. This allows the damaged battery to release its stored energy

---

[44] Ribière, P., Grugeon, S., Morcrette, M., Boyanov, S., Laruelle, S., & Marlair, G. (2011). Investigation on the fire-induced hazards of Li-ion battery cells by fire calorimetry. *Energy & Environmental Science*, *5*(1), 5271–5280. https://doi.org/10.1039/c1ee02218k
[45] Qiao, J., Wang, Y., Li, X., Wang, Y., Zhang, H., Liu, J., Su, W., & Yin, H. (2026). Battery pack jet fire modeling and vehicle fire spread simulation in Ro-Ro ships. *Applied Thermal Engineering*, 290, 130201.
[46] Ditch, B., FM Global, Zeng, D., & FM Global. (2019). ***Development of sprinkler protection guidance for lithium ion based energy storage systems***. FM Global. https://www.researchgate.net/publication/333653116
[47] Sun, P., Huang, X., Research Centre for Fire Engineering, Hong Kong Polytechnic University, Bisschop, R., Department of Fire Research, RISE Research Institutes of Sweden, Niu, H., & Guangzhou Industrial Technology Research Institute, Chinese Academy of Sciences. (2020). A review of battery fires in electric vehicles. In *Fire Technology* (Vols. 56–56, pp. 1361–1410) [Journal-article]. Springer Science+Business Media, LLC. https://doi.org/10.1007/s10694-019-00944-3

more gradually without destroying consequences, till the chemical components return to a natural stable equilibrium.

1.8.2) Influence of Sprinklers on Smoke Layer

Regarding water-based sprinkler systems, the available sources show mixed effects on gas toxicity. '*Development of sprinkler protection guidance for lithium ion based energy storage systems*' by Ditch et al.(2019) and the '*Fire protection solutions for EV charging zones in car parks*' by promat indicates that while water effectively reduces heat release, it does not stop toxic gas generation and may worsen smoke conditions by cooling the smoke, breaking stratification, and reducing visibility and tenability; battery casings further limit direct internal cooling, and HF-containing smoke remains a concern.[48] [49]

In contrast, '*Analysis of combustion gases from large-scale electric vehicle fire tests'* by Hynynen et al., (2023) demonstrates that water application can reduce certain toxic components in the air, because the toxic substances are absorbed into the water.[50] In sprinklered EV fire tests, HF concentrations were significantly lower, and no HF was detectable by Fourier-Transform Infrared spectroscopy (FTIR) during active water application; analysis of extinguishing water confirmed the presence of fluoride ions, indicating scrubbing of HF by water. On the other hand, this means that firefighting water from battery fires becomes heavily contaminated and should not be released into the environment without proper treatment. Additionally, soot emissions were reduced by approximately 50%, lowering the transport of particulate-bound toxins such as PAHs. However, water application also showed potential adverse effects, notably an increase in products of incomplete combustion, with total hydrocarbon content (THC) approximately doubling compared to free-burning tests.

Overall, sprinklers may reduce specific toxic species in the air such as HF and soot, but can simultaneously degrade visibility and increase other toxic or flammable gases, meaning their net effect on tenability and health risk during LIB fires remains highly scenario-dependent.

Due to the limited scope and timeframe of this thesis, smoke production in the FDS model is prescribed using a simplified approach rather than being derived from detailed combustion chemistry. Instead, smoke is represented using a surrogate fuel with predefined yields. Consequently, specific toxic species are not explicitly modeled, and a comprehensive assessment of smoke toxicity cannot be performed.

1.9) Experimental Data Available

As stated in the introduction, experimental data on full scale EVs fires remain rather limited. While individual battery cells and battery packs are increasingly studied in detail, full-scale EV testing is often constrained by the high costs of both the vehicles and the required testing

[48] Ditch, B., FM Global, Zeng, D., & FM Global. (2019). *Development of sprinkler protection guidance for lithium ion based energy storage systems*. FM Global. https://www.researchgate.net/publication/333653116
[49] Promat. (n.d.). FIRE PROTECTION SOLUTIONS FOR EV CHARGING ZONES IN CAR PARKS. In *WWW.PROMAT.COM* (pp. 3–4).
[50] Hynynen, J., Willstrand, O., Blomqvist, P., & Andersson, P. (2023). Analysis of combustion gases from large-scale electric vehicle fire tests. *Fire Safety Journal*, *139*, 103829. https://doi.org/10.1016/j.firesaf.2023.103829

infrastructure. In addition, EV technology continues to evolve rapidly, particularly through increasing battery pack capacities to extend driving range.[51] Consequently, EVs from ten years ago are no longer fully representative of current-generation vehicles.

Moreover, several factors as described in previous chapters of Part 1, influence the development and severity of a thermal runaway-induced EV fire. These include the chemical composition, the type of ignition source, the age of the battery, the state of charge (SOC), ventilation conditions, and the design of the battery pack. A Battery Management System (BMS) can also play a crucial role. The BMS continuously monitors the battery pack, protects it against adverse environmental conditions, and helps optimize both safety and performance.[52] As a result, EV fires can develop in significantly different ways and are difficult to reproduce consistently under experimental conditions.

Even when full-scale EV fire tests are conducted, they are typically performed in combination with a specific extinguishing method. This makes it difficult to isolate and study the natural fire development itself, as well as to use the results directly for validation of FDS simulations.

1.10) Analysis of an Experimental Data Set

The paper by Kang et al. (2023), entitled *"Full-scale fire testing of battery electric vehicles"*, presents several free-burning fire test configurations for an electric vehicle (EV). In this study, thermal runaway (TR) was initiated using a heating pad, after which the vehicle was allowed to burn freely. The experimental campaign included tests on the complete vehicle (BEV#4), the battery pack alone (64 kWh LIB pack), and the vehicle body without the battery pack (BEV body - ignited with a 300 kW propane burner), all based on the same EV model.

The battery state of charge (SOC) was set to 100%, since fully charged lithium-ion batteries generally exhibit the most severe fire behaviour and the highest potential for fire spread under well-ventilated conditions.

Because the paper provides a detailed heat release rate (HRR) dataset, it serves as a valuable reference for the development of the FDS model. The modelling approach consists of assigning a predefined HRR to the battery system while introducing combustible materials representing the vehicle interior and structural components. The objective is to reproduce the HRR curve reported in the experimental study. Therefore, the experimental data are analysed in detail to identify the contribution of the different combustible components and to establish suitable input parameters for the FDS simulations.

[51] Angeline, P. S., & Rajkumar, M. N. (2020). Evolution of electric vehicle and its future scope. *Materials Today Proceedings*, *33*, 3930–3936. https://doi.org/10.1016/j.matpr.2020.06.266
[52] Angeline, P. S., & Rajkumar, M. N. (2020). Evolution of electric vehicle and its future scope. *Materials Today Proceedings*, *33*, 3930–3936. https://doi.org/10.1016/j.matpr.2020.06.266

1.10.1) Key Fire Phenomena to be Reproduced in the FDS Model

Two important fire phenomena observed during the experiments must be accurately reproduced in the FDS model: accelerated fire growth leading to the peak heat release rate (pHRR), and the occurrence of jet flames.

The BEV_3 test exhibited a notably rapid fire growth rate (θ = 0.020), which is classified as fast-medium growth. Although the thermal runaway of the battery pack initiates the fire event, the study concludes that the majority of the fire load originates from the combustion of organic polymer materials within the passenger cabin, including plastics, upholstery, and other interior components. These combustible materials are therefore considered the dominant contributors to both the peak heat release rate (pHRR) and the total heat release (THR).

Compared to conventional combustible vehicle fires[53], the accelerated fire growth is attributed to high-velocity jet flames emerging from the battery pack during thermal runaway. These jet flames result from the ignition of flammable gases released through battery safety valves during cell venting. The flames typically appear before the passenger compartment becomes fully involved in the fire and contribute to the ignition of nearby combustible components through intense localized heating.

Since Kang et al. (2023) does not provide detailed quantitative data regarding the jet flame characteristics, supplementary information is obtained from Zhao et al. (2024), entitled *"Full-scale experimental study of the characteristics of electric vehicle fires process and response measures."*

1.10.2) Analysis of the HRR Curves

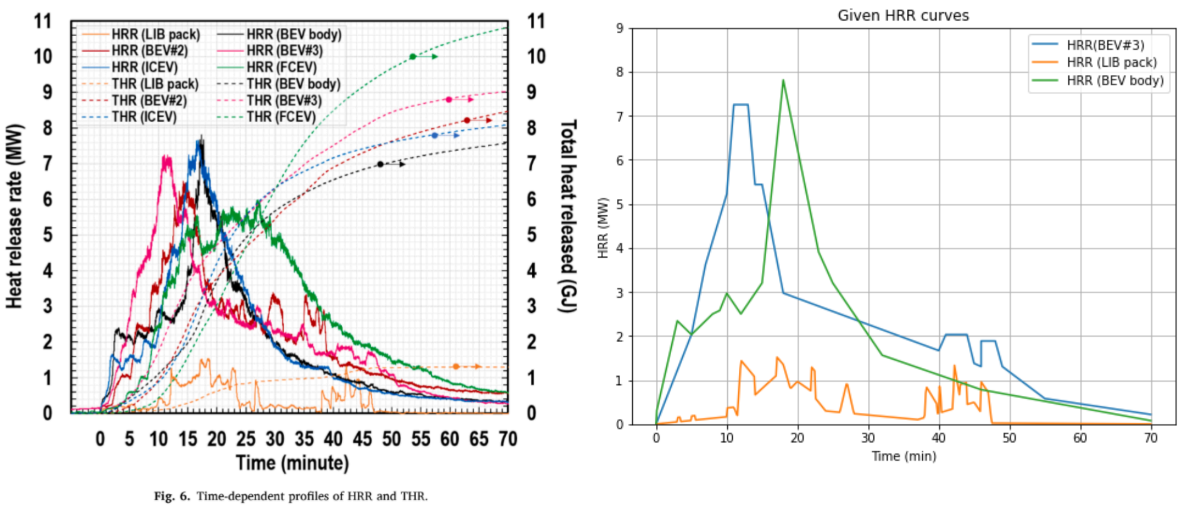

Figure 5: Original curves and curves created in Python

[53] Heinisuo, M., Partanen, M., Tampereen teknillinen yliopisto. Rakennustekniikan laitos. Rakennetekniikka, & Tampere University of Technology. Department of Civil Engineering. Structural Engineering. (2013). Modeling of Car Fires with Sprinklers. In *Tampere University of Technology. Department of Civil Engineering* (Research Report No. 161; p. 1).

All curves are shifted so that the moment of detected ignition corresponds to time zero. This means that the first 20 minutes of the tests with a TR as ignition source are excluded. because the heating sheet was active but no thermal runaway or significant fire growth had yet occurred. The simulation therefore focuses on the active combustion phase.The simulation therefore focuses on the active combustion phase.

The objective of this analysis is to determine the relationship between these curves. In principle, the combined contribution of the battery pack and the vehicle body should reproduce the HRR curve measured for the full vehicle fire. However, a simple summation of the curves does not reproduce the experimental result. This is due to the repeatability problem (see Experimental Data Available) and interactions between the battery pack and the car body.

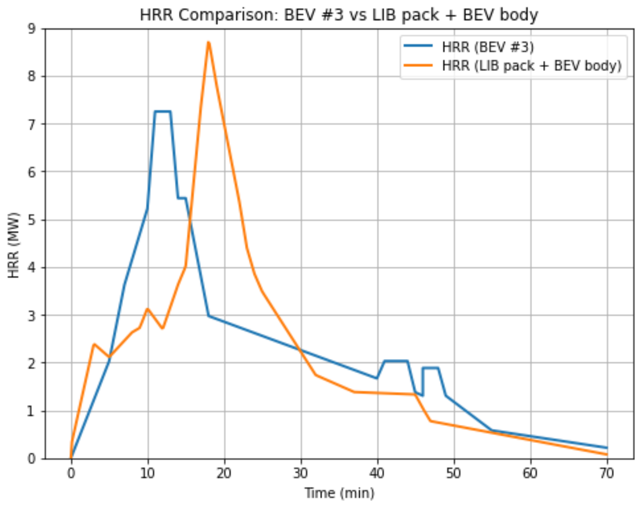

Figure 6: Full scale EV fire test and summation of the LIB pack fire test and the car body fire test

1.10.2.1) Behaviour of the Battery Pack

General

The HRR curve of the LIB pack shows relatively low activity during the first 10 minutes, followed by a rapid increase. Later in the test, a second smaller increase occurs after approximately 37 minutes.

The configuration of the battery pack consists of several isolated modules separated by small gaps to prevent fast spreading of a TR. The heating sheet is located in the centre of the pack. Consequently, thermal runaway initially occurs in this module and subsequently propagates to neighbouring modules. Other modules experience delayed thermal runaway later in the experiment.

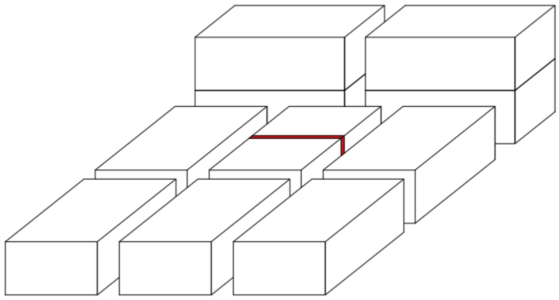

Figure 7: Configuration of the battery pack in the experiment

In the isolated battery pack test, heat can rise freely due to the absence of the vehicle body, resulting in limited thermal feedback. In a real vehicle configuration, however, the presence of the car body significantly increases thermal feedback, accelerating the transition from smouldering behaviour to rapid heat release.

To account for this effect in the full EV test, the early portion of the LIB pack HRR curve is shifted approximately 10 minutes earlier, while the later phase of the curve remains unchanged.

Jet flames

The HRR curve of the LIB pack also contains several short-duration peaks, each lasting approximately one minute. It is assumed that these peaks correspond to jet flame events generated during gas venting in the thermal runaway process. More specifically, the peaks are assumed to represent the heat release rate contribution of the jet flames alone. To avoid explicitly modelling these transient jet flame effects within the battery HRR input, the battery pack HRR curve was smoothed compared to the original experimental curve, as illustrated in Figure 8.

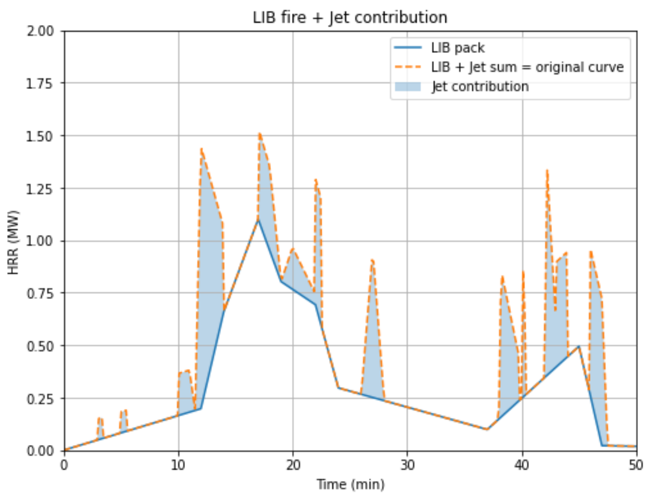

Figure 8: Graphs of the LIB pack

To assess whether this assumption is reasonable, findings from Cui et al. (2022) are considered. The study reports a maximum measured vent gas velocity of 42.1 m/s during thermal runaway. For the vent gas temperature, an average value of 800 °C is adopted based on the reported experimental measurements. (See main difference between ICEVs and EVs: Jet Flames)

Since the heat release rate (HRR) of jet flames is hard to measured directly in experiments, an approximate estimation is performed based on the mass flow rate of the vented gases:

$$HRR = m^{\circ}\, \Delta H_C = \rho v A \Delta H_C \qquad (1)$$

Where

m° = mass flow rate (kg/s)

ρ = gas density (kg/m³)

v = gas velocity (m/s)

A = vent opening area (m²)

ΔH_C = heat of combustion (MJ/kg)

In the FDS model, propylene is selected as the representative fuel for the jet flames. At room temperature, propylene has a density of 1.81 kg/m³. However, since the vented gases ignite immediately upon release during thermal runaway, the gas temperature is significantly elevated. Consequently, the gas density must be corrected to account for the high-temperature conditions using the ideal gas law density-temperature relationship:

$$\rho_T = \rho_0\, (T_0/T) \qquad (2)$$

Where:

T_0 = 293 K

T = 1073 K

This results in 0.494 kg/m³.

For the orifice area, an average safety valve diameter of 50 mm is assumed.

$$A = \pi * (d/2)^2 \qquad (3)$$

This results in 1.93 x 10^{-3}

Finally Kang et al. (2023) report a heat of combustion for the battery pack only of 45.9 MJ/kg.

The final result is:

$$HRR = 0.494 * 42.1 * 1.93 * 10^{-3} * 45.9 * 10^{6} = 1.88 * 10^{6} W = 1.9 MW$$

To account for uncertainty in vent velocities, additional calculations are performed using the minimum and maximum values reported in literature.

Lower bound velocity:

$$HRR = 0.494 * 16.6 * 1.93 * 10^{-3} * 45.9 * 10^{6} = 0.7 MW$$

Upper bound velocity:

$$HRR = 0.494 * 83.3 * 1.93 * 10^{-3} * 45.9 * 10^{6} = 3.7 MW$$

Thus, using representative values for gas density, vent velocity, and orifice area, the estimated heat release rate (HRR) of the jet flames ranges between approximately 0.7 MW and 3.6 MW. In comparison, the short-duration peaks observed in the LIB pack HRR curve reported by Kang et al. (2023) range between 0.1 MW and 1.25 MW, with a median value of approximately 0.7 MW. Although these values lie near the lower bound of the estimated range, the assumption remains plausible. Smaller jet flames may not always be visually identified or classified as distinct jet flame events during full-scale experiments. In addition, the well-ventilated laboratory conditions could have disturbed or diluted the vent flames, thereby reducing their apparent intensity and measured contribution to the overall HRR.

1.10.2.2) Behaviour of the Vehicle Body

The HRR curve of the BEV body test initially exhibits a rapid increase of approximately 0.3 MW, corresponding to the activation of the propane burner used to initiate the fire. Because the burner is positioned directly beneath the vehicle body, the thin metal plate separating the battery pack compartment from the passenger cabin heats up rapidly, resulting in the ignition of interior materials and tires. Following this initial growth phase, the fire stabilizes temporarily at approximately 2.1 MW. This plateau is attributed to limited oxygen availability while the vehicle windows remain intact, restricting ventilation to the passenger compartment. As the fire develops further, window breakage and structural deformation create additional openings, allowing increased airflow into the cabin and leading to renewed fire growth. Although the exact timing of window breakage is not reported by Kang et al. (2023), visual observations from experimental photographs at different time intervals provide an approximate indication of when these ventilation changes occur. Only one window was kept partially open from the start of the test to prevent self-extinguishment of the fire.

The peak HRR measured during the BEV body test is approximately 0.56 MW higher than that of the BEV_3 test. However, since the propane burner remained active throughout the experiment and continuously contributed approximately 0.3 MW, the effective difference attributable to the vehicle fire itself is estimated to be only about 0.26 MW.

If the LIB pack was added, the initial slope of the HRR curve should be reduced. In the BEV body experiment, the 300 kW propane burner provides an immediate and concentrated heat source. In the actual battery-initiated fire scenario, however, the battery pack does not produce a constant 300 kW from the first second. Instead, the heat release gradually increases during the first few minutes as thermal runaway develops, but the final ignition source would be bigger, resulting in both a medium fast growing fire. Furthermore, the burner acts as a localized ignition source, whereas the heat generated by a battery fire is distributed over a larger area. In addition, jet flames emerging from the battery pack can rapidly ignite components on the exterior of the vehicle. This can lead to earlier window failure and increased ventilation, shortening the temporary plateau observed in the BEV body test where limited oxygen supply slowed fire growth.

As a result of the stronger ignition source and the faster oxygen access, the HRR development in a battery-initiated fire is expected to occur earlier than in the burner-initiated experiment. To account for this effect, only the peak of the HRR (BEV body) curve is shifted six minutes earlier. The decay phase of the curve is assumed to remain unchanged, as it primarily reflects the burnout of combustible materials rather than the ignition mechanism. Finally, the entire HRR curve is shifted 0.3 MW downward to compensate for the constant heat input provided by the propane burner during the original experiment.

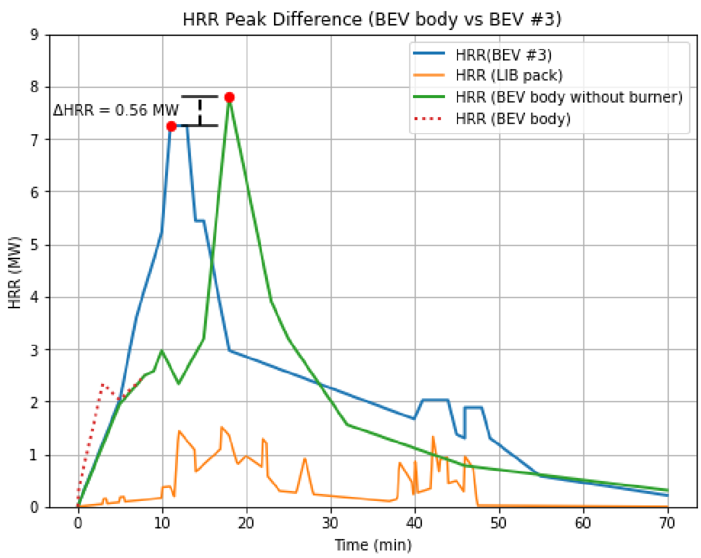

Figure 9: HRR curves

1.10.2.3) Combined HRR Curve

When the adjusted HRR curves of the LIB pack and the vehicle body are combined, the resulting curve closely resembles the HRR curve measured for the full BEV fire experiment.

This indicates that the interaction between the battery pack and the vehicle body, primarily through increased thermal feedback and thus a faster rise in temperature, accelerates fire growth, leading to earlier thermal runaway propagation and a faster increase toward the peak heat release rate.

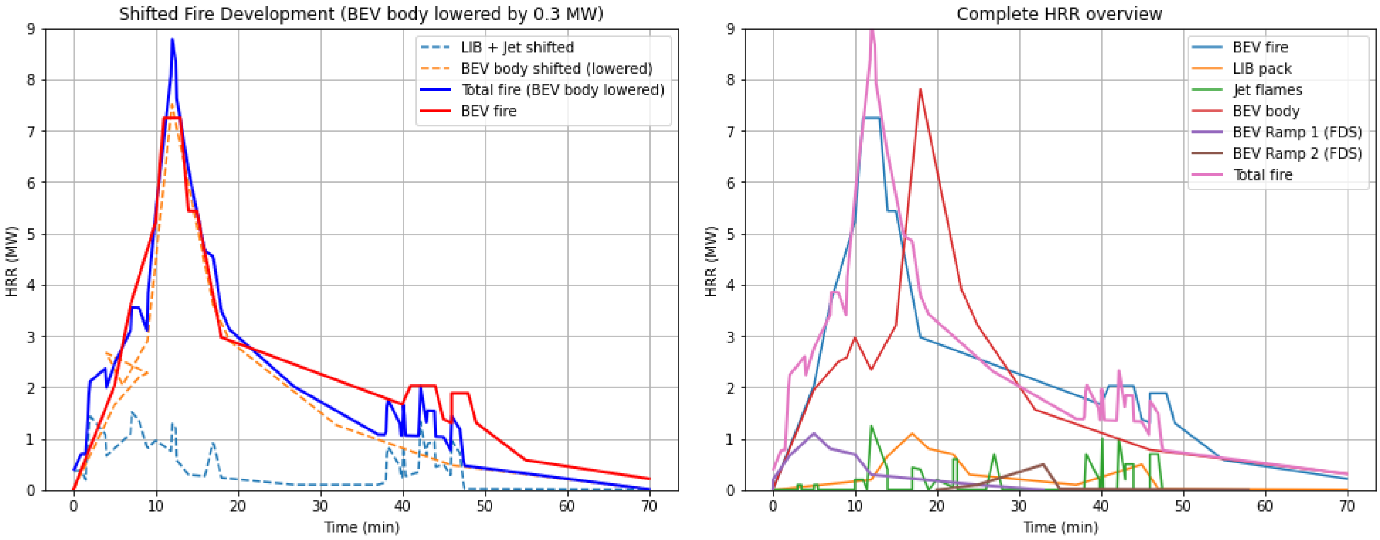

Figure 10: Left final HRR curve; Right: overview of all the HRR curves

Part 2: FDS model development

2.1) Modelling of the car

2.1.1) FDS set-up

The modelling procedure is structured in several steps. The final model can be found in Annex D. First, a simplified electric vehicle model within a 10 cm by 10 cm grid is created in AutoCAD based on the average dimensions of the nine best-selling electric passenger vehicles in 2025. (See annex E) and subsequently transferred to Revit to construct the three-dimensional geometry. This geometry is then imported into **Fire Dynamics Simulator (FDS) version 6.9.1** for the fire simulations. Finally, materials properties are assigned. The properties are primarily derived from the study “Modeling of Car Fires with Sprinklers” by Heinisuo et al. (2013). Although that study focuses on conventional combustion vehicles, the structural materials used in electric vehicles are largely similar. Therefore, the material properties reported in that work are considered representative for the present model. Because the geometry implemented in this study is more detailed than the model used by Heinisuo et al., minor adjustments to the material properties were introduced, while remaining within realistic ranges reported in literature. Steel is used as the primary material for the vehicle body because it remains one of the most common structural materials in passenger vehicles. Average values for density, thermal conductivity, and specific heat of structural steel are therefore applied.

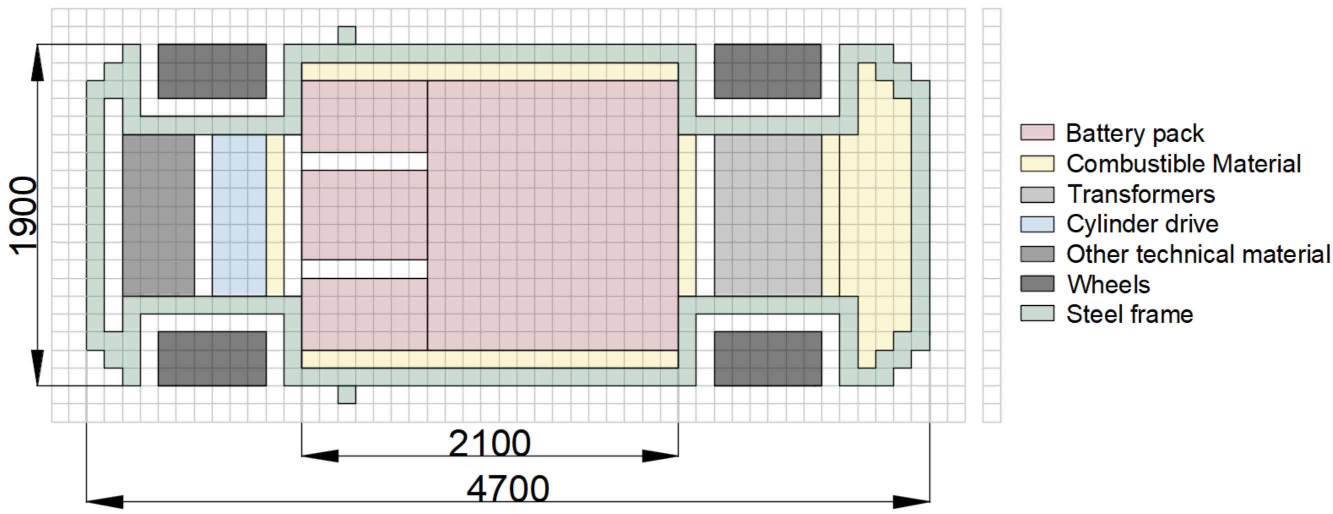

Figure 11: Initial Internal ground plan in Autocad

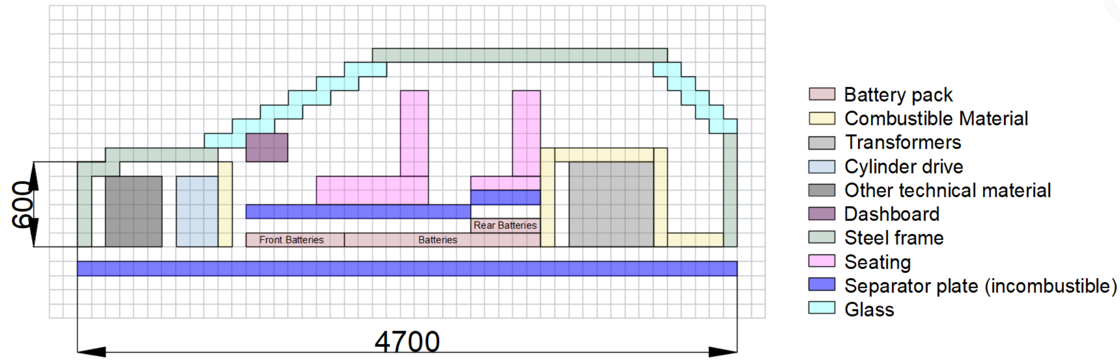

Figure 12: Cut-out view

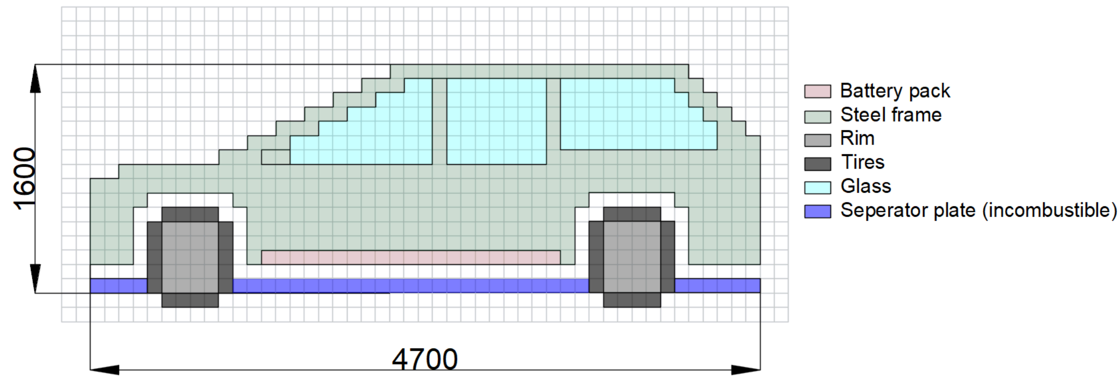

Figure 13: Side view

Surface/ component	Constituent Material(s)	Density [kg/m³]	Thermal Conductivity [W/(m*K)]	Specific Heat [kJ/(kg*K)]	Heat of Comb. [MJ/kg]	Ignition Temperature [C°]	Extinction temperature [C°]
Seating	Fabric Lining & Foam Filling	200/80	0.10/0.05	1.00/1.00	20/28	350	300
Cabin Insulation/interior	Fabric Lining & Polyproylene	200/900	0.10/0.16	1/1.9	20/48	450	400
Wheel Assembly (Tires)	Rubber (KUMI_CC)	910	0.13	1.88	32	300	250
Electronics/Dashboard	Electronic Plastic	1100	0.20	1.50	38	320	270
Battery Pack (Simple)	Battery Materials Simple	1500	0.20	1.50	39	270	220

Table 1: Materials characteristics and HRRPUA-values

In this study, combustible vehicle components and interior materials are represented using a simplified pyrolysis model in FDS. Rather than solving complex, multi-step chemical reaction kinetics (Arrhenius-based pyrolysis), solid fuel degradation is governed by a thermal threshold approach23. The 1D heat conduction equation is solved inside the solid material using specified thermal properties (density, thermal conductivity, and specific heat). Once a surface cell reaches its predefined ignition temperature, the material begins to burn at a fixed, prescribed HRRPUA. If water cooling reduces the surface temperature below the designated extinction temperature, or through the application of an empirical suppression coefficient, the heat release rate is reduced or terminated.

To ensure sufficient air access in the FDS model, gaps are introduced between the batteries and the separator plates. In addition, devices are assigned to each window to simulate failure at a temperature of 300 °C.[54] This simplified approach is based on the breakage of windows caused by thermal deformation of the frames or thermal shock induced by the fire.

The HRR of the LIB pack is predescribed with a surrogate fuel PROPANE with radiative fraction of 0.3 and, as mentioned before, based on experimental data from Kang et al. (2023) in "*Full-scale fire testing of battery electric vehicles*". The battery tested was a NCM battery with a 64 kWh capacity at 100% SOC, heated by a 575 W heating sheet (90 × 65 mm). To validate the model, the HRR of the whole car (BEV#3) of this paper will be used. In this experiment, the fire was also initiated using a 575 W heating sheet (90 × 65 mm) attached to a single lithium-ion battery cell located in the central battery module (Module 9). This setup simulates internal thermal runaway caused by a defect or mechanical abuse. A detailed analysis of the HRR curve presented in this study is discussed in 1.10. The experimental results indicate a total fire duration of at least 70 minutes, with a peak heat release rate (pHRR) of 7.25 MW, reached approximately 11 minutes after fire growth began. The total heat released (THR) during the experiment was 9.03 GJ. It is expected that these values will not be achieved exactly, but will correspond in magnitude.

Finally, a concrete wall is positioned 30 cm in front of the vehicle, while a floor and ceiling with a free height of 2.5 m are included to represent the enclosed underground parking environment.

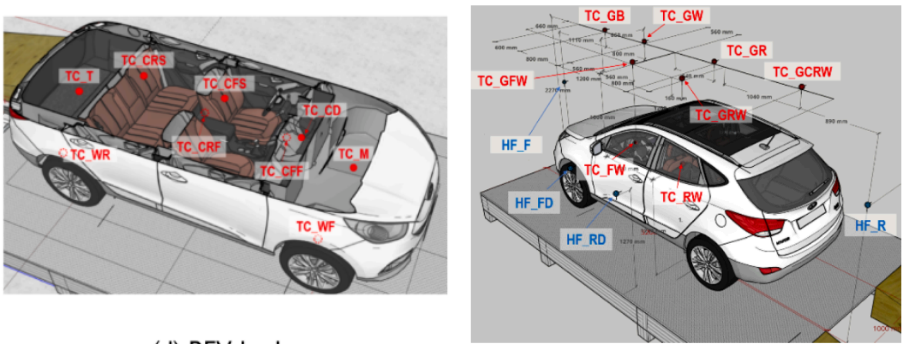

(d) BEV-body (b) Bird's-eye view

Figure 14: Locations of the thermocouples[55]

[54] Yang, Y., Miao, L., & Chow, C. L. (2017). Relative significance of temperature gradient components on cracking behavior in glass panes under thermal radiation. *Applied Thermal Engineering*, *131*, 837–848. https://doi.org/10.1016/j.applthermaleng.2017.12.060
[55] Kang, S., Kwon, M., Choi, J. Y., Sengkwan Choi, Fire Testing & Research Centre, Fire & Disaster Management Division, Korea Conformity Laboratories, Republic of Korea, Advanced Functional Nanohybrid Material Laboratory, Department of Chemistry, Dongkuk University, Republic of Korea, & School of the Built Environment, Ulster University, UK. (2023). Full-scale fire testing of battery electric vehicles [Journal-article]. *Applied Energy*, *332*, 120497. https://doi.org/10.1016/j.apenergy.2022.120497

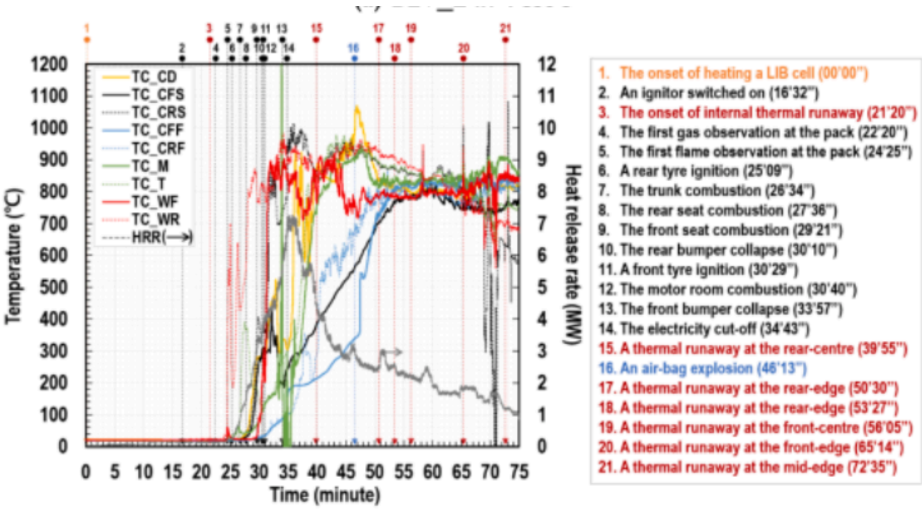

(b) BEV_3 in Test 4

Figure 15: Temperature measurements of the thermocouples and events[56]

2.1.2) Sensitivity analysis of a single EV fire without jet flames

2.1.2.1) Determination of the approximately cell size

For the initial validation of the test, a domain of 6 m × 6 m × 3 m (free height 2.5 m) was used, divided into eight equal meshes. To determine an appropriate cell size, an initial estimate was obtained using the resolution index formula:

$$RI = D^* / \Delta x = 10 \qquad (4)$$

With D* the characteristic fire diameter, obtained from equation:

$$D^* = \left(\frac{Q^{\circ}}{\rho_{\infty} * T_{\infty} * c_p * \sqrt{g}}\right)^{\frac{2}{5}} \qquad (5)$$

Where:

Q* = HRR at steady-state condition (equal to 7250 kW PHRR)

ρ_{∞} = density of ambient air (equal to 1.2 kg/m^3)

T_{∞} = temperature of ambient air (equal to 293 K)

[56] Kang, S., Kwon, M., Choi, J. Y., Sengkwan Choi, Fire Testing & Research Centre, Fire & Disaster Management Division, Korea Conformity Laboratories, Republic of Korea, Advanced Functional Nanohybrid Material Laboratory, Department of Chemistry, Dongkuk University, Republic of Korea, & School of the Built Environment, Ulster University, UK. (2023). Full-scale fire testing of battery electric vehicles [Journal-article]. *Applied Energy*, *332*, 120497. https://doi.org/10.1016/j.apenergy.2022.120497

c_p = specific heat of ambient air (equal to 1 kJ/kg×K)

g = gravitational acceleration (equal to 9.81 m/s^2).

It should be noted that using the Peak Heat Release Rate (PHRR) to determine D* yields a conservative estimate for grid resolution, as PHRR represents a single instantaneous peak value; adopting an average HRR value would provide a more representative characteristic fire diameter

Combining Equations (4) and (5) results in an estimated cell size Δx of approximately 0.21 m for a 7.25 MW fire. Based on this estimate, three cell sizes are selected for the sensitivity study: 2.5 cm, 5 cm, 10 cm, and 20 cm. For the sensitivity analysis, jet flames are not included. The underground parking is for the sensitivity analysis kept on 6.6 m by 7.3 m.

2.1.2.2) Results of the sensitivity analysis

Figure 16 compares the HRR predictions obtained using four mesh resolutions (2.5 cm, 5 cm, 10 cm, and 20 cm) for a single-car fire without jet flames. The 20 cm cell size shows significant deviations from the finer meshes, particularly during the fire growth phase and around the peak HRR, indicating that this resolution is too coarse to accurately capture the fire dynamics. This is mainly because the geometry was designed on a 10 cm × 10 cm grid, causing important geometrical details to be insufficiently resolved when using the 20 cm mesh.

In contrast, the 2.5 cm and 5 cm meshes show very similar behaviour during the first four minutes of the simulation. The 10 cm mesh exhibits a slightly delayed rise in HRR, but the overall behaviour remains sufficiently similar at the scale relevant for this study. Furthermore, the 5 cm and 10 cm meshes produce comparable HRR trends during the first 12 minutes, including similar fire growth rates and peak HRR values. Although the differences between the 5 cm and 10 cm meshes become more pronounced during the later stages of the simulation, a 10 cm cell size is ultimately selected for a suitable compromise between accuracy and computational cost. Since this early stage is the most critical period for sprinkler activation and fire spread assessment, the agreement between these two mesh resolutions is considered adequate for the objectives of the study.

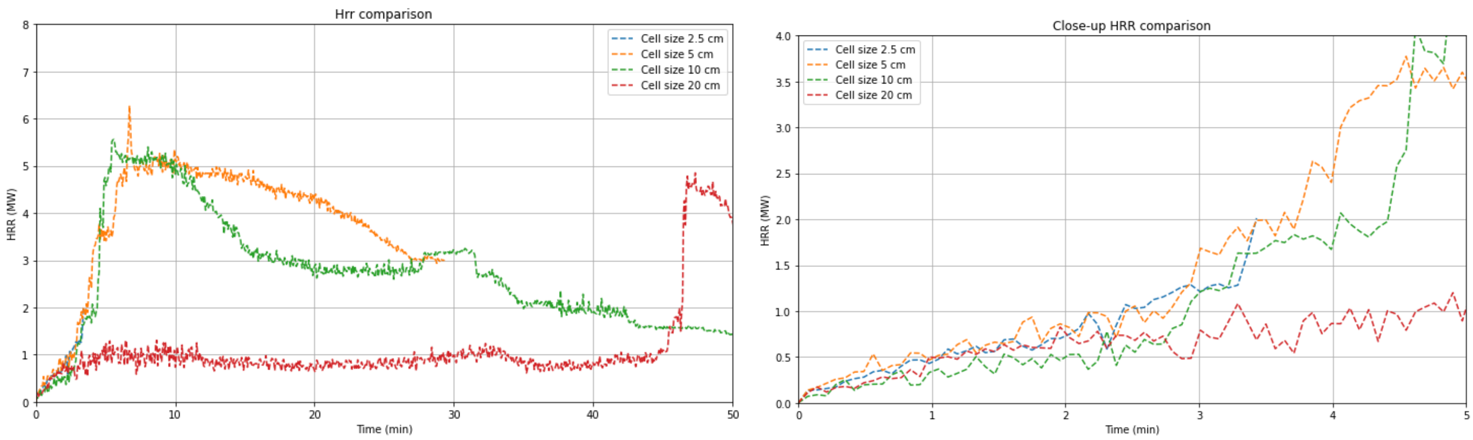

Figure 16: HRR of different cell sizes of a single car without jet flames

2.2) Modelling of the jet flames

2.2.1) Jet Flame Model Setup and Parametric Study

In the next stage of the study, jet flames are introduced into the numerical model. To accommodate the flame development, the computational domain is enlarged to **6.6 m × 7.3 m**. Since a surrogate fuel is used in the simulations, the jet flames must also be represented artificially. To achieve this, the side of the vehicle body adjacent to the battery pack is elevated by 10 cm, leaving the side of the battery pack exposed. Different &VENT configurations are then applied to this open surface. Each vent is defined by a time-dependent ramp and prescribed values for:

- jet velocity,
- gas temperature,
- horizontal orientation,
- fuel mass fraction,
- vent opening area.

This approach generates laterally projected jet flames, representing a battery pack configuration in which the safety valves are positioned on the sides of the battery cells. Such behaviour is consistent with observations reported in experimental studies on battery TR.[57] [58]

To isolate the effect of the jet flames, all combustible materials of the vehicle are removed from the model. In addition, the battery pack itself is assigned a reduced heat release rate per unit area (HRRPUA) of 10 kW/m², which is only sufficient to ignite the discharged flammable gases. As a result, the dominant heat release originates from the jet flames rather than from other burning vehicle components.

[57] Cui, Y., Liu, J., Cong, B., Han, X., & Yin, S. (2022). Characterization and assessment of fire evolution process of electric vehicles placed in parallel. *Process Safety and Environmental Protection*, *166*, 524–534. https://doi.org/10.1016/j.psep.2022.08.055
[58] Zhao, C., Hu, W., Meng, D., Mi, W., Wang, X., & Wang, J. (2023a). Full-scale experimental study of the characteristics of electric vehicle fires process and response measures. *Case Studies in Thermal Engineering*, *53*, 103889. https://doi.org/10.1016/j.csite.2023.103889

A parametric study is conducted to investigate the influence of jet flame parameters on flame behaviour. The parameters varied are:

- jet velocity,
- vent opening area, and
- gas temperature.

To ensure meaningful comparisons, the overall HRR is kept approximately constant for all cases. Therefore, the fuel mass fraction is adjusted according to the selected parameter combination. The mass flow rate is calculated using:

$$m^{\circ} = Y\rho v A \qquad (6)$$

Where

m° = mass flow rate (kg/s)

Y = mass fraction (-)

ρ = gas density (kg/m³)

v = gas velocity (m/s)

A = vent opening area (m²)

For temperature variations, the gas density is adjusted according to a simplified form of the ideal gas law:

$$\rho \propto 1/T \;\; => Y \propto T \qquad (7)$$

Based on these relationships, the mass fraction for each new configuration is determined using:

$$Y_{new} = Y_{old}(v_{old}/v_{new})(A_{old}/A_{new})(T_{new}/T_{old}) \qquad (8)$$

The objective of this chapter is to examine how variations in jet velocity, gas temperature, and vent area influence flame behaviour while maintaining approximately the same HRR. By varying one parameter at a time, systematic comparisons can be made regarding:

- flame shape,
- flame temperature, and
- overall flame behaviour.

This approach allows the observed differences in flame behaviour to be directly attributed to the selected parameter.

The underlying hypothesis is that identical HRRs can still produce significantly different jet flame characteristics depending on the flow conditions and vent geometry. This is particularly important in flame spread studies, where variations in jet flame behaviour may strongly influence fire propagation and interactions with the vehicle geometry and surrounding environment. Consequently, this chapter aims to demonstrate that HRR alone is insufficient to fully characterise flame spread behaviour, and that additional parameters and flame characteristics must also be considered.

The base-case jet flame configuration is defined by:

- fuel mass fraction: **6%**,
- jet velocity: **40 m/s**,
- gas temperature: **900 °C**,
- vent opening area: **10 × 10 cm²**.

2.2.2) Sensitivity analysis

Since the previous sensitivity analysis was performed without jet flames, an additional sensitivity study is conducted considering only the jet flame configuration. A coarser mesh resolution is not feasible in this case, due to the limited characteristic size of the jet flame region, which is approximately 10 × 10 cm. Based on equations (4) and (5), a maximum HRR of 375 kW (see Figure 17) results in an estimated required cell size of approximately 6.5 cm. This is smaller than the previously selected 10 cm mesh resolution. However, this relationship should be interpreted as an empirical guideline rather than an exact requirement, as it is derived from characteristic fire diameter scaling and therefore provides only an approximate estimate of the appropriate grid resolution. Furthermore, the jet flames used in this parametric study are relatively small compared to the full experimental configuration, where peak jet flames can reach up to 1.1 MW. This higher HRR corresponds more closely to a grid size of approximately 10 cm, which is consistent with the initially chosen mesh resolution for the full-scale case.

To ensure that the results are not sensitive to the chosen discretisation, an additional mesh sensitivity analysis is therefore performed using cell sizes of 2.5 cm, 5 cm, and 10 cm. This allows verification of the robustness of the simulation results with respect to grid resolution.

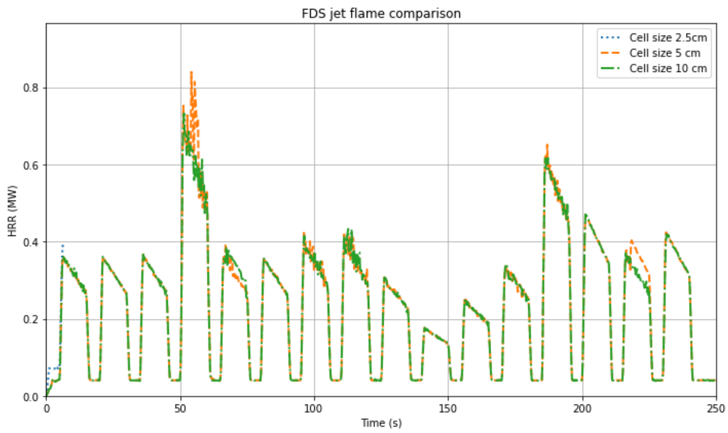

Figure 17: HRR of jet flames

A cell size of 2.5 cm exhibits numerical instability after approximately 7 seconds, corresponding to the moment when the first jet flame reaches its peak. This instability occurs because the minimum density drops below 0.12 kg/m³. Since FDS neglects pressure waves and averages the flow properties within each computational cell, at least one cell reaches a density that is too low for a grid resolution of 2.5 cm. For larger cell sizes, the averaged density remains sufficiently high, thereby preventing this error.

Consequently, a cell size of 10 cm × 10 cm was selected. Its results closely match those obtained with the 5 cm cell size, as long as the velocities exceed 20 m/s, while significantly reducing the risk of numerical instability caused by low-density cells. The jet flames remain similar up to at least 2.8 m from the vehicle, which corresponds to the boundary of the computational domain. These findings demonstrate that a 10 cm cell size provides sufficient accuracy for the application considered in this thesis.

2.2.3) HRR analysis

In the FDS model, the fuel flow rate for the vehicle fire and jet flames is governed by a prescribed HRRPUA combined with time-dependent ramp functions (RAMP_Q and RAMP_V). For the jet flames, the effective fuel mass flow rate is explicitly calculated using Equation (6). To isolate individual physical effects while keeping the total HRR constant across parametric cases, the fuel mass fraction Y of the surrogate fuel (propane) was systematically re-calibrated whenever jet velocity, vent opening area, or gas temperature was varied.

As shown in Figure 17, the HRR curves remain nearly identical for most cases, confirming that the adjustment of the mass fraction successfully compensates for the variations in velocity, temperature, and area. The observed deviations remain within approximately ±5% for all cases except Jet Flame 4. Jet Flame 4 corresponds to the case with a 50% reduction in velocity relative to the base case, resulting in a velocity of 20 m/s.

A closer investigation (see figure 18) using a more gradual reduction in velocity demonstrates that reductions up to 25% (corresponding to a velocity of 30 m/s) have little to no influence on the HRR. The hypothesis is that the deviation observed for the 50% velocity reduction is likely caused by the jet flame no longer transporting sufficient energy outside the computational domain. Consequently, a larger fraction of the released energy remains within the domain and contributes to the calculated HRR. A visual inspection of the flame behaviour is expected to confirm this hypothesis and will be performed in the next step of the analysis.

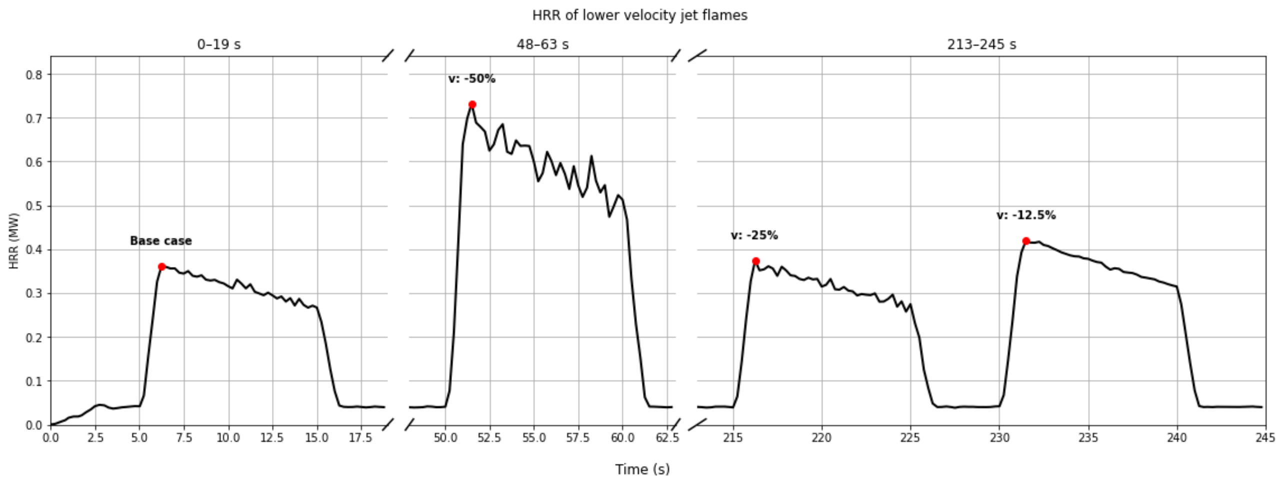

Figure 18: Closer investigation of lower velocity jet flames

2.2.4) Slice-Based Temperature Field Analysis

Using the *.smv* output files, a qualitative post-processing analysis is performed for selected jet flame cases at the time of peak heat release rate. For each case, vertical temperature slices are extracted along the VENT boundary at regular intervals of 0.2 m (x = 0.9, 1.1, 1.3, …, 2.9 m). In addition, horizontal temperature slices are generated at heights of z = 0.3 m and z = 0.6 m, corresponding to the location of the battery pack and an elevated reference plane.

This approach provides a reduced-order representation of the three-dimensional thermal field by combining multiple two-dimensional slices. Although it does not constitute a full volumetric analysis, it enables a consistent comparison of the spatial temperature distribution and flame development between different jet flame configurations.

Temperature is used as the primary diagnostic variable, as it serves as a proxy for thermal exposure and is strongly -however not the only parameter- correlated with the ignition potential of adjacent materials. Within this study, temperature fields are therefore used for comparative purposes, to identify differences in flame structure and the spatial extent of high-temperature regions between cases, rather than as a direct ignition criterion. The results are presented in Annex B.

From this study, it can be concluded that higher jet velocity results in a longer flame with increased momentum and greater penetration distance. The flame becomes more strongly directed, exhibiting a narrower and more coherent core structure. In contrast, lower velocities produce shorter flames with a more plume-like and diffuse shape. It also becomes evident that the observed increase in heat release rate (HRR) for the jet flame at a velocity of 20 m/s is indeed primarily attributed to a greater fraction of energy remaining within the computational domain and the hypothesis stated in the HRR analysis is therefore confirmed.

When increasing the vent area (decreasing is limited by the 10 cm × 10 cm cell size constraints), the jet becomes less needle-like, with increased radiative heating closer to the source. The flame appears broader and more diffused. Notably, at +200% area, the jet flame is observed to tilt more towards the ground. This suggests that the increased diffusion reduces the buoyancy-driven rise of the hotter gas regions, leading to a more downward-oriented flow pattern (see Figure 19).

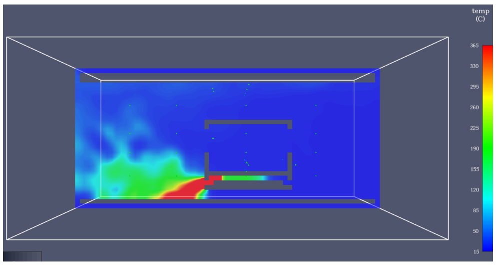

Figure 19: Jet flame at 85 sec with an area of 30 cm x 10 cm.

Third, when increasing temperature, the buoyancy effects are enhanced. The jet flame rises more rapidly, and the high-temperature region (red zone) becomes larger, indicating increased thermal intensity and higher heat flux. However, temperature increases have limited influence on extending the high-temperature zone beyond approximately 0.5 m from the source, where temperature differences between cases become less pronounced.

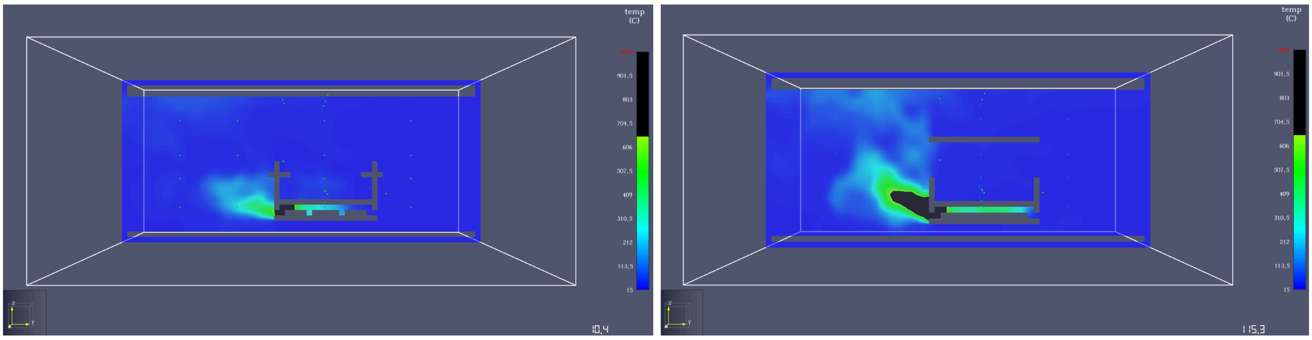

Figure 20: left: Base case jet flame; right +70% temperature jet flame (The black area is the zone with T > 650°C)

Summary of Parameter Effects:

- **Velocity:** primarily governs flame reach and penetration distance
- **Vent area:** mainly affects flame thickness, diffusion, and overall intensity
- **Temperature:** influences buoyancy strength and thermal intensity of the jet flame

Finally, a notable phenomenon was observed in two jet flame configurations: during the short activation period (~10 s), a weaker secondary jet flame intermittently appears on the opposite side of the system. The effect occurs in cases with a lower velocity (20 m/s, only with 5 cm cell size resolution) and in configurations with a doubled vent area (but not tripled area).

A possible explanation is the presence of a 10 cm gap between the battery pack and the vehicle floor, combined with vents positioned slightly beneath the vehicle body. This geometry may allow hot gases to recirculate into the gap region, creating a transient flow reversal or localized flashback effect that leads to a weaker jet flame emerging on the opposite side. This effect appears to be sensitive to momentum flux. At lower velocities, hot gases have sufficient residence time to penetrate the gap. Similarly, with increased vent area, the reduced momentum flux per unit area leads to a more diffuse and turbulent jet, allowing part of the flow to enter the gap and destabilize the internal air pocket. However, when the vent area becomes sufficiently large, the jet regains enough spatial freedom to exit more coherently, preventing this reversal phenomenon.

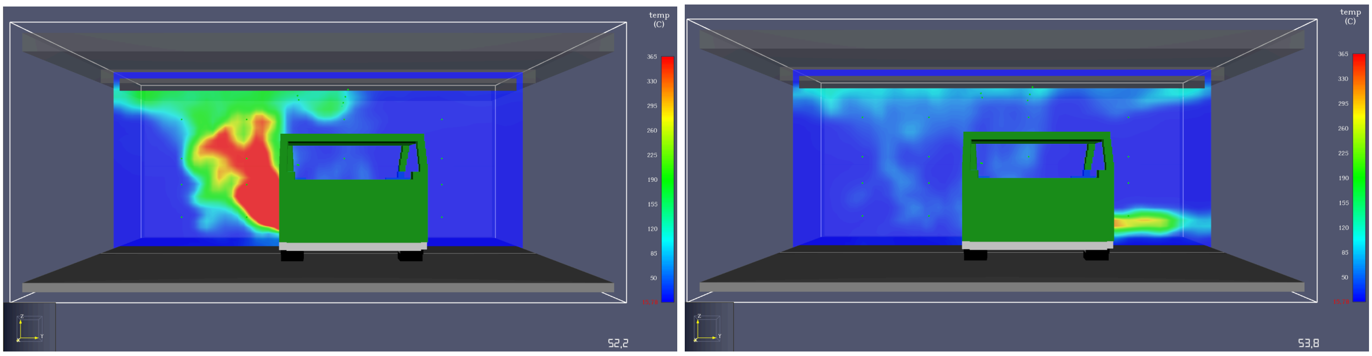

Figure 21: Left: Jet flame (velocity -50%) at 52.2 sec; Right: Rebounce jet flame (velocity -50%) at 53.8 sec.

2.2.5) Conclusion of the jet flame simulation

The simulations show that jet flame behaviour is primarily governed by momentum flux, which is controlled by the combined effect of velocity and vent area. Velocity mainly determines flame reach and penetration distance, while vent area influences jet diffusion and flame thickness. Temperature predominantly affects buoyancy and the thermal intensity of the flame.

Despite similar HRR, significant differences in flame structure and spatial temperature distribution were observed between cases, indicating that realistic jet flame parametrization is essential for accurate prediction of flame spread and thermal exposure. Furthermore, the geometric confinement and vent positioning can influence the flow field, potentially inducing localized recirculation and transient flow reversal at low momentum fluxes. These results demonstrate that HRR cannot be the only parameter measurement to predict flame spread.

Although the simulations provide valuable comparative insights into jet flame behavior, the results must be interpreted within the context of both code-inherent limitations and user-defined setup choices. Discrepancies between FDS predictions and experimental observations should not be viewed purely as intrinsic solver deficiencies. The simplified combustion modelling and numerical constraints, particularly for highly velocity flames (circa from 80 m/s there is a change for a numerical error and low-density (numerical error occurs with densities below 0.122 kg/m^3) combustion products, imply that the simulated jet flames should be interpreted as simplified representations of the physical phenomena rather than exact reproductions of reality. While FDS's low-Mach-number formulation inherently neglects pressure-driven expansion, causing the simulated jet flames to appear more buoyancy-dominated than in real-world experiments, the overall accuracy is equally governed by user responsibility in selecting appropriate input parameters. Factors such as the artificial representation of the vent area, surrogate fuel definitions, and simplified combustion settings play a significant role in flame structure and thermal exposure. Acknowledging both the solver's physical boundaries and the impact of these modeling assumptions is essential when interpreting the predicted fire spread.

Additional limitations include the mesh resolution, which is limited to 10 cm × 10 cm, and the modeled nozzle openings, which are often larger than in reality. In real battery failure scenarios, flammable gases from vaporized electrolyte are expelled through very narrow openings, such as small gaps or safety valves, typically around 100 mm^2 in area. These limitations must be carefully considered when using FDS to study fire spread initiated by EV battery thermal runaway.

2.3) Modelling of the underground parking & neighbouring vehicles

2.3.1) Modelling of the environment

To model the environment, the computational domain is extended to 16 m × 9.5 m. In addition, two neighbouring vehicles are added at a distance of 0.6 m on each side of the initial vehicle. These vehicles are coloured yellow and orange, while the green vehicle is defined as the initial burning car. The model is divided into eight equal meshes of 8 m x 4.8 m x 1.5 m. The study does not consider the complete fire duration until burn-out, but focuses instead on the first 12 - 15 minutes (700 - 900 s) of the event due to the maximum computational time of 72 hours. This period extends till the moment at which, according to Kang et al., the PHRR has already occurred.

The battery packs of the neighbouring vehicles are modelled as combustible materials with an ignition temperature of 250 °C, corresponding to the maximum value reported in literature beyond which thermal runaway can no longer be avoided. The green vehicle is assigned the prescribed HRR curve defined in Section 2.1.1.

Jet flames are only applied on one side of the burning vehicle, directed towards the yellow vehicle. The hypothesis is that the yellow vehicle will ignite earlier due to the additional flame impingement and thermal exposure. The timing of the jet flames and their respective HRR values are based on Figure 8 and Figure 10 (right) from Section 1.10.2. The geometry of the jet flames is derived from the parameter study presented in Section 2.2. This results in a total of 11 jet flames with HRR values as shown in Figure 22. The exact jet flame geometry based on temperature slices can be found in Annex C. This shows that the temperatures at which the jet flames impact the yellow car are relatively limited, ranging only between 450°C and 800°C. Only Jet Flames 4 and 10 maintain temperatures above 450°C that reach the yellow car throughout their entire duration of operation.

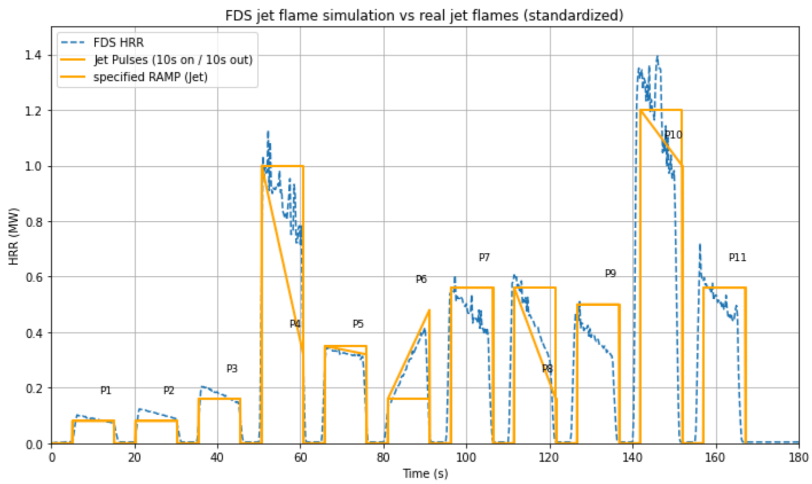

Figure 22: HRR of the jet flames used in the model (standardized)

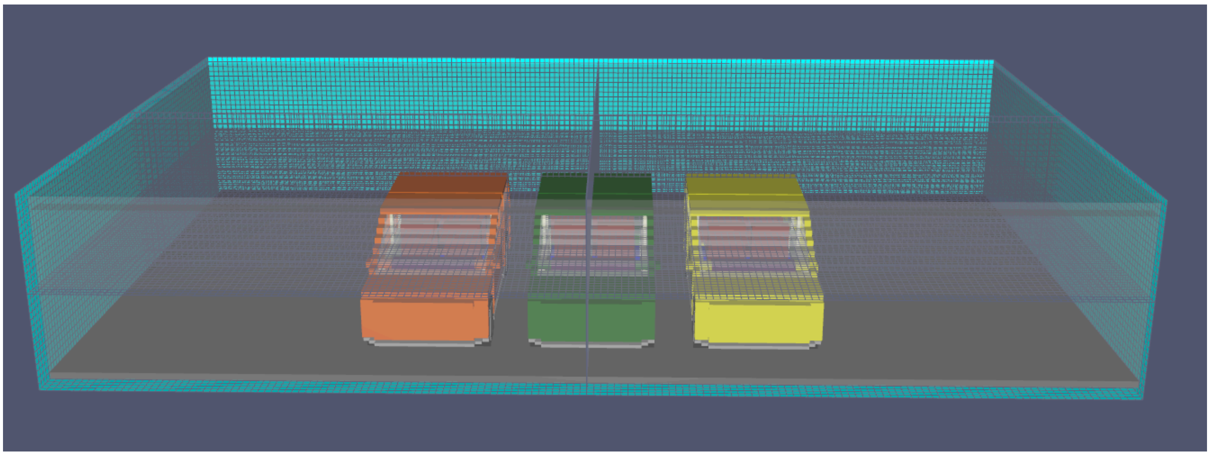

Figure 23: Final FDS model.

2.3.2) Model validation

Three simulations (grid size 10cm) containing only the green vehicle are performed and compared with the total BEV fire results reported by Kang et al. (2023) *"Full-scale fire testing of battery electric vehicles"* to verify whether the overall HRR evolution was broadly consistent with the reference study. An exact match is not expected, as BEV fires can vary significantly, as discussed in Section 1.9. The primary objective is to obtain a peak HRR between approximately 6 and 8 MW after around 10 minutes.

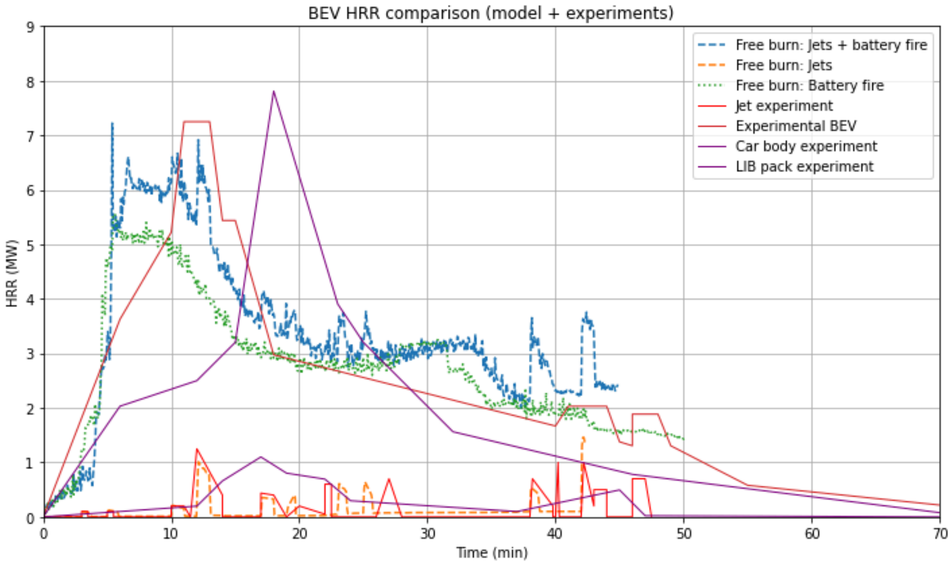

Figure 24: HRR of the single-vehicle model compared with the HRR curve from the reference study.

Although the HRR increases more rapidly than in the literature reference and the predicted PHRR reaches only 6.5 MW, the results are still considered sufficiently representative for the purposes of this study. The model reproduces the overall trend of the experimental HRR evolution reasonably well, particularly with respect to the duration and decay behaviour of the fire. Furthermore, given the significant variability observed in the experimental data (see 1.9), the model can be considered to capture the correct order of magnitude and the general fire development adequately.

In addition, the steeper HRR growth can be regarded as conservative with respect to flame spread prediction. A faster growth phase results in earlier and more severe thermal exposure to neighbouring vehicles, meaning that the model provides a safety-oriented estimate compared to the reference case.

It is also noteworthy that the scenario including only the jet flames (i.e., with the battery HRR set to 1 kW) is not capable of igniting the remainder of the vehicle, but it is able eventually at 779 sec to break the front window. In reality, jet flames propagating through gaps within the vehicle interior or a confined VCE explosion may compromise the separation between the battery pack and the passenger compartment. In this way, jet flames can contribute to the breach of internal barriers, enabling earlier ignition of adjacent vehicle components and thereby accelerating the overall fire development inside the car. However, since the primary focus of this study is flame spread to neighbouring vehicles rather than fire propagation within the vehicle itself, this limitation is not considered critical. Moreover, the growth phase in the model is already steeper than the experimental HRR data, which can be seen as compensation for the simplified jet flames.

As an additional analysis, a scenario was simulated in which only intermittent jet flames, but with three cars, were present, without any contribution from the LIB fire. The jet flames were activated for durations of 30 to 60 seconds, with 10-second pauses in between, to investigate whether they alone could ignite the adjacent vehicle (see Figure 25). The results indicate that the tires are only shortly ignited, but due to the set extinguishing temperature, extinguishes the fire again after the jet flame stops. However, in full-scale experimental testing it is currently not possible to isolate EV jet flames. Consequently, it remains uncertain whether, in real-world conditions, these jet flames alone are capable of igniting a nearby vehicle or whether, like in the model, their primary effect is to accelerate flame spread by locally increasing temperatures and enhancing radiative heat flux. Therefore, in this thesis, the jet flames are acknowledged as a weakness (See 5.1), but accepted as realistic in the model, also considering limitations within FDS.

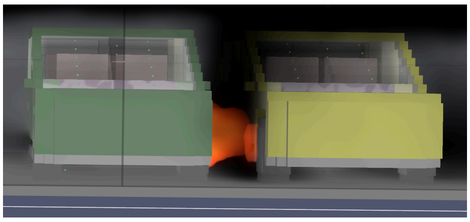

Figure 25: Short ignition of the tire

2.3.3) Sensitivity analysis

Since the computational domain is significantly larger than in the previous sensitivity studies and additional (combustible) geometry is introduced, a limited sensitivity analysis is carried out using cell sizes of 10 cm and 5 cm. A simulation with a 2.5 cm cell size is not feasible due to excessive computational time requirements. Furthermore, the 5 cm simulation can not be completed for the same reason. A cell size of 20 cm is not considered, as previous studies have demonstrated that this resolution is insufficiently accurate and unable to properly capture the jet flames and finer geometric details. Consequently, performing a simulation with a 20 cm cell size is deemed unnecessary. It is assumed that if the results obtained with 10 cm and 5 cm cell sizes show good agreement, the 10 cm cell size can be considered sufficiently accurate for the purposes of this study. The detailed analysis of this scenario will be conducted in 4.3.

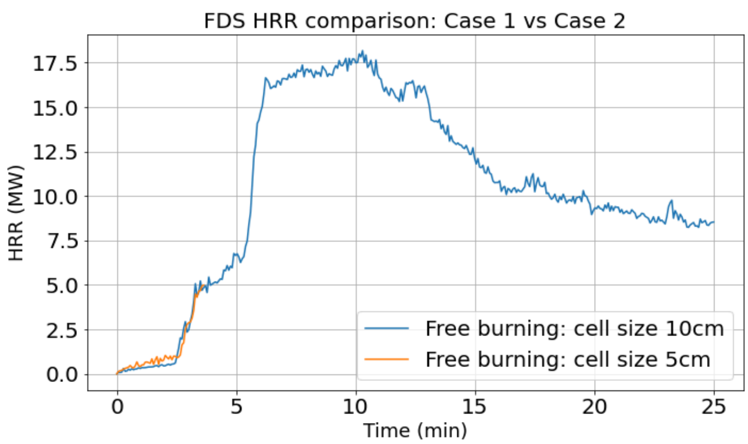

Figure 26: HRR of the complete model (three cars) cell size 5 cm and 10 cm

As shown in Figure 26, a cell size of 10 cm can be considered acceptable.

2.4) Conclusion of the FDS modelling approach

An FDS model of a battery electric vehicle fire in an **underground parking garage** with dimensions of **16 m × 9.5 m × 2.5 m** is developed and analysed using a combination of experimental data, sensitivity analyses, and parametric jet flame studies. The model consists of a **simplified three-dimensional green vehicle geometry** discretised on a **10 cm computational grid** and implemented in **Fire Dynamics Simulator (FDS) version 6.9.1**. Material properties are primarily derived from literature data for conventional vehicle structures reported by Heinisuo et al., while the battery fire behaviour and prescribed HRR are based on the experimental work of Kang et al.(2023).

The burning vehicle is positioned between **two identical neighbouring vehicles**, located at **a spacing of 0.6 m** on either side and represented in yellow and orange. The vehicles are placed inside an enclosed environment consisting of a **concrete wall** positioned **30 cm** in front of the cars, together with a concrete floor and **ceiling** with a **free height of 2.5 m**, representative of an underground parking configuration.

Several sensitivity analyses are performed to evaluate the influence of mesh resolution and jet flame parametrization. The results demonstrate that a **10 cm cell size** provides a **reasonable compromise between computational cost and numerical accuracy.** While finer meshes produce more detailed results, the overall HRR evolution, flame behaviour, and thermal exposure patterns remain sufficiently consistent for the engineering objectives of this study and reduces the risk of numerical errors.

The **jet flame** analysis, whereby the mass fraction is adjusted to maintain the same HRR with different velocity, temperature or area, shows that **flame behaviour is strongly influenced by momentum flux**, which is governed by the combined effect of jet velocity, density (influenced by temperature) and vent area. Velocity primarily controls flame reach and penetration distance, while vent area mainly affects flame diffusion and flame thickness and height. Temperature mainly influences buoyancy and thermal intensity. These simulations demonstrate that **similar HRR values can still produce substantially different jet flame structures and thermal exposure patterns**. This indicates that HRR alone is insufficient to fully characterise flame spread behaviour in BEV fires. Based on this analysis, the analysis of the HRR curve of Kang et al. (2023) and information given by Zhao et al. (2024) , 11 jet flames are chosen for the final model.

Due to **computational limitations** and the **limited scope of the study**, several **simplifications** are introduced in the numerical **model**:

1. The vehicle geometry was simplified and aligned to the 10 cm mesh resolution, limiting the representation of fine-scale details.
2. Openings and gaps are introduced around the battery pack to ensure numerical stability and to allow implementation of lateral jet flames.
3. Jet flames are represented using prescribed VENT boundary conditions with time-dependent ramp functions derived from experimental observations. Because

FDS is fundamentally a low-Mach-number solver, highly pressure-driven jet behaviour and compressibility effects could not be fully resolved, resulting in relatively more buoyancy-dominated flames and low density areas.

4. The thermal runaway behaviour of the lithium-ion battery pack is represented using prescribed HRR curves, meaning that suppression systems such as sprinklers could not directly influence the battery HRR itself, unless an E_COEFFICIENT is added (see 3.2.3.)
5. Propane is used as a surrogate fuel for all combustible components
6. Simplified pyrolysis models are used for the combustible materials
7. Temperature-controlled window failure mechanisms instead of temperature gradient devices are applied to reduce computational complexity.

Despite these simplifications, the developed model provides a stable and sufficiently representative engineering-scale approximation of BEV fire behaviour in underground parking structures. The simulations successfully captured the interaction between jet flames, thermal exposure, and fire spread towards neighbouring vehicles, thereby providing a suitable basis for the further analyses presented in this thesis.

Part 3: Sprinkler simulations

3.1) Sprinkler model implementation and Parameters in FDS

This section describes the implementation of the sprinkler system in Fire Dynamics Simulator (FDS) and the selection of the associated model parameters.[59] The objective is to define a consistent base-case sprinkler configuration that is used as a reference for all subsequent simulation scenarios unless explicitly stated otherwise. The chosen parameters are based on a combination of literature values, engineering standards (NFPA and EN 12845), and modelling assumptions required due to missing experimental data for electric vehicle fire scenarios.

3.1.1) Base Case sprinkler configuration

The sprinkler system is modelled in FDS as a combination of an activation mechanism and a Lagrangian droplet injection model. The activation is governed by a heat-sensitive link, while the hydraulic discharge and spray characteristics define the subsequent water application into the computational domain. According to the CEN standard NBN EN 12845, parking areas are classified as Ordinary Hazard (OH) occupancies, for which a maximum coverage area of 12 m² per sprinkler head is permitted. Consequently, the sprinklers are arranged in a staggered 3.5 m × 3.4 m grid, resulting in a coverage area of approximately 11.9 m² per sprinkler head. In addition, the sprinklers are positioned at least 1 m from the walls and installed 20 cm below the ceiling.

[59] Next chapter is based on the FDS Manuals: Release version: FDS 6.10.1

This results in a theoretical discharge density of:

$$Density\ (\frac{L/min}{m^2}) = \frac{Flow\ rate\ (L/min)}{Area\ per\ sprinkler(m^2)} \quad (9)$$

$$6.7\ \frac{L/min}{m^2} = \frac{80\ L/min}{11.9\ m^2}$$

Results from Scenario 1 (see Section 4.4) indicate that the sprinkler configuration in Columns B and D, particularly near the wall regions, provides insufficient water density (< 5 L/min). To achieve a more uniform water distribution and improve coverage in these critical areas, the sprinkler grid is modified to a 3-by-5 sprinkler row configuration (see Figure 27).

Because for the wall-mounted sprinklers, only 10 instead of 15 sprinklers are used, they need to cover more m². In the designed configuration, each sprinkler should cover 3.4m by 4.8m. This results in a theoretical discharge density of:

$$4.9\ \frac{L/min}{m^2} = \frac{80\ L/min * 10}{16.32\ m^2}$$

This is slightly below 5 L/min, but it is difficult for wall sprinklers to reach the middle of the parking. Raising the hypothesis that the flow density closer to the wall will be above 5 L/min and further away less than 5 L/min. Analysis of the results will control this hypothesis and will check if this flow rate is still sufficient.

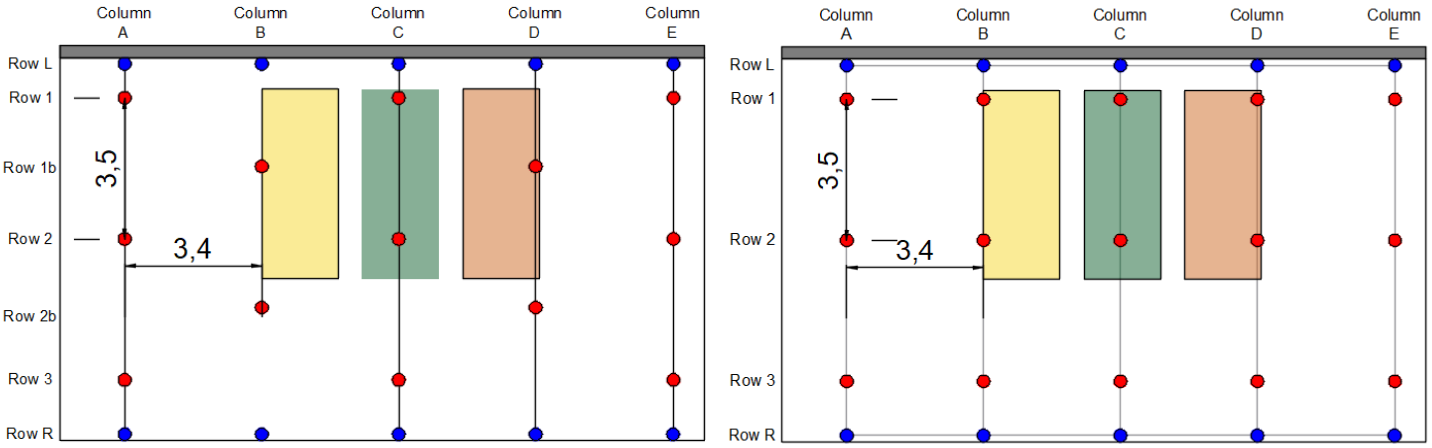

Figure 27: Staggered and non-staggered sprinkler configurations. Red: ceiling mounted sprinkler locations; Blue: Wall-mounted sprinkler locations.

The base case sprinkler configuration is defined using the following FDS input structure:

```
&SPEC ID='WATER VAPOR' /

&PART ID='waterdrops_FM',
    SPEC_ID='WATER VAPOR',
    DIAMETER=1000.0,
    SAMPLING_FACTOR=10 /

&PROP ID='FM_Global_QR_ESS',
    QUANTITY='SPRINKLER LINK TEMPERATURE',
```

```
RTI=100,
ACTIVATION_TEMPERATURE=68.0,
K_FACTOR=80.0,
PARTICLE_VELOCITY=10,
OPERATING_PRESSURE=1.0,
PART_ID='waterdrops_FM',
OFFSET=0.10,
SPRAY_ANGLE=30.0,90.0,
SMOKEVIEW_ID='sprinkler_pendent' /
```

3.1.1) Justification of the selected parameters

3.1.1.1) Activation Model Parameters

The sprinkler activation is based on a thermal response model representing the heating of a sprinkler link exposed to hot gases.

- **RTI (Response Time Index): Default & model value: 100 $(m\cdot s)^{1/2}$**
  The RTI defines the thermal sensitivity of the sprinkler link and governs the rate at which its temperature responds to surrounding gas temperatures. Fundamentally, it represents the balance between convective heat transfer and the thermal inertia of the link. A value of 100 is representative of standard-response sprinklers commonly used in building applications.

Category	RTI (meters-second)$^{1/2}$ [(ft-sec)$^{1/2}$]
Fast Response	50 or less (90 or less)
Standard Response	80 or more (145 or more)

Figure 28: RTI table of the NFPA[60]

- **C_FACTOR: Default & model value: 0 $(m\cdot s)^{1/2}$**
  This parameter accounts for heat losses from the sprinkler link to its mounting structure. This parameter is neglected to reduce model complexity and due to the absence of detailed mounting geometry.

- **ACTIVATION_TEMPERATURE: Default 74°C; model value: 68 °C**

  This parameter is defined in the numerical model to trigger sprinkler activation based on the link temperature. In practice, activation is mainly governed by the RTI value and the surrounding gas temperature development, while the activation temperature acts as a threshold condition.

  In parking garages, ambient temperatures typically range between 20–35 °C. To avoid premature activation under non-fire conditions, the activation temperature must

[60] *Basics of Sprinkler Thermal Characteristics | NFPA*. (2021, June 22). https://www.nfpa.org/news-blogs-and-articles/blogs/2021/06/22/the-basics-of-sprinkler-thermal-characteristics

be at least 30°C above ambient levels.[61] Therefore, an activation temperature of 68 °C is selected as the base case.

Max Ceiling Temperature °F (°C)	Temperature Rating °F (°C)	Temperature Classification	Glass Bulb Colors
100 (38)	135-170 (57-77)	Ordinary	Orange or Red
150 (66)	175-225 (79-107)	Intermediate	Yellow or Green

Figure 29: Sprinkler activation temperature rating according to NFPA

3.1.1.2) Hydraulic and Discharge Parameters

The water discharge is defined using either a direct flow rate or a pressure–orifice relationship:

- **K-factor: Default: 1.0 L/(min·bar½); model value: 80 L/(min·bar$^{1/2}$)**
  This value defines the relationship between flow rate and operating pressure according to:

$$q = K \times \sqrt{p} \qquad (10)$$

  It represents an average sprinkler discharge characteristic used in fire protection systems.

Page 10
EN 12259-1:1999 + A1:2001

Table 4 — K-factors

Nominal diameter of orifice mm	K-factor $l \cdot min^{-1} \cdot bar^{-1/2}$	
	Sprinklers other than dry types	Dry sprinklers
10 15 20	57 ± 3 80 ± 4 115 ± 6	57 ± 5 80 ± 6 115 ± 9

Figure 30: Table with K-factors according to EN 12259-1, Belgium norm

- **OPERATING_PRESSURE: Default & model value: 1.0 bar**
  Define the gauge pressure at the sprinkler. In addition to the flow rate, the operating pressure influences the initial droplet velocity and the median droplet diameter of the size distribution; The selected pressure corresponds to the lower end of the design pressure range commonly referenced in National Fire Protection Association NFPA standards. According to NFPA standards, the absolute minimum pressure at a sprinkler head is **0.5 bar**. Maximum operating pressures typically range between **7 and 12 bar**, while pressures exceeding **12 bar** are generally reserved for specialized

[61] Linton, M. (2026, February 8). *Sprinkler Temperature Ratings Explained. Choosing the Right Rating for the Right Environment — Fortis fire*. Fortis Fire. https://www.fortisfire.co.nz/insights/sprinkler-temperature-ratings

systems such as water mist installations.[62] The minimum water pressure for tap water in Belgium at the meter is 1.5 bar.[63] A pressure of 1.0 bar ensures a conservative but realistic lower-bound water discharge scenario.

- **FLOW_RATE: Default: 1 L/min; model value: 80 L/min**

According to National Fire Protection Association NFPA 13, parking garages are typically classified as Ordinary Hazard (OH1, recently, OH2 is suggested[64]) occupancies. Recent updates reflect increased fire severity from modern and electric vehicles, leading to higher expected design demands compared to conventional passenger car fires, with discharge rates of approximately 50–200 L/min for standard sprinkler heads, with higher values up to 300–400 L/min in high-demand or large-orifice configurations

Similarly, European Committee for Standardization EN 12845 bases sprinkler design on discharge density over a defined design area, rather than fixed per-sprinkler flows. Typical sprinkler coverage areas range from approximately 9 m² to 21 m² depending on the hazard classification and sprinkler arrangement.

The selected value of **80 L/min** therefore represents a value on the lower end (but not the minimum) of the design values for an EV parking fire scenario. This results in a theoretically Discharge density of 6.67 L/min/m².

Table 5 — Water distribution parameters

Column 1	Column 2	Column 3	Column 4	Column 5	Column 6
Nominal diameter of orifice mm	Flow rate per sprinkler l/min	Measurement area m^2	Sprinkler spacing m	Water coverage mm/min	Maximum number of containers with a lower content of water
10	50,6	20,25	4,5	2,5	8
15	61,3	12,25	3,5	5,0	5
15	135,0	9,00	3,0	15,0	4
20	90,0	9,00	3,0	10,0	4
20	187,5	6,25	2,5	30,0	3

Figure 31: Water distribution parameters according to EN 12259-1, Belgium norm

- **PARTICLE_VELOCITY: Default: 0 m/s; model value: 10 m/s**

[62] *Water mist Systems Overview | NFPA*. (2022, June 24). https://www.nfpa.org/news-blogs-and-articles/blogs/2022/06/24/water-mist-systems-overview
[63] *Druk in de woning altijd voldoende | De Watergroep*. (n.d.). De Watergroep. https://www.dewatergroep.be/nl-be/drinkwater/veelgestelde-vragen/binneninstallatie/is-de-druk-in-mijn-woning-altijd-voldoende
[64] *Parking garages and EVs*. (2024, July 12). https://www.nfpa.org/news-blogs-and-articles/blogs/2024/07/12/parking-garages-and-evs

The initial droplet velocity is assumed based on typical sprinkler discharge conditions in literature,[65] [66] in the absence of system-specific nozzle data.

- **OFFSET: Default: 0.05m; model value: 0.10 m**
  The offset defines the initial droplet release region, representing complete atomization within a spherical volume around the sprinkler head. This study adopts a value of 0.10 m to better represent the physical breakup process of the water jet into a fully developed spray.

3.1.1.3) Spray Parameters

- **SPRAY_PATTERN_SHAPE: Default & model value: Gaussian**
  Defines the general distribution shape of the spray. The Gaussian distribution is retained as the baseline assumption for droplet spatial distribution due to lack of detailed manufacturer spray data.
- **SPRAY_ANGLE: Default: 60° / 75°; model value: 30° / 90°**
  Specifies the angular extent of the spray cone or elliptical pattern. By default, the spray is conical. A dual-angle specification is used to represent an asymmetric conical spray distribution, improving realism compared to a purely axisymmetric cone. The 30°/90° specification replaces a generic default with a wider, head-specific distribution (30° to horizontal) that better represents the physical throw and provides a more stable, realistic interaction with the 10 cm grid used in the simulation.

3.1.1.4) Droplet Parameters

- **DIAMETER: Default: none; model value: 1000 µm**
  The median volumetric diameter (Dv,0.5) of droplets. This parameter determines the representative droplet size. Typical spray droplets have a size of approximately 1000 to 3000 µm, while droplets of approximately 100-10 µm are considered water mist.[67] The range in between is subject to interpretation. Since this study focuses on sprinklers, a minimum diameter of 1000 µm is maintained.

- **GAMMA_D: Default & model value: 2.4**
  Since real sprinklers produce droplets of varying sizes, FDS applies statistical distributions. This specific parameter controls the spread of the Rosin–Rammler distribution. Due to the lack of available data and to maintain model simplicity, the default setting is adopted.

- **SIGMA_D: Default & model value: 0.48**
  Defines the width of the log-normal distribution. The default setting is automatically calculated from:

[65] Heinisuo, M., Partanen, M., Tampereen teknillinen yliopisto. Rakennustekniikan laitos. Rakennetekniikka, & Tampere University of Technology. Department of Civil Engineering. Structural Engineering. (2013). Modeling of Car Fires with Sprinklers. In Tampere University of Technology. Department of Civil Engineering (Research Report No. 161; p. 1).
[66] Sheppard, D. T., & Lueptow, R. M. (2005). *Characterization of fire sprinkler sprays using particle image velocimetry*. **Atomization and Sprays, 15**(3), 341–362. https://doi.org/10.1615/atomizspr.v15.i3.50
[67] *Water mist Systems Overview | NFPA*. (2022, June 24). https://www.nfpa.org/news-blogs-and-articles/blogs/2022/06/24/water-mist-systems-overview

$$\sigma=1.15/\gamma \qquad (11)$$

- **SURFACE_DIAMETER: Default & model value: DIAMETER value**
  Defines the diameter (μm) of droplets that form when liquid detaches from a surface after forming a film. Due to the lack of available data and to maintain model simplicity, the default setting is adopted.

3.1.1.5) Orientation Parameter

- **ORIENTATION (x, y, z): Default & model value: (0, 0, −1), i.e. downward**
  Defines the direction in which the sprinkler discharges water.

3.1.1.6) Numerical Particle Injection

- **PARTICLES_PER_SECOND: Default & model value: 5000**
  This parameter defines the number of computational droplets injected per second per active sprinkler. It does not influence total mass flow but controls the resolution of the Lagrangian spray field and evaporation modelling accuracy. Due to the lack of available data and to maintain model simplicity, the default setting is adopted.

3.1.7) Duct Work Parameters

Since the focus of this thesis is not on achieving a fully accurate sprinkler system design, ductwork-related parameters will not be modeled. Only the OPERATING_PRESSURE is considered, specifically in relation to the FLOW_RATE (See 3.1.1.2.)

3.2) Suppression in FDS

FDS simulates sprinkler interaction through a dynamic exchange of mass, momentum, and energy between Lagrangian particles (representing droplets) and the Eulerian grid (representing the fire gas cells and solid surfaces).

3.2.1) Gas cooling

The cooling of the gas phase is governed by two main thermodynamic processes:

- **Convective Heat Transfer:** Energy is exchanged directly between the droplet surface and the gas. This is driven by the temperature difference ($T_p - T_g$) and a heat transfer coefficient (h_g).
- **Evaporative Cooling:** As droplets evaporate, they extract the latent heat of vaporization from the gas. The rate of evaporation ($\dot{m}_p$) is calculated using a mass transfer coefficient (h_m) and the difference between the vapor concentration between the droplet surface and the bulk gas.

Because FDS utilizes a low Mach number approximation, this energy exchange is not solved for explicitly but is instead implemented via a velocity divergence proxy ($\nabla \cdot u$); heat loss to droplets causes a negative divergence, which the solver interprets as a physical contraction or compression of the fluid element. Additionally, droplets provide radiative cooling by absorbing and scattering thermal radiation emitted by the fire, using properties derived from Mie theory. To maintain numerical stability and avoid non-physical temperature drops, the simulation must use an adequate number of PARTICLES_PER_SECOND to ensure the liquid mass is distributed uniformly.

3.2.2) Surface Cooling

In FDS, surface cooling occurs primarily through the interaction between a liquid film, formed when droplets hit a surface, and the solid-phase heat conduction model. When droplets strike a solid obstacle, they transform from airborne Lagrangian particles into a thin liquid film that extracts energy from the material. FDS calculates the film thickness (δ) by summing the volume of all droplets attached to a specific wall cell area. This heat transfer is governed by a heat transfer coefficient h_s, which can be user-defined or calculated from empirical turbulent correlations. FDS updates the surface temperature (T_s) by solving a 1D (or optional 3D) heat conduction model that accounts for energy loss to the liquid film. The film is also assumed opaque to thermal radiation, providing additional cooling by shielding the surface from incident radiant flux.

For combustible materials in the model, an *extinguishment temperature* is defined. When the surface temperature drops below this threshold due to cooling, the material ceases to produce HRRPUA, effectively representing local flame extinction. In this implementation, the extinguishment temperature is defined as 50°C lower than the ignition temperature, introducing a hysteresis between ignition and extinction behavior to improve numerical stability and avoid oscillatory re-ignition.

3.2.3) Fire Source Cooling

For materials defined with a prescribed HRRPUA, FDS models fire suppression using an empirical exponential approach. Because a HRRPUA fire behaves like a gas burner with a fixed heat release rate, it does not automatically respond to water cooling unless the E_COEFFICIENT suppression parameter is applied. This coefficient allows the user to reduce the local fuel mass loss rate based on the accumulated water mass per unit area $m_w''(t)$ on each fuel surface cell.

The local fuel mass loss rate ($\dot{m}_f''$) is reduced exponentially according to the water reaching the surface:

$$\dot{m}'''_f(t) = \dot{m}'''_{f,0}(t) e^{-\int k(t) dt} \qquad (12)$$

where $\dot{m}'''_{f,0}(t)$ is the user-specified burning rate without water, and the suppression factor k(t) is defined as:

$$k(t) = \text{E\_COEFFICIENT} \times m_w''(t) \qquad (13)$$

- $m_w''(t)$: is the local water mass per unit area (kg/m²) on the surface cell at time ttt
- E_COEFFICIENT: is the user-defined empirical constant (m²/(kg·s))

●

Here, the suppression factor k(t) is an empirical parameter representing the rate of local fire suppression, which directly depends on the accumulated water mass per unit surface area $m_{w''}(t)$.

Key Characteristics:

1. Empirical nature: The E_COEFFICIENT must be determined experimentally for each material and geometry.
2. Local calculation: Suppression is computed per surface cell, capturing spatial variations in water application, e.g., when one side of a burning object is wetted while the other remains dry.

Each material with a predefined HRRPUA is assigned an E_COEFFICIENT. As empirical values for these coefficients are rarely available, values of similar materials from the source: "Suppression of Rack-Storage Fires by Water." by Yu, Lee, en Kung (1994), the suggested source by the FDS Technical Reference Guide, were adopted. The base-case scenario (see Section 3.3.3) is simulated both with and without the application of E_COEFFICIENTS.
The following values are used:

- Standard Plastic Commodities: E_COEFFICIENT = 0.72, used for
  - FABRIC_LINING
  - FOAM_FILLING
  - POLYPROPYLENE_PLASTIC
  - ELECTRONIC_PLASTIC
- Class II Commodities: E_COEFFICIENT = 0.54, used for:
  - KUMI_CC (rubber tires)
- Batteries: Due to the limited suppression effectiveness, only a very low value of 0.1 is assigned.
  - BATTERY_MATERIAL_SIMPLE
  - BATTERY_FIRE

To maintain a conservative and straightforward modelling approach, all E_COEFFICIENT values are kept below 1.0. As a result, complete suppression of the EV fire is not achieved through the suppression model alone, unless the EXTINCTION_TEMPERATURE criterion is reached (see Section 3.2.2).

3.3) Simulation scenarios and case matrix

This section defines the simulation scenarios used to evaluate sprinkler performance in electric vehicle fire conditions. Seven cases are considered, ranging from a free-burning reference fire to multiple sprinkler configurations based on literature, standards, and sensitivity variations.

The scenarios systematically investigate the influence of key parameters such as activation temperature, hydraulic conditions, sprinkler placement, and discharge intensity. All cases use the same computational domain and fire source definition unless otherwise stated.

3.3.1) Overview of the simulation scenarios

The following scenarios are considered in this study:

- **Scenario Jet flames:** Single car + jet flames (constant HRR) + 2 sprinklers
- **Scenario 0:** Free-burning reference case (no suppression)
- **Scenario 1:** Realistic base-case sprinkler configuration
- **Scenario 2:** Literature-based sprinkler configuration (Heinisuo et al.)
- **Scenario 3:** BESS-based sprinkler configuration (adapted from energy storage systems)
- **Scenario 4:** Reduced activation temperature scenario
- **Scenario 5:** Wall-mounted sprinklers (height 2.3 m)
- **Scenario 6:** Wall-mounted sprinklers (height 1.5 m)
- **Scenario 7:** Increased flow rate case

Scenario 1 is used as the primary reference sprinkler configuration with the parameter settings discussed in 3.2. All other sprinkler cases are defined as deviations from this base case or literature based.

3.3.2) Scenario Jet Flames: Single car + jet flames + two sprinklers

This scenario considers a single vehicle exposed to prescribed jet flames, characteristic behaviour of electric vehicle fire development. The setup is based on Scenario 2.2, with two sprinklers added on the ceiling positioned 1 m from the vehicle. The flow rate is 56.5 L/min for each sprinkler, a high value to ensure influence on the jet flames. The activation temperature is set to 16°C to react immediately. The objective is to evaluate whether sprinkler discharge can directly interact with and suppress jet-flame-dominated fire behaviour under controlled conditions, independent of environmental influences. This idealised configuration isolates the interaction between water application and flame structure, and results are compared with the corresponding case without sprinklers to assess suppression effectiveness. The scenario will be conducted with and without E_COEFFICIENT.

3.3.3) Scenario 0: Free Burning Reference Case A &B

The free-burning Scenario 0A represents a fire without any active suppression system. This case is used as the baseline reference for evaluating the effectiveness of sprinkler interventions.

No sprinklers are included. The results of this scenario provide the baseline evolution of fire growth, heat release rate, and thermal conditions within the computational domain. This scenario is also simulated with a big jet flame before flash over, using “Jet 10,” with a PHRR of approximately 1.4 MW, applied starting at 160 s and lasting for 30 s. This scenario with the big jet flame is called Scenario 0B. The timing and duration are based on observations by Cui et al. (2022), who reported a jet flame of significant size and duration occurring at a similar stage of fire development. This 'Scenario 0B' setup is used to assess the contribution of a strong jet flame to flame spread during the early phase of the fire.

3.3.4) Scenario 1: Realistic Base Case Configuration A, B &

Scenario 1A defines the primary reference sprinkler configuration used for all comparative evaluations. It is intended to represent a realistic parking garage sprinkler system operating under standard design conditions. This scenario 1B will be conducted without E_COEFFICIENTs, while Scenario 1C will be conducted with a lower SETPOINT temperature for the windows of only 200°C.

3.3.5) Scenario 2: Literature-Based Benchmark (Heinisuo et al.)

This scenario is based on the study *"Modeling of Car Fires with Sprinklers"* by Heinisuo et al., and is used as a validation-oriented benchmark configuration. The geometry corresponds to an open parking environment of 8 × 16 m², consistent with the model domain used in this study.

Parameters of scenario 2			
Parameter	**Value**	**Parameter**	**Value**
Flow rate	45 L/min	**K-factor**	76.1 L/min·bar$^{1/2}$
Discharge density	5 L/min/m²	**Droplet velocity**	10 m/s
Coverage area	9 m² (3 m × 3 m)	**RTI**	150 (m·s)$^{1/2}$
Number of sprinklers	9	**Droplet diameter**	1000 µm
Activation temperature	68 °C	**Spray angle**	0–88°
Operating pressure	0.35 bar		

Table 2: Parameters of scenario 2

3.3.6) Scenario 3: BESS-Based Configuration

This scenario is adapted from research on sprinkler protection for lithium-ion Battery Energy Storage Systems (BESS).[68] Although the original study focuses on stationary energy storage units, the thermal behaviour of lithium-ion battery packs is considered sufficiently representative of electric vehicle fire conditions for comparative purposes.

[68] Ditch, B., FM Global, Zeng, D., & FM Global. (2019). *Development of sprinkler protection guidance for lithium ion based energy storage systems*. FM Global. https://www.researchgate.net/publication/333653116

The study highlights that ceiling-mounted sprinklers can limit fire spread but may not fully suppress fires within geometrically shielded configurations due to obstruction effects.

Parameters of scenario 3			
Parameter	**Value**	**Parameter**	**Value**
Flow rate	118.8 L/min	**K-factor**	84 L/min·bar$^{1/2}$
Discharge density	10 L/min/m²	**Droplet velocity**	10 m/s (assumed)
Coverage area	11.9 m² (3.5 m × 3.4 m)	**RTI**	27.6 (m·s)$^{1/2}$
Number of sprinklers	13 (original 1, central)	**Droplet diameter**	1000 µm (assumed)
Activation temperature	74 °C	**Spray angle**	30-90° (assumed)
Operating pressure	2.0 bar		

Table 3: Parameters of scenario 3

The configuration represents a high-intensity suppression scenario with reduced response time (faster activation) and increased discharge capacity compared to the base case.

3.3.7) Scenario 4: Reduced Activation Temperature

This scenario investigates the influence of earlier sprinkler activation on fire suppression performance. The activation temperature is reduced to 57 °C, representing a lower-bound practical value for fast-response sprinkler heads used in parking structures.

All other parameters are identical to Scenario 1.

3.3.8) Scenario 5: Wall-Mounted Sprinklers A & B & C

Located on the opposite side of the domain and aligned along the same axis as the ceiling-mounted sprinklers at a height of 2.3 m, this configuration changes the direction from which the sprinklers interact with the fire. As a result, cooling effectiveness in the near-field region of the fire plume may be enhanced. All other parameters of Scenario 5A remain identical to those used in Scenario 1A, but the amount of sprinklers is only 10. (See 3.1.1.)

Because sidewall sprinklers must also overcome the effects of gravity in the horizontal direction, it is not entirely appropriate to directly apply the same settings used for ceiling sprinklers. Therefore, Scenarios 5B and 5C were introduced.

First, the spray angle was adjusted to 0°–45° for Scenario 5B and to 10°–70° for Scenario 5C. Unlike ceiling sprinklers, sidewall sprinklers do not need to wet the ceiling surface, while

gravity naturally provides downward movement near the sprinkler head. In addition, the PARTICLE_VELOCITY was set to 15 m/s, which is the maximum value achievable without resorting to ad hoc parameter tuning.[69] Although this value is relatively high, it is necessary to ensure sufficient spray reach across the full rack length. In reality, however, achieving higher velocities would typically require an increase in driving pressure, but to keep the adjustments of the scenario simple, this is ignored. Finally, the DROPLET_DIAMETER was increased to 2000 μm for Scenario 5B and to 1500 μm for Scenario 5C. Both values remain within the range of realistic droplet diameters for sprinkler systems.
These modifications are intended to enhance the horizontal momentum of the droplets, enabling them to better overcome the effects of gravity.

3.3.9) Scenario 6: Low-Height Wall-Mounted Sprinkler Configuration with Heat-Triggered Ceiling Activation

This scenario is a theoretical experiment. It uses the same wall-mounted sprinkler configuration as Scenario 5C, but with the discharge height set to z = 1.5 m. The objective is to assess the sensitivity of suppression performance to the lateral placement of the water discharge source.

Since sprinklers installed at such a low height would typically respond relatively late, heat detectors are placed at the same locations as the ceiling-mounted sprinklers. When a heat detector on the same row as a wall-mounted sprinkler registers a temperature above 68°C, the corresponding sprinklers are activated after a certain time lag.

3.3.10) Scenario 7: Increased Flow Rate Sensitivity Case A - H

This scenario investigates the effect of increased water supply on suppression efficiency. The flow rate is doubled in Scenario 7A by elevating the pressure relative to Scenario 1 and the K factor is lowered to 10 in steps of 10 to create a theoretical flow density between 6.7L/min and 0.833 L/min, to find out the minimal flow rate needed. All other parameters remain unchanged.

This case is used to evaluate whether suppression performance is primarily limited by water availability or by geometric and thermal interaction effects.

3.4) Note on Scenario Consistency

All simulations use identical computational settings, fire source and jet flame definitions (unless stated otherwise), and mesh configurations. This ensures that observed differences between scenarios are attributable solely to variations in sprinkler parameters or placement.

[69] Sheppard, D. T., & Lueptow, R. M. (2005). *Characterization of fire sprinkler sprays using particle image velocimetry*. **Atomization and Sprays, 15**(3), 341–362. https://doi.org/10.1615/atomizspr.v15.i3.50

Part 4: Results

4.1 Monitored Parameters and Output Quantities

To evaluate the fire development and suppression performance in the simulated scenarios, several measurement devices and slice outputs were implemented in the FDS model. These measurements provide information on fire growth, heat transfer, sprinkler response, and fire spread between vehicles. While not every measurement will be discussed in detail, the most relevant parameters are analysed and compared across the different scenarios.

4.1.1) Heat Release Rate (HRR)

The fire development is primarily evaluated using the HRR obtained from the FDS simulation output. HRR is used to assess the intensity and growth of the vehicle fire and to compare the effectiveness of suppression measures between scenarios.

4.1.2) Temperature Trees

Five thermocouple trees, each consisting of sensors positioned at heights of 0.5 m, 1.0 m, 1.5 m, and 2.0 m, are used to monitor gas temperatures and evaluate fire spread between vehicles:

- T1: Centre of the green vehicle
- T2: 0.6 m from the green vehicle towards the orange vehicle
- T3: 0.6 m from the green vehicle towards the yellow vehicle
- T4: Centre of the orange vehicle
- T5: Centre of the yellow vehicle

TC_RW at height 1.3 m is also used to compare the temperature inside the car, just behind the driver's front window. Eight additional temperature devices are placed above the car at height z = 2.3m to measure the ceiling temperature above the green car.

These measurements provide insight into the thermal conditions around the vehicles and the progression of fire spread.

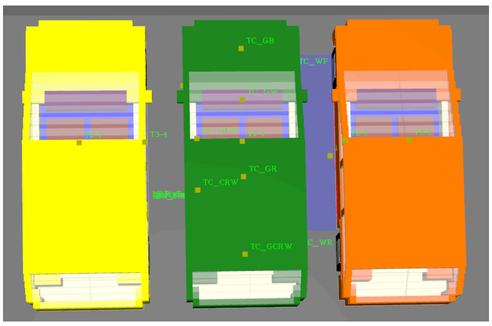

Figure: Locations of the thermocouples

4.1.3) Surface Temperature and Heat Flux

Incident heat fluxes and surface temperature measurements are recorded at the exposed sides doors of the neighbouring vehicles. A boundary file for the radiative and net heat flux are added. These measurements are used to evaluate thermal exposure and the potential for fire spread due to radiative and convective heat transfer. The threshold is set at 25 kW/m², which is identified as the exposure threshold for ignition of nearby vehicles in *Research Insights: Fire Safety for Electric Vehicles and Other Modern Vehicles in Parking Structures* by V.H. Lutz. Additionally, the threshold for thermal radiation exposure to combustible materials is 12.5 kW/m² according to EN standards.[70] Both values will be used as thresholds for flame spread.

4.1.4) Sprinkler Activation

Sprinkler activation times are analysed using activation state outputs and control log measurements. These data are used to assess the responsiveness of the sprinkler system in relation to fire growth and temperature development.

4.1.5) Water Mass Distribution

Water mass flow rate and distribution measurements are used to evaluate the effectiveness and coverage of the sprinkler system. A slice device is put at height 1.6 m and 0.5 m. The analysis focuses on how efficiently water reaches the fire area, adjacent vehicles and covers the whole surface of the parking.

4.1.6) Secondary Measurements

Additional performance indicators, including fire suppression effectiveness, fire spread behaviour, and EV fire containment, are derived from the previously described measurements. These secondary parameters are used to evaluate the overall performance of each simulated scenario. The sprinkler efficiency is explicitly defined as the relative reduction in Heat Release Rate (HRR) relative to the unsuppressed free-burning reference scenario (S_0).

4.2) Scenario Jet flames

There is little to no difference in the HRR between the jet flame scenarios with and without sprinklers, as shown in figure 32. This is because the fire is defined as a prescribed burner and with a lower E_COEFFICIENT, the water spray does not reduce the fuel supply. However, the HRR for the fourth jet flame appears slightly elevated in the sprinklered scenario. This indicates that the water droplets disrupt the high-velocity jet, reducing its momentum and ensuring that more fuel reacts within the computational domain rather than being projected beyond the mesh boundaries before burning.

[70] *Parking garages and EVs*. (2024b, July 12). https://www.nfpa.org/news-blogs-and-articles/blogs/2024/07/12/parking-garages-and-evs

Furthermore, temperature device T2_1 (located 60 cm from the source at 0.5 m height) recorded higher temperatures when sprinklers were active (see figure 33) . This is likely due to the jet being 'broken' by the spray, which causes the thermal energy to remain more concentrated near the source openings. At a distance of 120 cm, temperatures are systematically higher (see figure 33) due the same reason, but the average flame temperatures are generally lower due to the cooling effects of the water (see figure 34). Thus, the elevated temperature areas are more spread. The retention of energy closer to the origin limits the effectiveness of the sprinklers in this specific configuration. This phenomenon may be compounded by radiative scattering, as water droplets can redistribute thermal radiation toward lateral sensors. Additionally, the spray can induce air entrainment, pulling oxygen into the combustion zone and potentially intensifying local heat. Finally, these interactions are highly sensitive to grid resolution; a coarse mesh may over-predict the numerical spread of energy once the jet's momentum is disrupted. The final result is that the suppression factor is only maximum 13.4 % and -0.7% on average (see figure 34).

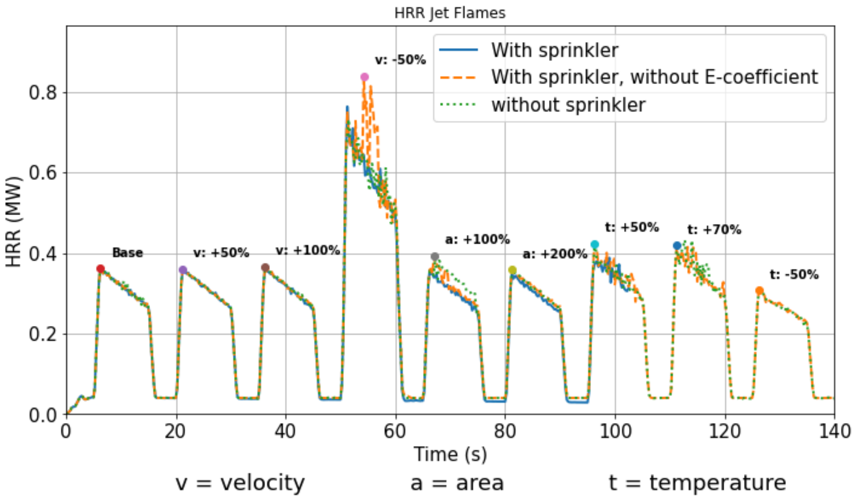

Figure 32: HRR of the jet flames with and without sprinklers

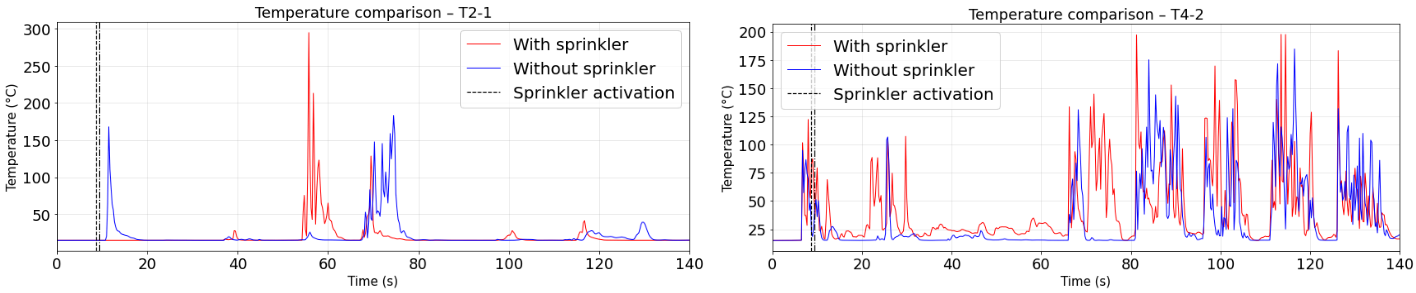

Figure 33: Right Temperature of T2_1; Left Temperature of T4_2

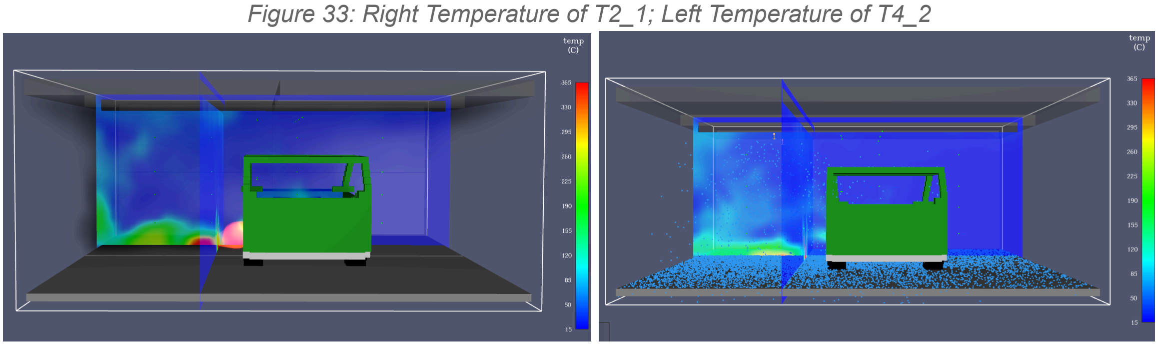

Figure 34: Left: Jet flame without sprinkles; Right: jet flame with sprinklers at time 86 sec (same temp.scale)

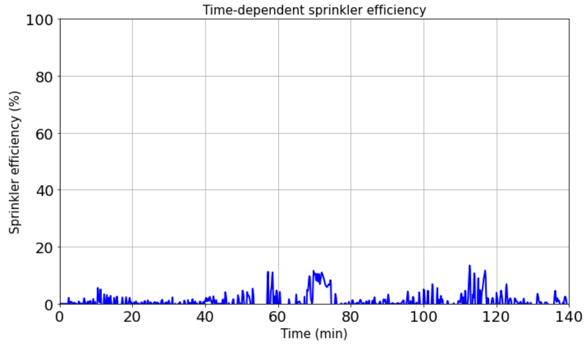

Figure 35: Cumulative HRR

4.3) Scenario 0: Free Burning Reference Case A & B

The fuel supply for the primary burning vehicle is governed by a prescribed multi-phase HRR curve derived from experimental baseline data (representing the combined LIB pack and vehicle body). However, as fire spread occurs to adjacent vehicles, the total fuel release rate is no longer constrained by this single prescribed curve. Instead, local fuel mass loss rates on neighboring car surfaces are dynamically activated once surface cell temperatures exceed their respective ignition thresholds, resulting in the rapid escalation of the overall HRR observed in Scenario 0A

Running the three-vehicle Scenario 0A shows a clear deviation from the expected heat release rate (HRR) based on the experimental data and the single-vehicle free-burning test. After approximately 3 minutes, the HRR increases exponentially as adjacent vehicles ignite (see Figure 36). The peak HRR exceeds 18 MW, which is roughly three times the peak HRR of a single vehicle, indicating that all three vehicles are burning at nearly full intensity simultaneously. This suggests that a vehicle ignites more rapidly when an adjacent vehicle is already fully involved in fire. If more vehicles were included, a chain reaction of fire spread would likely occur, leading to rapid and potentially uncontrollable fire propagation across multiple cars, as has also been observed in several real parking garage fire incidents reported in the media.[71] [72]

The first visible flames in the neighbouring yellow vehicle in smokeview appear at 237 s, followed by ignition of the orange vehicle at 271 s. A more precise comparison can be made using the activation of the window devices, which represent window failure and breakage. The first side window of the yellow vehicle activates at 216 s (Middle_window_passenger_2_2), while the corresponding window in the orange vehicle activates at 253 s (Middle_window_driver_Upper_3). In both cases, the seat located behind the window ignites approximately 20 seconds later.

---

[71] *Fire destroys 200 cars in Swedish car park – European Fire Sprinkler Network*. (n.d.). https://www.eurosprinkler.org/fire-destroys-200-cars-in-swedish-car-park/
[72] Electric vehicle fires on ships & ferries. (2025b, January 28). *EV Fire Safe*. https://www.evfiresafe.com/post/electric-vehicle-fires-on-ships-ferries

Since both ignition locations are positioned at the middle side windows - areas that are not directly exposed to intense jet flames - and the time difference is limited, the results suggest that jet flames in FDS are not the primary mechanism driving fire spread between vehicles. However, prior to flashover of the neighbouring vehicles, the selected jet flames exhibit a heat release rate of approximately 0.1 MW. To further assess their influence, Scenario 0B is simulated, with a larger jet flame case ("Jet 10") with a heat release rate of approximately 1.4 MW was simulated for 30 seconds starting at 160 s, based on observations by Cui et al. (2022), who reported a significant jet flame of comparable magnitude and duration at similar times.

In this Scenario 0B, the same window devices activate at 232 s and 273 s, which is approximately 20 s later than in the baseline case. The first visible flames in the neighbouring vehicles again appear about 20 s later. It can therefore be concluded that a large early-stage jet flame is not the dominant mechanism for flame spread between vehicles, as the jet flame primarily heats the lower sections of the adjacent vehicle, where combustible materials are protected by non-combustible components. More critical is the moment when the windows of the neighbouring vehicle fail, allowing external flames to make direct contact with interior combustible materials. When the overall HRR is considered, there is also no significant difference between the cases.

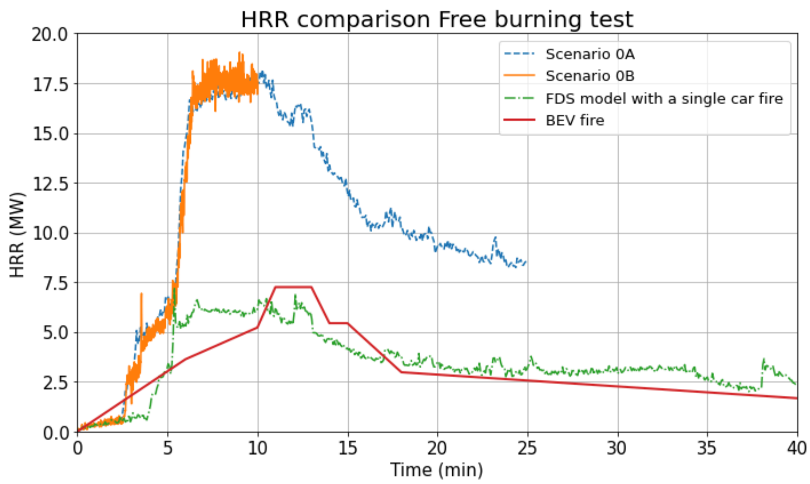

Figure 36: HRR scenario 0 (three cars & single car) and experimental data (single car)

4.4) Scenario 1: Realistic Base Case Configuration A & B

4.4.1) Water coverage

Before analysing the results of the scenarios with sprinklers, the discharge density is verified using the waterdrops_FM PARTICLE FLUX Z parameter (kg/s/m²) at a height of 1.6 m. (see figure 37, Right) From this value, the corresponding discharge rate in L/min/m² can be determined using the following conversion:

$$1 \text{ L} \approx 1 \text{ kg} \qquad (17)$$

Therefore

$$5\ L/min/m^2 = 5\ kg/min/m^2$$

Converting this to kg/s/m² results in:

$$5/60 = 0.833\ kg/s/m^2$$

Smokeview visualizations revealed that the rows containing only two sprinklers resulted in dry areas near the wall. To improve the water coverage, the sprinkler layout was modified to a uniform 5 × 3 sprinkler grid without staggering (see Section 3.1, Figure 27, Right). The updated configuration satisfies the required discharge density criterion of > 5 L/min/m² on average per m² (see Figure 37, Left).

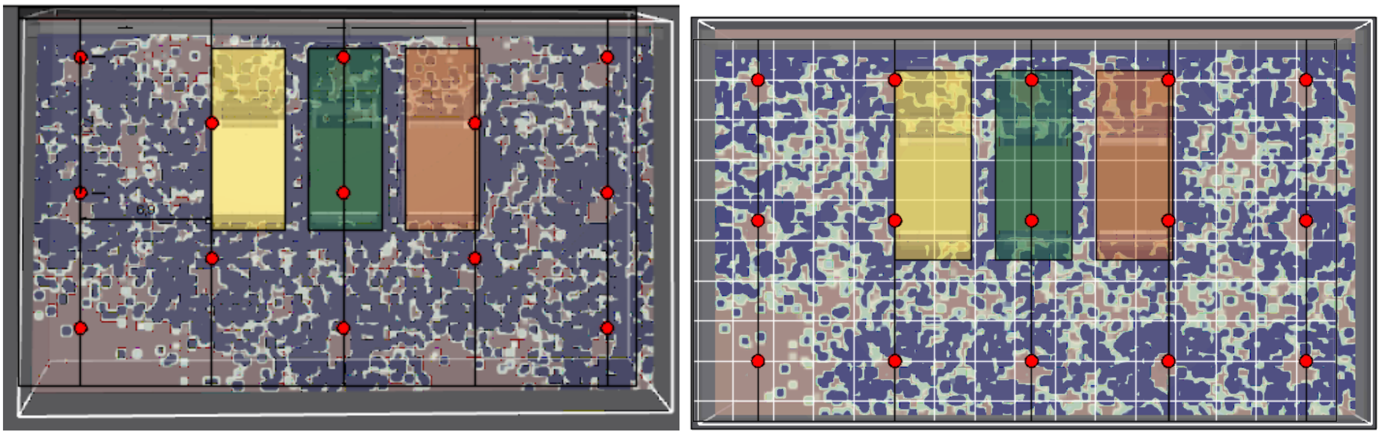

Figure 37: Locations of the sprinklers compared to sufficient water density (darker areas). Left: staggered configuration; Right: new configuration

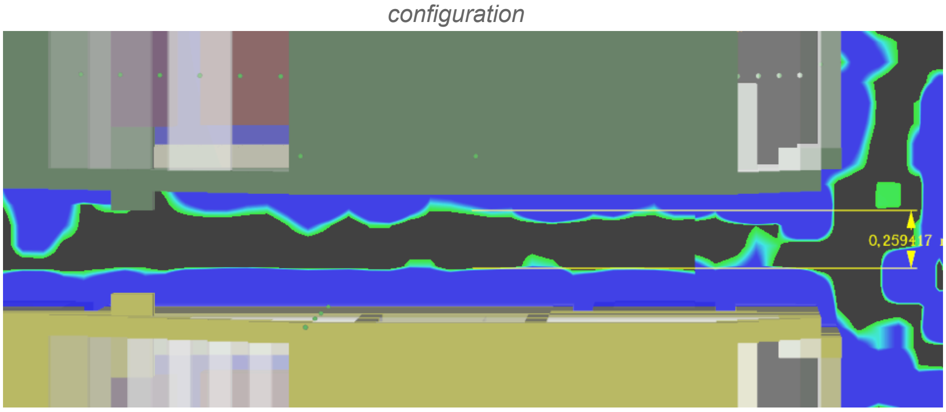

Figure 38: Water coverage between two cars

Additionally, it is immediately noticeable that the water from the sprinklers tends to coalesce, leaving a gap of approximately 25 cm that is not effectively covered by water (see Figure 38). This may reduce the effectiveness of jet flame suppression in that region. On the other hand, it provides a better thermal shielding effect by forming a continuous water film on the windows. Finally, Sprinkler A3 never activates.

4.4.2 Scenario 1A (with E_COEFFICIENT)

The HRR is plotted (see Figure 39 & Figure 40) and compared with Scenario 0A. All sprinklers, except one, activate within a time window between 165 s and 298 s, with seven activations occurring within a period of only 14 seconds. Around 190 s, the HRR begins to clearly deviate from the case without sprinklers.

Importantly, the second growth phase observed in Scenario 0A, occurring around 320 s, does not occur in this sprinkler case. This is attributed to the absence of fire spread to adjacent vehicles. Since Scenario 0A has shown that window failure is critical for fire propagation, the activation of window failure devices was also examined. At this stage, none of the windows have failed.

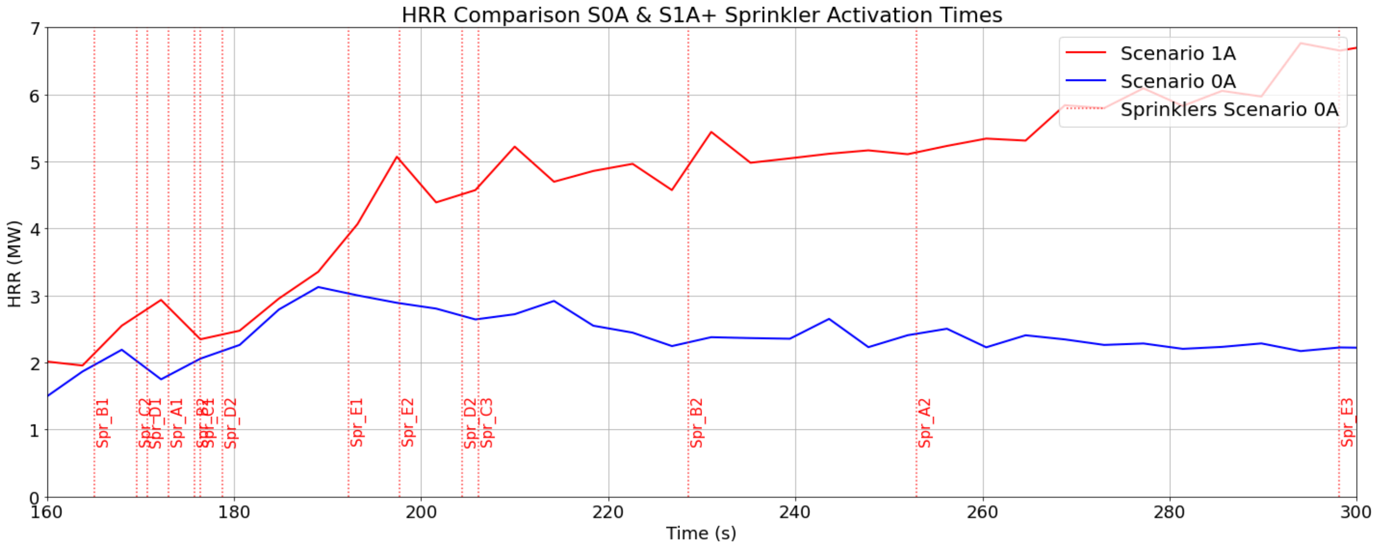

Figure 39: Sprinkler activation times and HRR of the scenario with and without sprinklers.

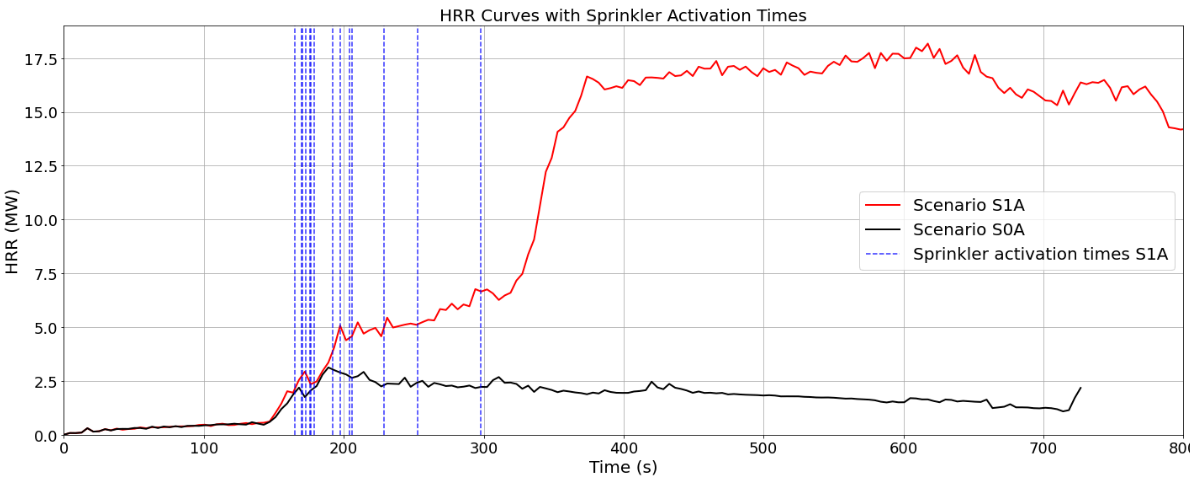

Figure 40: HRR of scenario 1 compared to Scenario 0

Data obtained from multiple temperature measurement devices clearly indicate that the sprinklers significantly reduce temperatures both inside and outside the vehicle, as well as in the surrounding environment (See figure 41 & 42). However, distinct temperature peaks remain visible in T3_during periods where jet flames are present. This indicates that the sprinkler water droplets have insufficient residence time and space (see figure 38) to effectively interact with these rapidly developing flames.

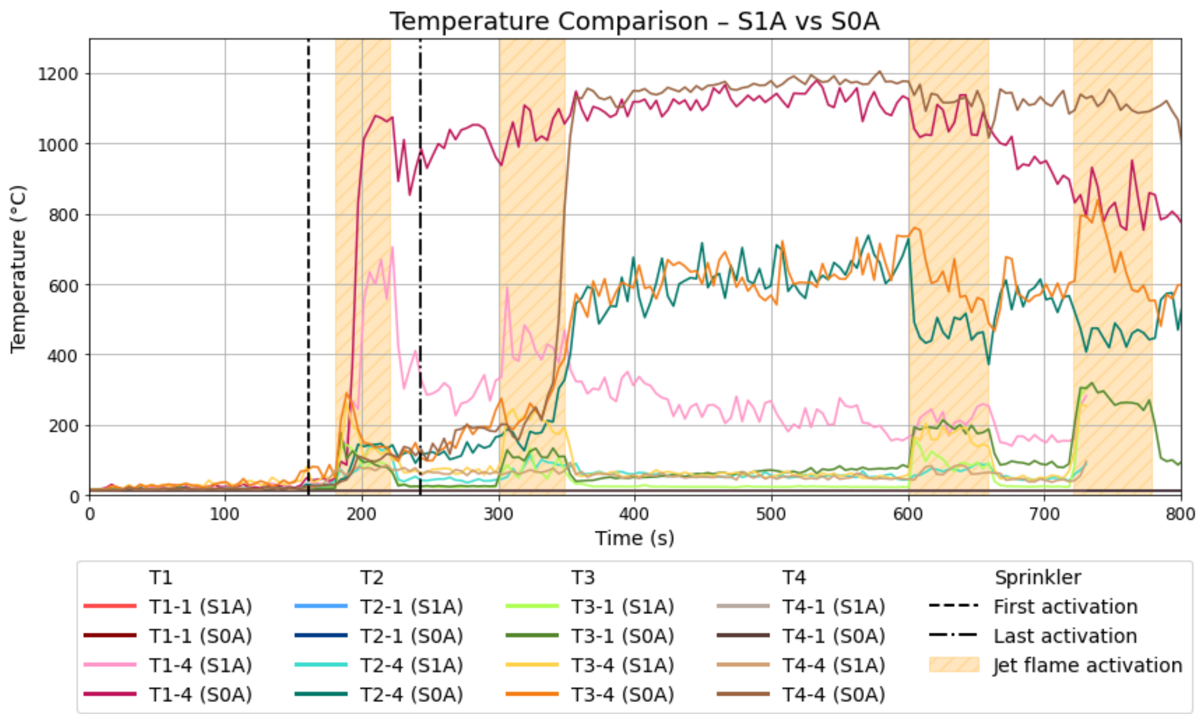

Figure 40: Upper and Lower temperature for each tree

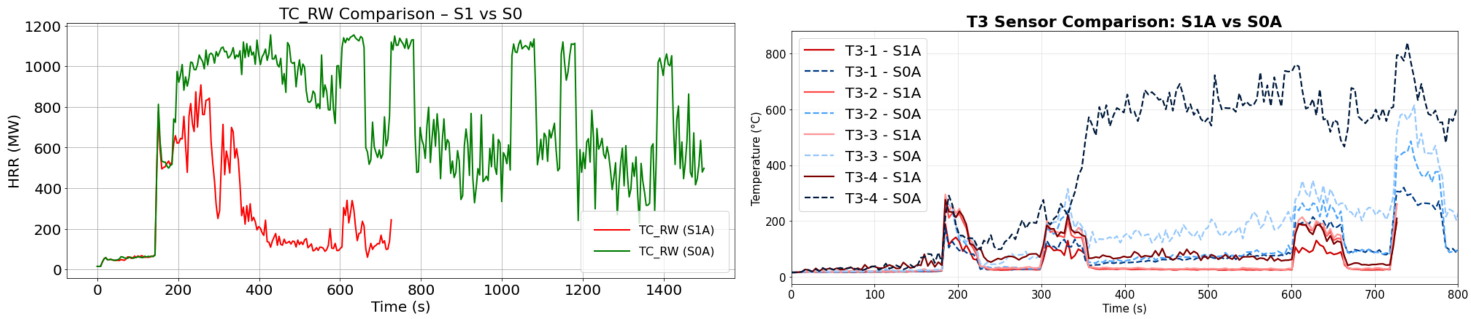

Figure 41: Left: Temperature inside the car; Right: Temperatures of tree 3 (The peaks are during the jet flames)

To assess the extent to which sprinklers influence smoke stratification, the soot visibility plane at 1 m height is compared with Scenario 0A. The results show that visibility decreases significantly when sprinklers are activated, which means destratification occurs.

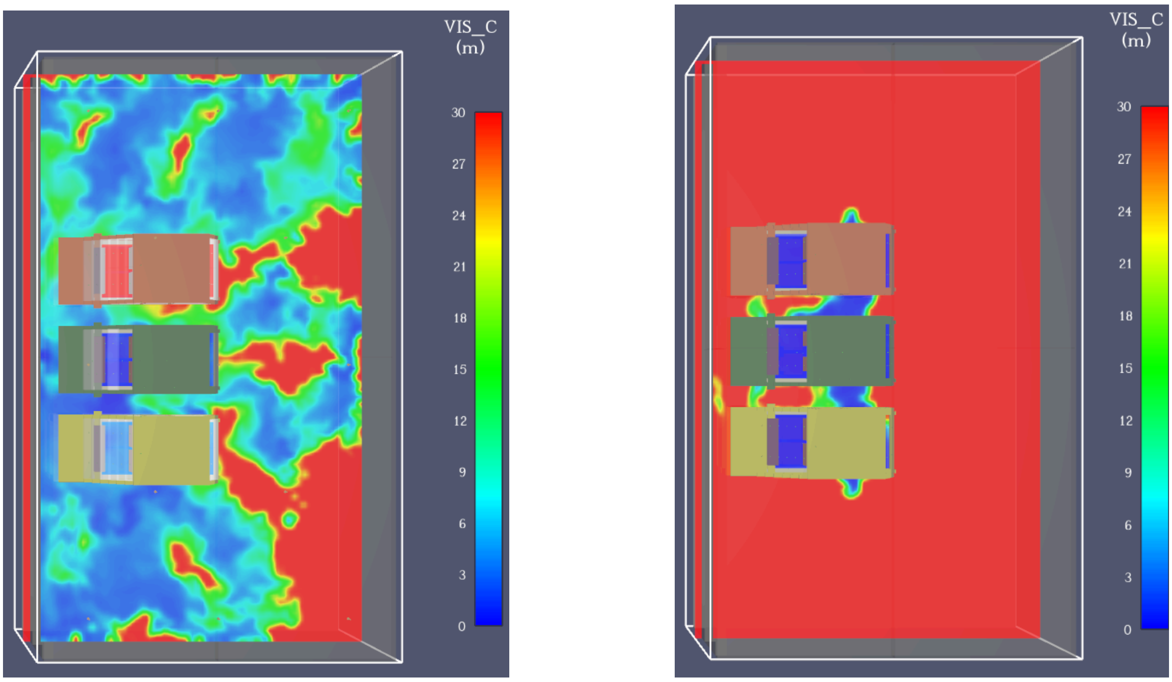

Figure 42: Visibility at 1 m height at 10 minutes (pHHR): Left: S1; Right: S0

Finally, the radiative heat flux and incident heat flux are examined (see Figure 43). As indicated, these values should remain below 25 kW/m², and below 12.5 kW/m² for combustible materials. A reference time of 235 seconds is used, corresponding to the moment in Scenario 0A when the seats of the yellow car are just about to ignite (as discussed in 4.3). At this point, it becomes clear that the radiative heat flux in the vicinity of the window is significantly lower. However, when considering the radiative heat flux at 10 minutes (PHRR), the side of the car is exposed to values exceeding 12.5 kW/m² (see figure 44). Furthermore, the temperature slice at y = −0.5 (parallel to the vehicles, at the height of the yellow car) shows temperatures fluctuating around 300°C. However, the windows don't fail and flame spread is avoided. Temperatures and heat fluxes are only higher than 300°C or 25 kW/m² when the jet flames are active and these aren't reaching the window heights.

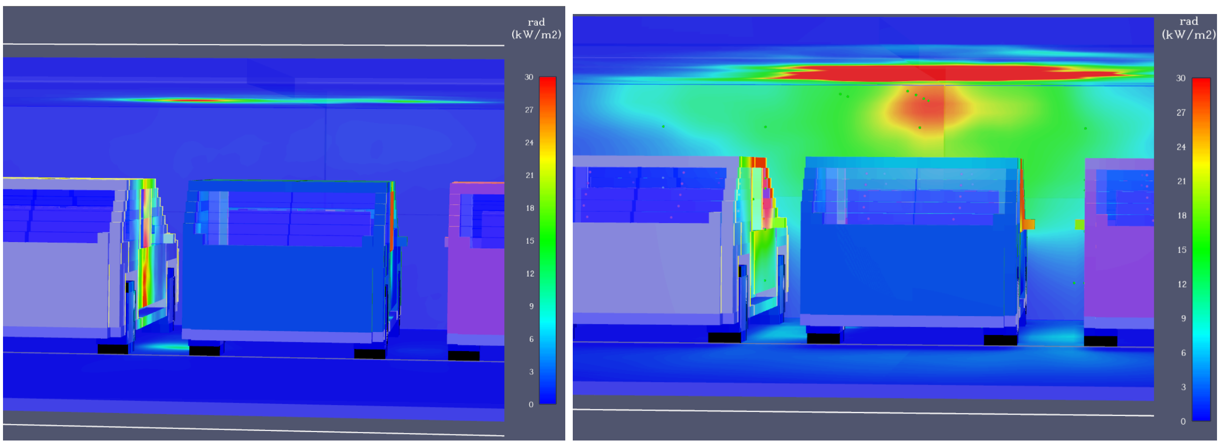

Figure 43: Radiative heat flux at time t = 350 sec (during jet flame). Left: Scenario 1; Right: Scenario 0 (all temperatures from orange to red exceed 25 kW/m²)

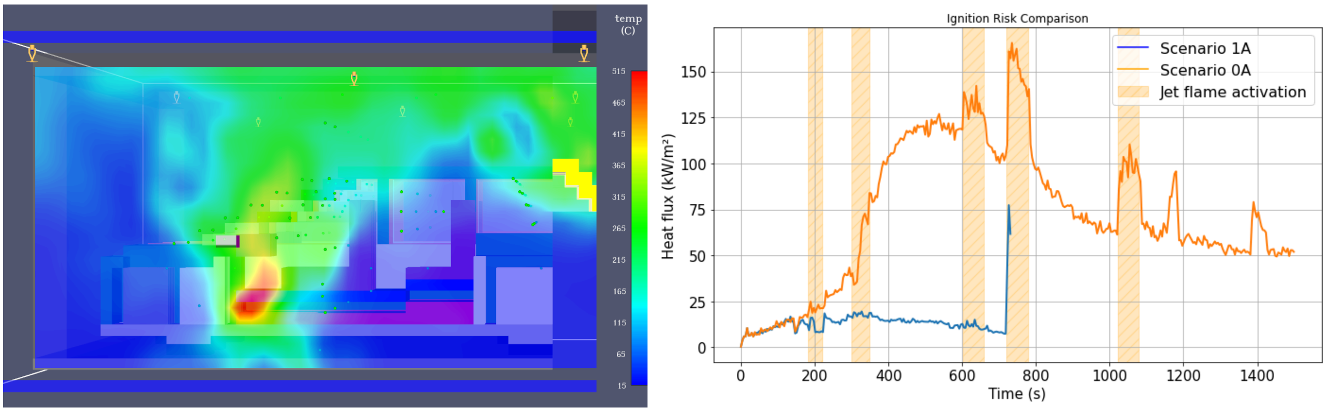

Figure 44: Left: Temperature near the yellow car (green corresponds to approximately 300°C); Right: Incident heat flux on the yellow door exposed to fire

Consequently, it can be concluded that the suppression system effectively limits fire spread under these conditions, preventing the transition to multi-vehicle involvement. The median efficiency is 91%, as shown in figure 45.

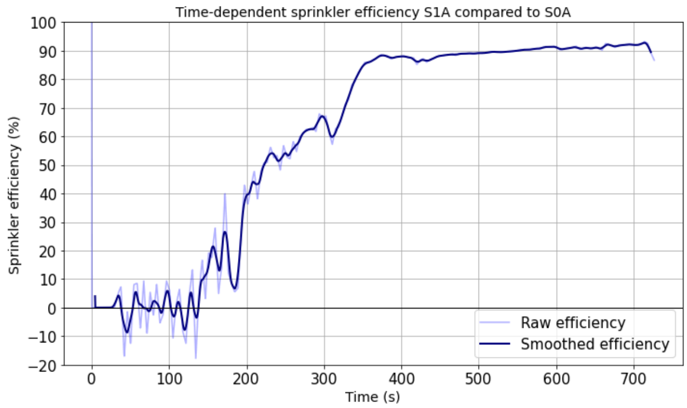

Figure 45: Time-depended sprinkler efficiency

4.4.3) Scenario 1B (without E_COEFFICIENT)

Finally, Scenario 1 with and without the E_Coefficient are compared. Firstly, both sprinklers demonstrate a highly effective fire suppression, successfully limiting the fire's growth. Sprinkler activations begin around 160 to 170 for both cases. Following these initial activations, both scenarios reach a suppressed PHRR between 3.0 MW and 3.3 MW. This represents a reduction of approximately 80-83% compared to the 18 MW free-burning Scenario 1A PHRR, indicating that both are successful in preventing a catastrophic fire spread.

In the long-term, the divergence between the scenarios becomes more and more apparent. Scenario S1A shows a consistent downward trend, dropping towards 1.5 MW and continuing to decline as the simulation progresses. In contrast, S1B fails to maintain the same level of decay. While the initial fire growth is suppressed, the HRR remains constant, hovering between 3 MW and 2.5 mw for a much longer duration. Also the temperatures can differ 0 till 200°C (see figure 46).

In terms of suppression efficiency, the difference is notable, Scenario S1A shows an active suppression, while S1B results in a sustained HRR that is nearly 1 MW more than S1A after 600 seconds. This suggests that the E_COEFFICIENT leads as expected to a more effective cooling and suppression effect than those in S1B. However, when compared to the temperatures and heat release rates (HRR) observed in Scenario 0A, the differences are negligible in magnitude, with a peak difference of approximately 1 MW on a maximum HRR of 18 MW (≈5.6%), which is generally within typical modelling and measurement uncertainty bounds in engineering fire safety studies and therefore not considered significant.

Two explanations can be given for this behaviour. First, the combustible materials (associated with a high E_coefficient, see 3.2.3.) are more difficult to reach due to the car's bodywork, limiting direct cooling. Second, sprinklers primarily act through a cooling mechanism via droplet evaporation and the resulting cooling of the smoke, rather than direct cooling of the fuel itself. Moreover, the relatively small droplet diameter reduces penetration depth, meaning droplets may evaporate before effectively reaching the fire source.

As described by Johansson et al. (2020), in *A Round Robin of fire modelling for performance-based design*"[73] the way a prescribed HRR is treated after sprinkler activation can significantly influence simulation outcomes. Since this study focuses on the suppression effectiveness of sprinklers in an electric vehicle fire scenario, the E_coefficient is included in the model despite its limited influence, in order to allow for adjustments in the prescribed HRR following sprinkler activation.

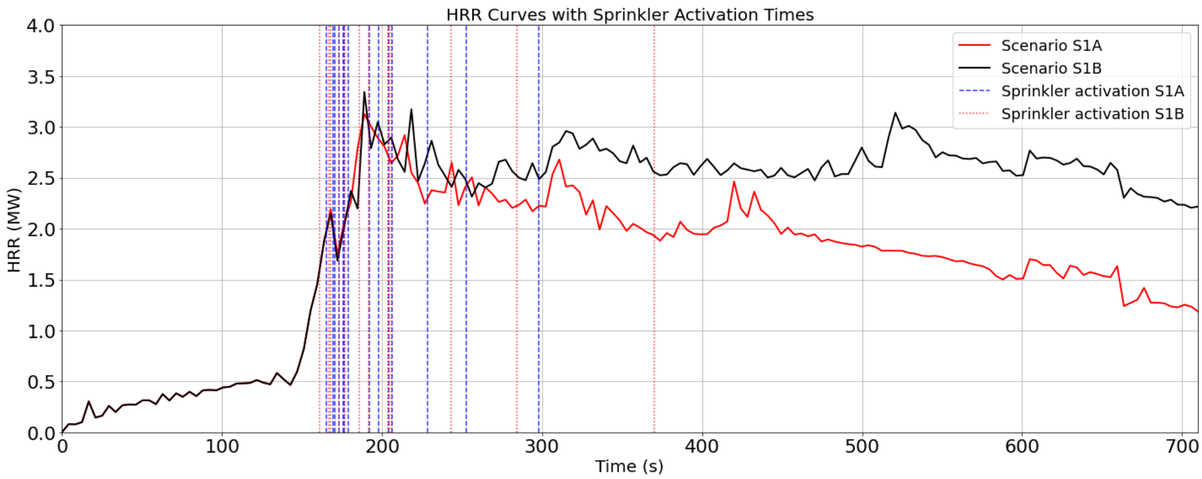

Figure 46: HRR of Scenario 1 with and without E_COEFFICIENT

[73] Johansson, N., Anderson, J., McNamee, R., & Pelo, C. (2020). A Round Robin of fire modelling for performance‐based design. *Fire and Materials*, *45*(8), 985–998. https://doi.org/10.1002/fam.2891

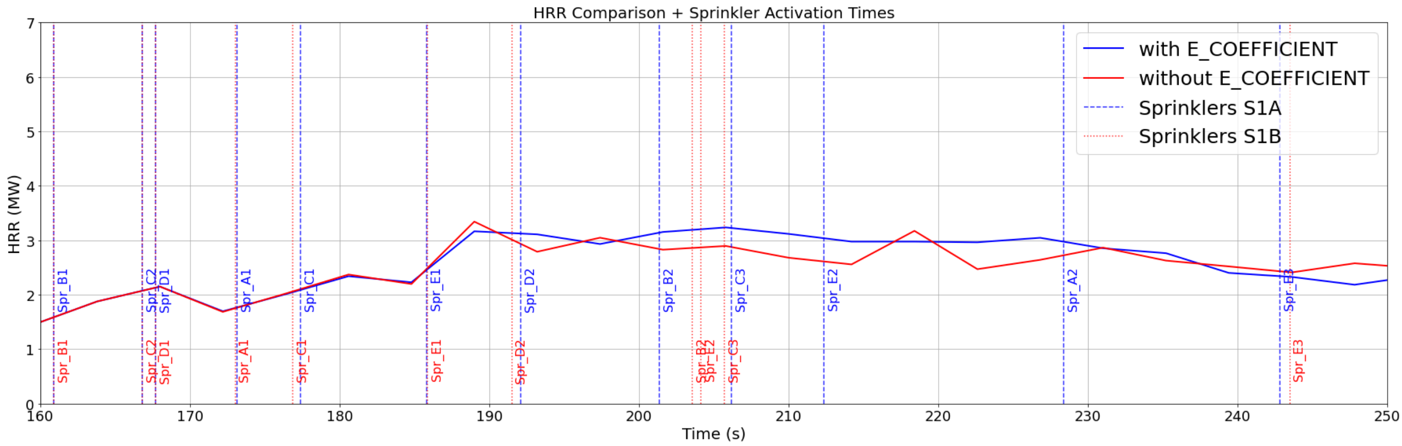

Figure 47: HRR and sprinkler activation times comparison

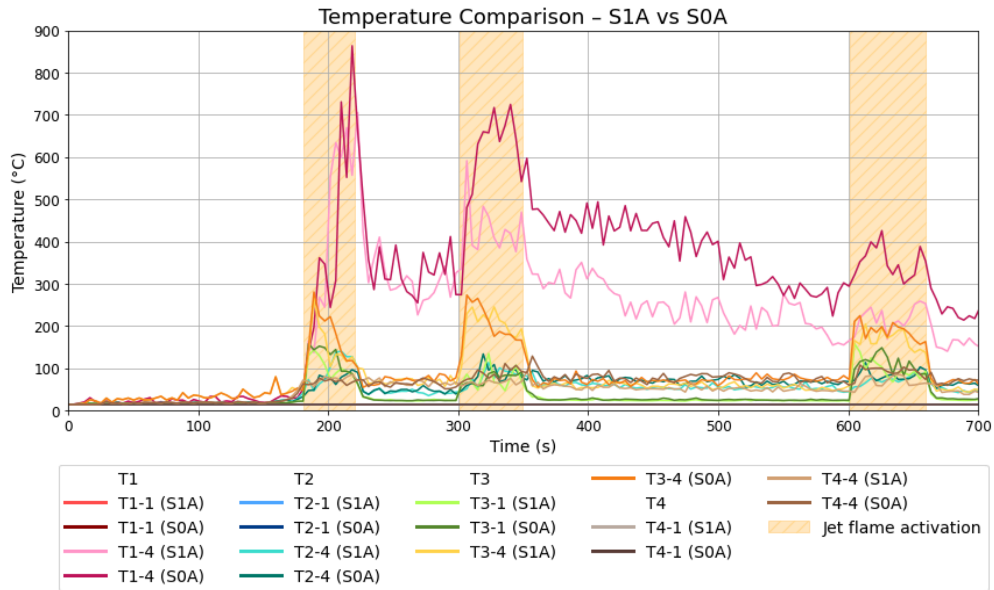

Figure 48: Upper and lower temperature comparison Scenario 1 with and without E_COEFFICIENT

4.4.4) Scenario 1C

As expected, the lower setpoint temperature for the windows leads to earlier window breakage, which in turn results in earlier sprinkler activation. However, despite this earlier activation, the sprinklers stabilize the HRR at a level similar to that observed in Scenario 1A. Furthermore, the windows of the yellow car appear to remain intact until at least 300 seconds, indicating a higher resistance to fire exposure over time.

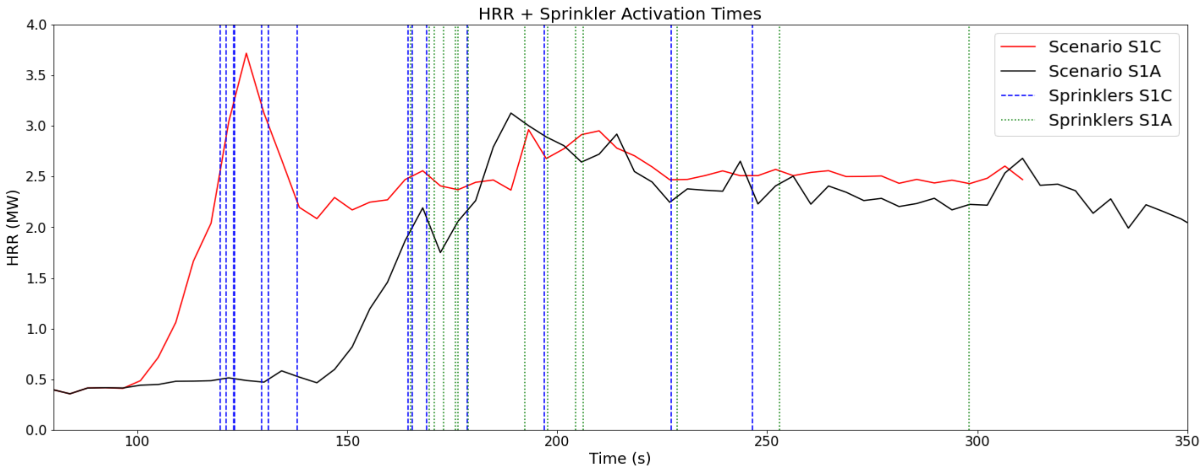

Figure 49: HRR comparison S1A & S1c + sprinkler activation times

Figure 50: HRR comparison + window breakage events

4.4) Scenario 2: Literature-Based Benchmark (Heinisuo et al.)

Since Scenario 2 involves a different sprinkler configuration and flow rate, the water density at a height of 0.5 m is first evaluated.

The results indicate that this configuration provides less coverage in the region located between two sprinklers. However, as the configuration is based on the study *"Modeling of Car Fires with Sprinklers"* by Heinisuo et al., no modifications are made. Instead, the analysis focuses on determining whether the sprinkler system is nevertheless capable of suppressing the fire and preventing fire spread. Interesting, due to the lower angle and good position of the sprinkler head, the water density between the yellow and green car is more sufficient than in Scenario 1 (See figure 37 & 51(Right)).

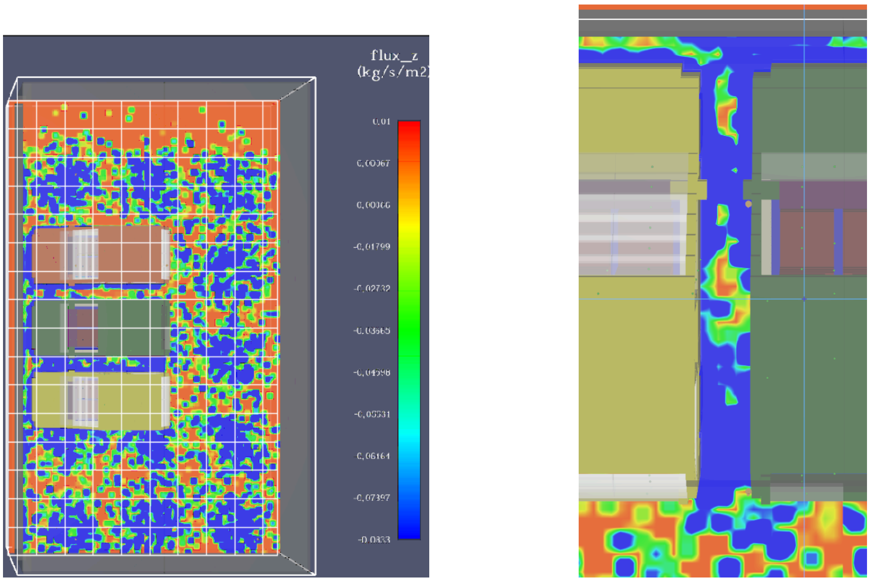

Figure 51: Left: Water flux at height 0.5m; Right: water density between cars (white grid is 1m², only the blue zones are sufficient)

Subsequently, the HRR is compared with that of Scenario 1. The results show that Scenario 2 is approximately 81%, 10% less effective in terms of suppression performance. (see figure 52) The first sprinkler, B1, activates at 177 seconds (165 seconds in Scenario 1). Since the difference is relatively small, it can be concluded that both systems activate within a similar time span. A key observation is that, in this case, the theoretical flow rate of 5 L/min just is achieved, whereas Scenario 1 reaches 6.7 L/min, corresponding to approximately 34% higher water discharge.

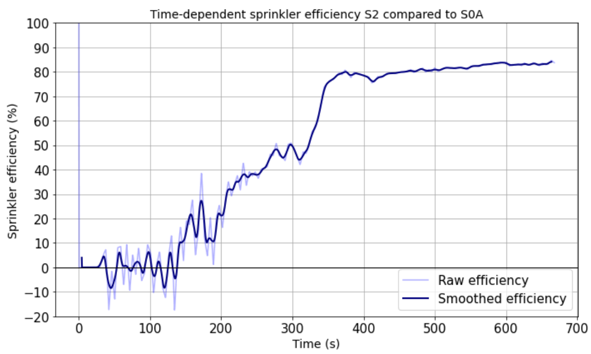

Figure 52: Efficiency S2

To assess whether this reduction in performance still allows prevention of fire spread, the incident heat flux on the side of the yellow car is analysed for both scenarios. (See figure 53) The results show that Scenario 2 exhibits peak values exceeding 25 kW/m². Based on this threshold, the yellow vehicle would be expected to ignite at approximately 338 seconds. Verification in Smokeview confirms this behaviour. This is roughly 100 seconds later than in Scenario 0. By analysing the *devc_ctrl_log.csv*, it is observed that the first window failure occurs at 291 seconds, which is 75 seconds later than in Scenario 0 (216 seconds).

The fire in the yellow car, however, appears to develop much more slowly than in Scenario 0. In contrast, the orange car seems to remain protected from fire spread. All windows of the orange vehicle remain intact and, although the middle window on this side of the green car breaks, the sprinklers ensure that the radiative heat flux remains close to 0 kW/m².

Overall, this configuration is therefore insufficient to prevent fire spread. While it does delay ignition and flame spread to some extent, the improvement is not significant enough to ensure effective prevention of fire spread under these conditions.

In addition, this scenario demonstrates that fire spread strongly depends on the fire development itself. Because the mesh containing the yellow car includes one cell more of the green car compared to the orange side, FDS systematically tends to model the first external flames on this side. Furthermore, the simulated jet flames are only implemented on the yellow car side and, as discussed previously, due to the neglect of pressure waves, the larger vent area, and the lower velocity, they are simulated more upwards than they would be in reality. These factors increase the likelihood of radiative heat transfer towards the yellow car window compared to the orange car side.

In reality, asymmetric scenarios are also highly plausible. According to Zhao et al. (2024), predicting on which side of the vehicle jet flames will occur or whether they will occur at all, is extremely difficult. Therefore, the fact that only one vehicle ignites in this simulation does not necessarily imply that the same outcome would occur in reality, but this scenario demonstrates that some sprinkler configurations can prevent partially fire spread to neighbouring vehicles.

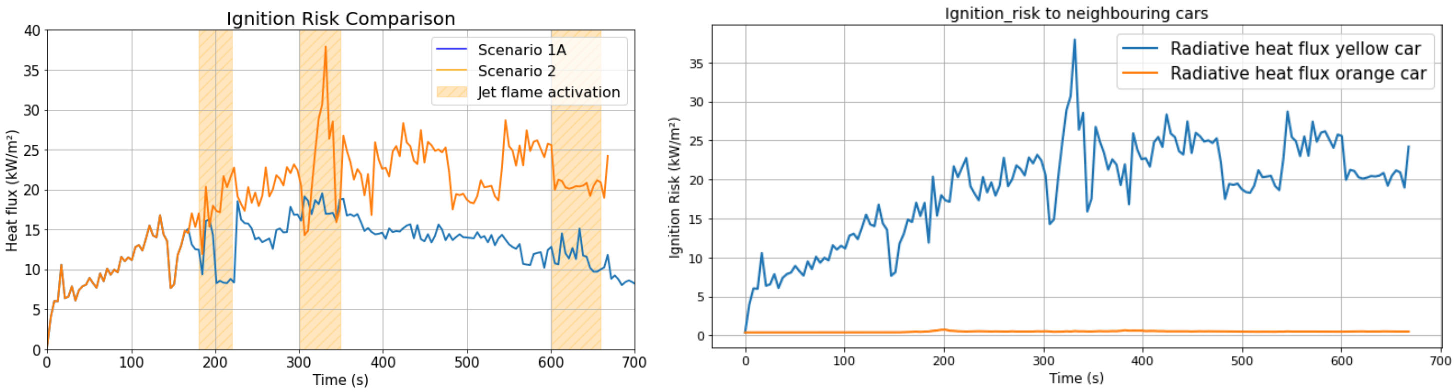

Figure 53: Left: Incident Heat flux (kW/m²) on the yellow car side S1 and S2; Right: Incident Heat flux Scenario 2

Since the water density results indicate that the water is more effectively distributed between the two vehicles, T3_2 (1 m, half a meter above the *&VENTS* of the jet flames) is plotted. (See figure 54) This shows that the sprinklers are again not capable of significantly reducing the intensity of the jet flames.

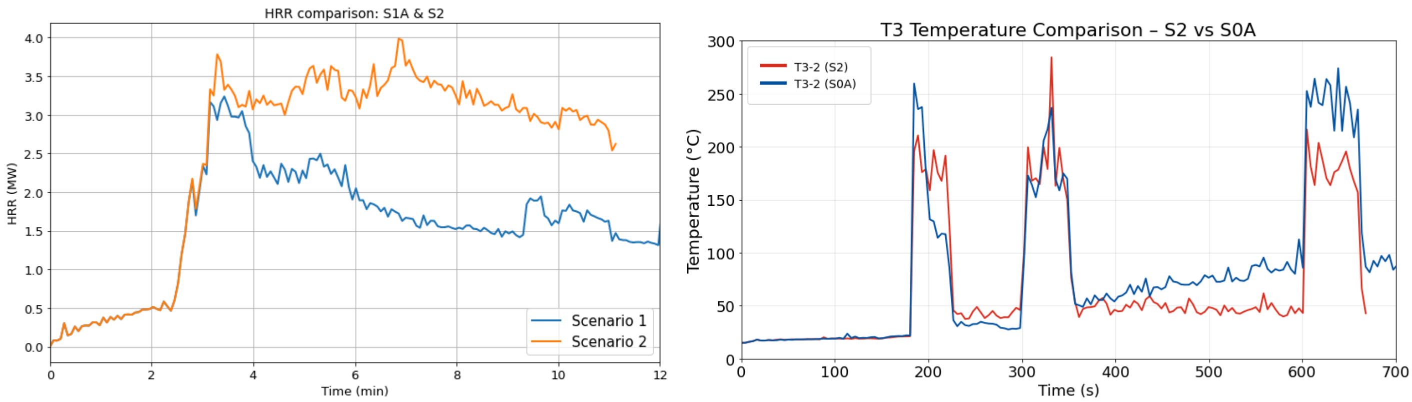

Figure 54: Left: HRR of Scenario 1 and Scenario 2 ; Right T3_2 of Scenario 1 and Scenario 2

4.5) Scenario 3: BESS-Based Configuration

This scenario is equipped with the most powerful sprinkler system, featuring twice the minimum required water density and a faster response time. When examining the HRR, it becomes evident that fire suppression is significantly more effective than in Scenario 1. (See figure 55, Left). This result is achieved with only 6 working sprinklers (activated between 111 seconds and 325 seconds), since the remaining sprinklers never reach their activation threshold.

Nevertheless, jet flames remain clearly present. For example, the jet flame initiating at approximately 12 minutes reaches a magnitude of about 1 MW (see Section 2.3.1). The sharp peak observed in the simulation increases from approximately 0.3 MW to 1.3 MW, indicating that neither gas-phase cooling, surface cooling, nor fire source cooling (see Section 3.2) is effectively suppressing this event. To evaluate the impact of these jet flames on the radiative heat flux towards the yellow vehicle, the incident heat flux is analysed. The results show that at around 12 minutes, the jet flame causes the threshold value of 25 kW/m² to be significantly exceeded. (see figure 55, Right)

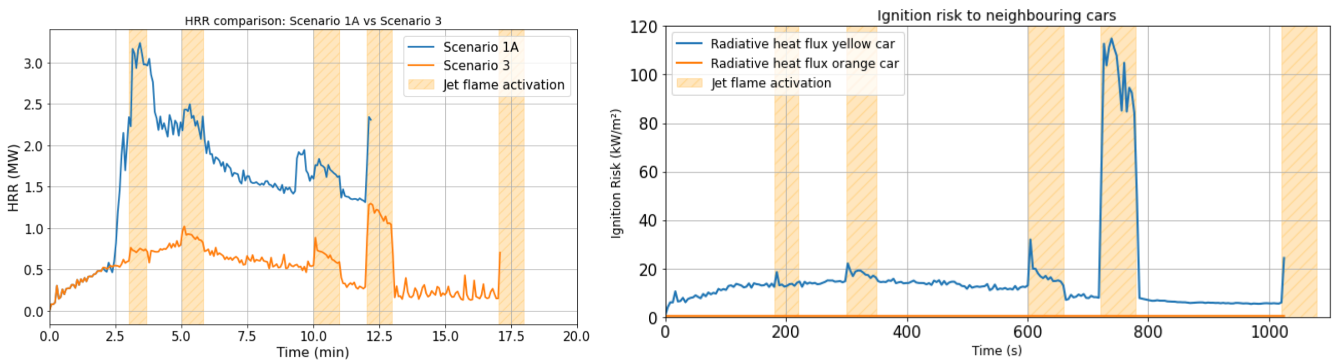

Figure: 55: Left: HRR of S 1 and S3; Right: Radiative heat flux to the yellow car S1 and S3

However, in this scenario, the location and dynamics of the jet flame prevent severe exposure of the yellow car. Due to a high jet velocity of approximately 60 m/s, the flame does not rise sufficiently to impinge on the windows. Instead, heat is primarily transferred to the steel door structure rather than directly to the combustible interior materials. Additionally, the jet flame duration is too short to ignite the materials behind the steel.

Overall, the sprinkler system achieves an estimated efficiency of 96% in limiting fire development and exposure.

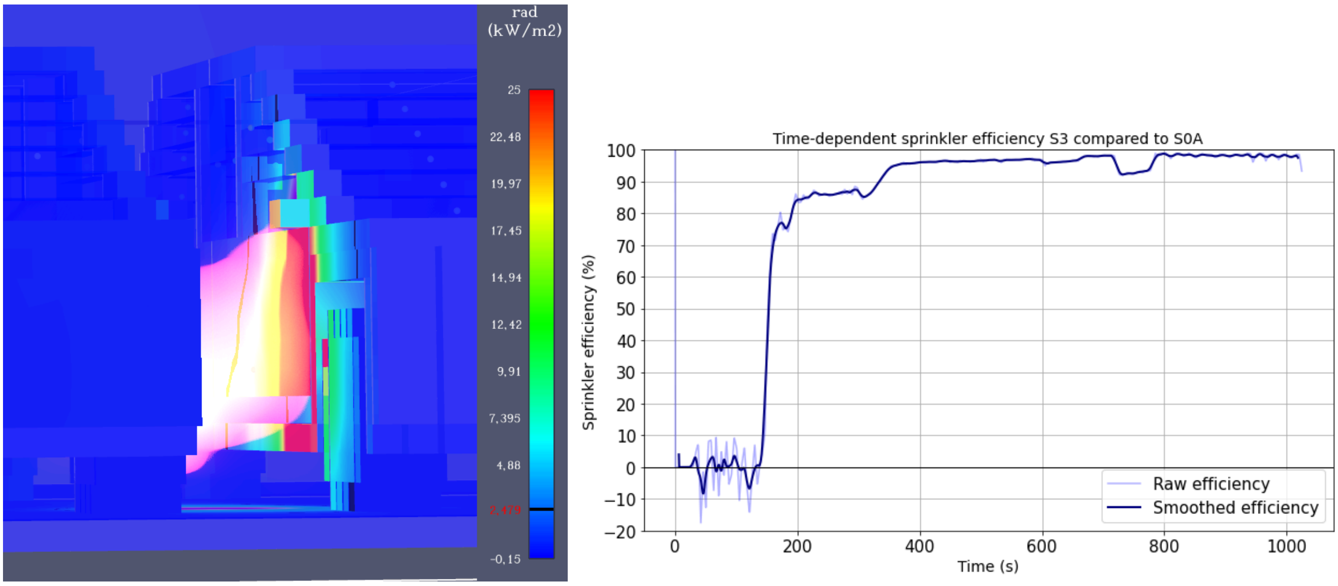

Figure 56: Left: Heat flux to the yellow car (red is > 25 kW/m²); Right Sprinkler efficiently S3 compared to S0

4.6) **Scenario 4: Reduced Activation Temperature**

The first sprinkler activates at 151 seconds, only about 10 seconds earlier than in Scenario 1A. While the remaining sprinklers in Scenario 4 activate slightly sooner, this difference does not lead to a meaningful reduction in the HRR. Once all sprinklers are fully activated, the initial temporal advantage is effectively lost.

This behavior can be explained by the rapid early-stage temperature increase directly above the vehicle, which triggers the first sprinkler activation in both scenarios. After the first window failure, smoke and flames are able to spread quickly along the ceiling layer, resulting in a sharp rise in ceiling temperatures. As a consequence, the subsequent sprinklers are activated in quick succession, with only minor differences in timing between the scenarios.

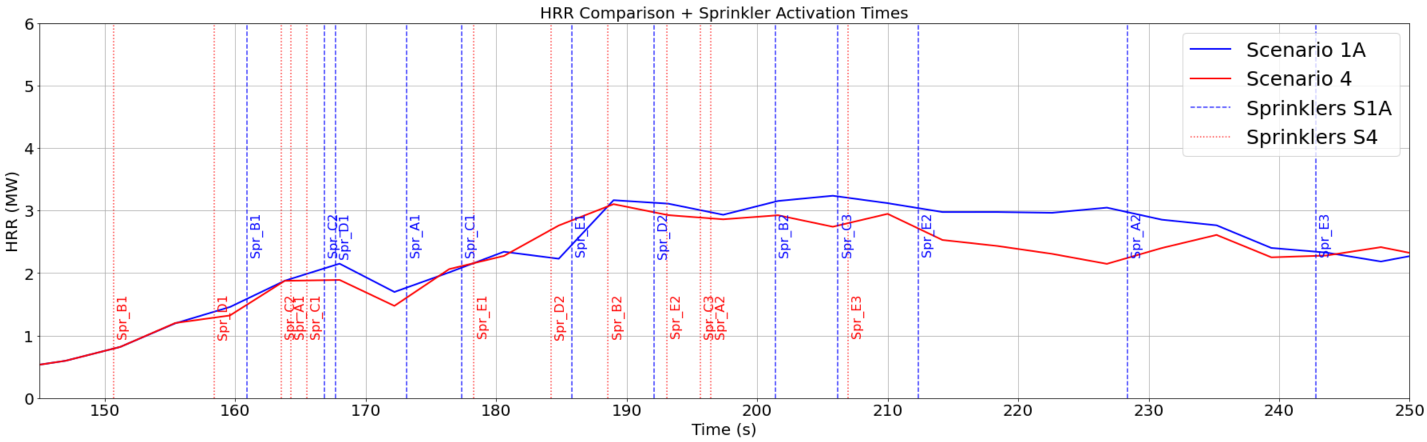

Figure 57: HRR comparison S1 and S4 and the sprinkler activation times

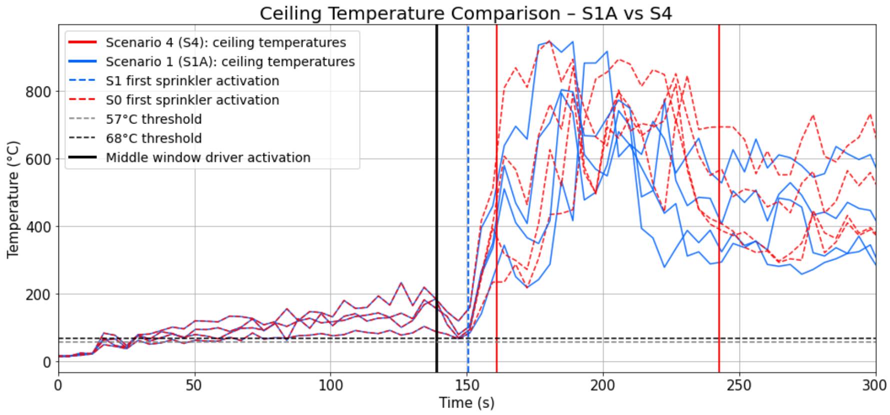

Figure 58: Ceiling temperature comparison S1 and S4

When comparing the ceiling temperatures of Scenario 1 and Scenario 4, a very rapid temperature increase is observed in both cases. The overall suppression efficiency of this scenario is 91%, the same as Scenario 1A.

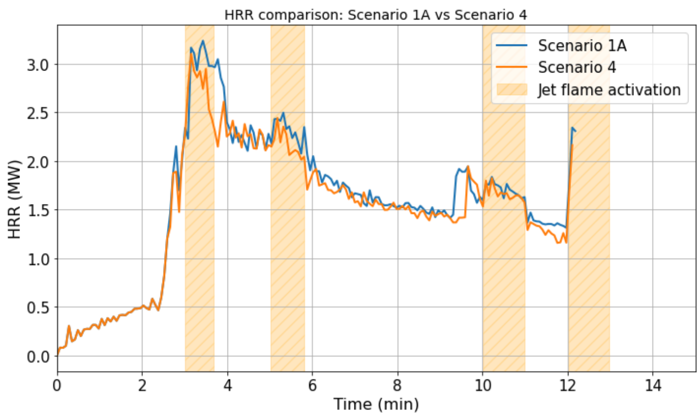

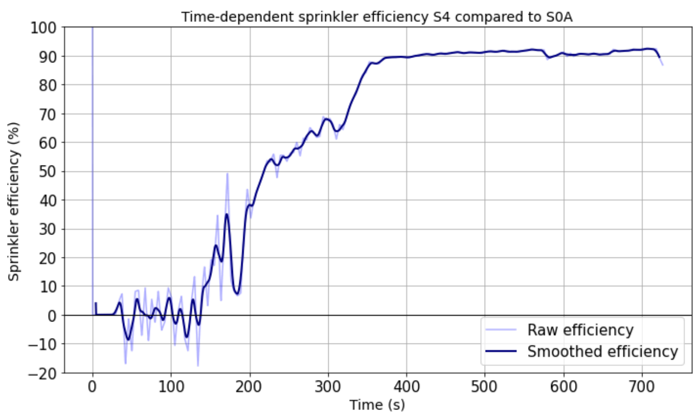

Figure 59:Left: HRR comparison S1 and S4; Right: Sprinkler efficiency

4.7) **Scenario 5: Wall-Mounted Sprinklers A, B & C**

4.7.1) Water coverage

The water flux slice at a height of 1.6 m shows that the coverage in Scenario 5A is highly concentrated within the first 70 cm from the wall. This suggests that, in Scenario 5A, the water is unable to reach all areas of the fire, making fire spread likely to occur.

Subsequently, Scenario 5B is evaluated. While this configuration is capable of reaching the central area, the limited spray angle results in large dry zones between the sprinklers near the wall.

Finally, Scenario 5C is considered. Its performance is clearly intermediate between the previous two scenarios. However, at a distance of 1.8 m from the wall, the required density of 5 L/min is not achieved.

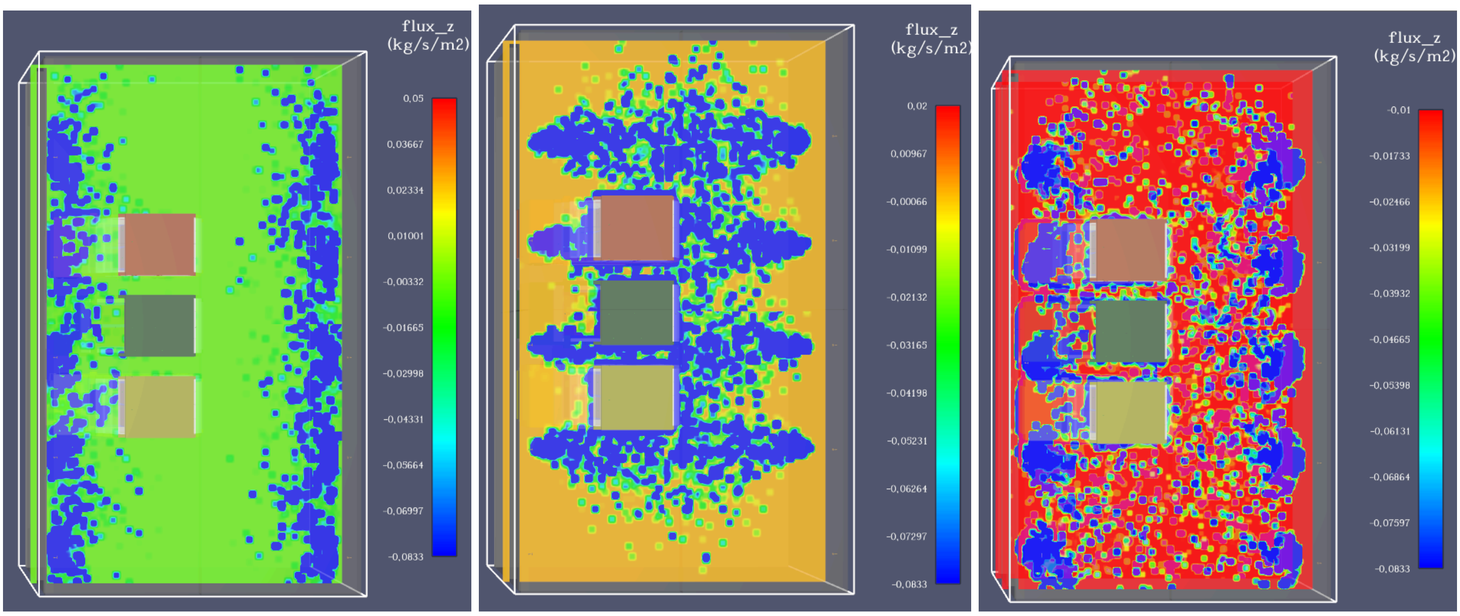

Figure 60: Water densities from Scenario 5; From left to right: S5A, S5B, S5C

4.7.2) Scenario 5A

The visual observation of fire spread in smokeview and the HRR curve confirm that this sprinkler configuration is indeed insufficient to prevent fire spread and flames become visible in SmokeView around 283 seconds. The first window failure of the yellow car is at 231 seconds. The primary cause is the inability of the sprinklers to adequately suppress the fire source and prevent propagation toward both the yellow and orange vehicles.

Nevertheless, the HRR results suggest that the growth phase of the fire is delayed. This indicates that the cooling effect of the hot gases, even indirectly, still has a measurable impact on fire development, this way, there is still an efficiency of 70%.

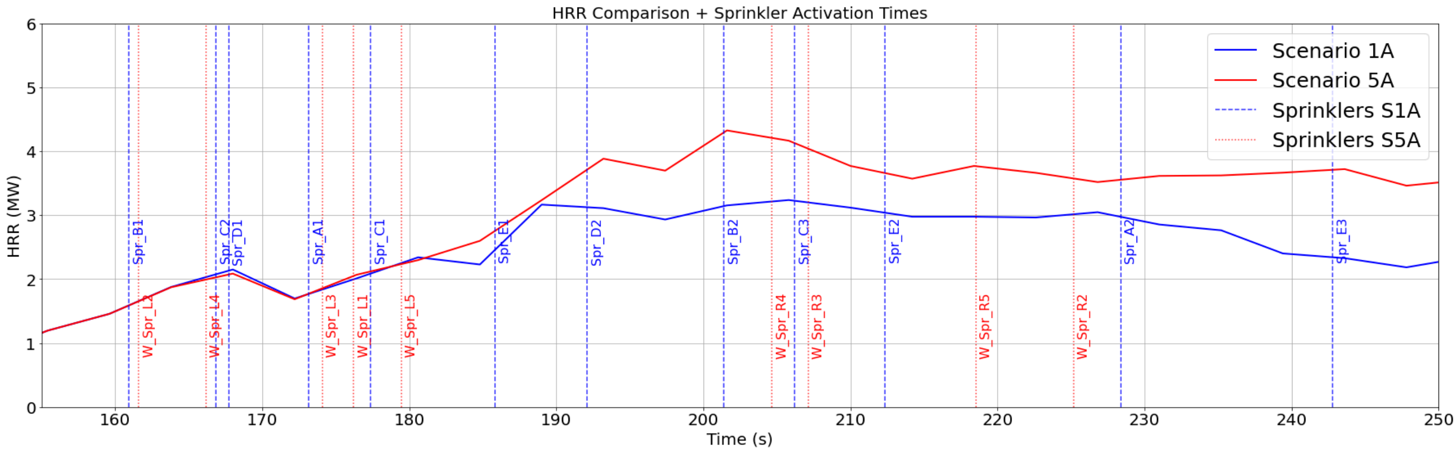

Figure 61: Activation times of the sprinklers Scenario 5A en Scenario 1A compared to S1

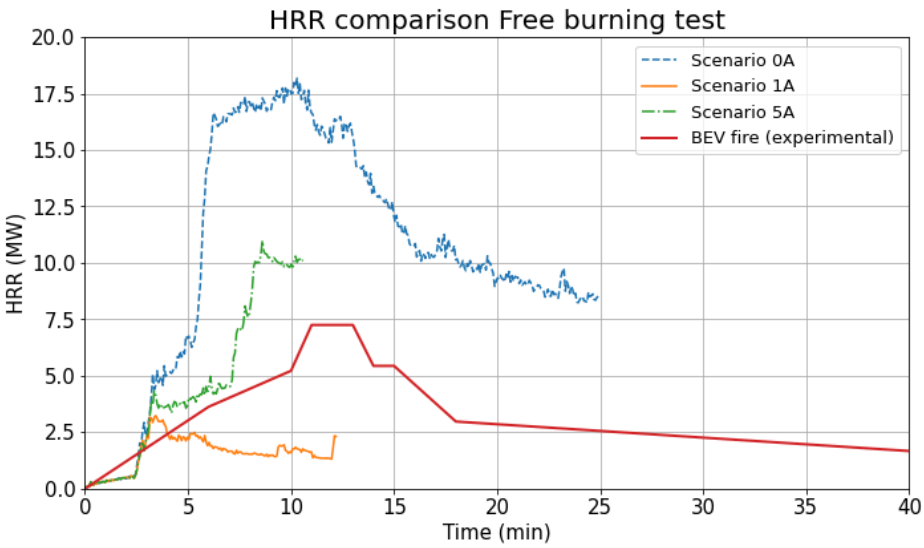

Figure 62: HRR of S0, S1, S5A and the single car burning of the experimental result.

4.7.3) Scenario 5B & 5C

The first activation of both the wall-mounted sprinklers and the ceiling-mounted sprinklers in Scenario 1 occurs roughly at the same time. (See figure 63) This is due to their installation at the same height. As previously indicated, once the window breaks, the ceiling temperature above the vehicle increases rapidly across the entire surface (see Figure 58). Sprinklers located further away from the fire source activate slightly later, as they are positioned at a greater distance from the fire origin.

The HRR response of the sprinklers generally follows the same HRR trend observed in Scenario 1. When examining the heat flux on the doors of adjacent vehicles, Scenario 5C reaches the critical threshold of 25 kW/m² at 315 seconds. However, at this time, the window temperature remains below 300°C and therefore has not yet reached the breaking point.

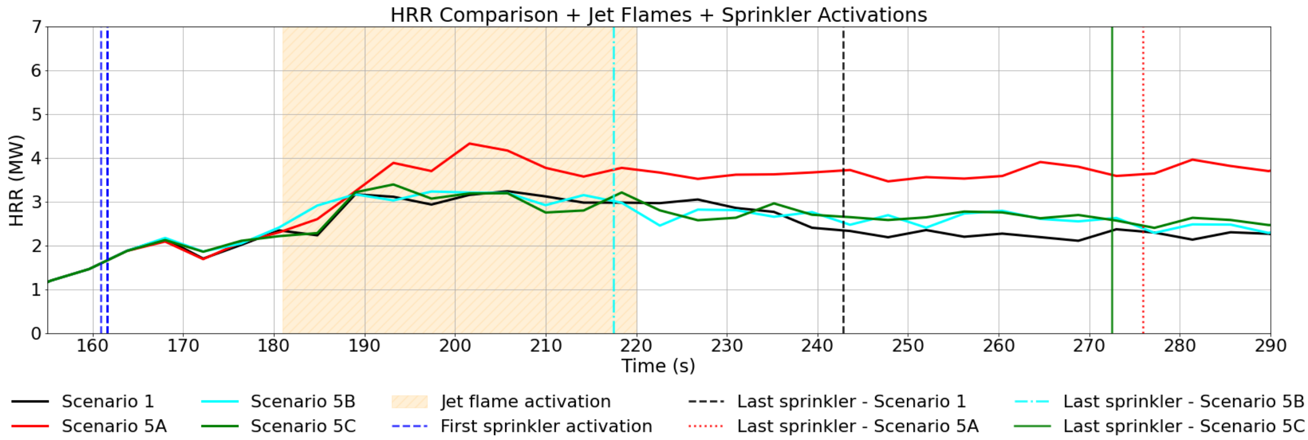

Figure 63: HRR of Scenario 1 and all scenarios 5 with sprinkler activation times

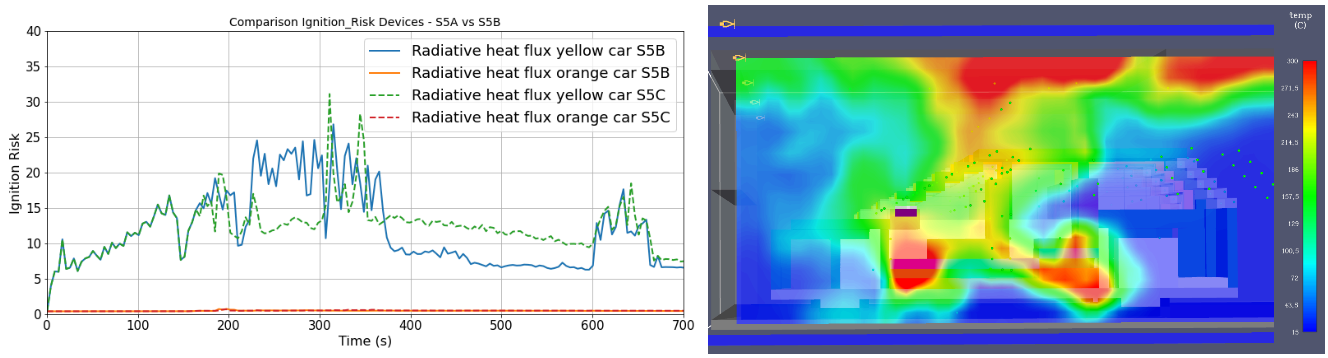

Figure 64: Left: Heat flux of S5B and S5C to neighbouring cars; Right Temperature device slice of Scenario 5C (Red is > 300°C)

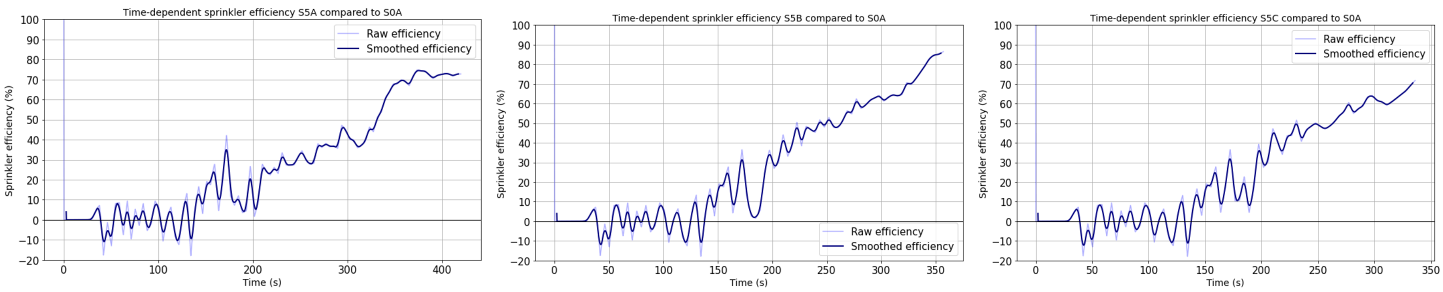

Figure 65: From left to right: Efficiency of Scenario 5A, 5B, 5C

4.8) Scenario 6

By installing the sprinklers at a lower height, a higher water flux is observed on the slice device at z = 0.5 m compared to the slice device at 1.6 m. Since this scenario differs from Scenario 5C only in terms of installation height and activation method, the two are directly compared.

The alternative detection mechanism results in faster sprinkler activation. Consequently, the sprinklers are able to respond before any of the green vehicle's windows fail. In all previous scenarios, window failure consistently coincided with a sharp increase in HRR, highlighting its critical role in fire development. However, due to prolonged external flame exposure and the sprinkler system’s insufficient suppression capacity, the first window of the green vehicle in Scenario 6 still fails at 259 seconds. Approximately 50 seconds later, a peak in HRR is observed as flashover occurs inside the green car. This further confirms that window breakage is a key driver of fire dynamics. Nevertheless, the sprinklers are still able to prevent flame spread to adjacent vehicles.

Secondly, the sprinklers show a slightly improved but not significant effect on the jet flames compared to the other scenarios, as shown in Figure 69.

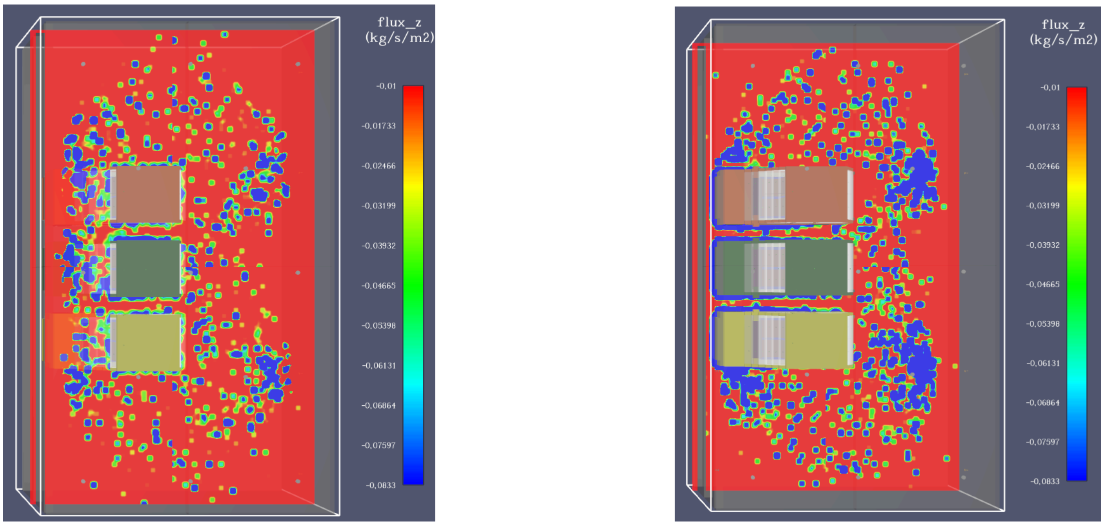

Figure 66: Water flux at height 1.6 m; Right: water flux at height 0.5 m

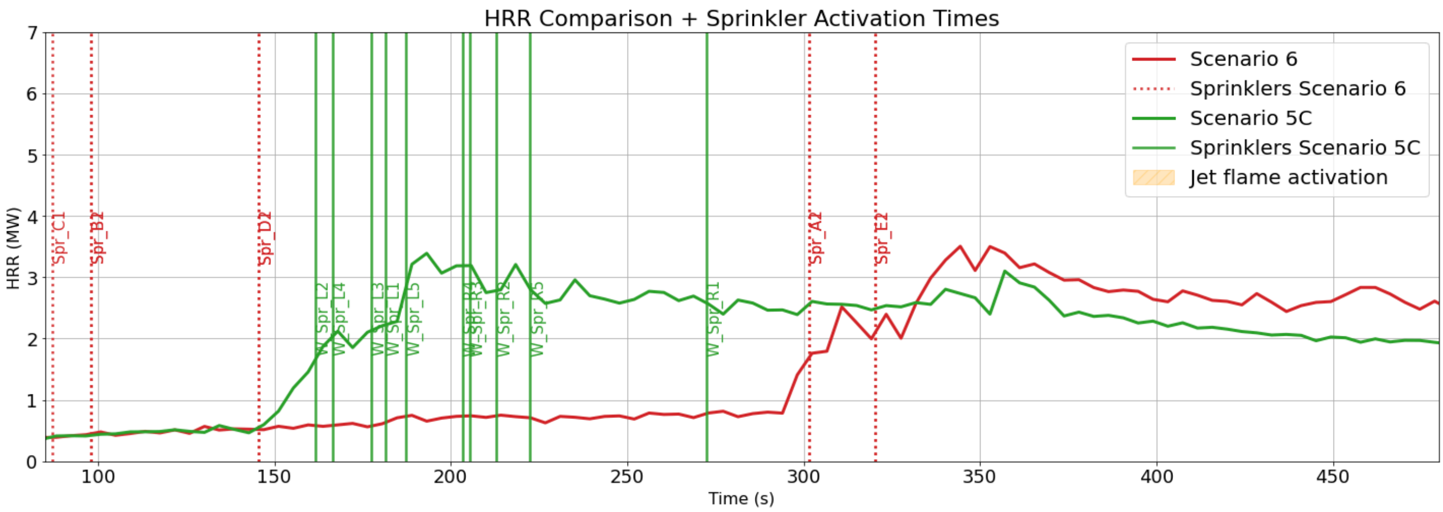

Figure 67: HRR of Scenario 6 and Scenario 5 and sprinkler activation times

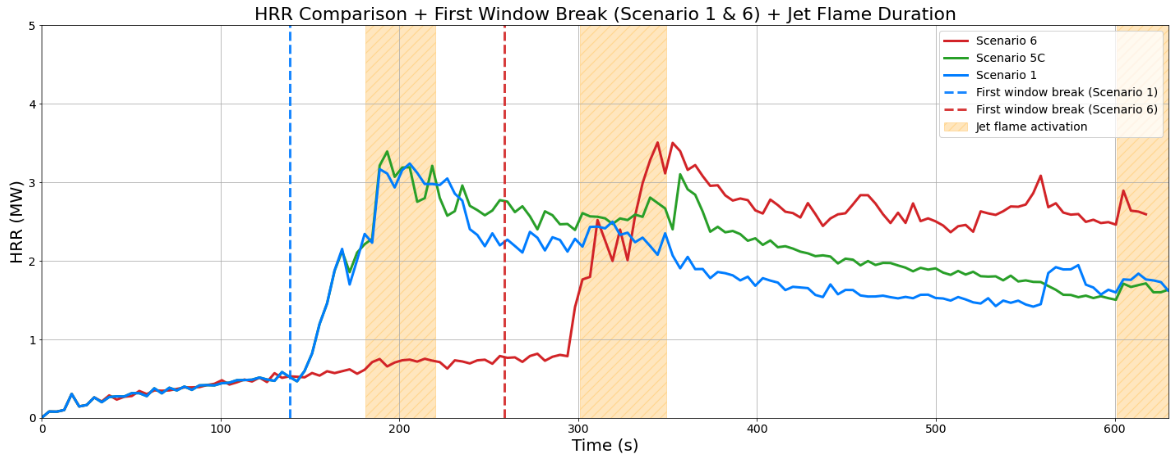

Figure 68: HRR of Scenario 1, 6 and 5C with the window break

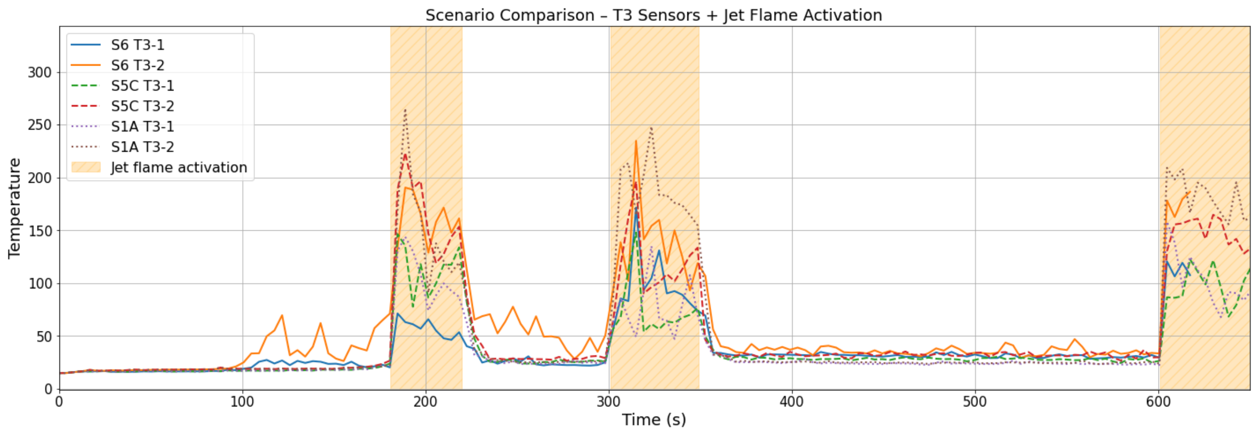

Figure 69: T3-2 and T3-1 of Scenario 1A and Scenario 6

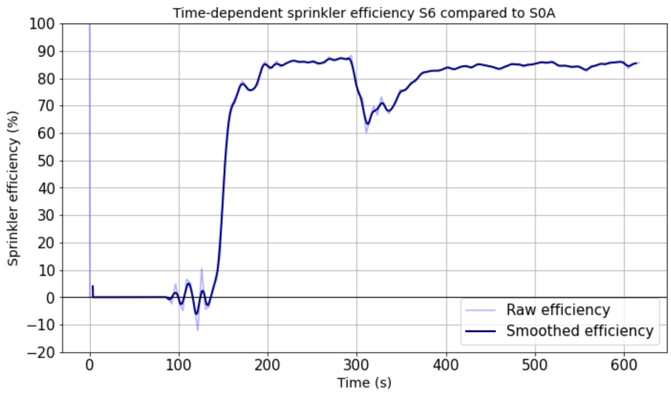

Figure 70: sprinkler efficiency Scenario 6

4.9) Scenario 7 A - H

Since the configuration of Scenario 7 has already been discussed, the focus here is solely on the heat release rate (HRR). The system interpretation is straightforward: when the HRR exceeds that of Scenario 2, flame spread can be considered likely, as in Scenario 2 the yellow vehicle did exhibit limited ignition. Conversely, when the HRR remains below this reference level, it is more probable that no flame spread to adjacent vehicles occurs.

A first observation is that doubling the flow rate does not result in a 50% reduction in HRR. (See figure 71) This is partly because the HRR is prescribed and therefore always maintains a minimum baseline value, and partly because the water is not fully effective in interacting with the fire. In practice, a significant portion of the water does not contribute to suppression but instead accumulates on the floor, reducing its cooling efficiency.

A second observation is that neither flame spread, nor window breakage of the neighbouring cars is observed once the flow rate exceeds a threshold of approximately 3.3 L/min for this configuration. The radiative heat flux exceeds 25 kW/m², however, the temperature device shows that in the region of the window, the temperature stays below 300°C. However, Scenario 2, which operates at a higher flow rate of 5 L/min, still exhibits flame spread. This indicates that the occurrence of flame spread is not solely governed by flow rate, but also depends on the overall system configuration and boundary conditions.

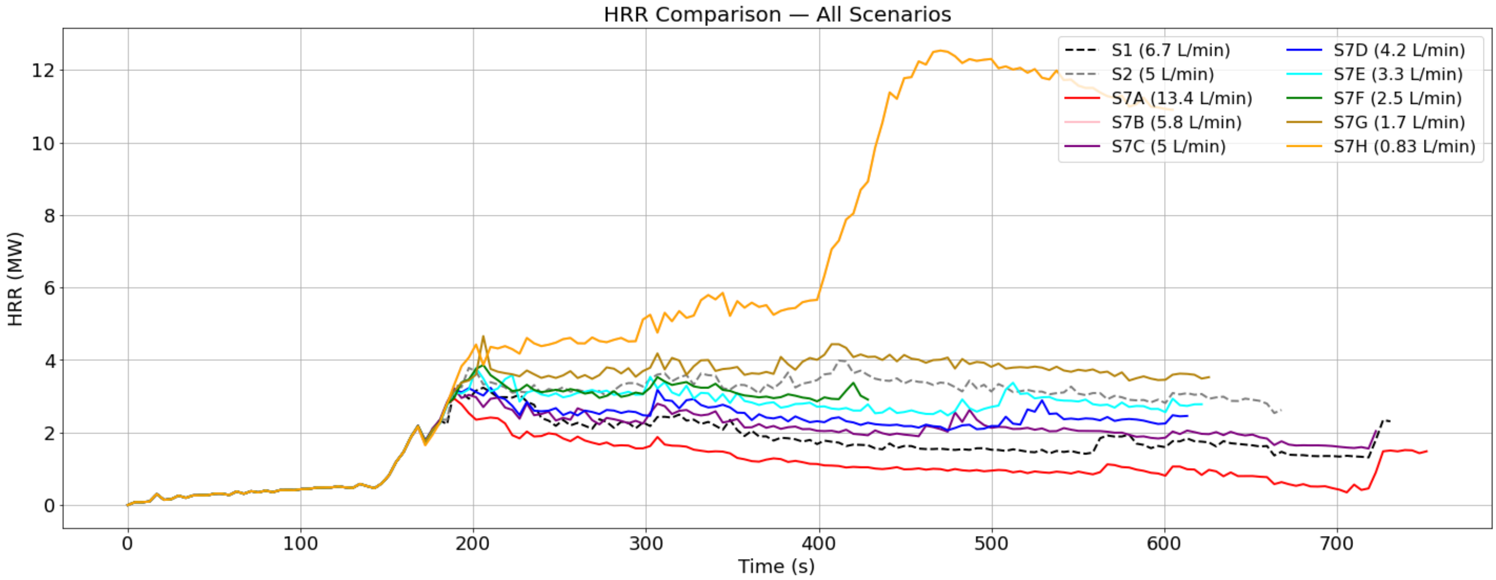

Figure 71: HRR of ceiling- mounted sprinklers with different flow rates.

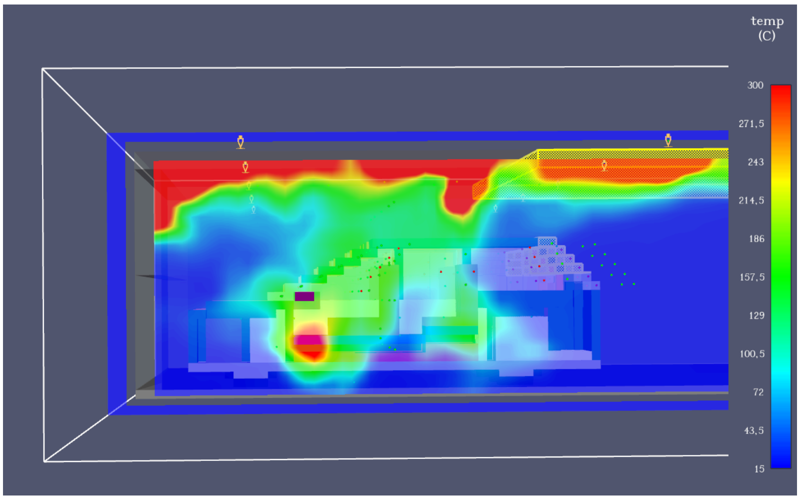

Figure 72: Temperature at the side of the yellow car. Red exceed 300°C

Part 5: Discussion & Conclusion

5.1) Discussion

5.1.1) Key Findings on EV Fire Dynamics and Sprinkler Suppression

The increasing electrification of the vehicle fleet has intensified concerns regarding the fire safety of enclosed parking structures. Existing literature consistently demonstrates that EV fires differ fundamentally from ICEV fires due to:

- the possible occurrence of thermal runaway (TR),
- the release of more toxic gases primarily originating from battery electrolytes
- an increased risk of vapor cloud explosions (VCE),
- and the unpredictable occurrence of high-intensity jet flames.

These characteristics can result in a faster peak heat release rate (PHRR) and, depending on the state of charge (SOC) and battery pack size, very different fire progression and potentially higher overall heat release rates.

However, the largest contributor to the total heat release rate (HRR) of a vehicle fire remains the car body itself, which consists of a significant amount of combustible polymers whose quantity has steadily increased over the years. Since the car bodies of ICEVs and EVs are broadly similar, it can be concluded that the significantly different fire development of EVs is primarily caused by the previously mentioned battery-related phenomena, which collectively create a distinct and elevated fire risk profile.

As a result, research into Li-ion battery fires has increased steadily in recent years. Nevertheless, despite the rapid growth in EV adoption, there remains a substantial lack of large-scale experimental vehicle fire tests and validated numerical studies investigating the interaction between EV fires and sprinkler systems in enclosed environments. This thesis therefore provides a numerical investigation of water-based sprinkler suppression of EV fires in enclosed parking structures using the Fire Dynamics Simulator (FDS).

In this way, the thesis contributes to the existing body of literature by combining:

- a literature-based EV fire representation in CFD,
- jet flame modelling,
- multi-vehicle fire spread analysis,
- and sprinkler suppression analysis within a confined underground parking environment.

The model was primarily validated against the studies of Kang et al. (2023) and Zhao et al. (2023), and further supported by the work of George (2023) and Ditch et al. (2019).

The simulations clearly demonstrate that an unsuppressed EV fire in an enclosed parking garage can rapidly escalate into a multi-vehicle fire scenario with a peak HRR exceeding 18

MW, corresponding to approximately three passenger vehicles burning simultaneously. The free-burning Scenarios 0A and 0B showed that neighbouring vehicles become involved primarily due to sustained thermal exposure and direct flame contact with combustible materials, rather than ignition caused solely by the battery jet flames. This finding was further confirmed through an additional simulation in which the HRR contribution of the battery pack was artificially set to zero. Furthermore, Scenarios 1 through 7 demonstrated that although the jet flames generated local heat fluxes exceeding 25 kW/m² at the vehicle doors, the short duration of these jet flames and their contact primarily with the steel vehicle body prevented direct ignition and subsequent fire spread.

According to the simulations, a much more critical parameter governing flame spread is window failure. Once the windows of a neighbouring vehicle break, the combustible interior materials become directly exposed to radiative heat fluxes exceeding 12.5 kW/m². In such cases, the sprinkler systems effectively act as a thermal shield that forms a water film over the windows preventing or at least delaying window breakage. Interestingly, the relatively limited spacing between vehicles may even become advantageous, since water droplets tend to flow and accumulate more effectively along the vehicle sides. This may partially explain why sprinkler systems with flow rates lower than the commonly proposed 5 L/min/m² can still prevent fire spread under certain conditions as proven in the Scenario 7 series.

The most effective suppression configuration was Scenario 3 (BESS-Based Configuration – Ditch & Zeng). This scenario employed high-intensity suppression and therefore unsurprisingly achieved the highest suppression efficiency coefficient of approximately 96% compared to the free burning Scenario 1A. These results are consistent with the findings of Ditch and Zeng (2019), who also identified high-density sprinkler configurations as the most effective strategy for overall fire suppression. Nevertheless, the simulations showed that even these powerful sprinklers were unable to significantly reduce the intensity of the simulated battery jet flames, which still caused local heat fluxes exceeding 25 kW/m² near the lower regions of the neighbouring vehicle.

Scenario 2, based on the literature benchmark by Heinisuo et al., applied a discharge density of 5 L/min/m², a pressure of only 0.35 bar and conservative activation sprinkler settings. In the original ICEV study, both experiments and simulations demonstrated that only the first vehicle burned when sprinklers were activated. In contrast, the EV simulations performed in this thesis resulted in limited ignition of the neighbouring vehicle, although ignition was delayed by approximately 100 seconds compared to the free-burning case. This discrepancy suggests that the unique characteristics of EV fires, combined with the modelling of a more modern and detailed vehicle geometry, may require higher protection levels than those traditionally designed for older conventional vehicles.

In Scenarios 5A, 5B, and 5C, wall-mounted sprinklers were investigated. An important disadvantage of wall-mounted sprinklers is that they lose the benefit of gravity-assisted water distribution and offer less flexibility regarding installation locations. Consequently, the simulations demonstrated that sprinklers with parameters identical to those of Scenario 1 were unable to provide a uniformly distributed water coverage throughout the parking compartment. A discharge density of > 5 L/min/m² was only achieved within approximately

1.8 m parallel to the wall. As a result, these sprinklers were unable to completely suppress fire spread, although they significantly delayed it by cooling the environment.

However, when the wall-mounted sprinkler parameters were adjusted by reducing the spray angle, increasing the particle velocity to 15 m/s, and increasing the droplet diameter to either 2000 µm or 1500 µm in order to better represent sprinklers specifically designed for wall-mounted applications, the simulations showed substantially improved performance, and fire spread could be prevented.

Another notable observation is that sprinkler activation times for sprinkler rows B, C, and D in Scenarios 1, 2, 4, 5, and 7 all occurred within a relatively narrow time interval between 155 and 230 seconds. The reason for this is that the ceiling temperature rises rapidly throughout the parking compartment once one of the windows of the burning green vehicle fails, mainly due to the limited ceiling height of the underground garage and the high temperature of the external flame. This statement is supported by the ceiling temperature measurements obtained from the simulations. Only Scenarios 3 and 6 showed significantly different activation behaviour. In Scenario 3, this is explained by the fact that only six sprinklers were required to suppress the fire effectively. In Scenario 6, a special activation strategy was applied in which sprinklers activated before any vehicle windows failed. Consequently, the first window failure of the green vehicle occurred later in the simulation, causing delayed activation of the remaining sprinklers.

Remarkably, both Scenario 6 (86% efficiency) and Scenario 4 (91% efficiency), despite exhibiting significantly different sprinkler activation timings, achieved suppression efficiencies comparable to Scenario 1 (91%) and avoided fire spread. As long as the sprinklers activated before a neighbouring vehicle ignited, the overall suppression effectiveness remained largely unchanged. This can be explained by the fact that the combustible materials within the vehicle body remain protected by the steel car body itself. As a result, sprinklers mainly contribute by cooling external flames and smoke gases rather than directly suppressing the combustible interior materials. This statement is supported by comparing Scenario 1A and 1B, where both are able to avoid fire spread, but 1B is modelled without possibilities to lower the predescribed HRRs.

The comparison of Scenario 1A and 1B leads to the broader discussion regarding fire source suppression modelling in FDS. Currently, there is no consensus on how sprinkler suppression should be incorporated into prescribed HRR fire models. A conservative approach is to entirely neglect suppression effects on the HRR. Another commonly used performance-based design (PBD) approach is to maintain the HRR constant from the moment of sprinkler activation, or approximately one minute thereafter. The FDS User's Guide additionally provides the option of applying an E_COEFFICIENT and is used in the scenarios of this thesis, however, this remains an empirical parameter for which little experimental validation data exists. A comparison between Scenarios 1A and 1B demonstrated that omitting the E_COEFFICIENT does produce a visible effect on the HRR evolution, although the influence on overall fire spread remained limited.

Overall, the most optimal sprinkler configuration was found to be Scenario 1, but with a minimum flow rate of 5 L/min/m² instead of 6.7 L/min/m². This conclusion is supported by the parametric study performed in Scenario 7, in which the flow rate was systematically reduced by adjusting the sprinkler K-factor. These results suggest that a minimum sprinkler installation designed according to current European standards and Belgian regulations is sufficient to prevent fire spread between multiple EVs when the initial vehicle fire originates from thermal runaway. This way, a catastrophic event in an (underground) parking can be avoided with a well designed sprinkler system.

The suppression efficiencies of the scenarios without ignition of neighbouring vehicles ranged between 86% and 96%. However, Scenario 2 demonstrated that fire spread may still occur at an efficiency level of approximately 81%. Although this scenario also applied a minimum flow rate of 5 L/min/m² and complied with the minimum European installation requirements (except for minimum pressure), it clearly indicates that not only flow rate, but also sprinkler location, spray angle, and operating pressure are critical design parameters.

Furthermore, ceiling-mounted sprinkler systems appear to be both more reliable and more realistically achievable than wall-mounted systems in underground parking applications.

Finally, the sprinkler activation temperature itself does not appear to be a dominant parameter, provided that the first sprinklers activate before the radiative heat flux exceeds 25 kW/m² at neighbouring vehicles or before window failure occurs.

5.1.2) Strengths and limitations

A key strength of CFD modelling lies in its ability to simulate multiple controllable scenarios in a cost-effective and repeatable manner. However, this thesis must critically acknowledge that FDS does not fully reproduce the complex dynamics of electric vehicle (EV) fires. This represents one of the most significant limitations of the present work. Therefore, the results provide an approximation of EV fire behaviour and should not be interpreted as definitive or fully representative predictions. A more suitable model simulation program is needed for the complex ignition and fire behaviour of battery packs.

FDS is fundamentally a low–Mach number CFD solver, optimized for buoyancy-driven fire and smoke transport. Thermal runaway jet flames, however, are highly transient phenomena governed by rapid pressure build-up, momentum-driven venting, and strong compressibility effects - none of which are explicitly resolved in FDS. Additional real-world effects such as intermittent venting, highly unsteady turbulent pulsations, and even localized explosion-like behaviour are therefore not fully captured. As a result, jet flames can only be represented in a highly simplified manner within the model.

The separate jet flame modelling showed that the flames became excessively buoyancy-dominated compared to experimental observations. This is not due to an overestimation of buoyancy, but rather the absence of competing physical mechanisms such as momentum-driven jetting and compressibility effects. Consequently:

- Flame impingement patterns may be inaccurate

- Jet flame penetration distances may be underestimated
- Localized heating may differ from real-world behaviour
- Local density fields may be distorted (and too low), introducing potential numerical errors

As a result, interactions between jet flames and neighbouring vehicles may not be fully captured, and the model should not be interpreted as a fully realistic representation of thermal runaway jet flame dynamics.

In addition, the chosen grid resolution of 10 cm is relatively coarse for resolving small-scale jet flame phenomena. This imposes a numerical constraint whereby vent areas must be at least 10 × 10 cm, whereas in reality vent openings can be significantly smaller. This discrepancy may influence the accuracy of localized flame development and jet behaviour.

Furthermore, results from the scenario analysis show that window breakage has a significant influence on whether fire spread occurs. In this model, window failure is simplified using a temperature device with a fixed activation threshold of 300 °C, after which the glass is removed from the simulation. In reality, glass failure is a far more complex process, governed by thermal gradients across the pane, material heterogeneity, and deformation of the surrounding frame. However, a sensitivity test scenario 1C with a lower activation threshold showed that the long-term results remain largely unchanged.

An additional limitation is that an EV fire is a chemically driven process initiated by a physical trigger. Representing this process using a surrogate fuel with a prescribed heat release rate (HRR) is therefore a simplification, and the model does not capture the battery's ability to internally generate oxygen during thermal runaway.

Furthermore, thermal runaway processes originate within the battery pack itself and can develop internally for several minutes before any external indicators such as visible smoke or flame become apparent. Experimental studies typically report this latent development phase to last approximately 6 to 20 minutes, during which significant internal degradation and heat accumulation occur without observable surface fire behaviour. This 'pre-time' is neglected in this study.

Moreover, the parameters SOOT_YIELD, RADIATIVE_FRACTION, and CO_YIELD are prescribed inputs in FDS that define combustion product composition and radiative energy distribution. The SOOT_YILED and RADIATIVE_FRACTION strongly influence fire development and spread, as soot is the primary driver of thermal radiation exchange. For instance, increasing soot yield significantly increases radiative heat transfer to surrounding combustible surfaces. Similarly, higher soot reduces the effective heat of combustion, thereby altering flame temperatures and the overall energy balance in the simulation.

A soot yield of 0.08 kg/kg lies within the range commonly reported for hydrocarbon-based and polymer-rich vehicle fires (approximately 0.05–0.15 kg/kg)[74], where combustion of interior plastics, insulation materials, and other synthetic components dominates smoke

[74] Hurley, M. J., Gottuk, D. T., Hall, J. R., Harada, K., Kuligowski, E., Puchovsky, M., Torero, J. L., Watts, J. M., & Wieczorek, C. (Eds.). (2016). *SFPE Handbook of Fire Protection Engineering* (5th ed.). Springer.

production and this value is conservative compared to typical experimental propane-based data. Nevertheless, further full-scale experimental studies of thermal runaway–induced EV fires are required to improve model fidelity and reduce uncertainty.

Furthermore, gas-phase combustion is modeled using a single-step, infinitely-fast reaction kinetics assumption (mixing-controlled combustion) using propane as a surrogate fuel. Importantly, the present FDS setup does not include an explicit gas-phase extinction sub-model (such as a critical flame temperature or strain-rate suppression limit). As a result, gas-phase flames cannot be extinguished purely through local flow strain or gas cooling, and extinguishment in the simulation occurs exclusively via surface cooling below specified extinction temperatures or through the empirical E_COEFFICIENT surface suppression parameter.

Finally, only a single representative parking layout was considered, limiting the generalizability of the results to other geometrical configurations.

Nevertheless, despite these limitations, the model is still capable of reproducing several key large-scale fire phenomena with reasonable accuracy, including:

- A progressively accelerating fire growth curve, consistent with experimental data sets.
- Thermal exposure between adjacent vehicles
- Multi-vehicle fire spread
- Sprinkler activation
- Water distribution effects
- Overall suppression behaviour

Finally, the modelling approach adopted in this thesis follows a systematic, step-by-step construction rather than a fully pre-built suppression scenario. This improves transparency and allows limitations to be identified more clearly. However, it also highlights that multiple simplifications were necessary to ensure computational feasibility. On the other hand, several of these simplified input parameters were intentionally chosen on the conservative side, meaning that the results are generally applicable to a wider range of parking configurations, including less critical scenarios. The model can therefore serve as a foundation for the development of a more advanced simulation framework, incorporating greater computational capacity and more detailed physical representations.

5.1.3) Further research recommendations

This study highlights several areas where further research is required to improve the understanding and modelling of electric vehicle (EV) fires in confined environments, particularly in sprinklered car parks.

5.1.3.1) Experimental validation of full-scale scenarios

The highest priority is validation of simulation results against **real-scale experimental data**, particularly in confined, sprinklered environments. A recommended next step is the execution of a full-scale test corresponding to Scenario 1A, involving three real EVs in a parking configuration. Such experiments would provide critical validation data for fire development, suppression effectiveness, and inter-vehicle fire spread under realistic boundary conditions.

5.1.3.2) Advanced CFD modelling of EV thermal runaway

The currently used CFD tool, FDS has limitations in accurately representing complex EV fire phenomena, including venting-driven jet flames and potential explosion-like behaviour (VCE). Further development or coupling of FDS with dedicated thermal runaway models is recommended. **An improved modelling framework** should ideally incorporate:

- Pressure-driven venting mechanisms
- Compressible or quasi-compressible flow behaviour
- Multi-phase gas release from battery cells
- Electrochemical degradation and cell-to-cell propagation models (for very detailed studies)

Such enhancements would significantly improve the physical realism of EV fire simulations. At present, FDS alone is insufficient to fully capture these coupled processes.

5.1.3.3) Smoke production and tenability analysis

This study primarily focused on fire spread; however, **toxic smoke production and movement** are equally critical for occupant safety and evacuation analysis. Further research is recommended into:

- Composition and yield of toxic gases from thermal runaway events
- Smoke layer development in confined parking structures (this can also influence the fire spread between vehicles)
- Impact on tenability conditions (visibility, toxicity, and temperature)
- Validation of smoke production models for EV-specific fires

Both experimental studies and improved numerical modelling approaches are needed in this area.

5.1.3.4) Scaling, geometry, and computational limitations

Future studies should extend the current work to **larger and more complex parking configurations**, including increased numbers of vehicles and multi-bay or multi-level structures. However, mesh resolution and computational constraints must be carefully addressed, as they significantly limit model scalability in high-resolution CFD simulations.

5.1.3.5) Improved incident data collection and classification

There is a need for more **reliable and structured data on EV fire incidents in Europe.** In particular, improved classification systems should distinguish between:

- Accident related fires
- Arson-related fires
- Thermal runaway–initiated fires

Better incident reporting would improve statistical reliability and support risk-based fire safety design. By establishing a reliable risk profile of TR fires, designers and supervisors can convincingly take more (or fewer) protective measures for both the car interior and the parking lot.

5.1.3.6) Experimental data of Car window failures

Since the breakage of the windows seems to be critical for the fire spread, further research into **car window failure mechanisms** under different thermal and mechanical loads could provide valuable insight. This includes exposing a car door with car glass to:

- Radiative heat flux thresholds
- Direct flames
- Pressure wave effects from potential (artificially induced) VCEs

Such experiments may offer a cost-effective alternative to full-scale vehicle fire tests while still providing relevant safety data.

5.1.3.7) Calibration of Heat Release Rate Suppression Factors in FDS for PBD

Additional research is needed into **appropriate E_COEFFICIENTs and related parameters used in FDS-based modelling for fire source cooling**. Improved calibration would allow more accurate representation of heat release rates (HRR) in performance-based design (PBD) studies, leading to more reliable fire safety assessments.

5.1.3.8) Future Research Directions on Electric Vehicle Fire Dynamics in Underground Parking Structures Beyond Flame Spread Analysis

Other relevant areas for future investigation include:

- Structural load investigations: EV fire dynamics in (**multi-storey parking) structures**, particularly under high HRR scenarios due to a multi-vehicle fire
- Interaction between EV fires and **charging infrastructure (EVSE systems)**
- Performance comparison in CFD of **different suppression strategies for EV**, including water mist, foam, and targeted cooling systems

5.2) Conclusion

This thesis demonstrates that **water-based sprinkler systems are highly effective** in mitigating large-scale fire propagation originating from electric vehicle (EV) battery thermal runaway events in enclosed parking structures using CFD. While the model is unable to suppress thermal runaway at the individual battery cell level, they significantly reduce overall fire severity, achieving up to an **82% reduction in peak heat release rate (PHRR)** for standard ceiling-mounted systems and up to **96% for high-intensity configurations compared to a free burning test with three vehicles**. A fundamental finding of this study is that **fire spread between adjacent vehicles is primarily driven by sustained thermal exposure** leading to window failure and the subsequent ignition of interior combustibles, rather than the high-velocity jet flames characteristic of lithium-ion battery fires. However, it should be noted that the representation of jet flames in the model is highly simplified.

The simulations indicate that an unsuppressed EV fire can rapidly escalate into a multi-vehicle catastrophe with a PHRR exceeding **18 MW**. However, sprinkler systems effectively act as a **thermal shield**, forming a water film over the windows of neighboring vehicles that prevents or at least delays their breakage.

This protective mechanism is sufficiently robust that a system designed in accordance with the **minimum European standard (5 L/min/m²) can effectively prevent fire spread between multiple electric vehicles.** However, the results also demonstrate that alternative sprinkler configurations play a significant role. In particular, the model shows that a sprinkler system with **an operating pressure of 1 bar, K-factor of 80, a droplet diameter of 1000 µm, an RTI of 100, an activation temperature of 68°C, a spacing of 3.5 × 3.4 m, ceiling-mounted installation, a spray angle of 30°–90°, and a droplet velocity of 10 m/s** provides a representative case for evaluating suppression performance.

Furthermore, **ceiling-mounted sprinklers were found to be more reliable** and realistically achievable than wall-mounted configurations, which required specific optimizations in droplet velocity and spray angle to achieve sufficient coverage.

Despite the inherent limitations of Fire Dynamics Simulator (FDS) as a low-Mach-number solver - resulting in simplified, more buoyancy-dominated jet flames -the model successfully captured the **critical interaction between water application and thermal exposure**. These findings provide a scientifically supported basis for fire safety design in modern parking environments. Nevertheless, **full-scale experimental validation** remains the highest priority for future research to confirm these numerical results, alongside more detailed investigations into the mechanisms of car window failure under combined thermal and mechanical loads. The outcome contributes to the fact that with a well-designed sprinkler protection, the potentially catastrophic risks associated with increasing EV adoption in underground structures can be effectively managed.

Part 6: Reference List & Annexes

6.1) Reference list

1. Angeline, P. S., & Rajkumar, M. N. (2020). Evolution of electric vehicle and its future scope. Materials Today Proceedings, 33, 3930–3936. https://doi.org/10.1016/j.matpr.2020.06.266
2. Basics of Sprinkler Thermal Characteristics | NFPA. (2021, June 22). https://www.nfpa.org/news-blogs-and-articles/blogs/2021/06/22/the-basics-of-sprinkler-thermal-characteristics
3. Cui, Y., Liu, J., Cong, B., Han, X., & Yin, S. (2022). Characterization and assessment of fire evolution process of electric vehicles placed in parallel. Process Safety and Environmental Protection, 166, 524–534. https://doi.org/10.1016/j.psep.2022.08.055
4. Ditch, B., FM Global, Zeng, D., & FM Global. (2019). Development of sprinkler protection guidance for lithium ion based energy storage systems. FM Global. https://www.researchgate.net/publication/333653116
5. Druk in de woning altijd voldoende | De Watergroep. (n.d.). De Watergroep. https://www.dewatergroep.be/nl-be/drinkwater/veelgestelde-vragen/binneninstallatie/is-de-druk-in-mijn-woning-altijd-voldoende
6. Electric vehicle fires on ships & ferries. (2025a, January 28). EV Fire Safe. https://www.evfiresafe.com/post/electric-vehicle-fires-on-ships-ferries
7. Electric vehicle fires on ships & ferries. (2025b, January 28). EV Fire Safe. https://www.evfiresafe.com/post/electric-vehicle-fires-on-ships-ferries
8. Eurostat. (2024, August 2). 1.5 million new battery-only electric cars in 2023. Eurostat. https://ec.europa.eu/eurostat/web/products-eurostat-news/w/ddn-20240802-1#:~:text=In%202023%2C%201.5%20million%20new,passenger%20cars%20in%20the%20EU.&text=When%20it%20comes%20to%20the,Poland%2C%20each%20at%200.2%25.
9. Eurostat. (2026). Passenger cars in the EU. Statistics Explained. https://ec.europa.eu/eurostat/statistics-explained/SEPDF/cache/25886.pdf
10. Fire destroys 200 cars in Swedish car park – European Fire Sprinkler Network. (n.d.). https://www.eurosprinkler.org/fire-destroys-200-cars-in-swedish-car-park/

11. George, J. (2023). Analysis of electric vehicle fire risks in car parks. In The University of Edinburgh, Master thesis submitted in the Erasmus+ Study Programme International Master of Science in Fire Safety Engineering.
12. Heinisuo, M., Partanen, M., Tampereen teknillinen yliopisto. Rakennustekniikan laitos. Rakennetekniikka, & Tampere University of Technology. Department of Civil Engineering. Structural Engineering. (2013). Modeling of Car Fires with Sprinklers. In Tampere University of Technology. Department of Civil Engineering (Research Report No. 161; p. 1).
13. How does a lithium-Ion battery work? (2019, September 23). Let's Talk Science. https://letstalkscience.ca/educational-resources/stem-explained/how-does-a-lithium-ion-battery-work
14. Hynynen, J., Willstrand, O., Blomqvist, P., & Andersson, P. (2023). Analysis of combustion gases from large-scale electric vehicle fire tests. Fire Safety Journal, 139, 103829. https://doi.org/10.1016/j.firesaf.2023.103829
15. Industrial VRLA Battery Safety Valve. (n.d.). http://www.oursun-power.com/product-industrial-vrla-battery-safety-valve.html
16. Jia, Z., Min, Y., Qin, P., Mei, W., Meng, X., Jin, K., Sun, J., & Wang, Q. (2023). Effect of safety valve types on the gas venting behavior and thermal runaway hazard severity of large-format prismatic lithium iron phosphate batteries. Journal of Energy Chemistry, 89, 195–207. https://doi.org/10.1016/j.jechem.2023.09.052
17. Johansson, N., Anderson, J., McNamee, R., & Pelo, C. (2020). A Round Robin of fire modelling for performance‐based design. Fire and Materials, 45(8), 985–998. https://doi.org/10.1002/fam.2891
18. Kang, S., Kwon, M., Choi, J. Y., Sengkwan Choi, Fire Testing & Research Centre, Fire & Disaster Management Division, Korea Conformity Laboratories, Republic of Korea, Advanced Functional Nanohybrid Material Laboratory, Department of Chemistry, Dongkuk University, Republic of Korea, & School of the Built Environment, Ulster University, UK. (2023). Full-scale fire testing of battery electric vehicles [Journal-article]. Applied Energy, 332, 120497. https://doi.org/10.1016/j.apenergy.2022.120497
19. Linton, M. (2026, February 8). Sprinkler Temperature Ratings Explained. Choosing the Right Rating for the Right Environment — Fortis fire. Fortis Fire. https://www.fortisfire.co.nz/insights/sprinkler-temperature-ratings
20. Lyon, R. E., & Walters, R. N. (2016). Energy release by rechargeable Lithium-Ion batteries in thermal runaway (By Federal Aviation Administration; Technical Note

DOT/FAA/TC-TN16/22; p. 26). Federal Aviation Administration. https://actlibrary.tc.faa.gov

21. New car registrations: -2.6% in January 2025; battery-electric 15% market share. (2025, February 28). ACEA - European Automobile Manufacturers' Association. https://www.acea.auto/pc-registrations/new-car-registrations-2-6-in-january-2025-battery-electric-15-market-share/
22. Parking garages and EVs. (2024b, July 12). https://www.nfpa.org/news-blogs-and-articles/blogs/2024/07/12/parking-garages-and-evs
23. Pastor, J. V., García, A., Monsalve-Serrano, J., & Golke, D. (2023). Analysis of the aging effects on the thermal runaway characteristics of Lithium-Ion cells through stepwise reactions. Applied Thermal Engineering, 230, 120685. https://doi.org/10.1016/j.applthermaleng.2023.120685
24. Precision Drive Systems. (2022). Elevator doors – more than just open and close. In Maxon – a Strong Global Brand (p. 2).
25. Pressure relief valves for Lithium-Ion battery packs that are reclosable, with high flow-rate, for multi-use | Nifco. (n.d.-a). Nifco. https://www.nifco.com/en/products/news/detail/kv9ihm0000000s2v.html
26. Promat. (n.d.). FIRE PROTECTION SOLUTIONS FOR EV CHARGING ZONES IN CAR PARKS. In WWW.PROMAT.COM (pp. 3–4).
27. Sheppard, D. T., & Lueptow, R. M. (2005). Characterization of fire sprinkler sprays using particle image velocimetry. Atomization and Sprays, 15(3), 341–362. https://doi.org/10.1615/atomizspr.v15.i3.50
28. Restuccia, F. (2025). A perspective on lithium-ion battery fire safety: from experiments to modelling approaches. Journal of Physics Conference Series, 3121(1), 012048. https://doi.org/10.1088/1742-6596/3121/1/012048
29. Ribière, P., Grugeon, S., Morcrette, M., Boyanov, S., Laruelle, S., & Marlair, G. (2011a). Investigation on the fire-induced hazards of Li-ion battery cells by fire calorimetry. Energy & Environmental Science, 5(1), 5271–5280. https://doi.org/10.1039/c1ee02218k
30. Sun, P., Huang, X., Research Centre for Fire Engineering, Hong Kong Polytechnic University, Bisschop, R., Department of Fire Research, RISE Research Institutes of Sweden, Niu, H., & Guangzhou Industrial Technology Research Institute, Chinese Academy of Sciences. (2020). A review of battery fires in electric vehicles. In Fire

Technology (Vols. 56–56, pp. 1361–1410) [Journal-article]. Springer Science+Business Media, LLC. https://doi.org/10.1007/s10694-019-00944-3

31. Tohir, M. Z. M., & Martín-Gómez, C. (2025). Evaluating fire severity in electric vehicles and internal combustion engine vehicles: A statistical approach to heat release rates. Fire Technology, 61(5), 2957–2998. https://doi.org/10.1007/s10694-025-01711-3
32. Veritasium. (2025, August 7). The perfect battery material is dangerous [Video]. YouTube. https://www.youtube.com/watch?v=AGglJehON5g
33. Wat is de snelheid van een lift en roltrap? - KONE België & Luxemburg. (n.d.). KONE België En Luxemburg. https://www.kone.be/nl/tools-downloads/faq/snelheid-lift-roltrap.aspx
34. Water mist Systems Overview | NFPA. (2022, June 24). https://www.nfpa.org/news-blogs-and-articles/blogs/2022/06/24/water-mist-systems-overview
35. Xie, L., & Liu, B. (2022). Electric vehicle battery charging interference intelligent protection device. Journal of Physics Conference Series, 2310(1), 012046. https://doi.org/10.1088/1742-6596/2310/1/012046
36. Yu, Lee, en Kung (1994). Suppression of Rack-Storage Fires by Water."
37. Zhao, C., Hu, W., Meng, D., Mi, W., Wang, X., & Wang, J. (2023a). Full-scale experimental study of the characteristics of electric vehicle fires process and response measures. Case Studies in Thermal Engineering, 53, 103889. https://doi.org/10.1016/j.csite.2023.103889
38. Zhong, G., Mao, B., Wang, C., Jiang, L., Xu, K., Sun, J., & Wang, Q. (2018). Thermal runaway and fire behavior investigation of lithium ion batteries using modified cone calorimeter. Journal of Thermal Analysis and Calorimetry, 135(5), 2879–2889. https://doi.org/10.1007/s10973-018-7599-7

6.2) Annexes

6.2.1) Annex A: EV vs ICE

	EV	ICE
Fuel Source	Lithium-ion batteries	Gasoline
Fire Causes	Short circuit, puncture, overheating, overcharging, over-discharging	Fuel or oil leak, overheating, worn out parts, loose electrical components
Suppression Time	~60–90+ min	~30 min
Water Usage (manual)	Reports of up to thousands of gallons of water have been used, requiring sustained water supply	~500 gallons
Reignition Potential	Likely, and fairly common	Rare
Fire Size	Avg Heat Release Rate: 1.5–8+ MW Avg Total Heat Release: 5.9 GJ Can be large if the initiating vehicle fire is allowed to propagate to an adjacent vehicle, but fires can typically be contained to one vehicle with protection by automatic sprinklers or intervention by the fire service prior to spread	Avg Heat Release Rate: 6.5–8 MW Avg Total Heat Release: 5.9 GJ Can be large if the initiating vehicle fire is allowed to propagate to an adjacent vehicle, but fires can typically be contained to one vehicle with protection by automatic sprinklers or intervention by the fire service prior to spread
Toxicity of Runoff	Water runoff has a pH of 7.3–7.7 Copper, antimony, and higher concentrations of manganese, nickel, cobalt, hydrogen fluoride, and lithium	Water runoff has a pH of 2.6–2.8 Higher concentrations of lead, copper, polycyclic aromatic hydrocarbons, and volatile organic compounds, testing showed higher toxicity towards aquatic species
Special Post-Fire Considerations	Often towed and recommended to be placed 50 ft away from all surroundings (due to reignition risk)	Vehicles/engines should be inspected to see how much damage was done to determine if repairs can occur
Additional Hazards	Stranded energy (reignition risk), electrocution risk, handling by secondary responders, projectiles and explosions, toxic gas release	Toxic gas release, lots of combustible fuel still accessible to the fire (i.e., a full gas tank)

[75]

[75] *Parking garages and EVs*. (2024, July 12). https://www.nfpa.org/news-blogs-and-articles/blogs/2024/07/12/parking-garages-and-evs

6.2.2) Annex B: Jet flame visualisation

Note: The distances shown on the visualisations are 0.5m, 1 m and 1.5 m; The temperature scale is from 15°C till 365°C; From the color shade strong green, the temperature is higher than 130°C, and a TR can occur with sufficiently long exposure; A car is typically parked 0.5m from the next car; A clear distinguishable jet flame in experimental results supposed to be around 1.5 to 3 meters with a temperature from at least 500°C.

Jet flame 1: Base Case

```
&SURF ID='JET_1',  SPEC_ID(1) = 'PROPANE',  MASS_FRACTION(1) = 0.06, RAMP_V = 'JET_ACT', VEL = -40.0, TMP_FRONT = 900.0,    COLOR = 'ORANGE' /

&RAMP ID='JET_ACT', T=5.0, F=0.0 /
&RAMP ID='JET_ACT', T=6, F=1.0 /
&RAMP ID='JET_ACT', T=15, F=0.7 /
&RAMP ID='JET_ACT', T=16, F=0.0 /

&VENT ID='Jet_Flame_1', SURF_ID='JET_1',XB=0.8,0.9, 0.2,0.2, 0.3,0.4, IOR=-2 /
```

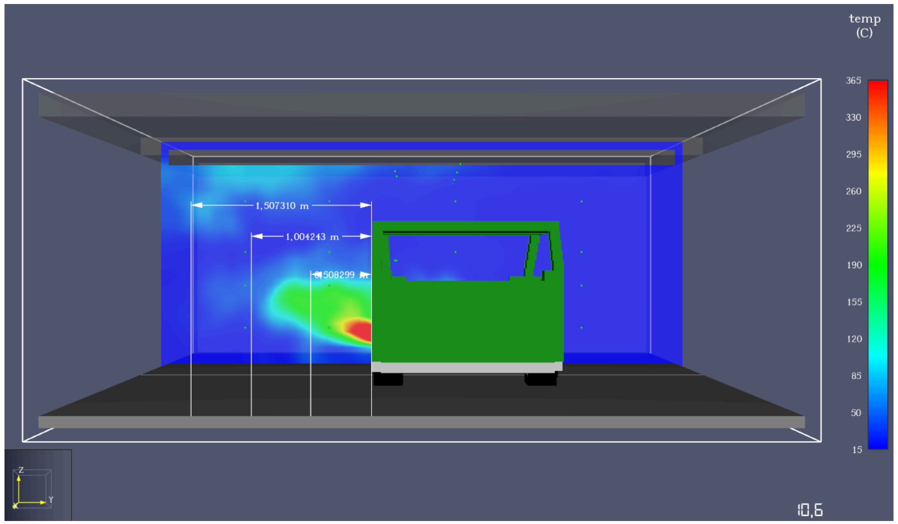

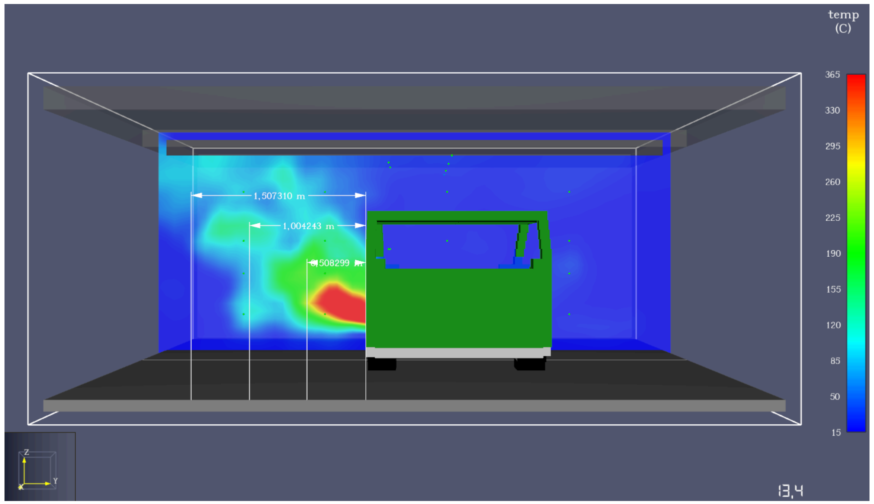

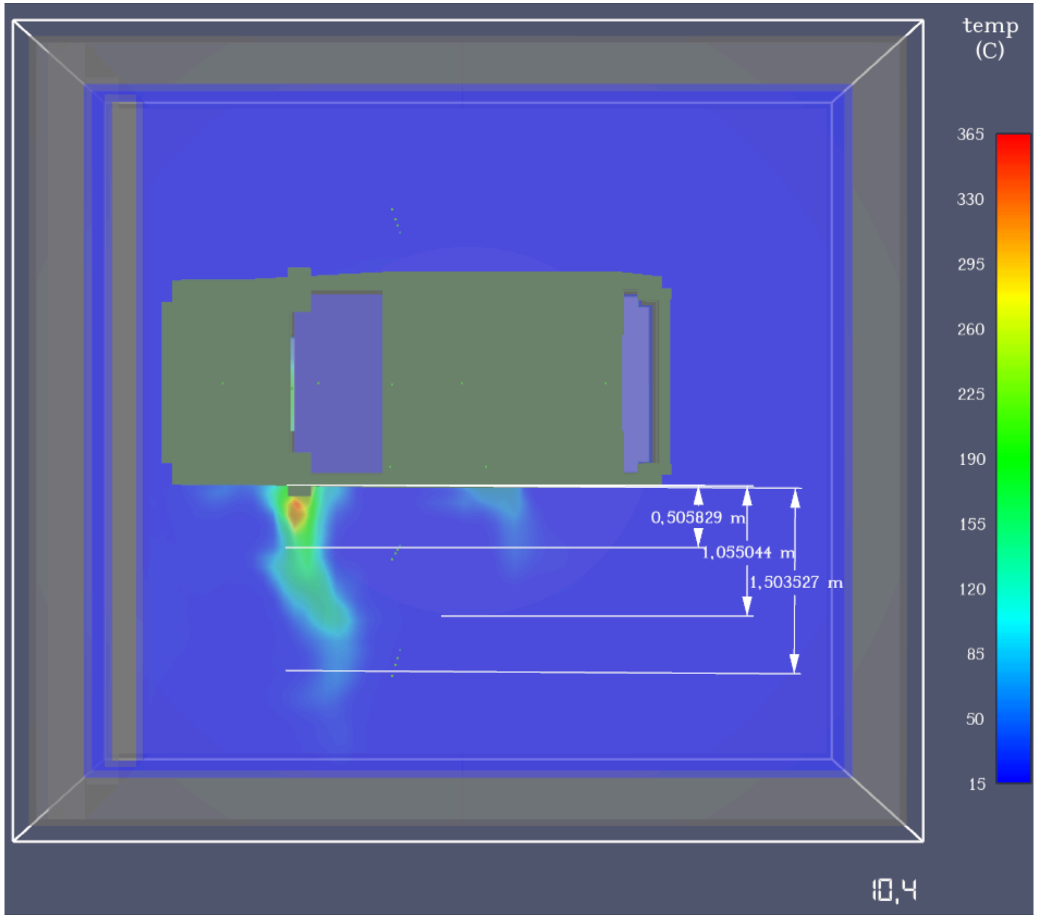temp
(C)
365
330
295
260
225
190
155
120
85
50
15
0,505829 m
1,055044 m
1,503527 m
10,4	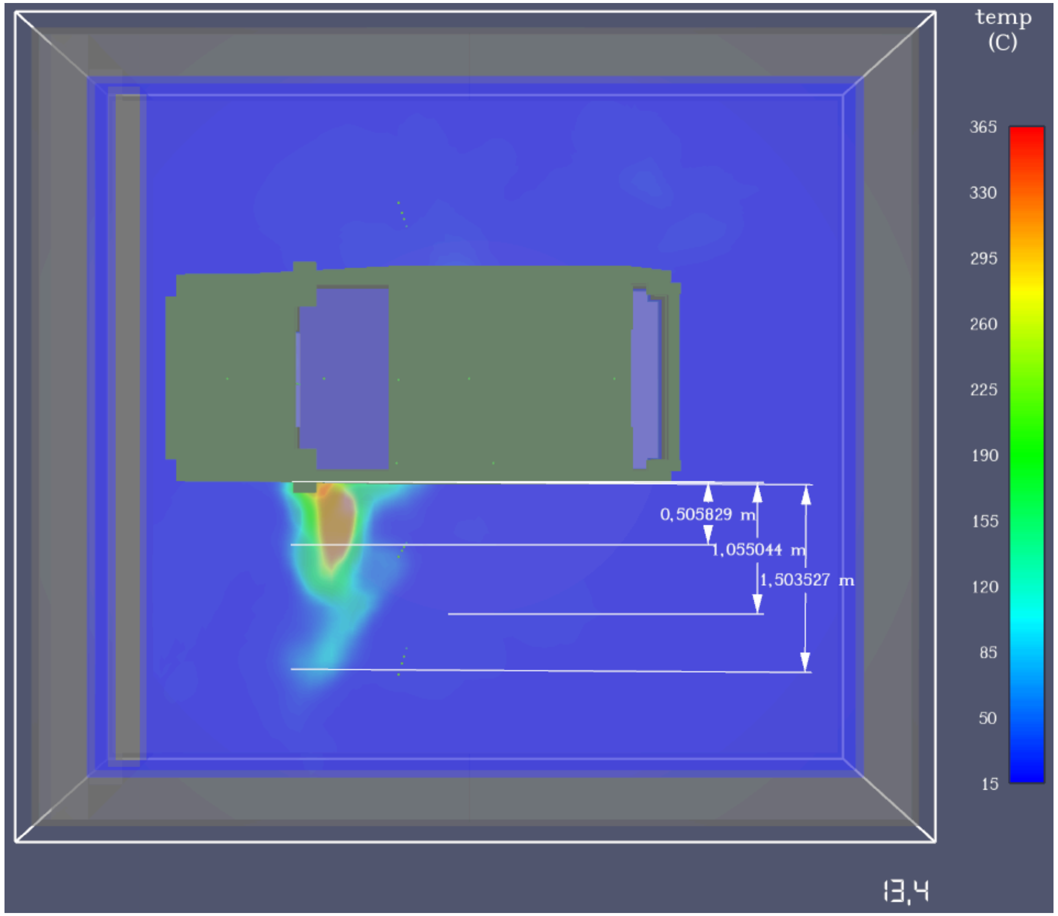temp
(C)
365
330
295
260
225
190
155
120
85
50
15
0,505829 m
1,055044 m
1,503527 m
13,4

Jet flame 2: Velocity +50%

&SURF ID='JET_2', SPEC_ID(1) = 'PROPANE', MASS_FRACTION(1) = 0.04, RAMP_V = 'JET_ACT_2', VEL = -60.0, TMP_FRONT = 900.0, COLOR = 'ORANGE' /

&RAMP ID='JET_ACT_2', T=20.0, F=0.0 /
&RAMP ID='JET_ACT_2', T=21, F=1.0 /
&RAMP ID='JET_ACT_2', T=30, F=0.7 /
&RAMP ID='JET_ACT_2', T=31, F=0.0 /

&VENT ID='Jet_Flame_2', SURF_ID='JET_2',XB=0.9,1.0, 0.2,0.2, 0.3,0.4, IOR=-2 /

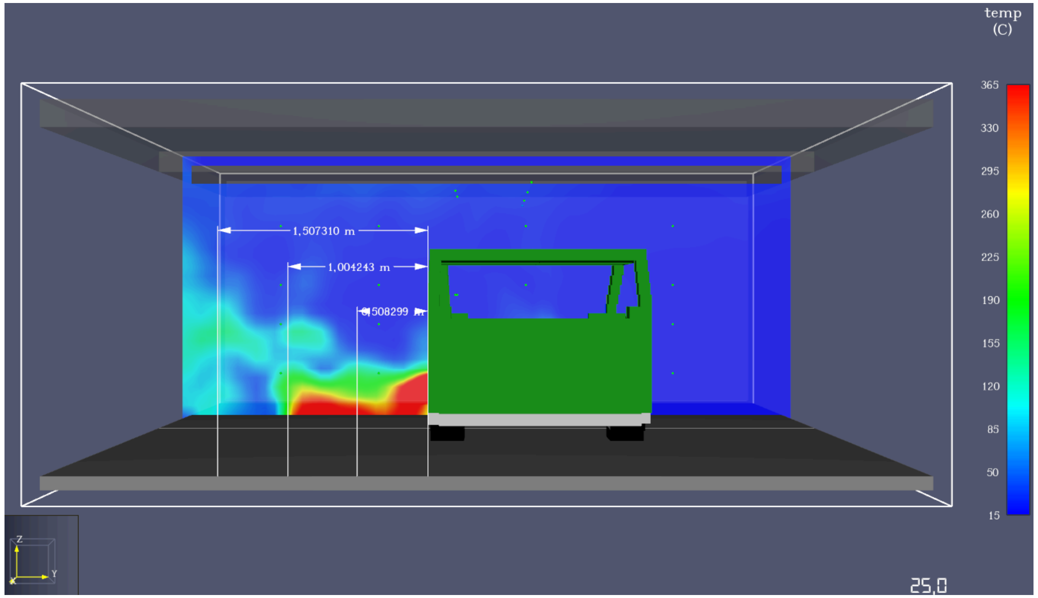

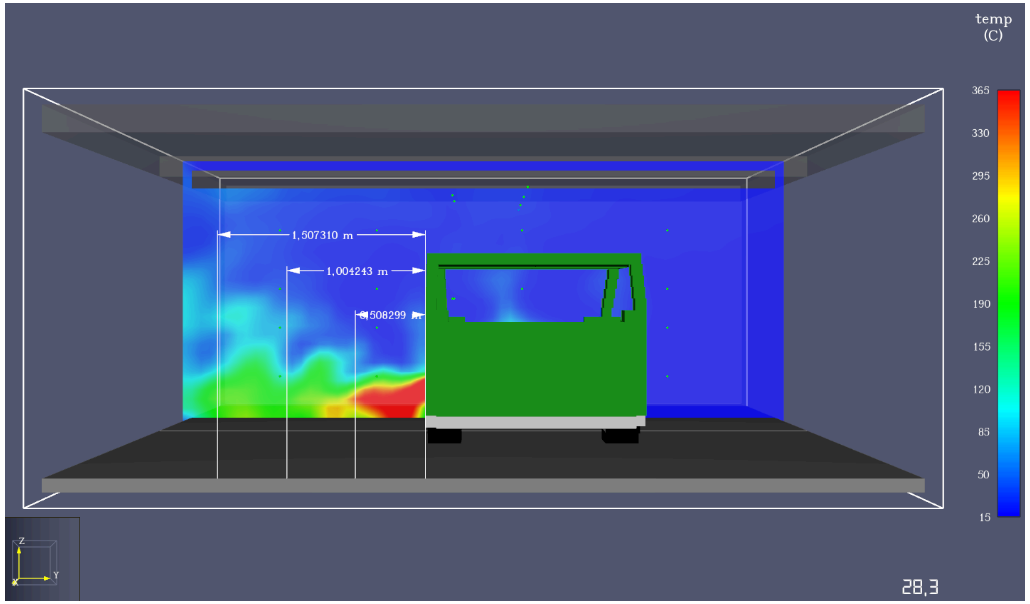

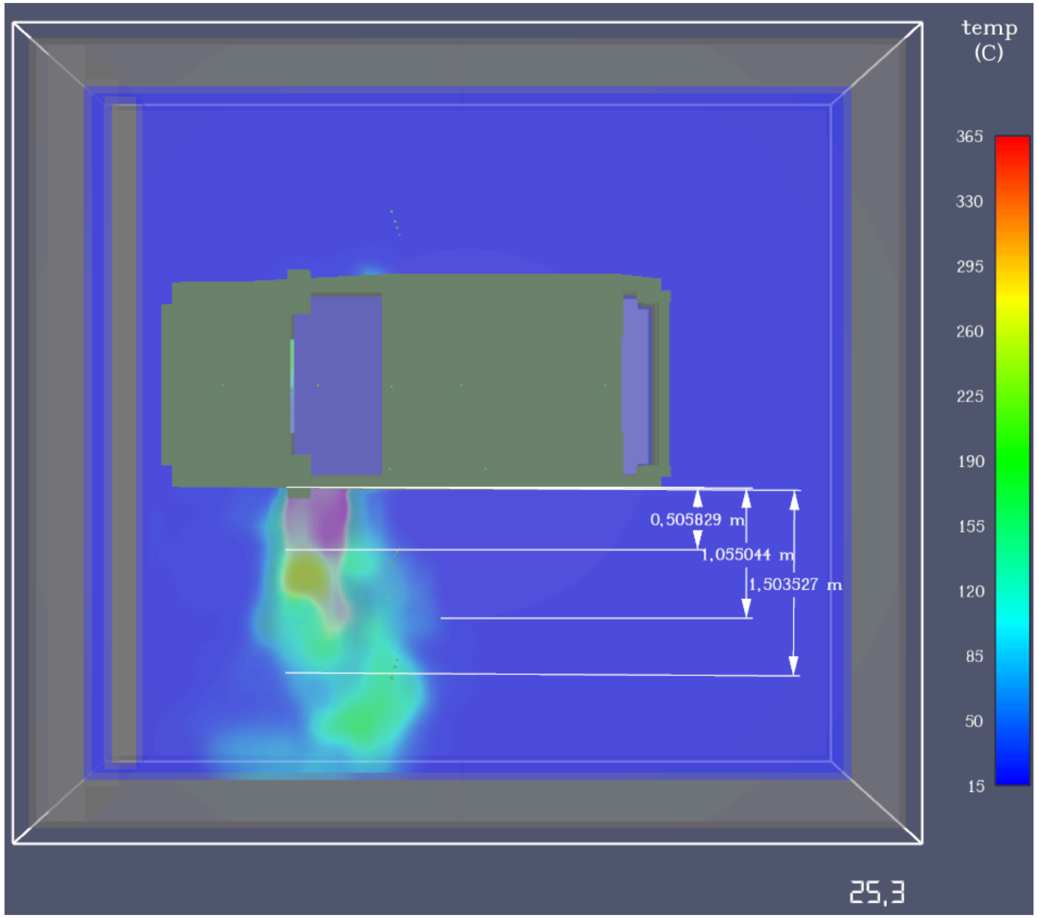
temp
(C)
365
330
295
260
225
190
155
120
85
50
15
0,505829 m
1,055044 m
1,503527 m
25,3

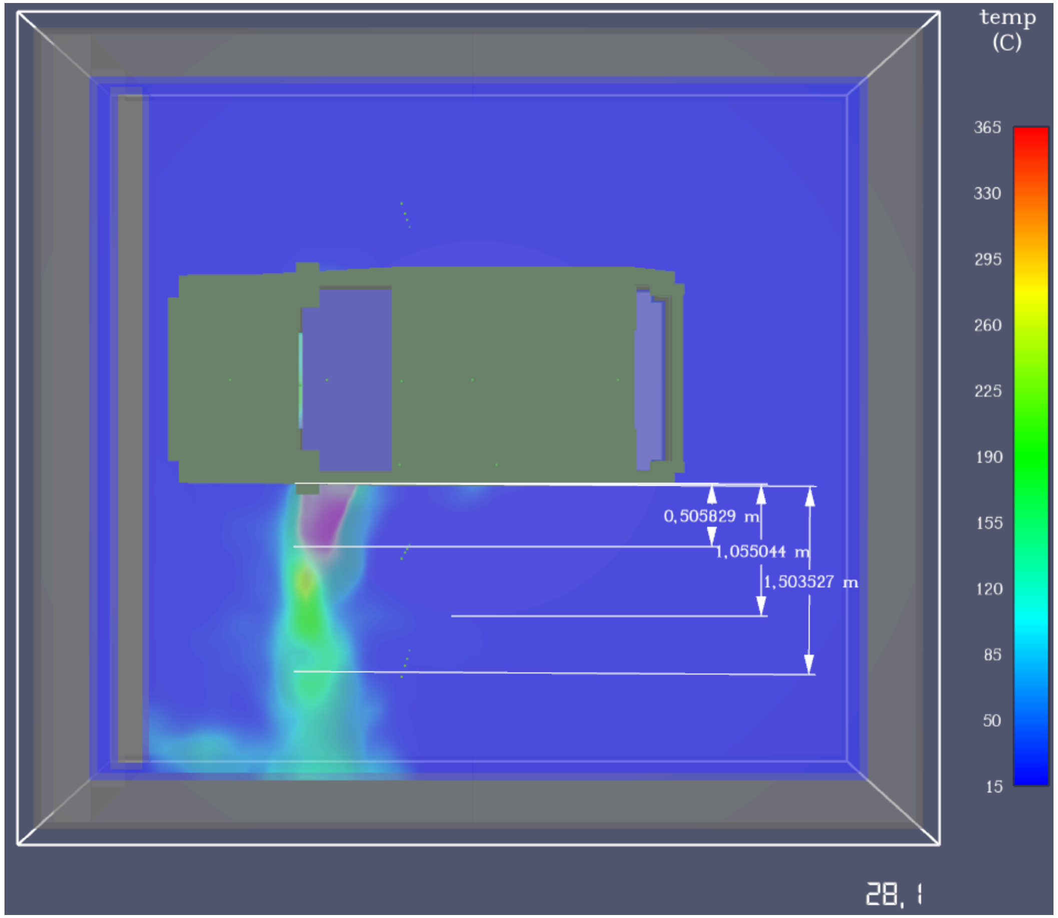
temp
(C)
365
330
295
260
225
190
155
120
85
50
15
0,505829 m
1,055044 m
1,503527 m
28,1

Jet flame 3: Velocity +100%	
&SURF ID='JET_3', SPEC_ID(1) = 'PROPANE', MASS_FRACTION(1) = 0.03, RAMP_V = 'JET_ACT_3', VEL = -80.0, TMP_FRONT = 900.0, COLOR = 'ORANGE' / &RAMP ID='JET_ACT_3', T=35.0, F=0.0 / &RAMP ID='JET_ACT_3', T=36, F=1.0 / &RAMP ID='JET_ACT_3', T=45, F=0.7 / &RAMP ID='JET_ACT_3', T=46, F=0.0 / &VENT ID='Jet_Flame_3', SURF_ID='JET_3',XB=1.0,1.1, 0.2,0.2, 0.3,0.4, IOR=-2 /	
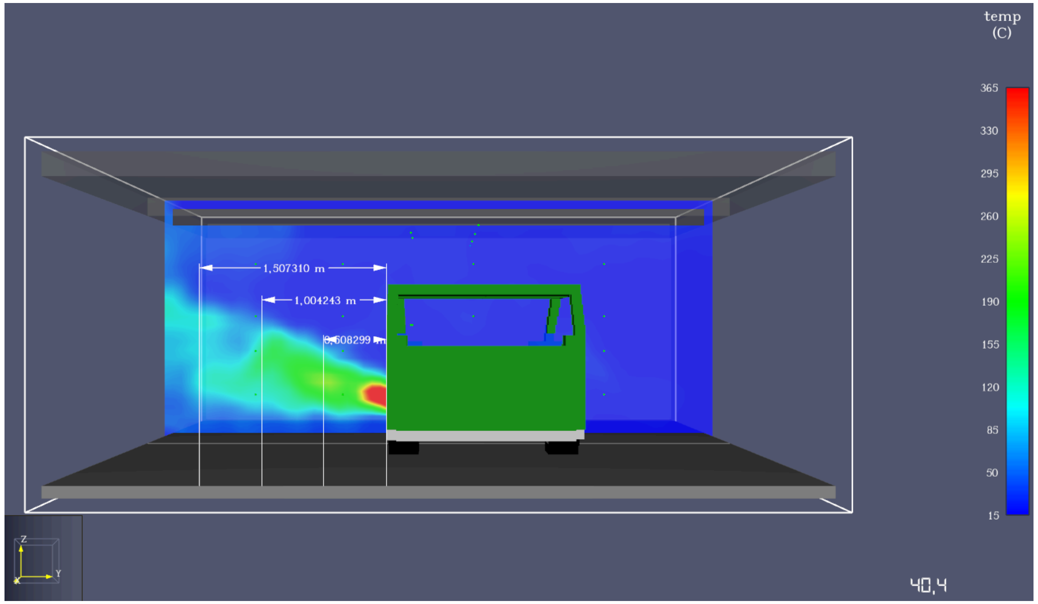	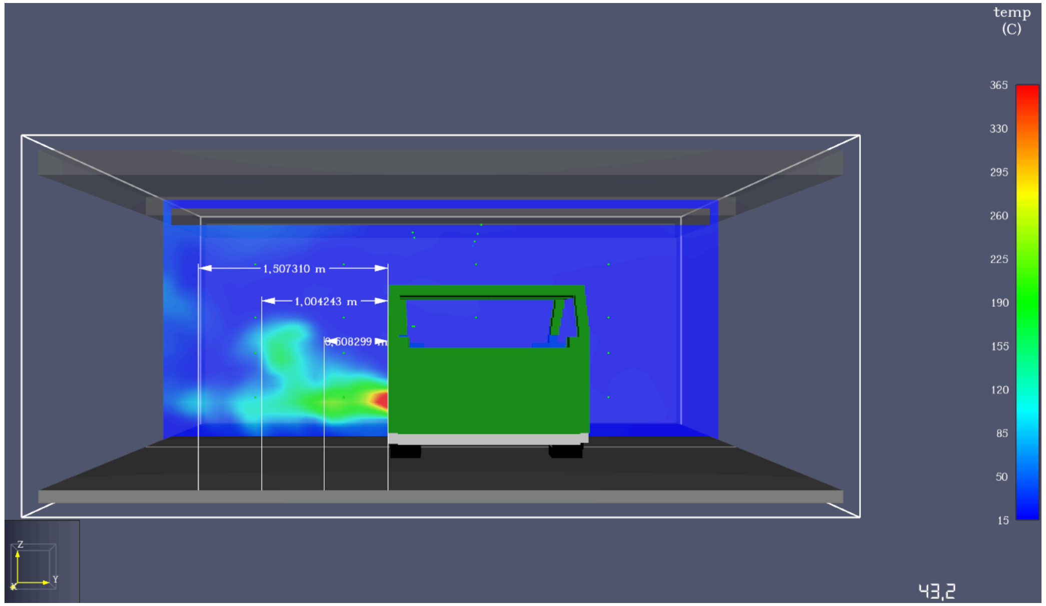

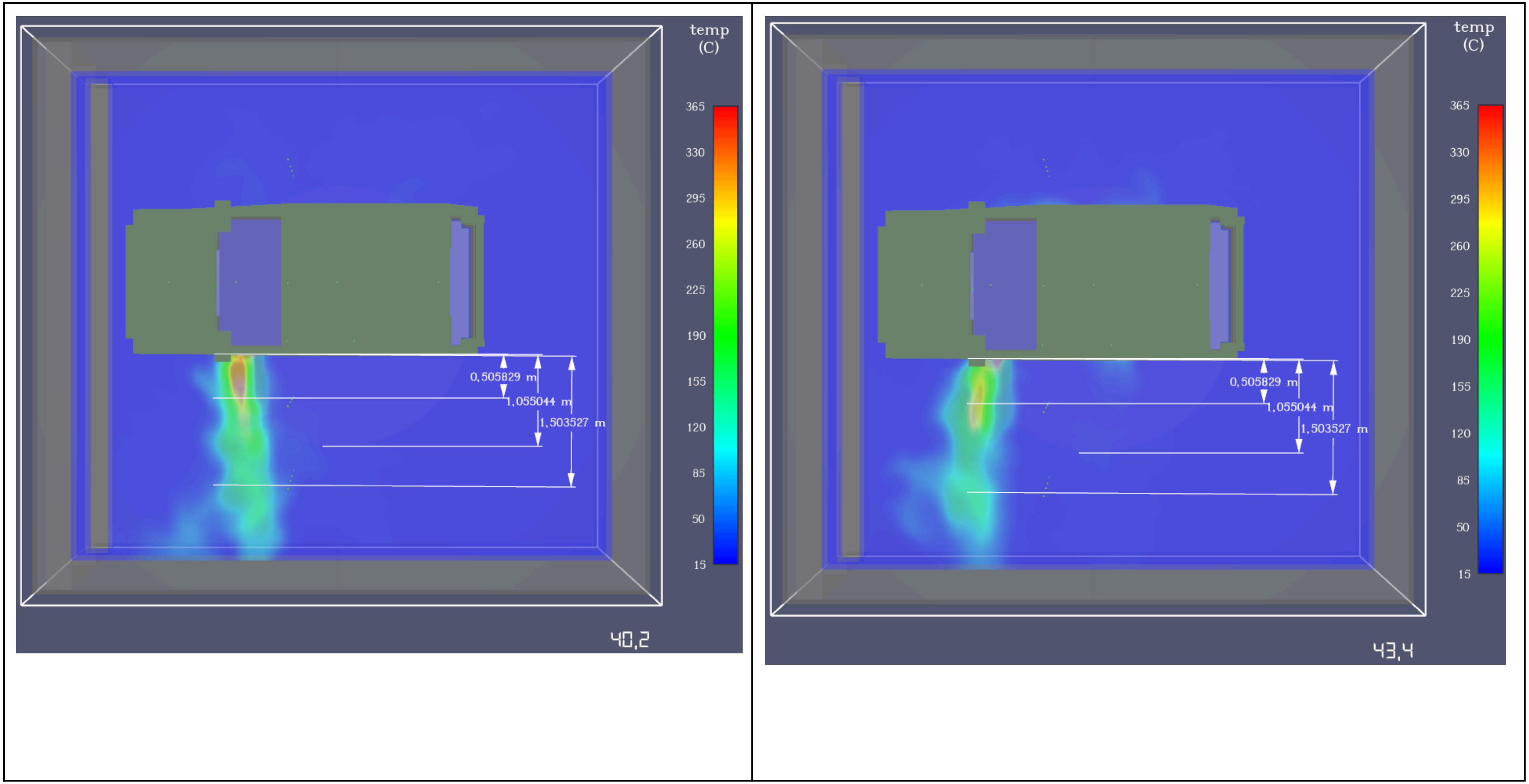
temp
(C)
365
330
295
260
225
190
155
120
85
50
15
0,505829 m
1,055044 m
1,503527 m
40,2
temp
(C)
365
330
295
260
225
190
155
120
85
50
15
0,505829 m
1,055044 m
1,503527 m
43,4

Jet flame 4: Velocity -50%	

```
&SURF ID='JET_4',
     SPEC_ID(1) = 'PROPANE',
     MASS_FRACTION(1) = 0.12,
     RAMP_V = 'JET_ACT_4',
     VEL = -20.0,
     TMP_FRONT = 900.0,
     COLOR = 'ORANGE' /

&RAMP ID='JET_ACT_4', T=50.0, F=0.0 /
&RAMP ID='JET_ACT_4', T=51, F=1.0 /
&RAMP ID='JET_ACT_4', T=60, F=0.7 /
&RAMP ID='JET_ACT_4', T=61, F=0.0 /

&VENT ID='Jet_Flame_4', SURF_ID='JET_4',XB=1.1,1.3, 0.2,0.2, 0.3,0.4, IOR=-2 /
```

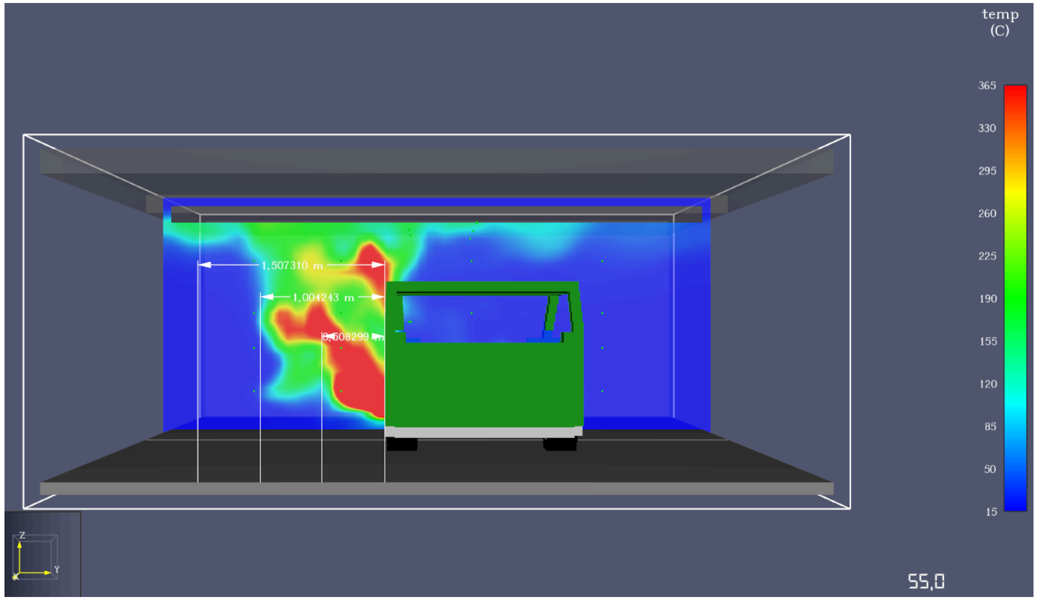
temp
(C)
365
330
295
260
225
190
155
120
85
50
15
1,507310 m
1,004243 m
55,0

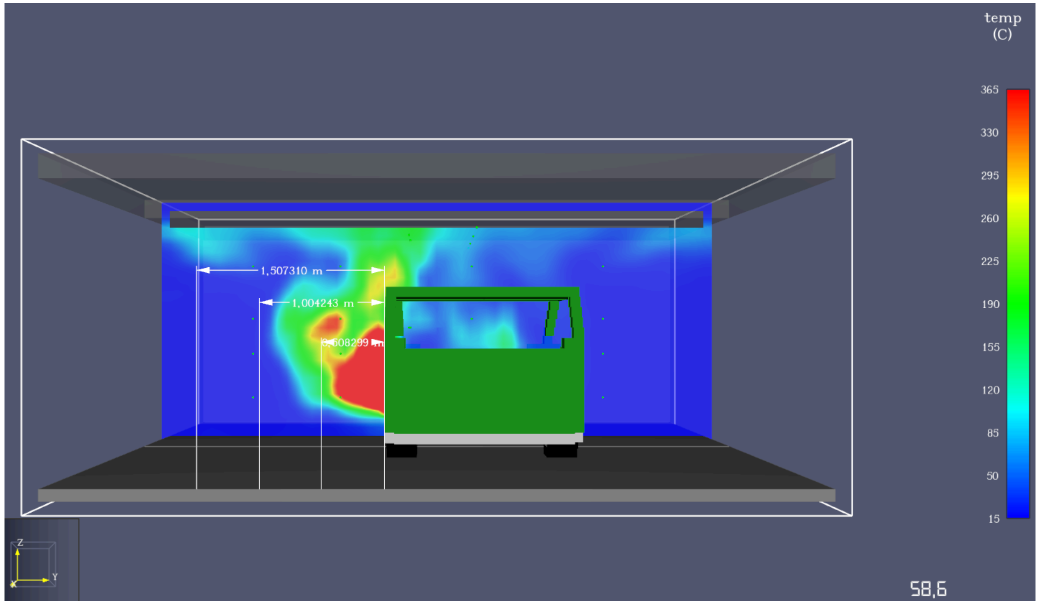
temp
(C)
365
330
295
260
225
190
155
120
85
50
15
1,507310 m
1,004243 m
58,6

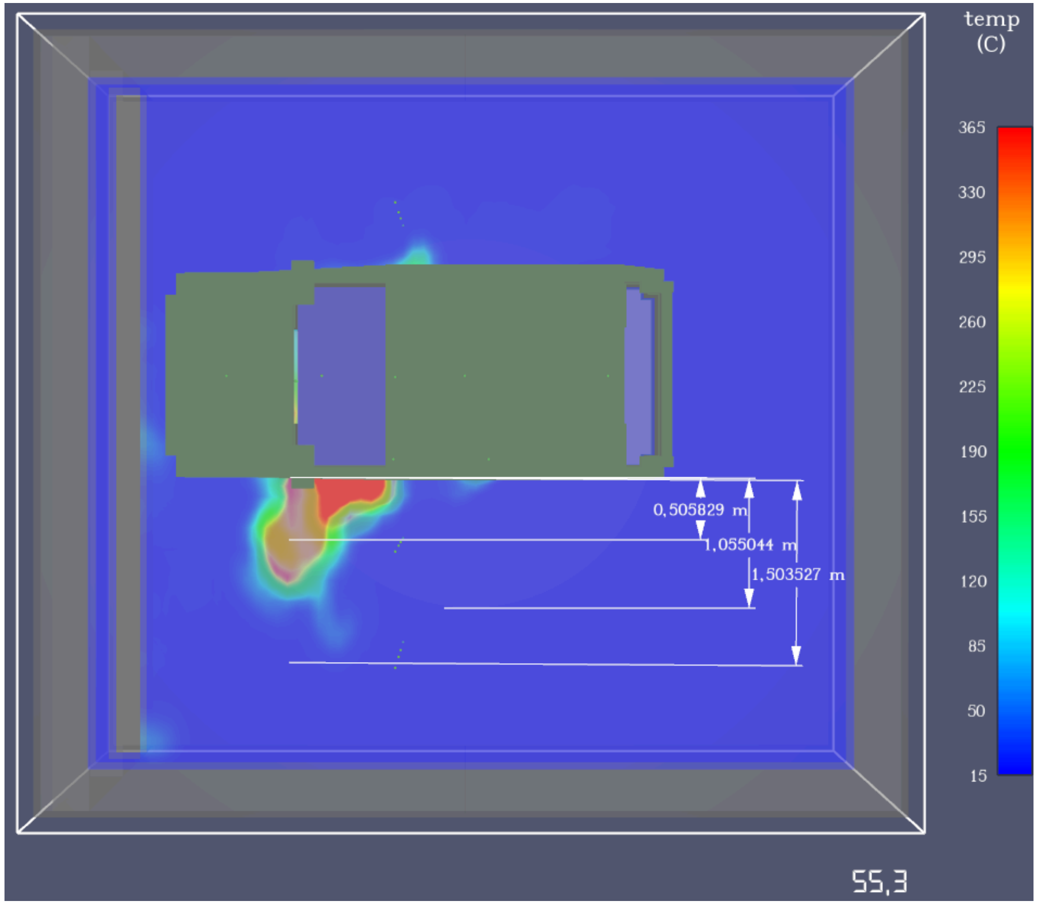
temp
(C)
365
330
295
260
225
190
155
120
85
50
15
0,505829 m
1,055044 m
1,503527 m
55,3

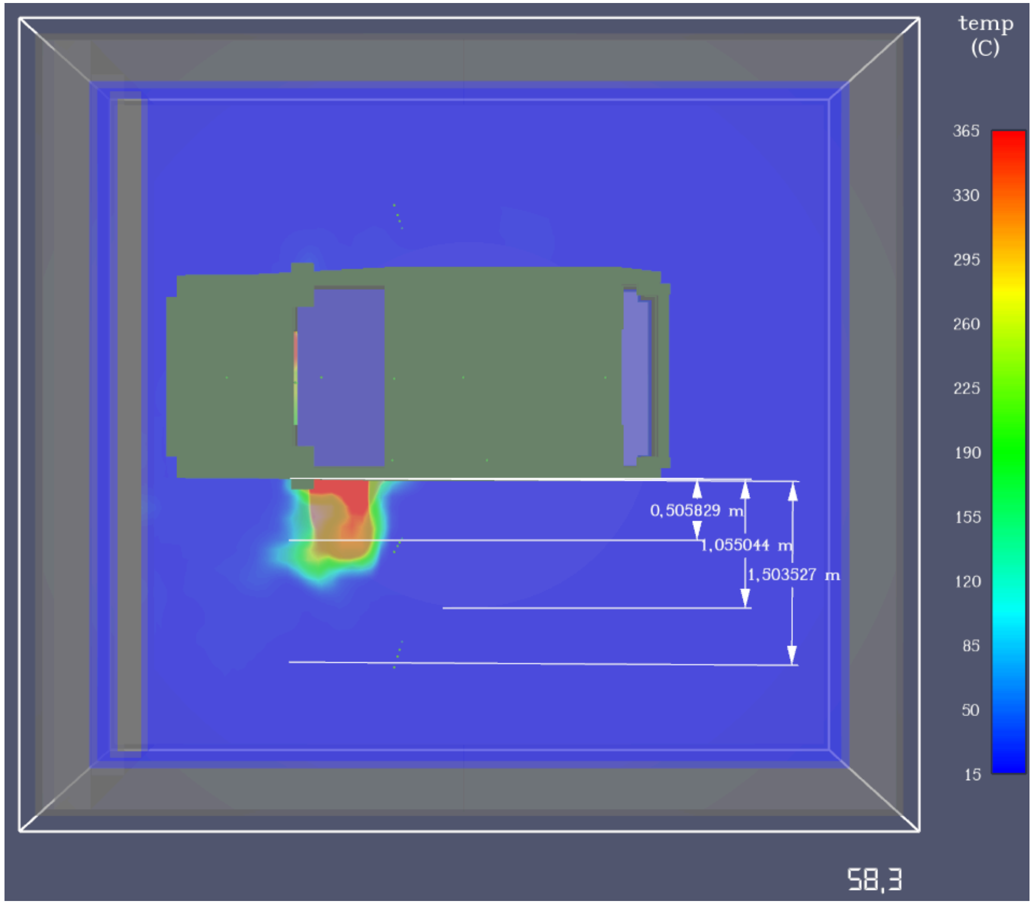
temp
(C)
365
330
295
260
225
190
155
120
85
50
15
0,505829 m
1,055044 m
1,503527 m
58,3

Jet flame 4_1: Velocity -25%

```
&SURF ID='JET_4_1',
     SPEC_ID(1) = 'PROPANE',
     MASS_FRACTION(1) = 0.08,
     RAMP_V = 'JET_ACT_4_1',
     VEL = -30.0,
     TMP_FRONT = 900.0,
     COLOR = 'ORANGE' /

&RAMP ID='JET_ACT_4_1', T=215.0, F=0.0 /
&RAMP ID='JET_ACT_4_1', T=216, F=1.0 /
&RAMP ID='JET_ACT_4_1', T=225, F=0.7 /
&RAMP ID='JET_ACT_4_1', T=226, F=0.0 /

&VENT ID='Jet_Flame_4_1', SURF_ID='JET_4_1',XB=2.6,2.7, 0.2,0.2, 0.3,0.4, IOR=-2 /
```

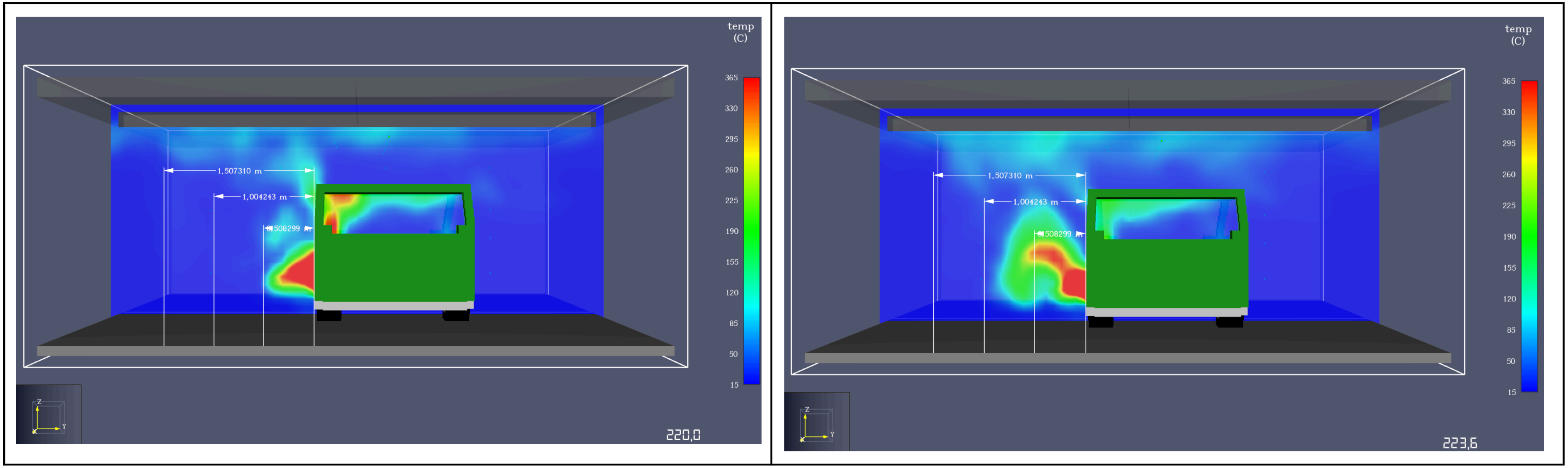
temp
(C)
365
330
295
260
225
190
155
120
85
50
15
1,507310 m
1,004243 m
220,0
223,6

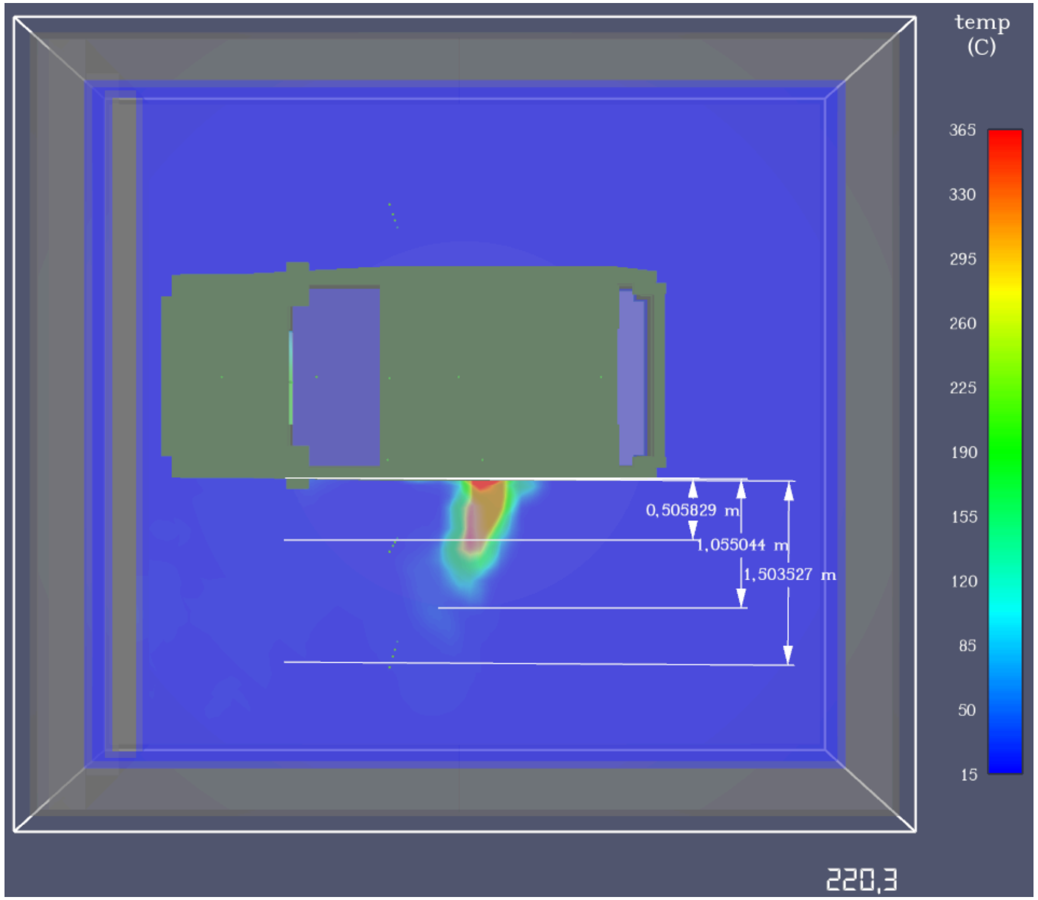temp
(C)
365
330
295
260
225
190
155
120
85
50
15
0,505829 m
1,055044 m
1,503527 m
220,3	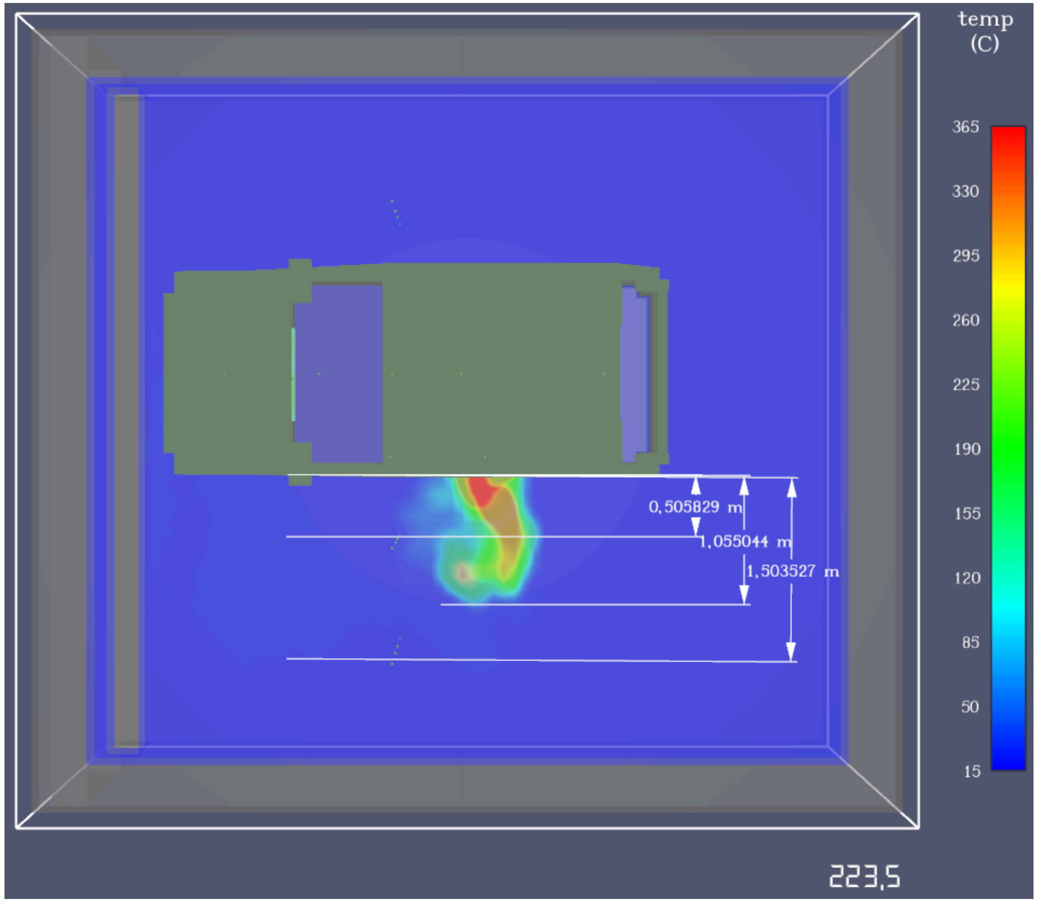temp
(C)
365
330
295
260
225
190
155
120
85
50
15
0,505829 m
1,055044 m
1,503527 m
223,5

Jet flame 4_2: Velocity -12.5%

```
&SURF ID='JET_4_2',
     SPEC_ID(1) = 'PROPANE',
     MASS_FRACTION(1) = 0.069,
     RAMP_V = 'JET_ACT_4_2',
     VEL = -35.0,
     TMP_FRONT = 900.0,
     COLOR = 'ORANGE' /

&RAMP ID='JET_ACT_4_2', T=230.0, F=0.0 /
&RAMP ID='JET_ACT_4_2', T=231, F=1.0 /
&RAMP ID='JET_ACT_4_2', T=240, F=0.7 /
&RAMP ID='JET_ACT_4_2', T=241, F=0.0 /

&VENT ID='Jet_Flame_4_2', SURF_ID='JET_4_2',XB=2.7,2.8, 0.2,0.2, 0.3,0.4, IOR=-2 /
```

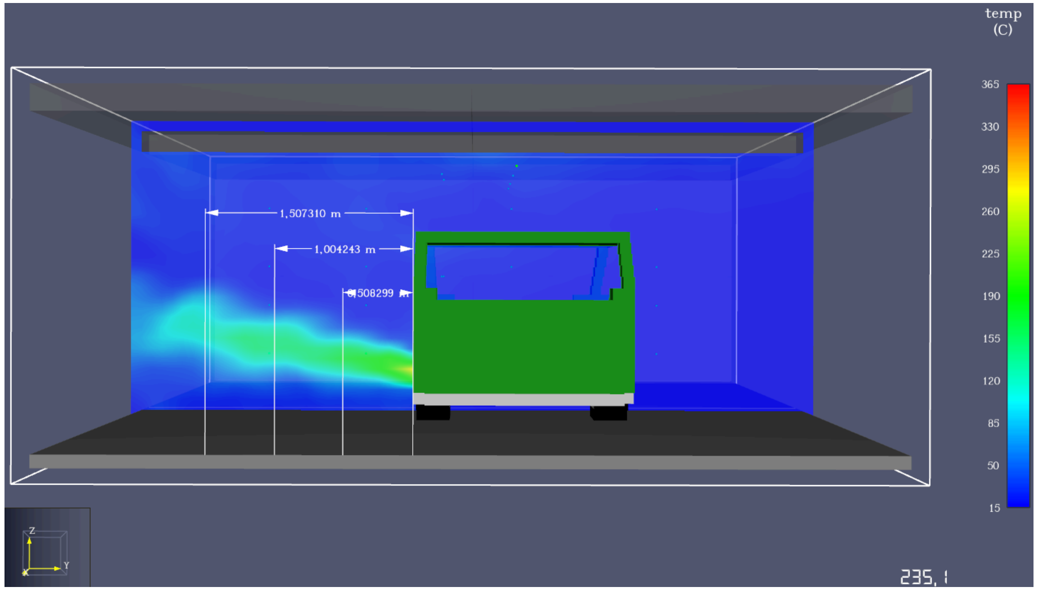
temp
(C)
365
330
295
260
225
190
155
120
85
50
15
1,507310 m
1,004243 m
508299
Z
Y
235,1

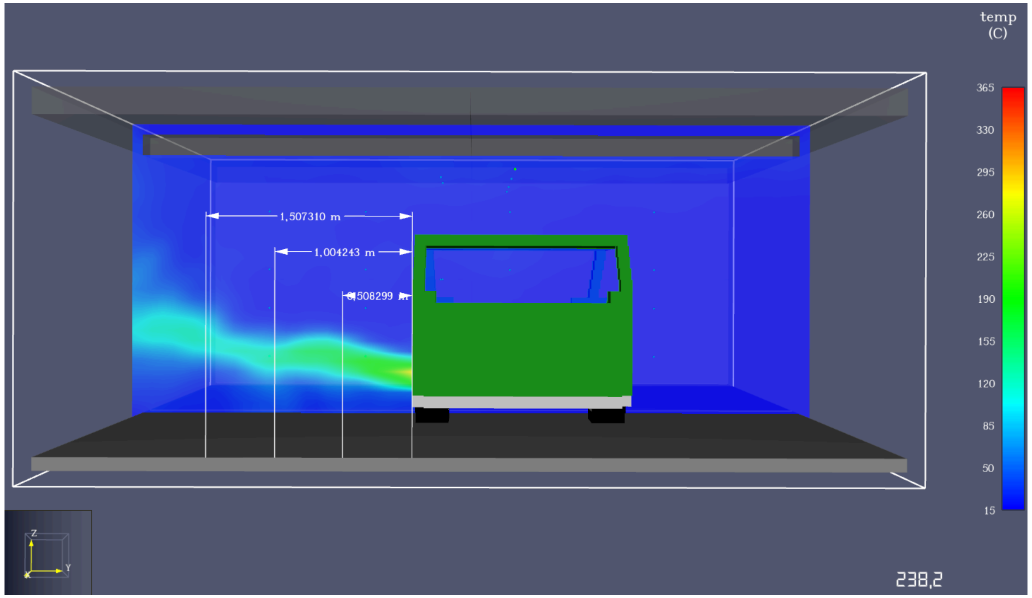
temp
(C)
365
330
295
260
225
190
155
120
85
50
15
1,507310 m
1,004243 m
508299
Z
Y
238,2

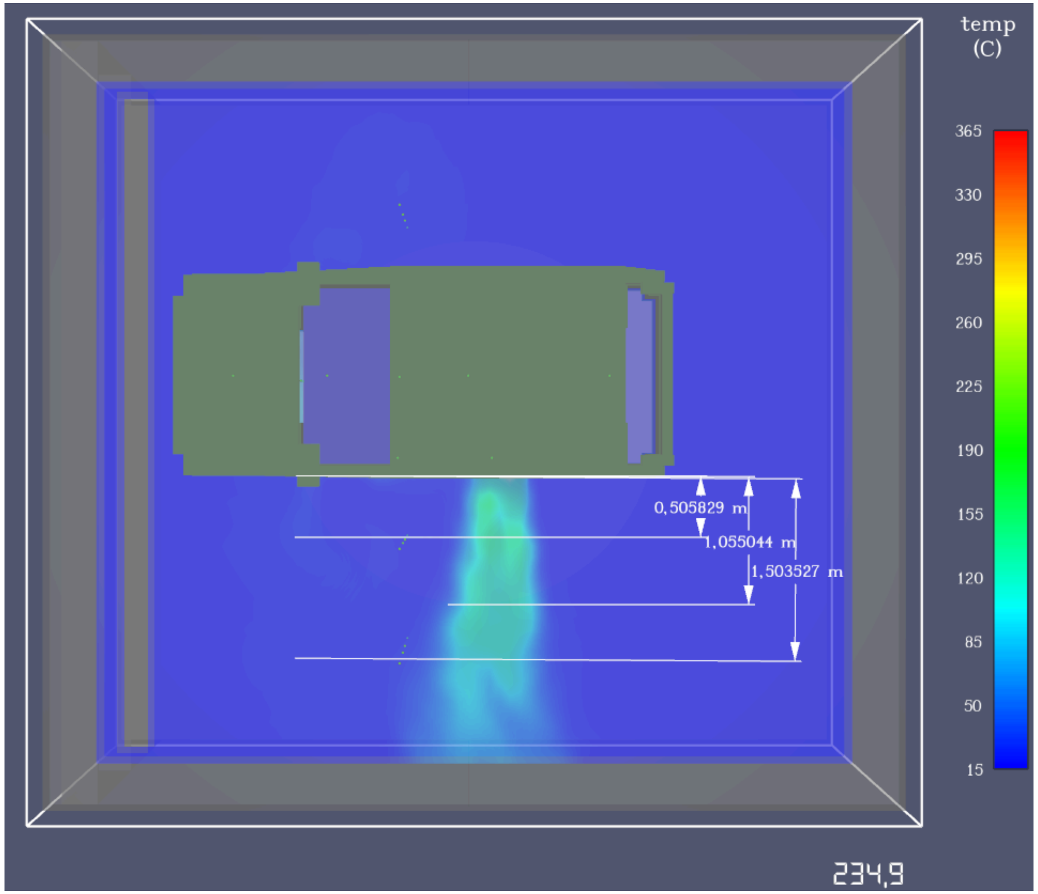
temp
(C)
365
330
295
260
225
190
155
120
85
50
15
0,505829 m
1,055044 m
1,503527 m
234,9

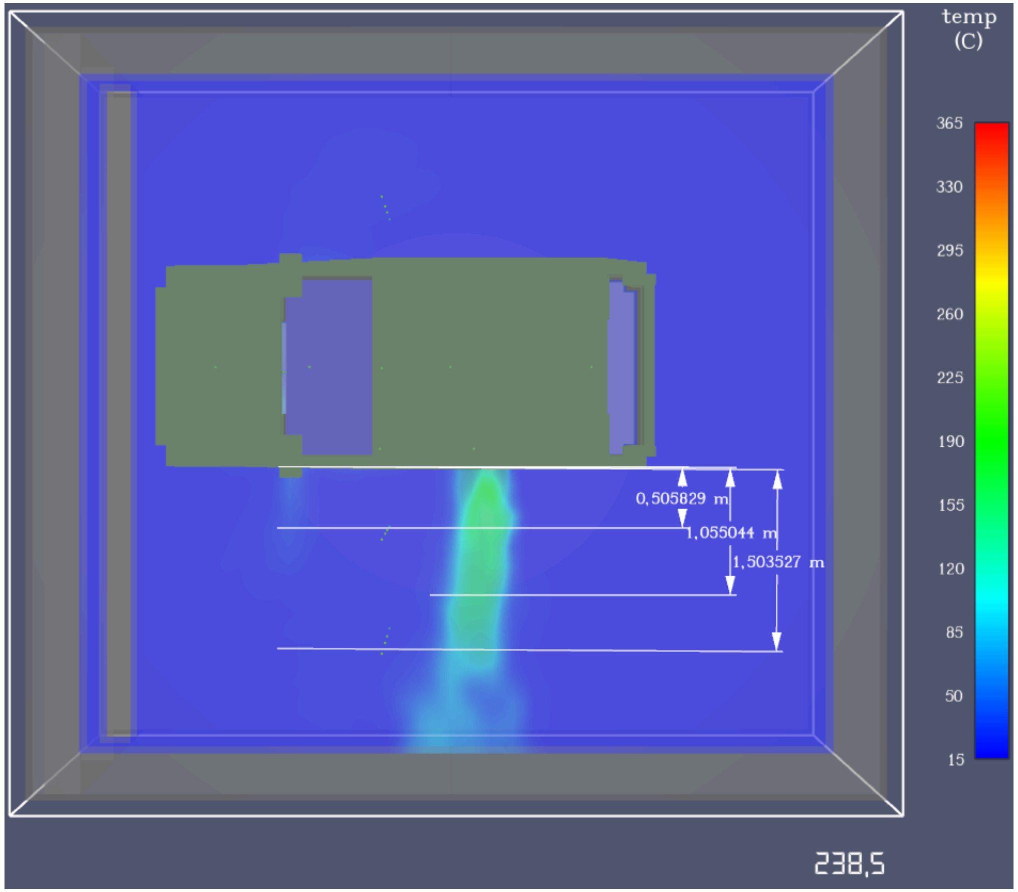
temp
(C)
365
330
295
260
225
190
155
120
85
50
15
0,505829 m
1,055044 m
1,503527 m
238,5

Jet flame 5: area +100%	

```
&SURF ID='JET_5',
     SPEC_ID(1) = 'PROPANE',
     MASS_FRACTION(1) = 0.03,
     RAMP_V = 'JET_ACT_5',
     VEL = -40.0,
     TMP_FRONT = 900.0,
     COLOR = 'ORANGE' /

&RAMP ID='JET_ACT_5', T=65.0, F=0.0 /
&RAMP ID='JET_ACT_5', T=66, F=1.0 /
&RAMP ID='JET_ACT_5', T=75, F=0.7 /
&RAMP ID='JET_ACT_5', T=76, F=0.0 /

&VENT ID='Jet_Flame_5', SURF_ID='JET_5',XB=1.3,1.5, 0.2,0.2, 0.3,0.4, IOR=-2 /
```

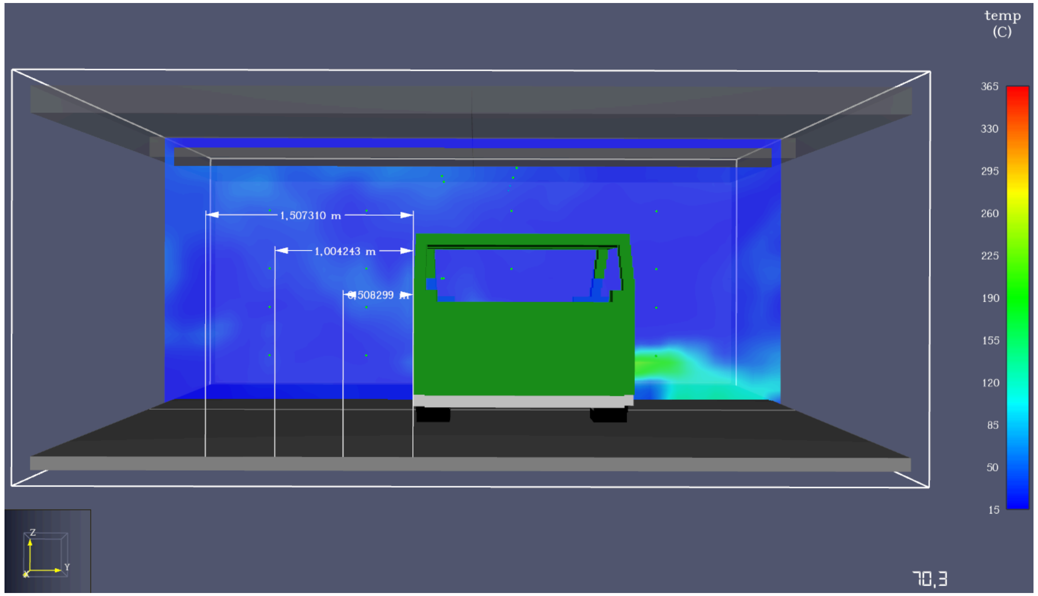
temp
(C)
365
330
295
260
225
190
155
120
85
50
15
1,507310 m
1,004243 m
508299
70,3

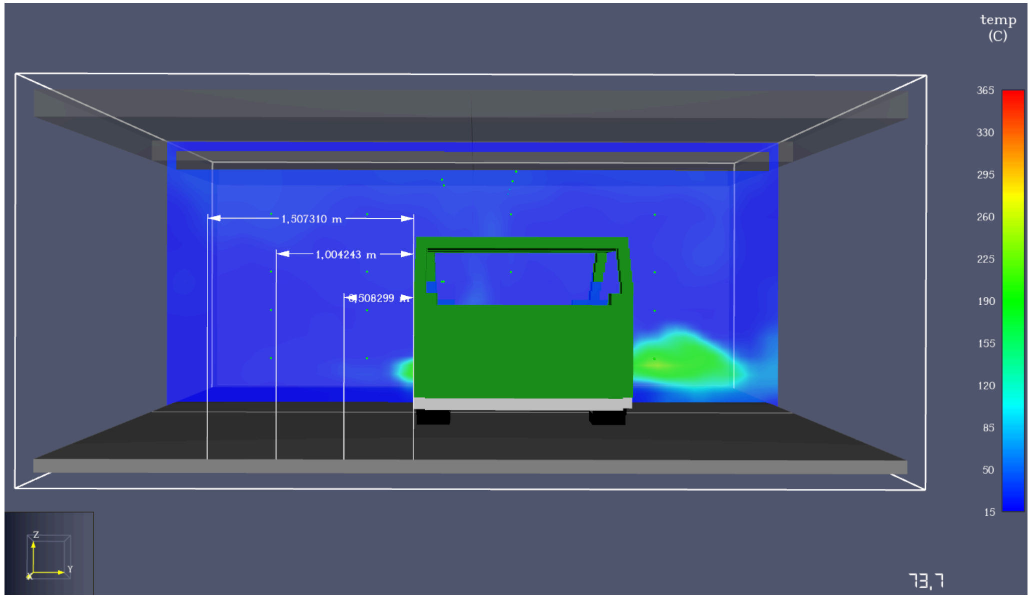
temp
(C)
365
330
295
260
225
190
155
120
85
50
15
1,507310 m
1,004243 m
508299
73,7

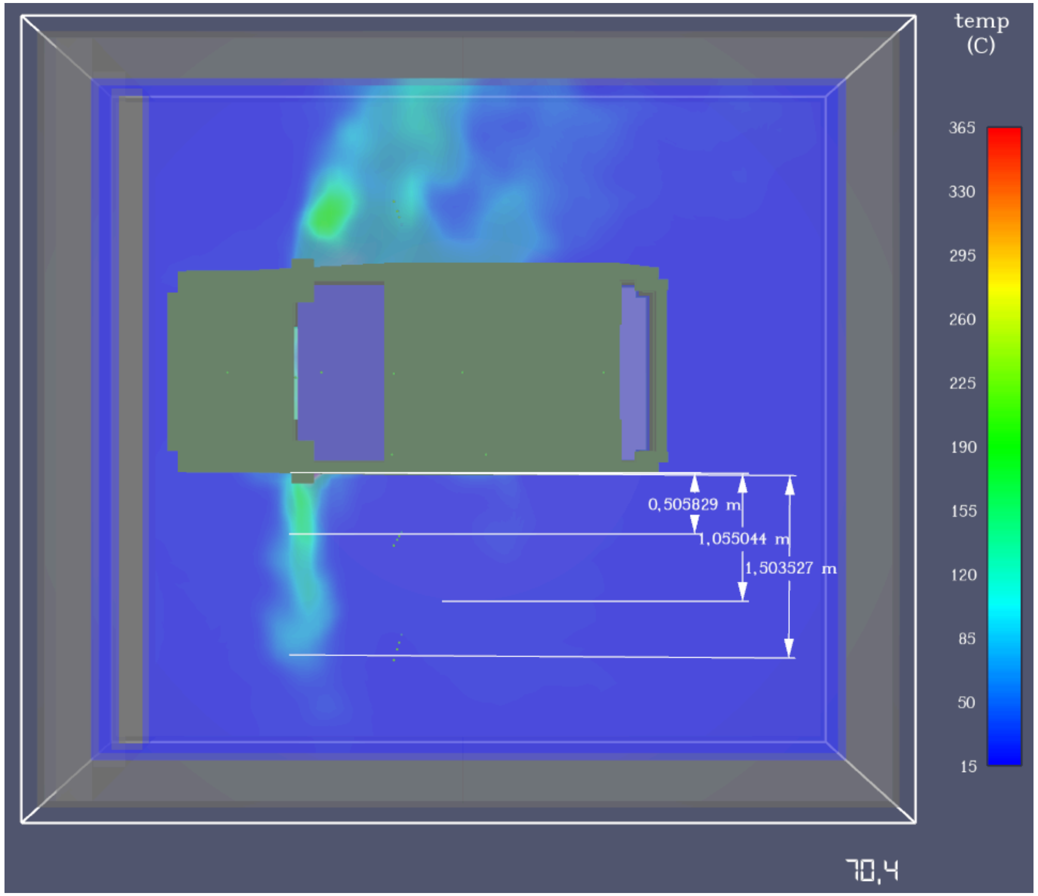
temp
(C)
365
330
295
260
225
190
155
120
85
50
15
0,505829 m
1,055044 m
1,503527 m
70,4
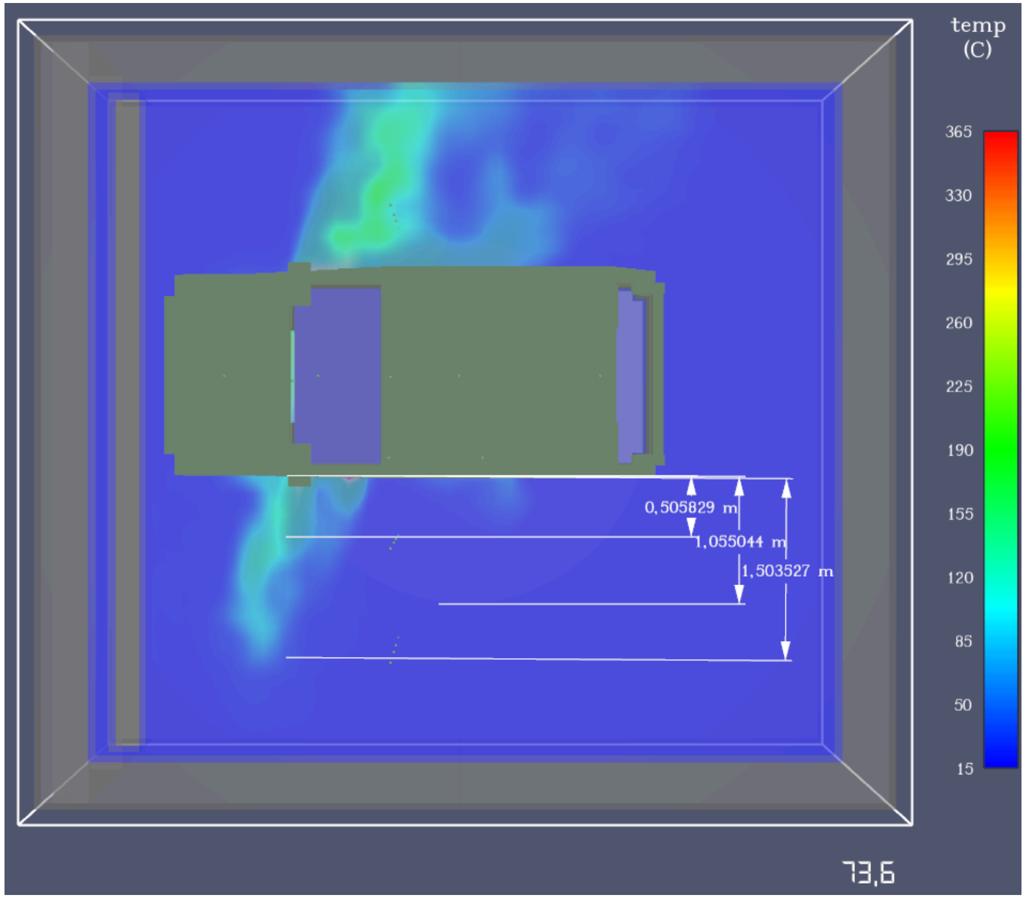
temp
(C)
365
330
295
260
225
190
155
120
85
50
15
0,505829 m
1,055044 m
1,503527 m
73,6

Jet flame 6: Area +200%

```
&SURF ID='JET_6',
     SPEC_ID(1) = 'PROPANE',
     MASS_FRACTION(1) = 0.02,
     RAMP_V = 'JET_ACT_6',
     VEL = -40.0,
     TMP_FRONT = 900.0,
     COLOR = 'ORANGE' /

&RAMP ID='JET_ACT_6', T=80.0, F=0.0 /
&RAMP ID='JET_ACT_6', T=81, F=1.0 /
&RAMP ID='JET_ACT_6', T=90, F=0.7 /
&RAMP ID='JET_ACT_6', T=91, F=0.0 /

&VENT ID='Jet_Flame_6', SURF_ID='JET_6',XB=1.5,1.8, 0.2,0.2, 0.3,0.4, IOR=-2 /
```

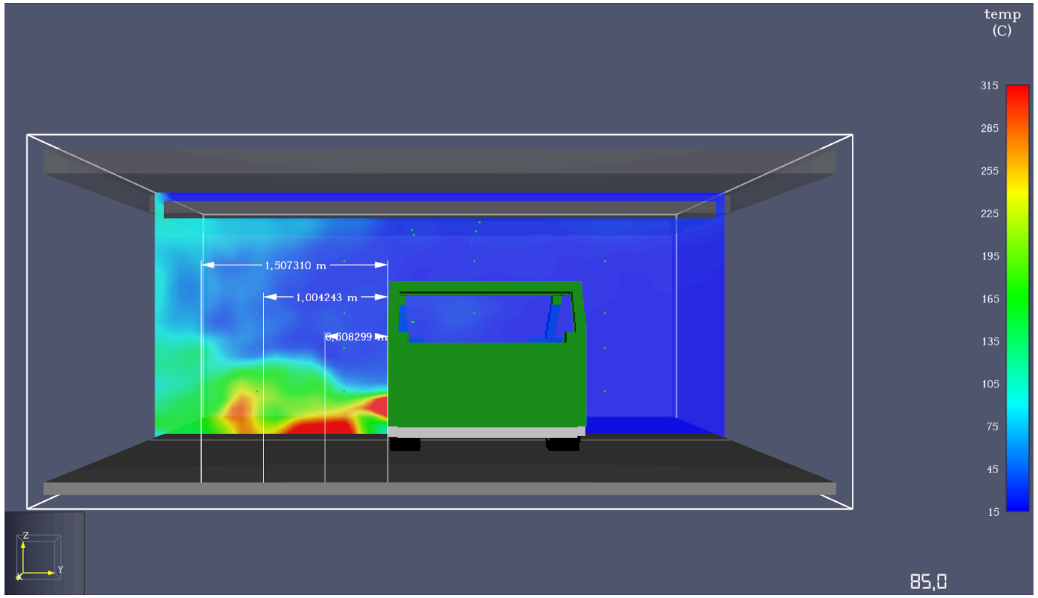
temp
(C)
315
285
255
225
195
165
135
105
75
45
15
1,507310 m
1,004243 m
85,0

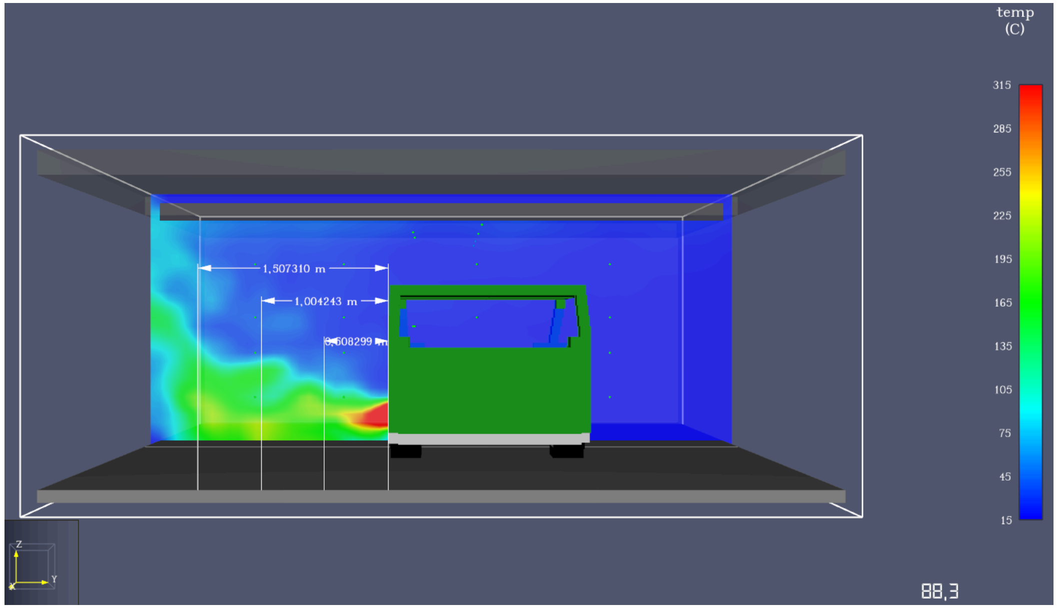
temp
(C)
315
285
255
225
195
165
135
105
75
45
15
1,507310 m
1,004243 m
88,3

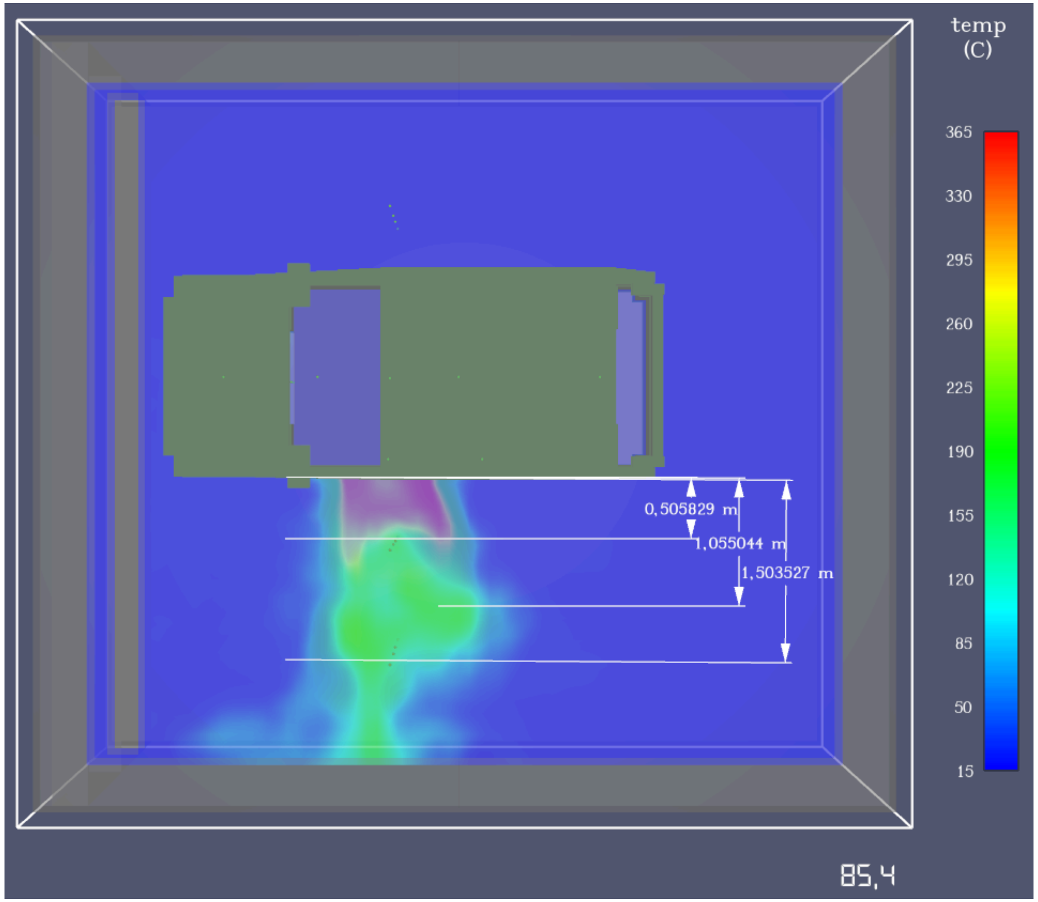
temp
(C)
365
330
295
260
225
190
155
120
85
50
15
0,505829 m
1,055044 m
1,503527 m
85,4

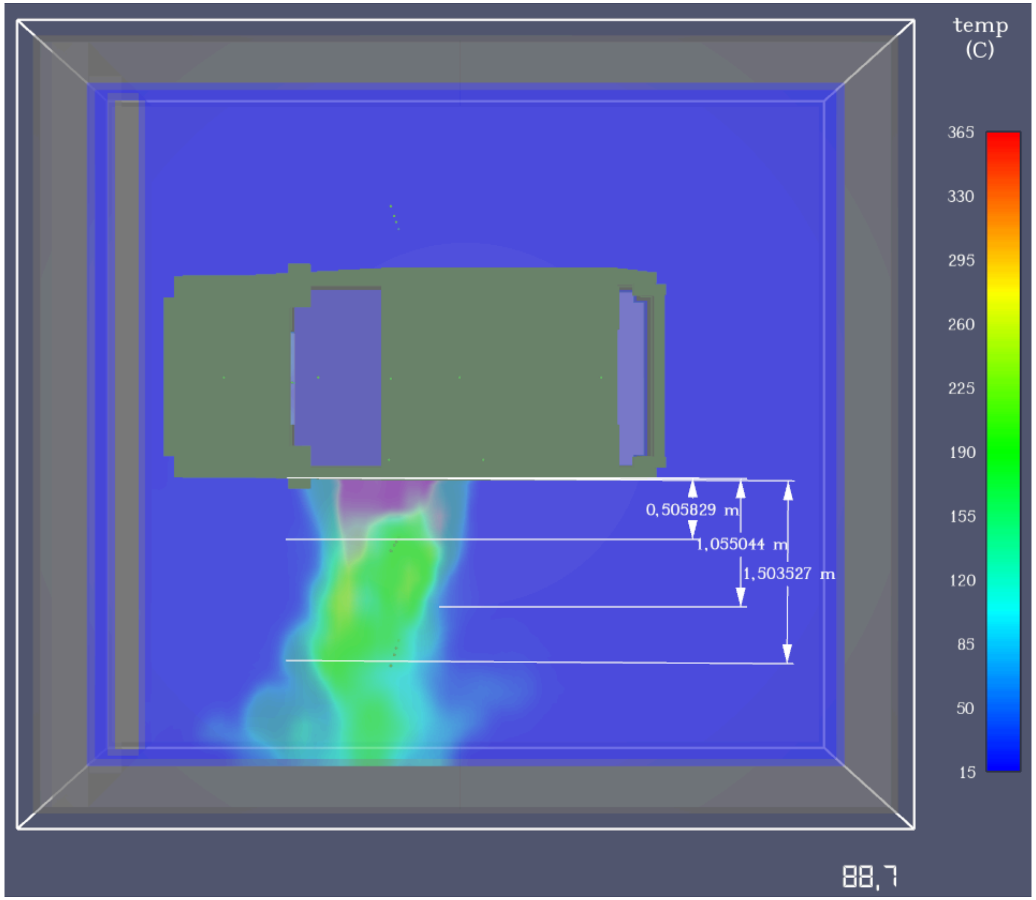
temp
(C)
365
330
295
260
225
190
155
120
85
50
15
0,505829 m
1,055044 m
1,503527 m
88,7

Jet flame 7: Temperature +50%

```
&SURF ID='JET_7',
     SPEC_ID(1) = 'PROPANE',
     MASS_FRACTION(1) = 0.09,
     RAMP_V = 'JET_ACT_7',
     VEL = -40.0,
     TMP_FRONT = 1350.0,
     COLOR = 'ORANGE' /

&RAMP ID='JET_ACT_7', T=95.0, F=0.0 /
&RAMP ID='JET_ACT_7', T=96, F=1.0 /
&RAMP ID='JET_ACT_7', T=105, F=0.7 /
&RAMP ID='JET_ACT_7', T=106, F=0.0 /

&VENT ID='Jet_Flame_7', SURF_ID='JET_7',XB=1.8,1.9, 0.2,0.2, 0.3,0.4, IOR=-2 /
```

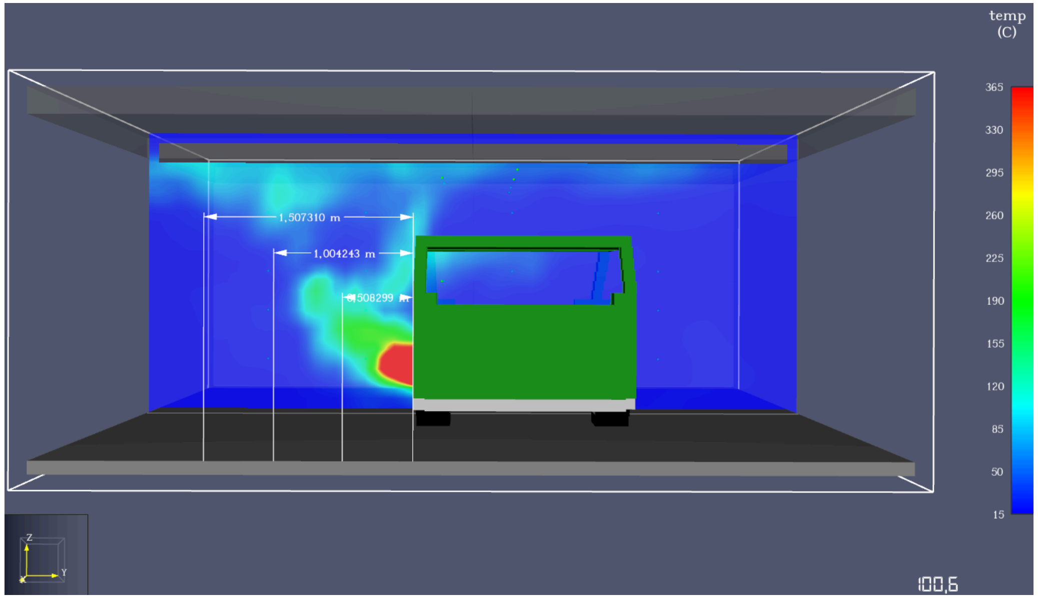
temp
(C)
365
330
295
260
225
190
155
120
85
50
15
1,507310 m
1,004243 m
100,6

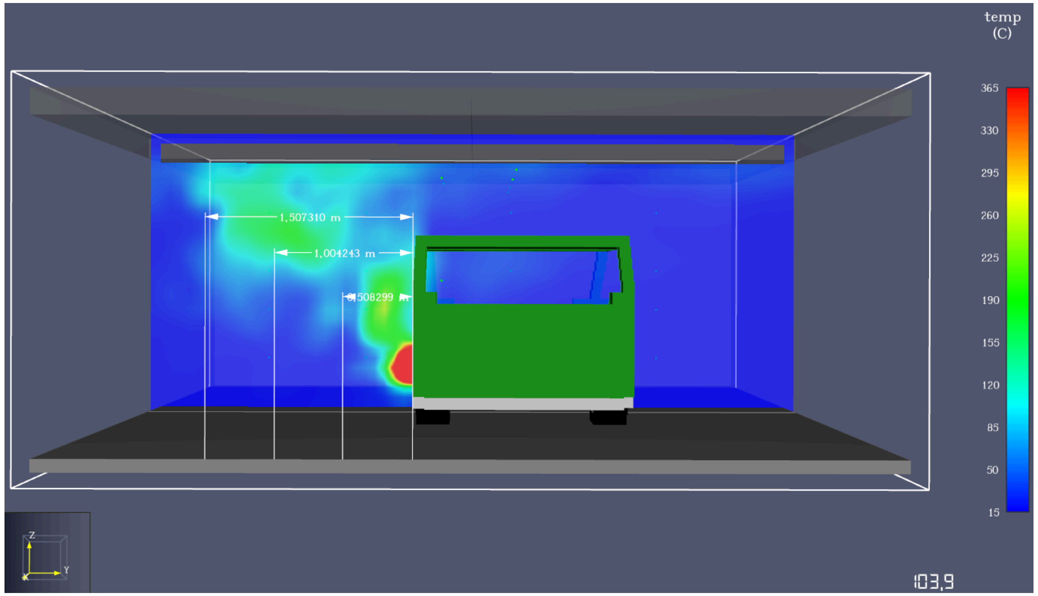
temp
(C)
365
330
295
260
225
190
155
120
85
50
15
1,507310 m
1,004243 m
103,9

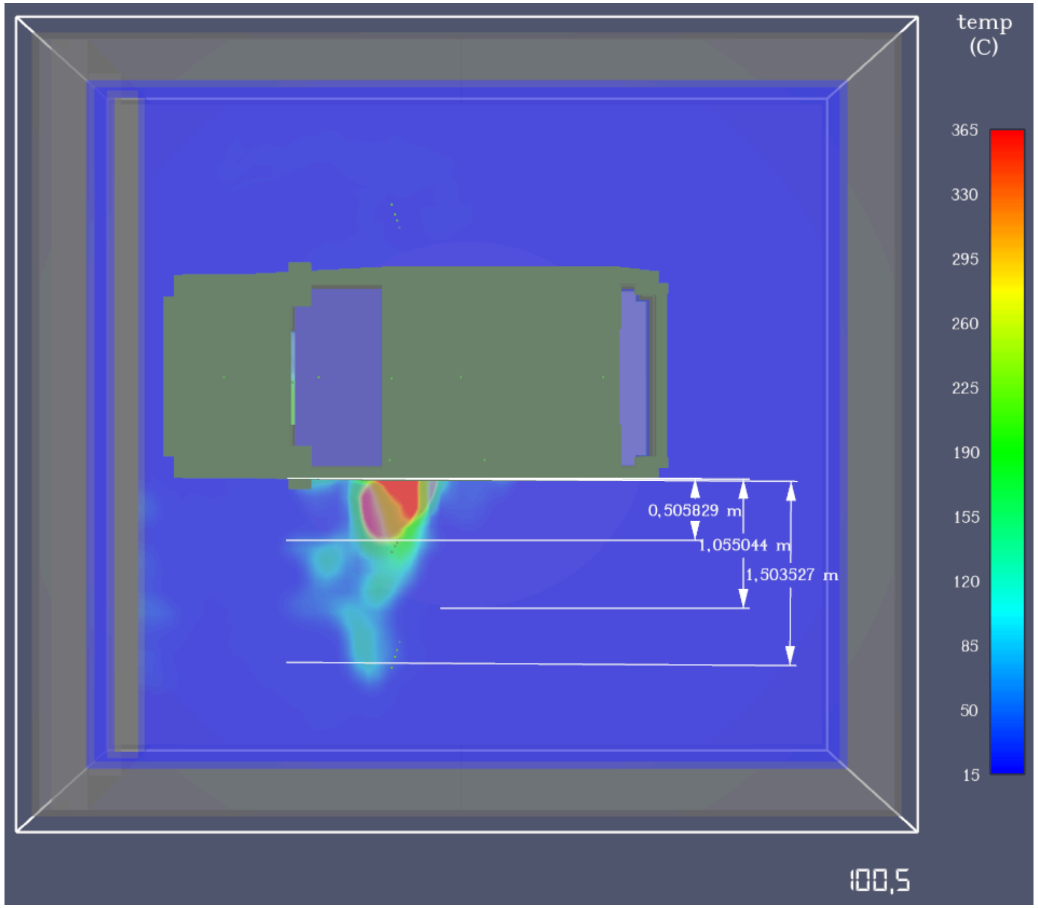
temp
(C)
365
330
295
260
225
190
155
120
85
50
15
0,505829 m
1,055044 m
1,503527 m
100,5

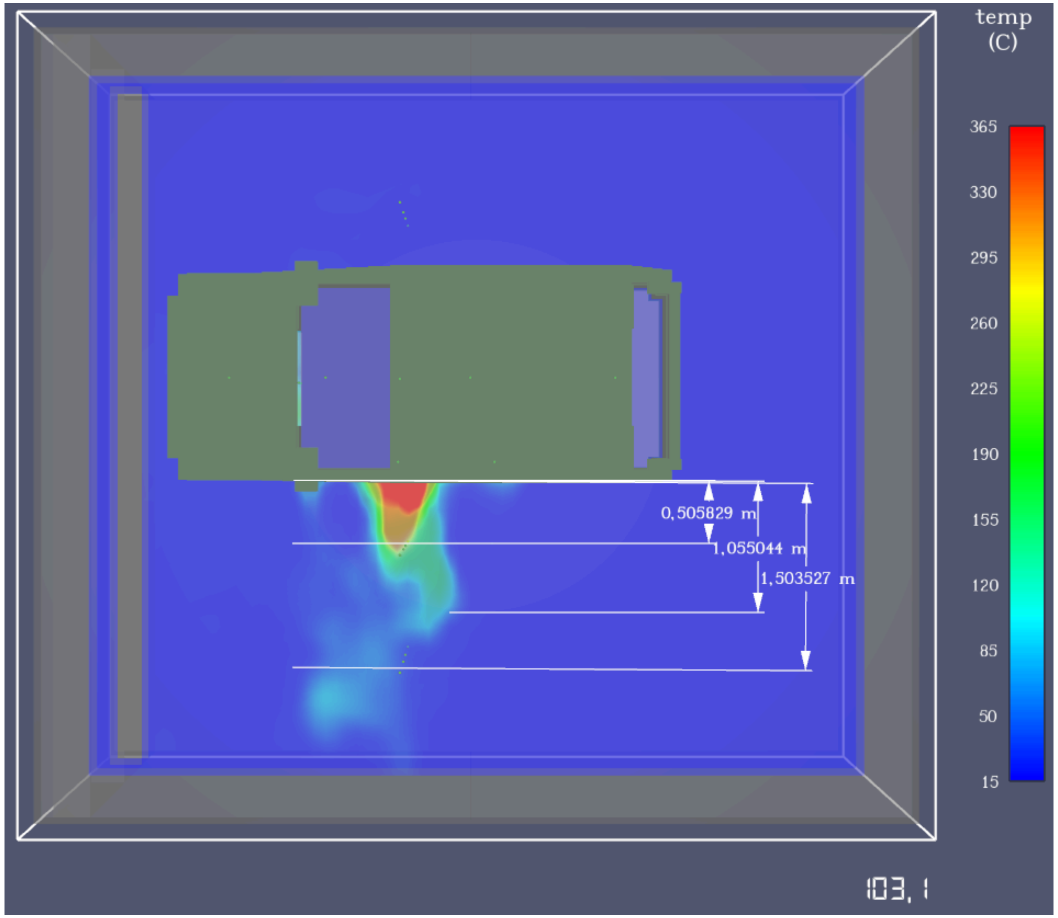
temp
(C)
365
330
295
260
225
190
155
120
85
50
15
0,505829 m
1,055044 m
1,503527 m
103,1

Jet flame 8: Temperature +70%

```
&SURF ID='JET_8',
     SPEC_ID(1) = 'PROPANE',
     MASS_FRACTION(1) = 0.096,
     RAMP_V = 'JET_ACT_8',
     VEL = -40.0,
     TMP_FRONT = 1440.0,
     COLOR = 'ORANGE' /

&RAMP ID='JET_ACT_8', T=110.0, F=0.0 /
&RAMP ID='JET_ACT_8', T=111, F=1.0 /
&RAMP ID='JET_ACT_8', T=120, F=0.7 /
&RAMP ID='JET_ACT_8', T=121, F=0.0 /

&VENT ID='Jet_Flame_8', SURF_ID='JET_8',XB=1.9,2.0, 0.2,0.2, 0.3,0.4, IOR=-2 /
```

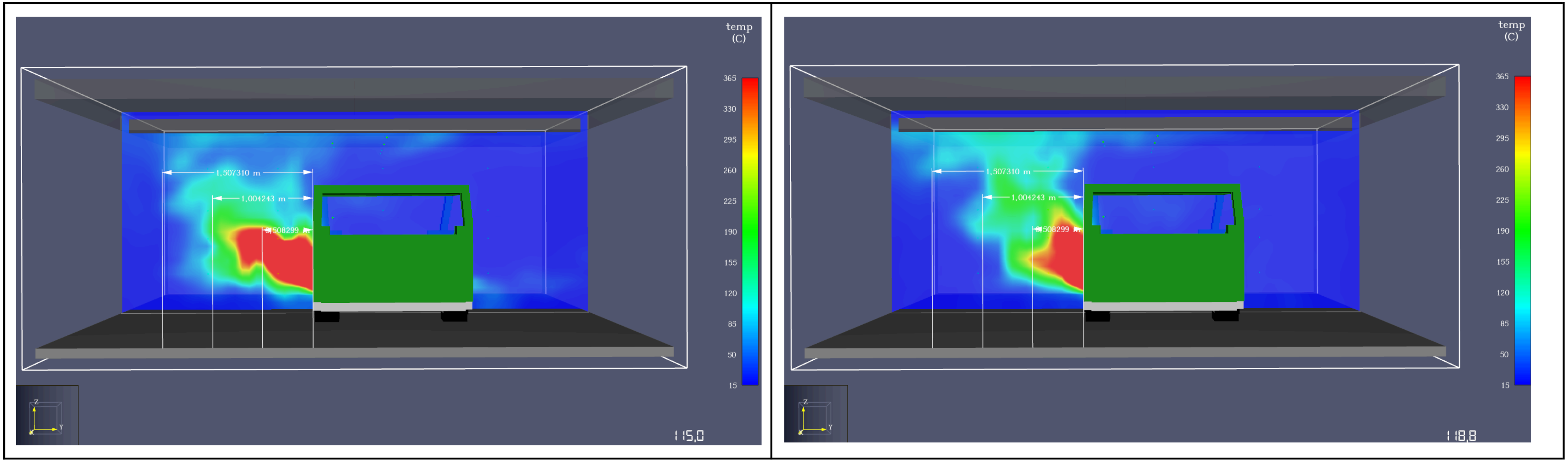
temp
(C)
365
330
295
260
225
190
155
120
85
50
15
1,507310 m
1,004243 m
115,0
temp
(C)
365
330
295
260
225
190
155
120
85
50
15
1,507310 m
1,004243 m
118,8

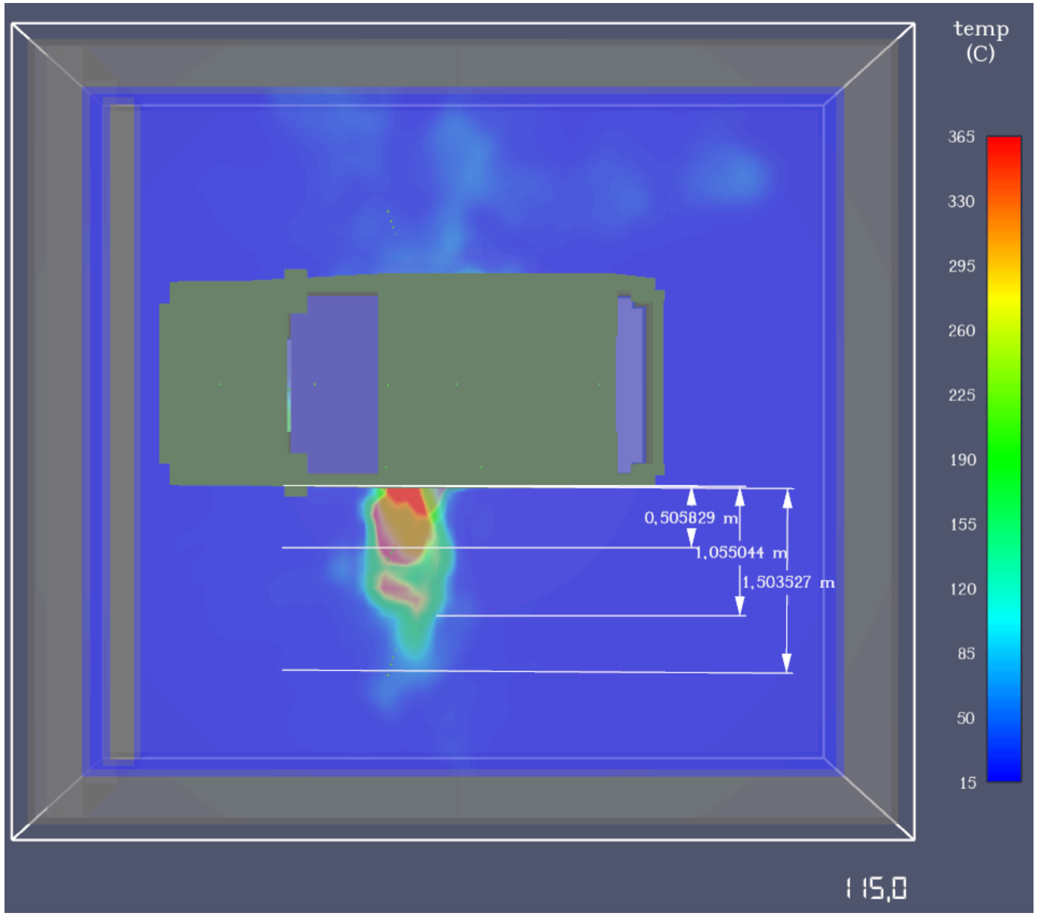
temp
(C)
365
330
295
260
225
190
155
120
85
50
15
0,505829 m
1,055044 m
1,503527 m
115,0

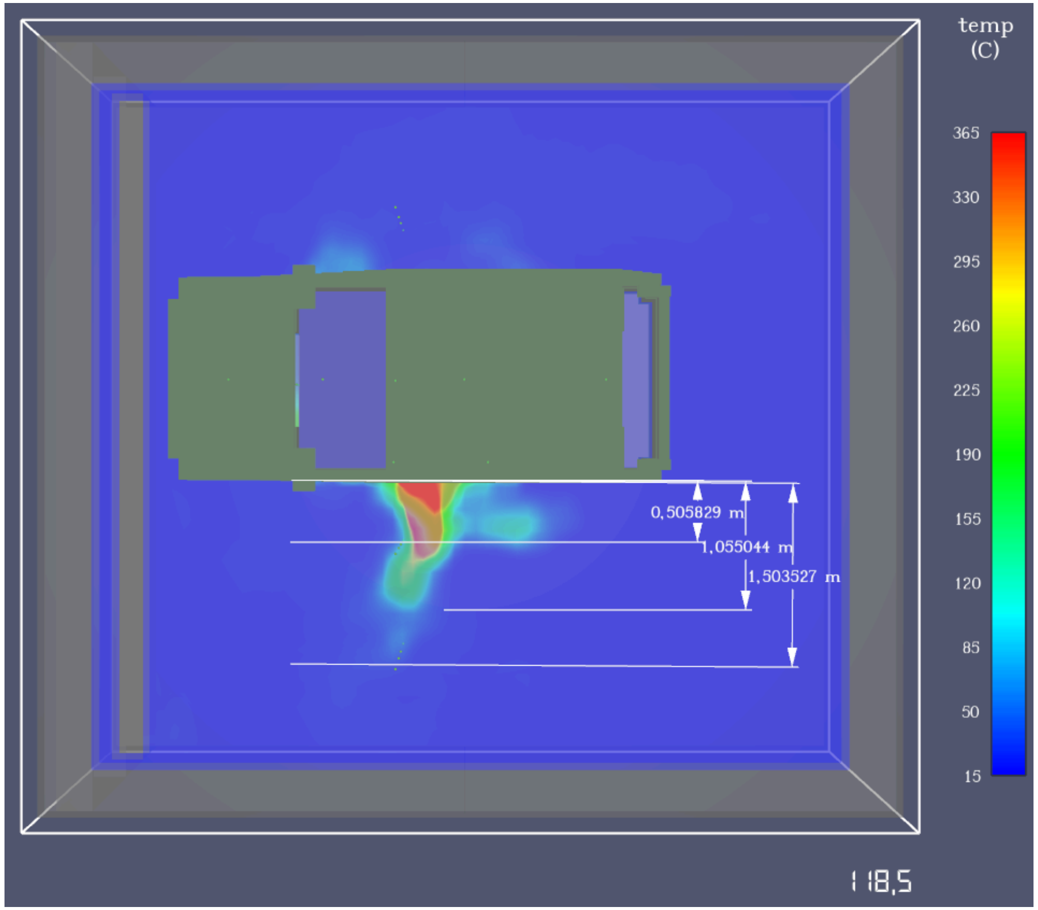
temp
(C)
365
330
295
260
225
190
155
120
85
50
15
0,505829 m
1,055044 m
1,503527 m
118,5

Jet flame 9: Temperature - 50%

```
&SURF ID='JET_9',
     SPEC_ID(1) = 'PROPANE',
     MASS_FRACTION(1) = 0.03,
     RAMP_V = 'JET_ACT_9',
     VEL = -40.0,
     TMP_FRONT = 450.0,
     COLOR = 'ORANGE' /

&RAMP ID='JET_ACT_9', T=125.0, F=0.0 /
&RAMP ID='JET_ACT_9', T=126, F=1.0 /
&RAMP ID='JET_ACT_9', T=135, F=0.7 /
&RAMP ID='JET_ACT_9', T=136, F=0.0 /

&VENT ID='Jet_Flame_9', SURF_ID='JET_9',XB=2.0,2.1, 0.2,0.2, 0.3,0.5, IOR=-2 /
```

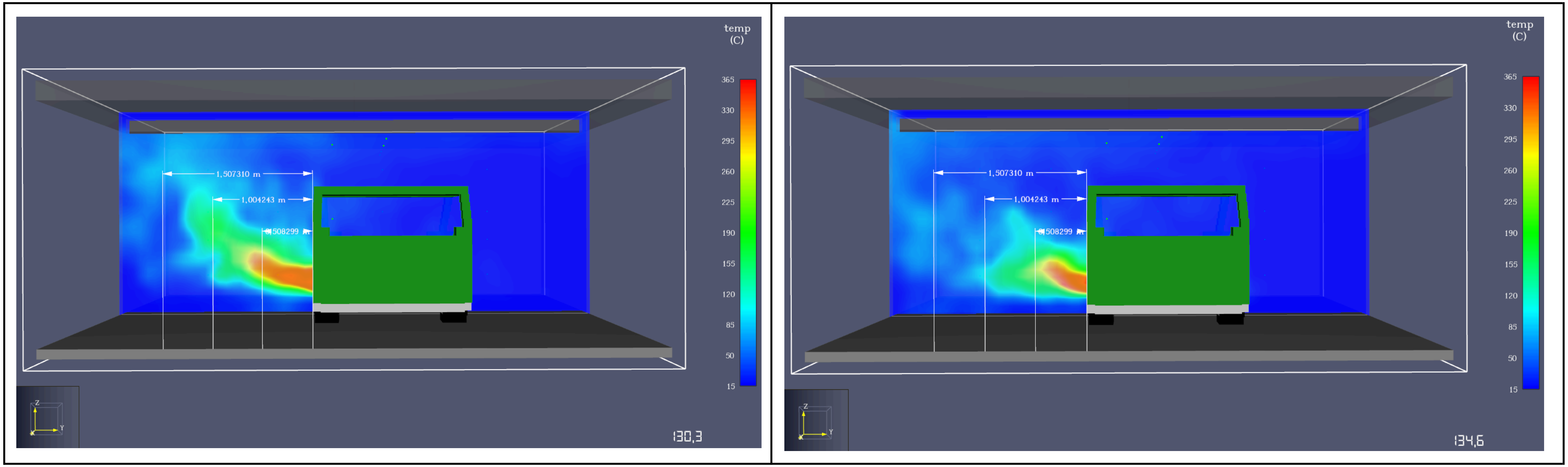
temp
(C)
365
330
295
260
225
190
155
120
85
50
15
1,507310 m
1,004243 m
130,3
134,6

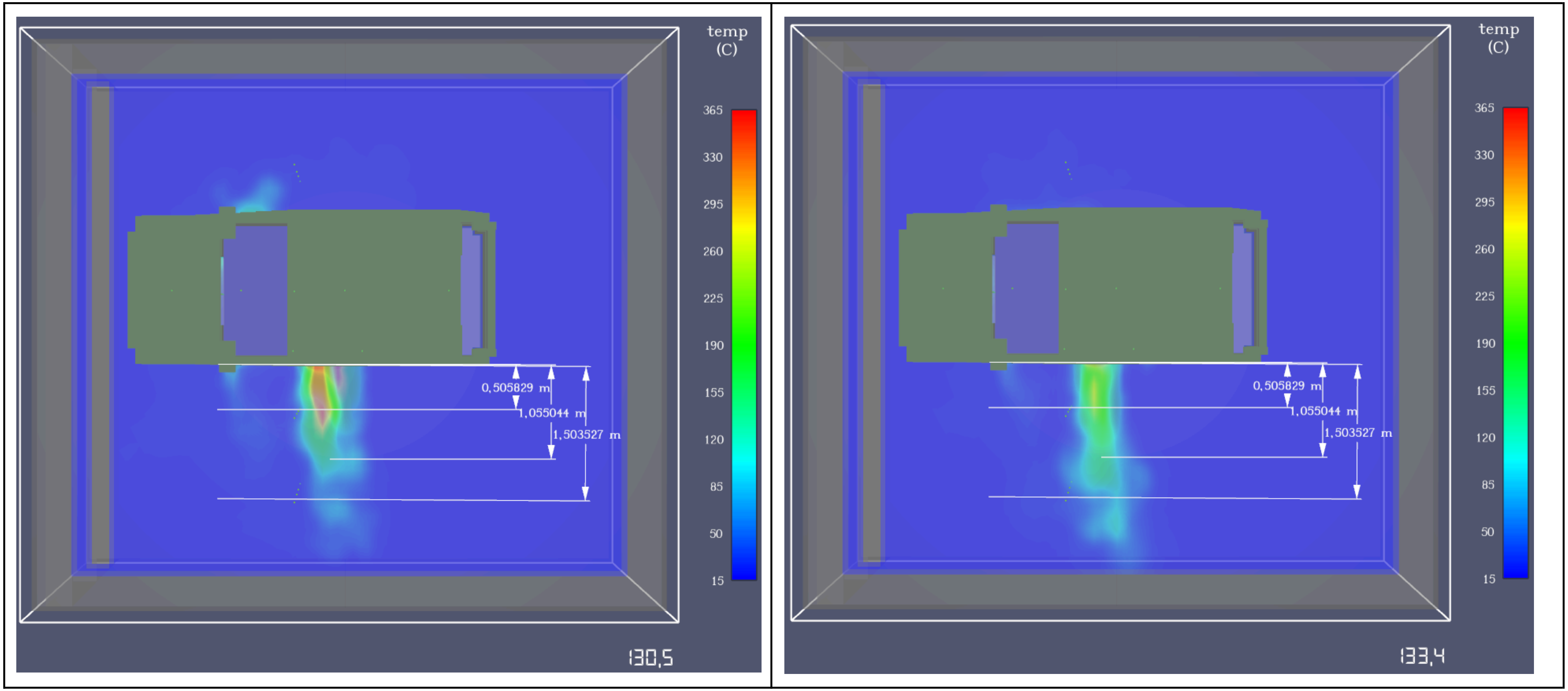
temp
(C)
365
330
295
260
225
190
155
120
85
50
15
0,505829 m
1,055044 m
1,503527 m
130,5
temp
(C)
365
330
295
260
225
190
155
120
85
50
15
0,505829 m
1,055044 m
1,503527 m
133,4

6.2.3) Annex C: Jet flames model

Note: temperature bar: 450°C (red- max. temp. of ignition for the highest ignition temp of the combustible materials); 250°C (green); 15°C (darkblue). The perpendicular slice device stands 0.6m from the green car (distance neighbouring vehicle) .

```
&SURF ID='JET_1',
     SPEC_ID(1) = 'PROPANE',
     MASS_FRACTION(1) = 0.017,
     RAMP_V = 'JET_ACT_1',
     VEL = -60.0,
     TMP_FRONT = 1350.0,
     COLOR = 'ORANGE' / 10% is propane, the other is air

&RAMP ID='JET_ACT_1', T=180.0, F=0.0 /
&RAMP ID='JET_ACT_1', T=181, F=1.0 /
&RAMP ID='JET_ACT_1', T=220, F=0.7 /
&RAMP ID='JET_ACT_1', T=221, F=0.0 /

&VENT ID='Jet_Flame_1', SURF_ID='JET_1',XB=0.8,0.9, 0.2,0.2, 0.3,0.4, IOR=-2 /
```

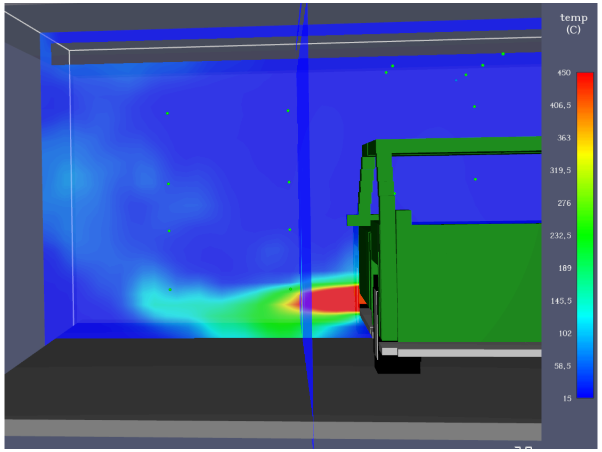


```
&SURF ID='JET_2',
     SPEC_ID(1) = 'PROPANE',
     MASS_FRACTION(1) = 0.019,
     RAMP_V = 'JET_ACT_2',
     VEL = -60.0,
     TMP_FRONT = 1200.0,
     COLOR = 'ORANGE' /

&RAMP ID='JET_ACT_2', T=300.0, F=0.0 /
&RAMP ID='JET_ACT_2', T=301, F=1.0 /
&RAMP ID='JET_ACT_2', T=349, F=0.7 /
&RAMP ID='JET_ACT_2', T=350, F=0.0 /

&VENT ID='Jet_Flame_2', SURF_ID='JET_2',XB=0.9,1.0, 0.2,0.2, 0.3,0.4, IOR=-2 /
```

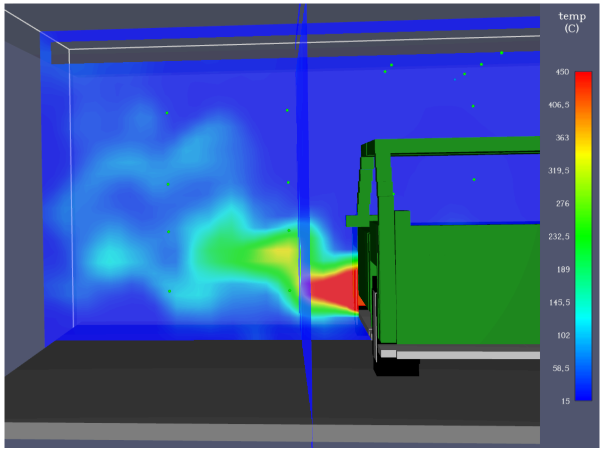

&SURF ID='JET_3', SPEC_ID(1) = 'PROPANE', MASS_FRACTION(1) = 0.03, RAMP_V = 'JET_ACT_3', VEL = -70.0, TMP_FRONT = 1350.0, COLOR = 'ORANGE' / &RAMP ID='JET_ACT_3', T=600.0, F=0.0 / &RAMP ID='JET_ACT_3', T=601, F=1.0 / &RAMP ID='JET_ACT_3', T=659, F=0.7 / &RAMP ID='JET_ACT_3', T=660, F=0.0 / &VENT ID='Jet_Flame_3', SURF_ID='JET_3',XB=1.0,1.1, 0.2,0.2, 0.3,0.4, IOR=-2 /	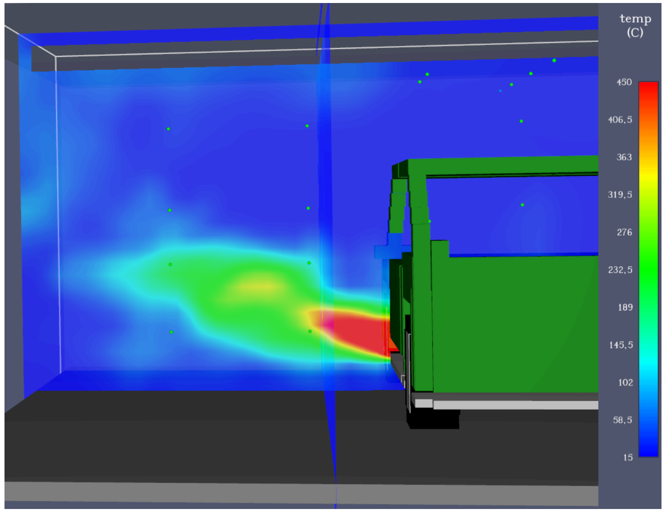
&SURF ID='JET_4', SPEC_ID(1) = 'PROPANE', MASS_FRACTION(1) = 0.11, RAMP_V = 'JET_ACT_4', VEL = -60.0, TMP_FRONT = 800.0, COLOR = 'ORANGE' / &RAMP ID='JET_ACT_4', T=720.0, F=0.0 / &RAMP ID='JET_ACT_4', T=721, F=1.0 / &RAMP ID='JET_ACT_4', T=779, F=0.7 / &RAMP ID='JET_ACT_4', T=780, F=0.0 / &VENT ID='Jet_Flame_4', SURF_ID='JET_4',XB=1.1,1.2, 0.2,0.2, 0.3,0.4, IOR=-2 /	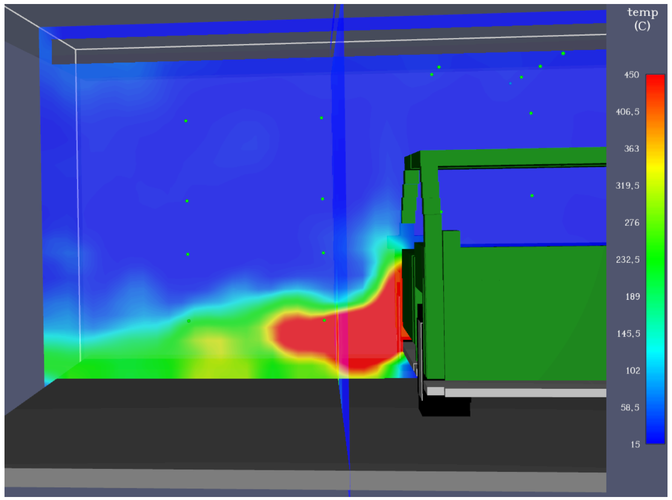

```
&SURF ID='JET_5',
     SPEC_ID(1) = 'PROPANE',
     MASS_FRACTION(1) = 0.03,
     RAMP_V = 'JET_ACT_5',
     VEL = -70.0,
     TMP_FRONT = 700.0,
     COLOR = 'ORANGE' /

&RAMP ID='JET_ACT_5', T=1020.0, F=0.0 /
&RAMP ID='JET_ACT_5', T=1021, F=1.0 /
&RAMP ID='JET_ACT_5', T=1079, F=0.9 /
&RAMP ID='JET_ACT_5', T=1080, F=0.0 /

&VENT ID='Jet_Flame_5', SURF_ID='JET_5',XB=1.2,1.3, 0.2,0.2, 0.3,0.4, IOR=-2 /
```

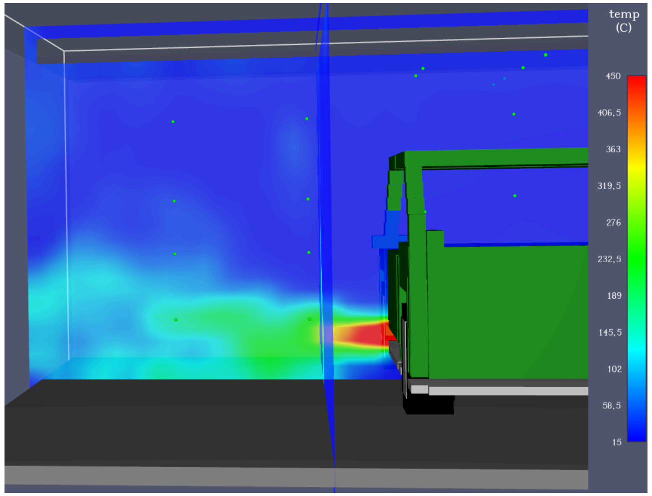


```
&SURF ID='JET_6',
     SPEC_ID(1) = 'PROPANE',
     MASS_FRACTION(1) = 0.048,
     RAMP_V = 'JET_ACT_6',
     VEL = -70.0,
     TMP_FRONT = 1000.0,
     COLOR = 'ORANGE' /

&RAMP ID='JET_ACT_6', T=1140.0, F=0.0 /
&RAMP ID='JET_ACT_6', T=1141, F=0.3 /
&RAMP ID='JET_ACT_6', T=1179, F=1.0 /
&RAMP ID='JET_ACT_6', T=1180, F=0.0 /

&VENT ID='Jet_Flame_6', SURF_ID='JET_6',XB=1.3,1.4, 0.2,0.2, 0.3,0.4, IOR=-2 /
```

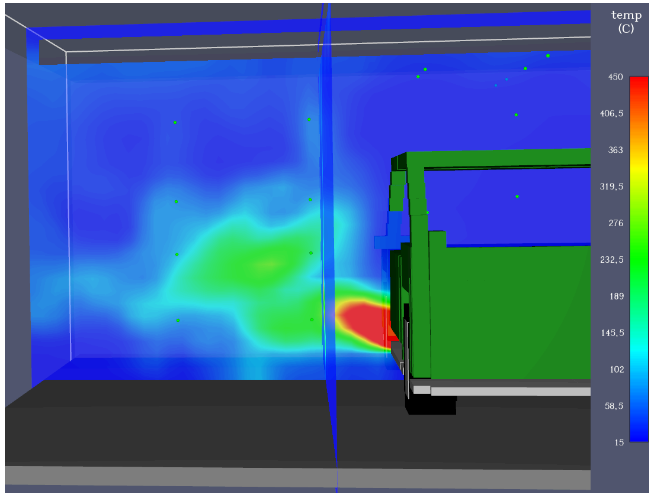

```
&SURF ID='JET_7',
     SPEC_ID(1) = 'PROPANE',
     MASS_FRACTION(1) = 0.085,
     RAMP_V = 'JET_ACT_7',
     VEL = -40.0,
     TMP_FRONT = 700.0,
     COLOR = 'ORANGE' /

&RAMP ID='JET_ACT_7', T=1380.0, F=0.0 /
&RAMP ID='JET_ACT_7', T=1381, F=1.0 /
&RAMP ID='JET_ACT_7', T=1420, F=0.7 /
&RAMP ID='JET_ACT_7', T=1421, F=0.0 /

&VENT ID='Jet_Flame_7', SURF_ID='JET_7',XB=1.4,1.5, 0.2,0.2, 0.3,0.4, IOR=-2 /
```

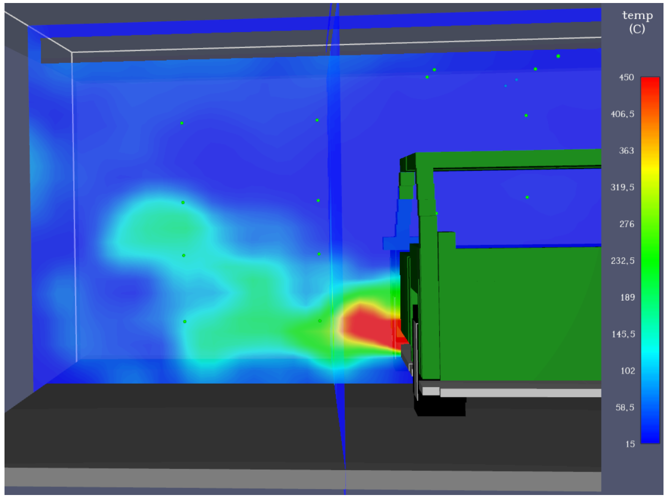


```
&SURF ID='JET_8',
     SPEC_ID(1) = 'PROPANE',
     MASS_FRACTION(1) = 0.08,
     RAMP_V = 'JET_ACT_8',
     VEL = -60.0,
     TMP_FRONT = 1000.0,
     COLOR = 'ORANGE' /

&RAMP ID='JET_ACT_8', T=1500.0, F=0.0 /
&RAMP ID='JET_ACT_8', T=1501, F=1.0 /
&RAMP ID='JET_ACT_8', T=1540, F=0.5 /
&RAMP ID='JET_ACT_8', T=1541, F=0.0 /

&VENT ID='Jet_Flame_8', SURF_ID='JET_8',XB=1.5,1.6, 0.2,0.2, 0.3,0.4, IOR=-2 /
```

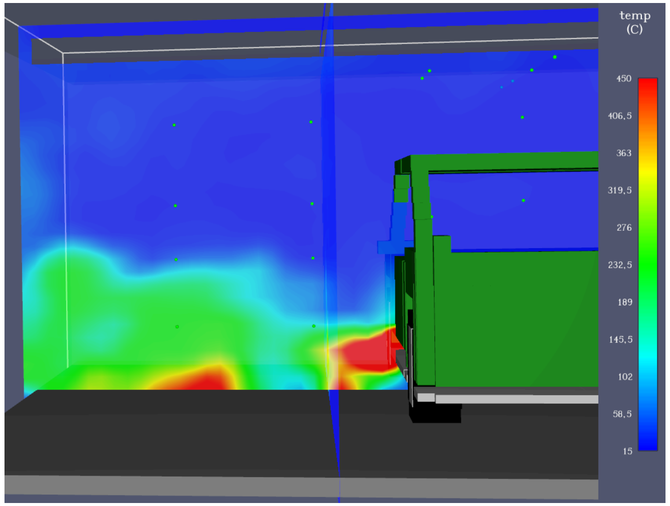

```
&SURF ID='JET_9',
     SPEC_ID(1) = 'PROPANE',
     MASS_FRACTION(1) = 0.06,
     RAMP_V = 'JET_ACT_9',
     VEL = -55.0,
     TMP_FRONT = 900.0,
     COLOR = 'ORANGE' /

&RAMP ID='JET_ACT_9', T=2280.0, F=0.0 /
&RAMP ID='JET_ACT_9', T=2281, F=1.0 /
&RAMP ID='JET_ACT_9', T=2320, F=0.7 /
&RAMP ID='JET_ACT_9', T=2321, F=0.0 /

&VENT ID='Jet_Flame_9', SURF_ID='JET_9',XB=1.6,1.7, 0.2,0.2, 0.3,0.4, IOR=-2 /
```

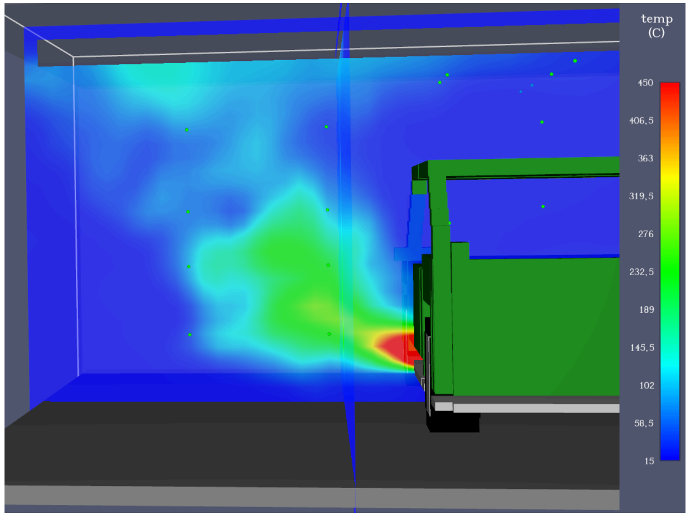


```
&SURF ID='JET_10',
     SPEC_ID(1) = 'PROPANE',
     MASS_FRACTION(1) = 0.1,
     RAMP_V = 'JET_ACT_10',
     VEL = -50.0,
     TMP_FRONT = 900.0,
     COLOR = 'ORANGE' /

&RAMP ID='JET_ACT_10', T=2520.0, F=0.0 /
&RAMP ID='JET_ACT_10', T=2521, F=1.0 /
&RAMP ID='JET_ACT_10', T=2580, F=0.7 /
&RAMP ID='JET_ACT_10', T=2581, F=0.0 /

&VENT ID='Jet_Flame_10', SURF_ID='JET_10',XB=1.7,1.9, 0.2,0.2, 0.3,0.4,
IOR=-2 /
```

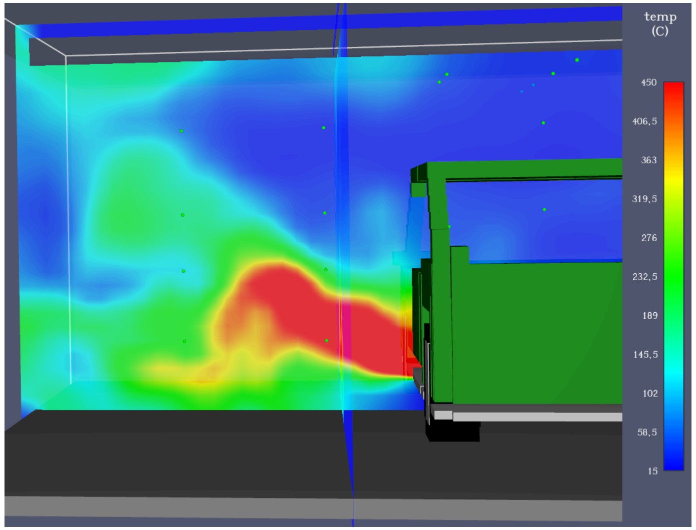

```
&SURF ID='JET_11',
     SPEC_ID(1) = 'PROPANE',
     MASS_FRACTION(1) = 0.09,
     RAMP_V = 'JET_ACT_11',
     VEL = -45.0,
     TMP_FRONT = 800.0,
     COLOR = 'ORANGE' /

&RAMP ID='JET_ACT_11', T=2280.0, F=0.0 /
&RAMP ID='JET_ACT_11', T=2281 F=1.0 /
&RAMP ID='JET_ACT_11', T=2920, F=0.7 /
&RAMP ID='JET_ACT_11', T=2921, F=0.0 /

&VENT ID='Jet_Flame_11', SURF_ID='JET_11',XB=1.9,2.0, 0.2,0.2, 0.3,0.5,
IOR=-2 /
```

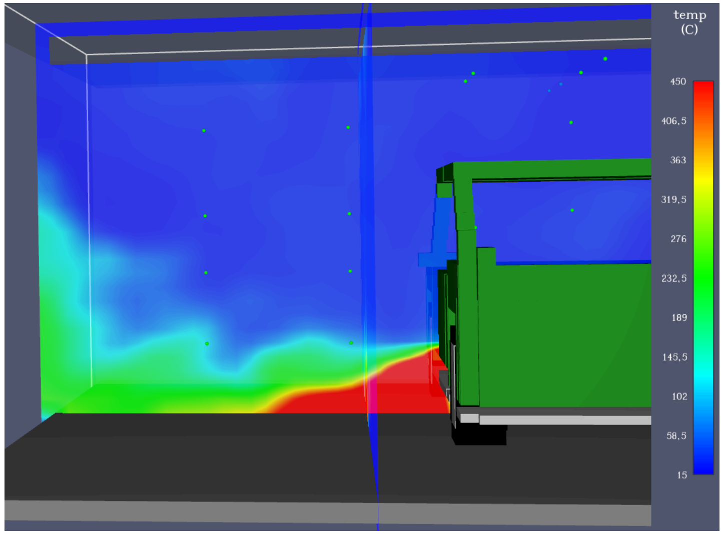

6.2.4) Annex D: FDS model (Scenario 1)

```
&HEAD CHID='Scenario_1', TITLE='Scenario_1'/
&TIME T_END=4200.0/70 min
&DUMP DT_RESTART=900.0, DT_SL3D=5.0, SMOKE3D=.TRUE. /
&MISC TMPA=15.0,CFL_VELOCITY_NORM=2, MPI_TIMEOUT=1200.0/
/______________________________________________________________________ meshes
&MESH ID='M1', IJK=48,80,15, XB=-1.2,3.6, -7.0,1.0, -0.2,1.3 /
&MESH ID='M2', IJK=48,80,15, XB=3.6,8.4, -7.0,1.0, -0.2,1.3 /

&MESH ID='M3', IJK=48,80,15, XB=-1.2,3.6, 1.0,9.0, -0.2,1.3 /
&MESH ID='M4', IJK=48,80,15, XB=3.6,8.4, 1.0,9.0, -0.2,1.3 /

&MESH ID='M5', IJK=48,80,15, XB=-1.2,3.6, -7.0,1.0, 1.3,2.8 /
&MESH ID='M6', IJK=48,80,15, XB=3.6,8.4, -7.0,1.0, 1.3,2.8 /

&MESH ID='M7', IJK=48,80,15, XB=-1.2,3.6, 1.0,9.0, 1.3,2.8 /
&MESH ID='M8', IJK=48,80,15, XB=3.6,8.4, 1.0,9.0, 1.3,2.8 /
/__________________________________________________________________________________________battery fire

&REAC FUEL='PROPANE',
      SOOT_YIELD=0.08,
      CO_YIELD=0.02,
      RADIATIVE_FRACTION = 0.3 /

&SURF ID='BATTERY_FIRE',
     SPEC_ID ='PROPANE',
     HRRPUA=300,
     RAMP_Q='BEV_FIRE',
     COLOR='RED',
      E_COEFFICIENT=0.1/

&RAMP ID='BEV_FIRE', T=0.0, F=0.0 /
&RAMP ID='BEV_FIRE', T=1.0, F=0.0 /
&RAMP ID='BEV_FIRE', T=2.0, F=0.18 /
```

```
&RAMP ID='BEV_FIRE', T=120.0, F=0.6 /
&RAMP ID='BEV_FIRE', T=300.0, F=1.0/
&RAMP ID='BEV_FIRE', T=420.0, F=0.73 /
&RAMP ID='BEV_FIRE', T=600.0, F=0.63/
&RAMP ID='BEV_FIRE', T=720.0, F=0.27 /
&RAMP ID='BEV_FIRE', T=1500.0, F=0.09 /
&RAMP ID='BEV_FIRE', T=3480.0, F=0.0 /

&OBST ID='Battery', XB=1.5,2.9, 0.2,1.7, 0.3,0.4, SURF_ID='BATTERY_FIRE'/
&OBST ID='Battery_rear', XB=2.3, 2.9, 0.2, 1.7, 0.4, 0.5, SURF_ID='BATTERY_FIRE'/

&SURF ID='BATTERY_FIRE_FRONT',
      SPEC_ID ='PROPANE',
      HRRPUA=440,
      RAMP_Q='BEV_FIRE_2',
      COLOR='RED',
       E_COEFFICIENT=0.1/

&RAMP ID='BEV_FIRE_2', T=1200.0, F=0.0 /
&RAMP ID='BEV_FIRE_2', T=1500.0, F=0.09 /
&RAMP ID='BEV_FIRE_2', T=1980.0, F=0.45 /
&RAMP ID='BEV_FIRE_2', T=2100.0, F=0.02 /
&RAMP ID='BEV_FIRE_2', T=3480.0, F=0.0 /

&OBST ID='Battery:1667225_front', XB=0.8, 1.5, 0.2, 0.6, 0.3, 0.4, SURF_ID='BATTERY_FIRE_FRONT'/
&OBST ID='Battery:1667226_front', XB=0.8, 1.5, 0.7, 1.2, 0.3, 0.4, SURF_ID='BATTERY_FIRE_FRONT'/
&OBST ID='Battery:1667227_front', XB=0.8, 1.5, 1.3, 1.7, 0.3, 0.4, SURF_ID='BATTERY_FIRE_FRONT'/

/_____________________________________________________________________________________Jet flames
&SURF ID='JET_1',
      SPEC_ID(1) = 'PROPANE',
      MASS_FRACTION(1) = 0.017,
      RAMP_V = 'JET_ACT_1',
      VEL = -60.0,
      TMP_FRONT = 1350.0,
```

```
    COLOR = 'ORANGE' / 10% is propane, the other is air

&RAMP ID='JET_ACT_1', T=180.0, F=0.0 /
&RAMP ID='JET_ACT_1', T=181, F=1.0 /
&RAMP ID='JET_ACT_1', T=220, F=0.7 /
&RAMP ID='JET_ACT_1', T=221, F=0.0 /

&VENT ID='Jet_Flame_1', SURF_ID='JET_1',XB=0.8,0.9, 0.2,0.2, 0.3,0.4, IOR=-2 /

&SURF ID='JET_2',
    SPEC_ID(1) = 'PROPANE',
    MASS_FRACTION(1) = 0.019,
    RAMP_V = 'JET_ACT_2',
    VEL = -60.0,
    TMP_FRONT = 1200.0,
    COLOR = 'ORANGE' /

&RAMP ID='JET_ACT_2', T=300.0, F=0.0 /
&RAMP ID='JET_ACT_2', T=301, F=1.0 /
&RAMP ID='JET_ACT_2', T=349, F=0.7 /
&RAMP ID='JET_ACT_2', T=350, F=0.0 /

&VENT ID='Jet_Flame_2', SURF_ID='JET_2',XB=0.9,1.0, 0.2,0.2, 0.3,0.4, IOR=-2 /

&SURF ID='JET_3',
    SPEC_ID(1) = 'PROPANE',
    MASS_FRACTION(1) = 0.03,
    RAMP_V = 'JET_ACT_3',
    VEL = -70.0,
    TMP_FRONT = 1350.0,
    COLOR = 'ORANGE' /

&RAMP ID='JET_ACT_3', T=600.0, F=0.0 /
&RAMP ID='JET_ACT_3', T=601, F=1.0 /
&RAMP ID='JET_ACT_3', T=659, F=0.7 /
```

```
&RAMP ID='JET_ACT_3', T=660, F=0.0 /

&VENT ID='Jet_Flame_3', SURF_ID='JET_3',XB=1.0,1.1, 0.2,0.2, 0.3,0.4, IOR=-2 /

&SURF ID='JET_4',
    SPEC_ID(1) = 'PROPANE',
    MASS_FRACTION(1) = 0.11,
    RAMP_V = 'JET_ACT_4',
    VEL = -60.0,
    TMP_FRONT = 800.0,
    COLOR = 'ORANGE' /

&RAMP ID='JET_ACT_4', T=720.0, F=0.0 /
&RAMP ID='JET_ACT_4', T=721, F=1.0 /
&RAMP ID='JET_ACT_4', T=779, F=0.7 /
&RAMP ID='JET_ACT_4', T=780, F=0.0 /

&VENT ID='Jet_Flame_4', SURF_ID='JET_4',XB=1.1,1.2, 0.2,0.2, 0.3,0.4, IOR=-2 /

&SURF ID='JET_5',
    SPEC_ID(1) = 'PROPANE',
    MASS_FRACTION(1) = 0.03,
    RAMP_V = 'JET_ACT_5',
    VEL = -70.0,
    TMP_FRONT = 700.0,
    COLOR = 'ORANGE' /

&RAMP ID='JET_ACT_5', T=1020.0, F=0.0 /
&RAMP ID='JET_ACT_5', T=1021, F=1.0 /
&RAMP ID='JET_ACT_5', T=1079, F=0.9 /
&RAMP ID='JET_ACT_5', T=1080, F=0.0 /

&VENT ID='Jet_Flame_5', SURF_ID='JET_5',XB=1.2,1.3, 0.2,0.2, 0.3,0.4, IOR=-2 /
```

```
&SURF ID='JET_6',
    SPEC_ID(1) = 'PROPANE',
    MASS_FRACTION(1) = 0.048,
    RAMP_V = 'JET_ACT_6',
    VEL = -70.0,
    TMP_FRONT = 1000.0,
    COLOR = 'ORANGE' /

&RAMP ID='JET_ACT_6', T=1140.0, F=0.0 /
&RAMP ID='JET_ACT_6', T=1141, F=0.3 /
&RAMP ID='JET_ACT_6', T=1179, F=1.0 /
&RAMP ID='JET_ACT_6', T=1180, F=0.0 /

&VENT ID='Jet_Flame_6', SURF_ID='JET_6',XB=1.3,1.4, 0.2,0.2, 0.3,0.4, IOR=-2 /


&SURF ID='JET_7',
    SPEC_ID(1) = 'PROPANE',
    MASS_FRACTION(1) = 0.085,
    RAMP_V = 'JET_ACT_7',
    VEL = -40.0,
    TMP_FRONT = 700.0,
    COLOR = 'ORANGE' /

&RAMP ID='JET_ACT_7', T=1380.0, F=0.0 /
&RAMP ID='JET_ACT_7', T=1381, F=1.0 /
&RAMP ID='JET_ACT_7', T=1420, F=0.7 /
&RAMP ID='JET_ACT_7', T=1421, F=0.0 /

&VENT ID='Jet_Flame_7', SURF_ID='JET_7',XB=1.4,1.5, 0.2,0.2, 0.3,0.4, IOR=-2 /

&SURF ID='JET_8',
    SPEC_ID(1) = 'PROPANE',
    MASS_FRACTION(1) = 0.08,
    RAMP_V = 'JET_ACT_8',
```

```
    VEL = -60.0,
    TMP_FRONT = 1000.0,
    COLOR = 'ORANGE' /

&RAMP ID='JET_ACT_8', T=1500.0, F=0.0 /
&RAMP ID='JET_ACT_8', T=1501, F=1.0 /
&RAMP ID='JET_ACT_8', T=1540, F=0.5 /
&RAMP ID='JET_ACT_8', T=1541, F=0.0 /

&VENT ID='Jet_Flame_8', SURF_ID='JET_8',XB=1.5,1.6, 0.2,0.2, 0.3,0.4, IOR=-2 /

&SURF ID='JET_9',
    SPEC_ID(1) = 'PROPANE',
    MASS_FRACTION(1) = 0.06,
    RAMP_V = 'JET_ACT_9',
    VEL = -55.0,
    TMP_FRONT = 900.0,
    COLOR = 'ORANGE' /

&RAMP ID='JET_ACT_9', T=2280.0, F=0.0 /
&RAMP ID='JET_ACT_9', T=2281, F=1.0 /
&RAMP ID='JET_ACT_9', T=2320, F=0.7 /
&RAMP ID='JET_ACT_9', T=2321, F=0.0 /

&VENT ID='Jet_Flame_9', SURF_ID='JET_9',XB=1.6,1.7, 0.2,0.2, 0.3,0.4, IOR=-2 /

&SURF ID='JET_10',
    SPEC_ID(1) = 'PROPANE',
    MASS_FRACTION(1) = 0.1,
    RAMP_V = 'JET_ACT_10',
    VEL = -50.0,
    TMP_FRONT = 900.0,
    COLOR = 'ORANGE' /

&RAMP ID='JET_ACT_10', T=2520.0, F=0.0 /
```

```
&RAMP ID='JET_ACT_10', T=2521, F=1.0 /
&RAMP ID='JET_ACT_10', T=2580, F=0.7 /
&RAMP ID='JET_ACT_10', T=2581, F=0.0 /

&VENT ID='Jet_Flame_10', SURF_ID='JET_10',XB=1.7,1.9, 0.2,0.2, 0.3,0.4, IOR=-2 /

&SURF ID='JET_11',
    SPEC_ID(1) = 'PROPANE',
    MASS_FRACTION(1) = 0.09,
    RAMP_V = 'JET_ACT_11',
    VEL = -45.0,
    TMP_FRONT = 800.0,
    COLOR = 'ORANGE' /

&RAMP ID='JET_ACT_11', T=2280.0, F=0.0 /
&RAMP ID='JET_ACT_11', T=2281 F=1.0 /
&RAMP ID='JET_ACT_11', T=2920, F=0.7 /
&RAMP ID='JET_ACT_11', T=2921, F=0.0 /

&VENT ID='Jet_Flame_11', SURF_ID='JET_11',XB=1.9,2.0, 0.2,0.2, 0.3,0.5, IOR=-2 /
/____________________________________________________________________________non-combustible materials

&MATL ID='CONCRETE',
    CONDUCTIVITY=1.37,
    SPECIFIC_HEAT=0.88,
    DENSITY=2400. / based combustible car

&MATL ID='CYLINDER_ALUMINIUM',
    CONDUCTIVITY=180.0,
    SPECIFIC_HEAT=0.897,
    DENSITY=2710.0 /

&MATL ID        = 'TEMPERED_GLASS'
    SPECIFIC_HEAT = 0.8
    DENSITY     = 2500.
```

```
    CONDUCTIVITY = 0.8 /

&MATL ID='CAR_STEEL',
    CONDUCTIVITY=50.0,
    SPECIFIC_HEAT=0.50,
    DENSITY=7850.0,
    EMISSIVITY=0.9 /

&MATL ID='INCOMBUSTIBLE_INSULATOR',
    CONDUCTIVITY=0.04,
    SPECIFIC_HEAT=0.85,
    DENSITY=100.0 /

&MATL ID='TRANS_STEEL',
    CONDUCTIVITY=50.0,
    SPECIFIC_HEAT=0.50,
    DENSITY=7850.0 /

&SURF ID='Concrete',
    COLOR='GRAY',
    TRANSPARENCY=0.4,
    MATL_ID='CONCRETE',
    THICKNESS=0.30,
    BACKING='VOID' /based on combustible car, but thicker

&SURF ID       = 'Glass'
    RGB = 249,250,249,
    TRANSPARENCY = 0.211765,
    MATL_ID   = 'TEMPERED_GLASS'
    THICKNESS = 0.006 / Based Combustible car

&SURF ID='steel',
    COLOR='SILVER',
    MATL_ID='CAR_STEEL',
    THICKNESS=0.005,
```

```
    BACKING='EXPOSED' / /Normal construction steel

&SURF ID='Insulation_batteries',
    COLOR='GOLDENROD',
    MATL_ID='INCOMBUSTIBLE_INSULATOR',
    THICKNESS=0.05,
    BACKING='EXPOSED' /Average values of rock wool

&SURF ID='transformer',
    RGB=245,245,243,
    MATL_ID='TRANS_STEEL',
    THICKNESS=0.01,
    EMISSIVITY=0.9,
    BACKING='EXPOSED' /transformator is basically a big metal object

&SURF ID='Cylinders',
    RGB=200,200,200,
    MATL_ID='CYLINDER_ALUMINIUM',
    THICKNESS=0.01,
    EMISSIVITY=0.4,
    BACKING='EXPOSED' /based on aluminium of combustible car

/__________________________________________________________________________________combustible materials

&MATL ID='BATTERY_MATERIAL_SIMPLE',
    CONDUCTIVITY=0.2,
    SPECIFIC_HEAT=1.5,
    DENSITY=1500.0 /
    HEAT_OF_COMBUSTION=39000 /


&MATL ID          = 'FABRIC_LINING',
    CONDUCTIVITY = 0.1,
    SPECIFIC_HEAT = 1.0,
    DENSITY      = 200.,
```

```
    HEAT_OF_COMBUSTION=20000 /

&MATL ID          = 'FOAM_FILLING',
    CONDUCTIVITY = 0.05,
    SPECIFIC_HEAT = 1.0,
    DENSITY      = 80.,
    HEAT_OF_COMBUSTION=28000 /

&MATL ID          = 'POLYPROPYLENE_PLASTIC',
    CONDUCTIVITY = 0.16,
    SPECIFIC_HEAT = 1.9,
    DENSITY      = 900,
    HEAT_OF_COMBUSTION=48000 /

&MATL ID='ELECTRONIC_PLASTIC',
    CONDUCTIVITY=0.20,
    SPECIFIC_HEAT=1.5,
    DENSITY=1100.0,
    HEAT_OF_COMBUSTION=38000 /

&MATL ID          = 'KUMI_CC'
    CONDUCTIVITY = 0.13
    SPECIFIC_HEAT = 1.88
    DENSITY      = 910.
    HEAT_OF_COMBUSTION = 32000. /


&SURF ID='SIMPLE_BATTERY_SURFACE',
    COLOR='RED' /
    HRRPUA=440.0,
    BURN_AWAY      = T,
    IGNITION_TEMPERATURE = 270,
    EXTINCTION_TEMPERATURE = 220,
    MATL_ID='BATTERY_MATERIAL_SIMPLE',
    THICKNESS=0.03,
```

```
     E_COEFFICIENT=0.1 /

&SURF ID            = 'Seating',
     COLOR          = 'BROWN'
     HRRPUA         = 500,
     BURN_AWAY      = T,
     IGNITION_TEMPERATURE = 350,
     EXTINCTION_TEMPERATURE = 300,
     MATL_ID(1:3,1) = 'FABRIC_LINING','FOAM_FILLING',
     THICKNESS(1:3) = 0.002, 0.2,
      E_COEFFICIENT=0.72 /

&SURF ID          = 'Wheel_Assembly',
     COLOR        = 'BLACK'
     HRRPUA       = 300,
     BURN_AWAY      = T,
     IGNITION_TEMPERATURE = 300,
     EXTINCTION_TEMPERATURE = 250,
     MATL_ID      = 'KUMI_CC',
     THICKNESS    = 0.03,
      E_COEFFICIENT=0.54  /

&SURF ID            = 'Insulation_car_cabine',
     RGB=255,255,224,
     HRRPUA         = 500,
     BURN_AWAY      = T,
     IGNITION_TEMPERATURE = 450,
     EXTINCTION_TEMPERATURE = 400,
     MATL_ID = 'FABRIC_LINING','POLYPROPYLENE_PLASTIC',
     THICKNESS = 0.002, 0.05,
      E_COEFFICIENT=0.72 /

&SURF ID='electronic',
     RGB=80,80,80,
     HRRPUA=300,
```

```
      BURN_AWAY= T,
      IGNITION_TEMPERATURE=320,
      EXTINCTION_TEMPERATURE = 270,
      MATL_ID='ELECTRONIC_PLASTIC',
      THICKNESS=0.004,
       E_COEFFICIENT=0.72 /
/_______________________________________________________________________________underground parking
&OBST ID='Concrete_Floor', XB=-1.0,8.3,-7.0,8.9,-0.1,0.0, COLOR='GRAY', TRANSPARENCY=1.0, SURF_ID='Concrete' /
&OBST ID='Concrete_wall:1692812', XB=-1.0,-0.7,-7.0,8.9,0.0,2.5, SURF_ID='Concrete' /
&OBST ID='Concrete_ceiling', XB=-1.0,8.3,-7.0,8.9,2.5,2.7, SURF_ID='Concrete'/

/_______________________________________________________________________________________Green car
&OBST ID='Bottom_car', XB=-0.4,-0.1,0.2,0.4,0.2,0.25, COLOR='SILVER', SURF_ID='steel'/
&OBST ID='Bottom_car', XB=-0.4,2.6,0.4,1.0,0.2,0.25, COLOR='SILVER', SURF_ID='steel'/
&OBST ID='Bottom_car', XB=-0.3,-0.1,0.1,0.2,0.2,0.25, COLOR='SILVER', SURF_ID='steel'/
&OBST ID='Bottom_car', XB=-0.2,-0.1,0.0,0.1,0.2,0.25, COLOR='SILVER', SURF_ID='steel'/
&OBST ID='Bottom_car', XB=0.7,2.6,0.0,0.4,0.2,0.25, COLOR='SILVER', SURF_ID='steel'/
&OBST ID='Bottom_car', XB=2.6,3.0,0.0,0.4,0.2,0.25, COLOR='SILVER', SURF_ID='steel'/
&OBST ID='Bottom_car', XB=2.6,4.3,0.4,1.0,0.2,0.25, COLOR='SILVER', SURF_ID='steel'/
&OBST ID='Bottom_car', XB=3.8,4.2,0.0,0.1,0.2,0.25, COLOR='SILVER', SURF_ID='steel'/
&OBST ID='Bottom_car', XB=3.8,4.3,0.1,0.4,0.2,0.25, COLOR='SILVER', SURF_ID='steel'/
&OBST ID='Bottom_car', XB=2.6,3.0,1.5,1.9,0.2,0.25, COLOR='SILVER', SURF_ID='steel'/
&OBST ID='Bottom_car', XB=2.6,4.3,1.0,1.5,0.2,0.25, COLOR='SILVER', SURF_ID='steel'/
&OBST ID='Bottom_car', XB=3.8,4.1,1.8,1.9,0.2,0.25, COLOR='SILVER', SURF_ID='steel'/
&OBST ID='Bottom_car', XB=3.8,4.3,1.5,1.8,0.2,0.25, COLOR='SILVER', SURF_ID='steel'/
&OBST ID='Bottom_car', XB=-0.4,-0.1,1.5,1.7,0.2,0.25, COLOR='SILVER', SURF_ID='steel'/
&OBST ID='Bottom_car', XB=-0.4,2.6,1.0,1.5,0.2,0.25, COLOR='SILVER', SURF_ID='steel'/
&OBST ID='Bottom_car', XB=-0.3,-0.1,1.7,1.8,0.2,0.25, COLOR='SILVER', SURF_ID='steel'/
&OBST ID='Bottom_car', XB=-0.2,-0.1,1.8,1.9,0.2,0.25, COLOR='SILVER', SURF_ID='steel'/
&OBST ID='Bottom_car', XB=0.7,2.6,1.5,1.9,0.2,0.25, COLOR='SILVER', SURF_ID='steel'/

&OBST ID='Covering_batteries', XB=0.8,2.3, 0.1,1.8, 0.5,0.6, COLOR='BLUE', SURF_ID='steel'/  seperation between seating and batteries for oxygen
&OBST ID='Covering_batteries_back', XB=2.3,2.9, 0.2,1.7, 0.6,0.7, COLOR='BLUE', SURF_ID='steel'/  seperation between seating and batteries for oxygen

/_________________________________________________________________________green car frame
```

```
&OBST ID='car_body_front', XB=-0.4,-0.2,0.2,1.0,0.8,0.9, COLOR='FOREST GREEN', SURF_ID='steel'/
&OBST ID='car_body_front', XB=-0.3,-0.2,0.0,0.2,0.8,0.9, COLOR='FOREST GREEN', SURF_ID='steel'/
&OBST ID='car_body_front', XB=-0.4,-0.2,1.0,1.7,0.8,0.9, COLOR='FOREST GREEN', SURF_ID='steel'/
&OBST ID='car_body_front', XB=-0.3,-0.2,1.7,1.9,0.8,0.9, COLOR='FOREST GREEN', SURF_ID='steel'/
&OBST ID='car_body_above_wheels:1678653', XB=-0.2,0.8,0.0,0.5,0.8,0.9, COLOR='FOREST GREEN', SURF_ID='steel'/
&OBST ID='car_body_above_wheels:1678732', XB=-0.2,0.8,1.4,1.9,0.8,0.9, COLOR='FOREST GREEN', SURF_ID='steel'/
&OBST ID='car_body_above_wheels:1678748', XB=2.9,3.9,1.4,1.9,0.8,0.9, COLOR='FOREST GREEN', SURF_ID='steel'/
&OBST ID='car_body_above_wheels:1678762', XB=2.9,3.9,0.0,0.5,0.8,0.9, COLOR='FOREST GREEN', SURF_ID='steel'/
&OBST ID='Car_body:1673246', XB=-0.4,-0.2,1.6,1.7,0.3,0.8, COLOR='FOREST GREEN', SURF_ID='steel'/
&OBST ID='Car_body:1673275', XB=-0.3,-0.2,1.7,1.9,0.3,0.8, COLOR='FOREST GREEN', SURF_ID='steel'/
&OBST ID='Car_body:1673381', XB=-0.2,-0.1,1.8,1.9,0.3,0.8, COLOR='FOREST GREEN', SURF_ID='steel'/
&OBST ID='Car_body:1673471', XB=-0.2,-0.1,1.4,1.8,0.3,0.8, COLOR='FOREST GREEN', SURF_ID='steel'/
&OBST ID='Car_body:1673520', XB=-0.1,0.8,1.4,1.5,0.3,0.8, COLOR='FOREST GREEN', SURF_ID='steel'/
&OBST ID='Car_body:1673573', XB=0.7,0.8,1.5,1.9,0.3,0.8, COLOR='FOREST GREEN', SURF_ID='steel'/
&OBST ID='Car_body:1673628', XB=2.6,2.9,1.8,1.9,0.4,1.0, COLOR='FOREST GREEN', SURF_ID='steel'/
&OBST ID='Car_body:1673628', XB=0.8,2.6,1.8,1.9,0.4,1.0, COLOR='FOREST GREEN', SURF_ID='steel'/
&OBST ID='Car_body:1673732', XB=2.9,3.9,1.4,1.5,0.3,0.8, COLOR='FOREST GREEN', SURF_ID='steel'/
&OBST ID='Car_body:1673763', XB=3.8,3.9,1.5,1.9,0.3,0.8, COLOR='FOREST GREEN', SURF_ID='steel'/
&OBST ID='Car_body:1673788', XB=3.9,4.2,1.8,1.9,0.3,0.9, COLOR='FOREST GREEN', SURF_ID='steel'/
&OBST ID='Car_body:1673830', XB=4.1,4.2,1.7,1.8,0.3,0.9, COLOR='FOREST GREEN', SURF_ID='steel'/
&OBST ID='Car_body:1673916', XB=4.2,4.3,0.1,1.0,0.3,0.9, COLOR='FOREST GREEN', SURF_ID='steel'/
&OBST ID='Car_body:1673916', XB=4.2,4.3,1.0,1.8,0.3,0.9, COLOR='FOREST GREEN', SURF_ID='steel'/
&OBST ID='Car_body:1673967', XB=4.1,4.2,0.0,0.2,0.3,0.9, COLOR='FOREST GREEN', SURF_ID='steel'/
&OBST ID='Car_body:1673995', XB=4.1,4.2,0.1,0.2,0.3,0.9, COLOR='FOREST GREEN', SURF_ID='steel'/
&OBST ID='Car_body:1674064', XB=3.9,4.1,0.0,0.1,0.3,0.9, COLOR='FOREST GREEN', SURF_ID='steel'/
&OBST ID='Car_body:1674105', XB=3.8,3.9,0.0,0.5,0.3,0.8, COLOR='FOREST GREEN', SURF_ID='steel'/
&OBST ID='Car_body:1674245', XB=0.8,2.6,0.0,0.1,0.4,1.0, COLOR='FOREST GREEN', SURF_ID='steel'/
&OBST ID='Car_body:1674245', XB=2.6,2.9,0.0,0.1,0.4,1.0, COLOR='FOREST GREEN', SURF_ID='steel'/
&OBST ID='Car_body:1674536', XB=0.7,0.8,0.0,0.5,0.3,0.8, COLOR='FOREST GREEN', SURF_ID='steel'/
&OBST ID='Car_body:1674582', XB=-0.2,0.7,0.4,0.5,0.3,0.8, COLOR='FOREST GREEN', SURF_ID='steel'/
&OBST ID='Car_body:1674615', XB=-0.2,-0.1,0.0,0.4,0.3,0.8, COLOR='FOREST GREEN', SURF_ID='steel'/
&OBST ID='Car_body:1674733', XB=-0.3,-0.2,0.0,0.3,0.3,0.8, COLOR='FOREST GREEN', SURF_ID='steel'/
&OBST ID='Car_body:1674759', XB=-0.4,-0.3,0.2,0.3,0.3,0.8, COLOR='FOREST GREEN', SURF_ID='steel'/
&OBST ID='Car_body:1674792', XB=-0.4,-0.3,0.3,1.0,0.3,0.8, COLOR='FOREST GREEN', SURF_ID='steel'/
```

```
&OBST ID='Car_body:1674792', XB=-0.4,-0.3,1.0,1.6,0.3,0.8, COLOR='FOREST GREEN', SURF_ID='steel'/
&OBST ID='Car_body:1679523', XB=2.9,3.8,0.4,0.5,0.3,0.8, COLOR='FOREST GREEN', SURF_ID='steel'/
&OBST ID='Car_body:1679563', XB=2.9,3.0,0.0,0.4,0.3,0.8, COLOR='FOREST GREEN', SURF_ID='steel'/
&OBST ID='Car_body_roof', XB=1.7,2.6,0.0,1.0,1.6,1.7, COLOR='FOREST GREEN', SURF_ID='steel'/
&OBST ID='Car_body_roof', XB=2.6,3.8,0.0,1.0,1.6,1.7, COLOR='FOREST GREEN', SURF_ID='steel'/
&OBST ID='Car_body_roof', XB=2.6,3.8,1.0,1.9,1.6,1.7, COLOR='FOREST GREEN', SURF_ID='steel'/
&OBST ID='Car_body_roof', XB=1.7,2.6,1.0,1.9,1.6,1.7, COLOR='FOREST GREEN', SURF_ID='steel'/
&OBST ID='engine cover:1685928', XB=-0.2,0.8,0.0,1.0,0.9,1.0, COLOR='FOREST GREEN', SURF_ID='steel'/
&OBST ID='engine cover:1685928', XB=-0.2,0.8,1.0,1.9,0.9,1.0, COLOR='FOREST GREEN', SURF_ID='steel'/
&OBST ID=' Frame_front_window:1690476', XB=0.5,0.8,0.0,0.1,1.0,1.1, COLOR='FOREST GREEN', SURF_ID='steel'/
&OBST ID=' Frame_front_window:1690483', XB=0.7,1.0,0.0,0.1,1.1,1.2, COLOR='FOREST GREEN', SURF_ID='steel'/
&OBST ID=' Frame_front_window:1690490', XB=0.9,1.2,0.0,0.1,1.2,1.3, COLOR='FOREST GREEN', SURF_ID='steel'/
&OBST ID=' Frame_front_window:1690497', XB=1.1,1.4,0.0,0.1,1.3,1.4, COLOR='FOREST GREEN', SURF_ID='steel'/
&OBST ID=' Frame_front_window:1690504', XB=1.3,1.6,0.0,0.1,1.4,1.5, COLOR='FOREST GREEN', SURF_ID='steel'/
&OBST ID=' Frame_front_window:1690511', XB=1.5,1.8,0.0,0.1,1.5,1.6, COLOR='FOREST GREEN', SURF_ID='steel'/
&OBST ID=' Frame_front_window:1690660', XB=0.5,0.8,1.8,1.9,1.0,1.1, COLOR='FOREST GREEN', SURF_ID='steel'/
&OBST ID=' Frame_front_window:1690667', XB=0.7,1.0,1.8,1.9,1.1,1.2, COLOR='FOREST GREEN', SURF_ID='steel'/
&OBST ID=' Frame_front_window:1690674', XB=0.9,1.2,1.8,1.9,1.2,1.3, COLOR='FOREST GREEN', SURF_ID='steel'/
&OBST ID=' Frame_front_window:1690681', XB=1.1,1.4,1.8,1.9,1.3,1.4, COLOR='FOREST GREEN', SURF_ID='steel'/
&OBST ID=' Frame_front_window:1690688', XB=1.3,1.6,1.8,1.9,1.4,1.5, COLOR='FOREST GREEN', SURF_ID='steel'/
&OBST ID=' Frame_front_window:1690695', XB=1.5,1.8,1.8,1.9,1.5,1.6, COLOR='FOREST GREEN', SURF_ID='steel'/
&OBST ID=' Frame_back_window:1690745', XB=3.7,3.9,0.0,0.1,1.5,1.6, COLOR='FOREST GREEN', SURF_ID='steel'/
&OBST ID=' Frame_back_window:1690752', XB=3.8,4.0,0.0,0.1,1.4,1.5, COLOR='FOREST GREEN', SURF_ID='steel'/
&OBST ID=' Frame_back_window:1690759', XB=3.9,4.1,0.0,0.1,1.3,1.4, COLOR='FOREST GREEN', SURF_ID='steel'/
&OBST ID=' Frame_back_window:1690766', XB=4.0,4.2,0.0,0.1,1.2,1.3, COLOR='FOREST GREEN', SURF_ID='steel'/
&OBST ID=' Frame_back_window:1690773', XB=4.0,4.2,0.0,0.1,1.1,1.2, COLOR='FOREST GREEN', SURF_ID='steel'/
&OBST ID=' Frame_back_window:1690773', XB=4.0,4.3,0.1,0.2,1.1,1.2, COLOR='FOREST GREEN', SURF_ID='steel'/
&OBST ID=' Frame_back_window:1691187', XB=3.7,3.9,1.8,1.9,1.5,1.6, COLOR='FOREST GREEN', SURF_ID='steel'/
&OBST ID=' Frame_back_window:1691194', XB=3.8,4.0,1.8,1.9,1.4,1.5, COLOR='FOREST GREEN', SURF_ID='steel'/
&OBST ID=' Frame_back_window:1691201', XB=3.9,4.1,1.8,1.9,1.3,1.4, COLOR='FOREST GREEN', SURF_ID='steel'/
&OBST ID=' Frame_back_window:1691208', XB=4.0,4.2,1.8,1.9,1.2,1.3, COLOR='FOREST GREEN', SURF_ID='steel'/
&OBST ID=' Frame_back_window:1691285', XB=4.0,4.2,1.8,1.9,1.1,1.2, COLOR='FOREST GREEN', SURF_ID='steel'/
&OBST ID=' Frame_back_window:1691285', XB=4.0,4.3,1.7,1.8,1.1,1.2, COLOR='FOREST GREEN', SURF_ID='steel'/
&OBST ID=' Frame_back_window:1691348', XB=0.8,1.0,-0.1,0.3,1.0,1.1, COLOR='FOREST GREEN', SURF_ID='steel'/
&OBST ID=' Frame_back_window:1691491', XB=0.8,1.0,1.6,2.0,1.0,1.1, COLOR='FOREST GREEN', SURF_ID='steel'/
```

```
&OBST ID='Car_body:1689403', XB=2.9,4.1,1.8,1.9,0.9,1.1, COLOR='FOREST GREEN', SURF_ID='steel'/
&OBST ID='Car_body:1689425', XB=4.1,4.2,1.7,1.9,0.9,1.1, COLOR='FOREST GREEN', SURF_ID='steel'/
&OBST ID='Car_body:1689461', XB=4.2,4.3,1.7,1.8,0.9,1.1, COLOR='FOREST GREEN', SURF_ID='steel'/
&OBST ID='Car_body:1689516', XB=4.2,4.3,0.2,1.0,0.9,1.1, COLOR='FOREST GREEN', SURF_ID='steel'/
&OBST ID='Car_body:1689516', XB=4.2,4.3,1.0,1.7,0.9,1.1, COLOR='FOREST GREEN', SURF_ID='steel'/
&OBST ID='Car_body:1689545', XB=4.1,4.3,0.1,0.2,0.9,1.1, COLOR='FOREST GREEN', SURF_ID='steel'/
&OBST ID='Car_body:1689567', XB=4.1,4.2,0.0,0.1,0.9,1.1, COLOR='FOREST GREEN', SURF_ID='steel'/
&OBST ID='Car_body:1689617', XB=2.9,4.1,-0,0.1,0.9,1.1, COLOR='FOREST GREEN', SURF_ID='steel'/
&OBST ID='Car_body:1680322', XB=2.9,3.0,1.5,1.9,0.3,0.8, COLOR='FOREST GREEN', SURF_ID='steel'/


&OBST ID='Covering_trunk', XB=3.7,4.2,0.5,1.0,0.3,0.35, SURF_ID='Insulation_car_cabine', BULK_DENSITY=900. /
&OBST ID='Covering_trunk', XB=3.9,4.1,0.1,0.2,0.3,0.35, SURF_ID='Insulation_car_cabine', BULK_DENSITY=900. /
&OBST ID='Covering_trunk', XB=3.9,4.2,0.2,0.5,0.3,0.35, SURF_ID='Insulation_car_cabine', BULK_DENSITY=900. /
&OBST ID='Covering_trunk', XB=3.7,4.2,1.0,1.4,0.3,0.35, SURF_ID='Insulation_car_cabine', BULK_DENSITY=900. /
&OBST ID='Covering_trunk', XB=3.9,4.1,1.7,1.8,0.3,0.35, SURF_ID='Insulation_car_cabine', BULK_DENSITY=900. /
&OBST ID='Covering_trunk', XB=3.9,4.2,1.4,1.7,0.3,0.35, SURF_ID='Insulation_car_cabine', BULK_DENSITY=900. /
&OBST ID='Covering_wheels', XB=2.9,3.8,0.5,1.0,0.85,0.9, SURF_ID='Insulation_car_cabine', BULK_DENSITY=900. /
&OBST ID='Covering_wheels', XB=2.9,3.8,1.0,1.4,0.85,0.9, SURF_ID='Insulation_car_cabine', BULK_DENSITY=900. /

&OBST ID='Wheel:1665075', XB=0.1,0.5,1.6,1.9,0.0,0.1, COLOR='BLACK', SURF_ID='Wheel_Assembly', BULK_DENSITY=910. /
&OBST ID='Wheel:1665075_rim', XB=0.1,0.5,1.6,1.9,0.1,0.6, COLOR='SILVER', SURF_ID='steel'/
&OBST ID='Wheel:1665075', XB=0.1,0.5,1.6,1.9,0.6,0.7, COLOR='BLACK', SURF_ID='Wheel_Assembly', BULK_DENSITY=910. /
&OBST ID='Wheel:1665344', XB=0.5,0.6,1.6,1.9,0.1,0.6, COLOR='BLACK', SURF_ID='Wheel_Assembly', BULK_DENSITY=910. /
&OBST ID=' Wheel:1666370', XB=0.0,0.1,1.6,1.9,0.1,0.6, COLOR='BLACK', SURF_ID='Wheel_Assembly', BULK_DENSITY=910. /
&OBST ID='Wheel:1666668', XB=0.1,0.5,0.0,0.3,0.0,0.1, COLOR='BLACK', SURF_ID='Wheel_Assembly', BULK_DENSITY=910. /
&OBST ID='Wheel_rim:1666668', XB=0.1,0.5,0.0,0.3,0.1,0.6, COLOR='SILVER', SURF_ID='steel'/
&OBST ID='Wheel:1666668', XB=0.1,0.5,0.0,0.3,0.6,0.7, COLOR='BLACK', SURF_ID='Wheel_Assembly', BULK_DENSITY=910. /
&OBST ID=' Wheel:1666669', XB=0.5,0.6,0.0,0.3,0.1,0.6, COLOR='BLACK', SURF_ID='Wheel_Assembly', BULK_DENSITY=910. /
&OBST ID=' Wheel:1666670', XB=0.0,0.1,0.0,0.3,0.1,0.6, COLOR='BLACK', SURF_ID='Wheel_Assembly', BULK_DENSITY=910. /
&OBST ID='Wheel:1666678', XB=3.2,3.6,0.0,0.3,0.0,0.1, COLOR='BLACK', SURF_ID='Wheel_Assembly', BULK_DENSITY=910. /
&OBST ID='Wheel:1666678_rim', XB=3.2,3.6,0.0,0.3,0.1,0.6, COLOR='SILVER', SURF_ID='steel'/
&OBST ID='Wheel:1666678', XB=3.2,3.6,0.0,0.3,0.6,0.7, COLOR='BLACK', SURF_ID='Wheel_Assembly', BULK_DENSITY=910. /
&OBST ID=' Wheel:1666679', XB=3.6,3.7,0.0,0.3,0.1,0.6, COLOR='BLACK', SURF_ID='Wheel_Assembly', BULK_DENSITY=910. /
&OBST ID=' Wheel:1666680', XB=3.1,3.2,0.0,0.3,0.1,0.6, COLOR='BLACK', SURF_ID='Wheel_Assembly', BULK_DENSITY=910. /
```

```
&OBST ID='Wheel:1679782', XB=3.2,3.6,1.6,1.9,0.0,0.1, COLOR='BLACK', SURF_ID='Wheel_Assembly', BULK_DENSITY=910. /
&OBST ID='Wheel:1679782_rim', XB=3.2,3.6,1.6,1.9,0.1,0.6, COLOR='SILVER', SURF_ID='steel'/
&OBST ID='Wheel:1679782', XB=3.2,3.6,1.6,1.9,0.6,0.7, COLOR='BLACK', SURF_ID='Wheel_Assembly', BULK_DENSITY=910. /
&OBST ID='Wheel 2:1679783', XB=3.6,3.7,1.6,1.9,0.1,0.6, COLOR='BLACK', SURF_ID='Wheel_Assembly', BULK_DENSITY=910. /
&OBST ID='Wheel 2:1679784', XB=3.1,3.2,1.6,1.9,0.1,0.6, COLOR='BLACK', SURF_ID='Wheel_Assembly', BULK_DENSITY=910. /
/&OBST ID='Division_insulation_battery_rows', XB=0.8,2.6,0.9,1.0,0.3,0.5, SURF_ID='Insulation_batteries'/
/&OBST ID='Division_insulation_battery_rows', XB=2.6,2.9,0.9,1.0,0.3,0.5, SURF_ID='Insulation_batteries'/
/&OBST ID='Insulation_battery_rows:1671243', XB=2.6,2.9,1.7,1.8,0.3,0.5, SURF_ID='Insulation_batteries'/
/&OBST ID='Insulation_battery_rows:1671243', XB=0.8,2.6,1.7,1.8,0.3,0.5, SURF_ID='Insulation_batteries'/
/&OBST ID='Insulation_battery_rows:1672588', XB=0.8,2.6,0.1,0.2,0.3,0.5, SURF_ID='Insulation_batteries'/
/&OBST ID='Insulation_battery_rows:1672588', XB=2.6,2.9,0.1,0.2,0.3,0.5, SURF_ID='Insulation_batteries'/
&OBST ID='Technical_stuff_front:1676605', XB=-0.2,0.2,0.5,1.0,0.3,0.8, COLOR='GRAY 47', SURF_ID='electronic', BULK_DENSITY=1100. /
&OBST ID='Technical_stuff_front:1676605', XB=-0.2,0.2,1.0,1.4,0.3,0.8, COLOR='GRAY 47', SURF_ID='electronic', BULK_DENSITY=1100. /
&OBST ID='Cylinders:1677342', XB=0.3,0.6,0.5,1.0,0.3,0.8, RGB=244,245,246, SURF_ID='Cylinders'/
&OBST ID='Cylinders:1677342', XB=0.3,0.6,1.0,1.4,0.3,0.8, RGB=244,245,246, SURF_ID='Cylinders'/
&OBST ID='Buffer_behind_engine:1677885', XB=0.6,0.65,0.5,1.0,0.3,0.9,  SURF_ID='Insulation_car_cabine', BULK_DENSITY=900. /
&OBST ID='Buffer_behind_engine:1677885', XB=0.6,0.65,1.0,1.4,0.3,0.9,  SURF_ID='Insulation_car_cabine', BULK_DENSITY=900. /
&OBST ID='Buffer_behind_Transformer:1683239', XB=3.7,3.75,0.5,1.0,0.3,0.9, SURF_ID='Insulation_car_cabine', BULK_DENSITY=900. /
&OBST ID='Buffer_behind_Transformer:1683239', XB=3.7,3.75,1.0,1.4,0.3,0.9, SURF_ID='Insulation_car_cabine', BULK_DENSITY=900. /
&OBST ID='Cover_befor_transformer:1683732', XB=2.9,2.95,0.5,1.0,0.3,0.9, SURF_ID='Insulation_car_cabine', BULK_DENSITY=900. /
&OBST ID='Cover_befor_transformer:1683732', XB=2.9,2.95,1.0,1.4,0.3,0.9, SURF_ID='Insulation_car_cabine', BULK_DENSITY=900. /
&OBST ID='Transformer:1678843', XB=3.1,3.7,0.5,1.0,0.3,0.8, SURF_ID='transformer'/
&OBST ID='Transformer:1678843', XB=3.1,3.7,1.0,1.4,0.3,0.8, SURF_ID='transformer'/
&OBST ID='Seating:1684541', XB=1.2,2.0,1.0,1.6,0.6,0.8, SURF_ID='Seating', /
&OBST ID='Seating:1684640', XB=1.2,2.0,0.3,0.9,0.6,0.8, SURF_ID='Seating' /
&OBST ID='Seating:1685527', XB=2.3,2.6,0.3,1.0,0.7,0.8, SURF_ID='Seating' /
&OBST ID='Seating:1685527', XB=2.6,2.9,0.3,1.0,0.7,0.8, SURF_ID='Seating' /
&OBST ID='Seating:1685527', XB=2.6,2.9,1.0,1.6,0.7,0.8, SURF_ID='Seating' /
&OBST ID='Seating:1685527', XB=2.3,2.6,1.0,1.6,0.7,0.8, SURF_ID='Seating' /
&OBST ID='Dashboard:1686413', XB=0.8,1.1,0.3,1.0,0.9,1.1, COLOR='PURPLE', SURF_ID='electronic', BULK_DENSITY=1100. /
&OBST ID='Dashboard:1686413', XB=0.8,1.1,1.0,1.6,0.9,1.1, COLOR='PURPLE', SURF_ID='electronic', BULK_DENSITY=1100. /
&OBST ID='Seating_backrest:1684772', XB=1.8,2.0,0.3,0.9,0.8,1.4, SURF_ID='Seating' /
&OBST ID='Seating_backrest:1685038', XB=1.8,2.0,1.0,1.6,0.8,1.4, SURF_ID='Seating' /
&OBST ID='Seating_backrest:1685444', XB=2.7,2.9,0.3,1.0,0.8,1.4, SURF_ID='Seating' /
&OBST ID='Seating_backrest:1685444', XB=2.7,2.9,1.0,1.7,0.8,1.4, SURF_ID='Seating' /
```

```
/xmin, xmax, ymin, ymax, zmin, zmax
&OBST ID='safety cage finishing:1685633', XB=0.8,2.6,0.1,0.2,0.6,1.0,
SURF_ID6='Insulation_car_cabine','Insulation_car_cabine','INERT','Insulation_car_cabine','Insulation_car_cabine','Insulation_car_cabine', BULK_DENSITY=900. /
&OBST ID='safety cage finishing:1685633', XB=2.6,2.9,0.1,0.2,0.6,1.0,
SURF_ID6='Insulation_car_cabine','Insulation_car_cabine','INERT','Insulation_car_cabine','Insulation_car_cabine','Insulation_car_cabine', BULK_DENSITY=900. /
&OBST ID='safety cage finishing:1685910', XB=2.6,2.9,1.7,1.8,0.6,1.0,
SURF_ID6='Insulation_car_cabine','Insulation_car_cabine','Insulation_car_cabine','INERT','Insulation_car_cabine','Insulation_car_cabine', BULK_DENSITY=900. /
&OBST ID='safety cage finishing:1685910', XB=0.8,2.6,1.7,1.8,0.6,1.0,
SURF_ID6='Insulation_car_cabine','Insulation_car_cabine','Insulation_car_cabine','INERT','Insulation_car_cabine','Insulation_car_cabine', BULK_DENSITY=900. /

&OBST ID=' Window_frame_middle:1687323', XB=2.0,2.1,0.0,0.1,1.0,1.6, COLOR='FOREST GREEN', SURF_ID='steel'/
&OBST ID='Window_frame_middle_safety_cage_finishing:1687719', XB=2.0,2.1,0.1,0.15,1.0,1.6, SURF_ID='Insulation_car_cabine', BULK_DENSITY=900. /
&OBST ID='Window_frame_middle:1687903', XB=2.8,2.9,0.0,0.1,1.0,1.6,COLOR='FOREST GREEN', SURF_ID='steel'/
&OBST ID='Window_frame_middle_safety_cage_finishinge:1687904', XB=2.8,2.9,0.1,0.15,1.0,1.6, SURF_ID='Insulation_car_cabine', BULK_DENSITY=900. /
&OBST ID='Window_frame_middle:1687988', XB=2.0,2.1,1.8,1.9,1.0,1.6, COLOR='FOREST GREEN', SURF_ID='steel'/
&OBST ID='Window_frame_middle_safety_cage_finishing:1687989', XB=2.0,2.1,1.75,1.8,1.0,1.6, SURF_ID='Insulation_car_cabine', BULK_DENSITY=900. /
&OBST ID='Window_frame_middle:1687990', XB=2.8,2.9,1.8,1.9,1.0,1.6, COLOR='FOREST GREEN', SURF_ID='steel'/
&OBST ID='Window_frame_middle_safety_cage_finishing:1687991', XB=2.8,2.9,1.75,1.8,1.0,1.6, SURF_ID='Insulation_car_cabine', BULK_DENSITY=900. /

/______________________________________________________________________________________________windows green car
&DEVC ID='Window_driver_1', SURF_ID='Glass', XB=1.0,2.0,0.0,0.1,1.0,1.2, QUANTITY='WALL TEMPERATURE', SPATIAL_STATISTIC='MAX', SETPOINT=300.,
INITIAL_STATE=T. /
&DEVC ID='Window_driver_2', SURF_ID='Glass', XB=1.2,2.0,0.0,0.1,1.2,1.3, QUANTITY='WALL TEMPERATURE', SPATIAL_STATISTIC='MAX', SETPOINT=300.,
INITIAL_STATE=T. /
&DEVC ID='Window_driver_3', SURF_ID='Glass', XB=1.4,2.0,0.0,0.1,1.3,1.4, QUANTITY='WALL TEMPERATURE', SPATIAL_STATISTIC='MAX', SETPOINT=300.,
INITIAL_STATE=T. /
&DEVC ID='Window_driver_4', SURF_ID='Glass', XB=1.6,2.0,0.0,0.1,1.4,1.5, QUANTITY='WALL TEMPERATURE', SPATIAL_STATISTIC='MAX', SETPOINT=300.,
INITIAL_STATE=T. /
&DEVC ID='Window_driver_5', SURF_ID='Glass', XB=1.8,2.0,0.0,0.1,1.5,1.6, QUANTITY='WALL TEMPERATURE', SPATIAL_STATISTIC='MAX', SETPOINT=300.,
INITIAL_STATE=T. /

&DEVC ID='Window_passenger_1', SURF_ID='Glass', XB=1.0,2.0,1.8,1.9,1.0,1.2, QUANTITY='WALL TEMPERATURE', SPATIAL_STATISTIC='MAX', SETPOINT=300.,
INITIAL_STATE=T. /
```

```
&DEVC ID='Window_passenger_2', SURF_ID='Glass', XB=1.2,2.0,1.8,1.9,1.2,1.3, QUANTITY='WALL TEMPERATURE', SPATIAL_STATISTIC='MAX', SETPOINT=300., INITIAL_STATE=T. /
&DEVC ID='Window_passenger_3', SURF_ID='Glass', XB=1.4,2.0,1.8,1.9,1.3,1.4, QUANTITY='WALL TEMPERATURE', SPATIAL_STATISTIC='MAX', SETPOINT=300., INITIAL_STATE=T. /
&DEVC ID='Window_passenger_4', SURF_ID='Glass', XB=1.6,2.0,1.8,1.9,1.4,1.5, QUANTITY='WALL TEMPERATURE', SPATIAL_STATISTIC='MAX', SETPOINT=300., INITIAL_STATE=T. /
&DEVC ID='Window_passenger_5', SURF_ID='Glass', XB=1.8,2.0,1.8,1.9,1.5,1.6, QUANTITY='WALL TEMPERATURE', SPATIAL_STATISTIC='MAX', SETPOINT=300., INITIAL_STATE=T. /

&DEVC ID='Back_window_passenger_1', SURF_ID='Glass', XB=2.9,4.0,1.8,1.9,1.1,1.3, QUANTITY='WALL TEMPERATURE', SPATIAL_STATISTIC='MAX', SETPOINT=300., INITIAL_STATE=T. /
&DEVC ID='Back_window_passenger_2', SURF_ID='Glass', XB=2.9,3.9,1.8,1.9,1.3,1.4, QUANTITY='WALL TEMPERATURE', SPATIAL_STATISTIC='MAX', SETPOINT=300., INITIAL_STATE=T. /
&DEVC ID='Back_window_passenger_3', SURF_ID='Glass', XB=2.9,3.8,1.8,1.9,1.4,1.5, QUANTITY='WALL TEMPERATURE', SPATIAL_STATISTIC='MAX', SETPOINT=300., INITIAL_STATE=T. /
&DEVC ID='Back_window_passenger_4', SURF_ID='Glass', XB=2.9,3.7,1.8,1.9,1.5,1.6, QUANTITY='WALL TEMPERATURE', SPATIAL_STATISTIC='MAX', SETPOINT=300., INITIAL_STATE=T. /

&DEVC ID='Back_window_driver_1', SURF_ID='Glass', XB=2.9,4.0,0.0,0.1,1.1,1.3, QUANTITY='WALL TEMPERATURE', SPATIAL_STATISTIC='MAX', SETPOINT=300., INITIAL_STATE=T. /
&DEVC ID='Back_window_driver_2', SURF_ID='Glass', XB=2.9,3.9,0.0,0.1,1.3,1.4, QUANTITY='WALL TEMPERATURE', SPATIAL_STATISTIC='MAX', SETPOINT=300., INITIAL_STATE=T. /
&DEVC ID='Back_window_driver_3', SURF_ID='Glass', XB=2.9,3.8,0.0,0.1,1.4,1.5, QUANTITY='WALL TEMPERATURE', SPATIAL_STATISTIC='MAX', SETPOINT=300., INITIAL_STATE=T. /
&DEVC ID='Back_window_driver_4', XB=2.9,3.7,0.0,0.1,1.5,1.6, QUANTITY='WALL TEMPERATURE', SPATIAL_STATISTIC='MAX', SETPOINT=300., SURF_ID='Glass', INITIAL_STATE=T. /

&DEVC ID='Middle_window_driver_Lower', XB=2.1,2.8,0.0,0.1,1.0,1.3, QUANTITY='WALL TEMPERATURE', SPATIAL_STATISTIC='MAX', SETPOINT=300., SURF_ID='Glass', INITIAL_STATE=T./
&DEVC ID='Middle_window_driver_Upper', XB=2.1,2.8,0.0,0.1,1.3,1.6, QUANTITY='WALL TEMPERATURE', SPATIAL_STATISTIC='MAX', SETPOINT=300., SURF_ID='Glass', INITIAL_STATE=T./

&DEVC ID='Middle_window_passenger_1', XB=2.6,2.8,1.8,1.9,1.0,1.6, QUANTITY='WALL TEMPERATURE', SPATIAL_STATISTIC='MAX', SETPOINT=300., SURF_ID='Glass', INITIAL_STATE=T./
```

```
&DEVC ID='Middle_window_passenger_2', XB=2.1,2.6,1.8,1.9,1.0,1.6, QUANTITY='WALL TEMPERATURE', SPATIAL_STATISTIC='MAX', SETPOINT=300., SURF_ID='Glass', INITIAL_STATE=T./

&DEVC ID='Front_window_1', XB=0.5,0.8,0.1,1.0,1.0,1.1, QUANTITY='WALL TEMPERATURE', SPATIAL_STATISTIC='MAX', SETPOINT=300., SURF_ID='Glass', INITIAL_STATE=T./
&DEVC ID='Front_window_2', XB=0.5,0.8,1.0,1.8,1.0,1.1, QUANTITY='WALL TEMPERATURE', SPATIAL_STATISTIC='MAX', SETPOINT=300., SURF_ID='Glass', INITIAL_STATE=T./
&DEVC ID='Front_window_3', XB=0.7,1.0,0.1,1.0,1.1,1.2, QUANTITY='WALL TEMPERATURE', SPATIAL_STATISTIC='MAX', SETPOINT=300., SURF_ID='Glass', INITIAL_STATE=T./
&DEVC ID='Front_window_4', XB=0.7,1.0,1.0,1.8,1.1,1.2, QUANTITY='WALL TEMPERATURE', SPATIAL_STATISTIC='MAX', SETPOINT=300., SURF_ID='Glass', INITIAL_STATE=T./
&DEVC ID='Front_window_5', XB=0.9,1.2,0.1,1.0,1.2,1.3, QUANTITY='WALL TEMPERATURE', SPATIAL_STATISTIC='MAX', SETPOINT=300., SURF_ID='Glass', INITIAL_STATE=T./
&DEVC ID='Front_window_6', XB=0.9,1.2,1.0,1.8,1.2,1.3, QUANTITY='WALL TEMPERATURE', SPATIAL_STATISTIC='MAX', SETPOINT=300., SURF_ID='Glass', INITIAL_STATE=T./
&DEVC ID='Front_window_7', XB=1.1,1.4,0.1,1.0,1.3,1.4, QUANTITY='WALL TEMPERATURE', SPATIAL_STATISTIC='MAX', SETPOINT=300., SURF_ID='Glass', INITIAL_STATE=T./
&DEVC ID='Front_window_8', XB=1.1,1.4,1.0,1.8,1.3,1.4, QUANTITY='WALL TEMPERATURE', SPATIAL_STATISTIC='MAX', SETPOINT=300., SURF_ID='Glass', INITIAL_STATE=T./
&DEVC ID='Front_window_9', XB=1.3,1.6,0.1,1.0,1.4,1.5, QUANTITY='WALL TEMPERATURE', SPATIAL_STATISTIC='MAX', SETPOINT=300., SURF_ID='Glass', INITIAL_STATE=T./
&DEVC ID='Front_window_10', XB=1.3,1.6,1.0,1.8,1.4,1.5, QUANTITY='WALL TEMPERATURE', SPATIAL_STATISTIC='MAX', SETPOINT=300., SURF_ID='Glass', INITIAL_STATE=T./
&DEVC ID='Front_window_11', XB=1.5,1.8,0.1,1.0,1.5,1.6, QUANTITY='WALL TEMPERATURE', SPATIAL_STATISTIC='MAX', SETPOINT=300., SURF_ID='Glass', INITIAL_STATE=T./
&DEVC ID='Front_window_12', XB=1.5,1.8,1.0,1.8,1.5,1.6, QUANTITY='WALL TEMPERATURE', SPATIAL_STATISTIC='MAX', SETPOINT=300., SURF_ID='Glass', INITIAL_STATE=T./

&DEVC ID='Back_window_1', XB=3.7,3.9,0.1,1.0,1.5,1.6, QUANTITY='WALL TEMPERATURE', SPATIAL_STATISTIC='MAX', SETPOINT=300., SURF_ID='Glass', INITIAL_STATE=T./
&DEVC ID='Back_window_2', XB=3.7,3.9,1.0,1.8,1.5,1.6, QUANTITY='WALL TEMPERATURE', SPATIAL_STATISTIC='MAX', SETPOINT=300., SURF_ID='Glass', INITIAL_STATE=T./
&DEVC ID='Back_window_3', XB=3.8,4.0,0.1,1.0,1.4,1.5, QUANTITY='WALL TEMPERATURE', SPATIAL_STATISTIC='MAX', SETPOINT=300., SURF_ID='Glass', INITIAL_STATE=T./
```

```
&DEVC ID='Back_window_4', XB=3.8,4.0,1.0,1.8,1.4,1.5, QUANTITY='WALL TEMPERATURE', SPATIAL_STATISTIC='MAX', SETPOINT=300., SURF_ID='Glass',
INITIAL_STATE=T./
&DEVC ID='Back_window_5', XB=3.9,4.1,0.1,1.0,1.3,1.4, QUANTITY='WALL TEMPERATURE', SPATIAL_STATISTIC='MAX', SETPOINT=300., SURF_ID='Glass',
INITIAL_STATE=T./
&DEVC ID='Back_window_6', XB=3.9,4.1,1.0,1.8,1.3,1.4, QUANTITY='WALL TEMPERATURE', SPATIAL_STATISTIC='MAX', SETPOINT=300., SURF_ID='Glass',
INITIAL_STATE=T./
&DEVC ID='Back_window_7', XB=4.0,4.2,0.1,1.0,1.2,1.3, QUANTITY='WALL TEMPERATURE', SPATIAL_STATISTIC='MAX', SETPOINT=300., SURF_ID='Glass',
INITIAL_STATE=T./
&DEVC ID='Back_window_8', XB=4.0,4.2,1.0,1.8,1.2,1.3, QUANTITY='WALL TEMPERATURE', SPATIAL_STATISTIC='MAX', SETPOINT=300., SURF_ID='Glass',
INITIAL_STATE=T./
&DEVC ID='Back_window_9', XB=4.1,4.3,0.2,1.0,1.1,1.2, QUANTITY='WALL TEMPERATURE', SPATIAL_STATISTIC='MAX', SETPOINT=300., SURF_ID='Glass',
INITIAL_STATE=T./
&DEVC ID='Back_window_10', XB=4.1,4.3,1.0,1.7,1.1,1.2, QUANTITY='WALL TEMPERATURE', SPATIAL_STATISTIC='MAX', SETPOINT=300., SURF_ID='Glass',
INITIAL_STATE=T./


&OBST ID='Window_driver_1', XB=1.0,2.0,0.0,0.1,1.0,1.2, SURF_ID='Glass', DEVC_ID='Window_driver_1'/
&OBST ID='Window_driver_2', XB=1.2,2.0,0.0,0.1,1.2,1.3, SURF_ID='Glass', DEVC_ID='Window_driver_2'/
&OBST ID='Window_driver_3', XB=1.4,2.0,0.0,0.1,1.3,1.4, SURF_ID='Glass', DEVC_ID='Window_driver_3'/
&OBST ID='Window_driver_4', XB=1.6,2.0,0.0,0.1,1.4,1.5, SURF_ID='Glass', DEVC_ID='Window_driver_4'/
&OBST ID='Window_driver_5', XB=1.8,2.0,0.0,0.1,1.5,1.6, SURF_ID='Glass', DEVC_ID='Window_driver_5'/

&OBST ID='Middle_window_driver_Lower', XB=2.1,2.8,0.0,0.1,1.0,1.3, SURF_ID='Glass', DEVC_ID='Middle_window_driver_Lower'/
&OBST ID='Middle_window_driver_Upper', XB=2.1,2.8,0.0,0.1,1.3,1.6, SURF_ID='Glass', DEVC_ID='Middle_window_driver_Upper'/

&OBST ID='Window_passenger_1', XB=1.0,2.0,1.8,1.9,1.0,1.2, SURF_ID='Glass', DEVC_ID='Window_passenger_1'/
&OBST ID='Window_passenger_2', XB=1.2,2.0,1.8,1.9,1.2,1.3, SURF_ID='Glass', DEVC_ID='Window_passenger_2'/
&OBST ID='Window_passenger_3', XB=1.4,2.0,1.8,1.9,1.3,1.4, SURF_ID='Glass', DEVC_ID='Window_passenger_3'/
&OBST ID='Window_passenger_4', XB=1.6,2.0,1.8,1.9,1.4,1.5, SURF_ID='Glass', DEVC_ID='Window_passenger_4'/
&OBST ID='Window_passenger_5', XB=1.8,2.0,1.8,1.9,1.5,1.6, SURF_ID='Glass', DEVC_ID='Window_passenger_5'/

&OBST ID='Middle_window_passenger', XB=2.6,2.8,1.8,1.9,1.0,1.6, SURF_ID='Glass', DEVC_ID='Middle_window_passenger_1'/
&OBST ID='Middle_window_passenger', XB=2.1,2.6,1.8,1.9,1.0,1.6, SURF_ID='Glass', DEVC_ID='Middle_window_passenger_2'/
&OBST ID='Back_window_driver_1', XB=2.9,4.0,0.0,0.1,1.1,1.3, SURF_ID='Glass', DEVC_ID='Back_window_driver_1'/
&OBST ID='Back_window_driver_2', XB=2.9,3.9,0.0,0.1,1.3,1.4, SURF_ID='Glass', DEVC_ID='Back_window_driver_2'/
```

```
&OBST ID='Back_window_driver_3', XB=2.9,3.8,0.0,0.1,1.4,1.5, SURF_ID='Glass', DEVC_ID='Back_window_driver_3'/
&OBST ID='Back_window_driver_4', XB=2.9,3.7,0.0,0.1,1.5,1.6, SURF_ID='Glass', DEVC_ID='Back_window_driver_4'/

&OBST ID='Back_window_passenger_1', XB=2.9,4.0,1.8,1.9,1.1,1.3, SURF_ID='Glass', DEVC_ID='Back_window_passenger_1'/
&OBST ID='Back_window_passenger_2', XB=2.9,3.9,1.8,1.9,1.3,1.4, SURF_ID='Glass', DEVC_ID='Back_window_passenger_2'/
&OBST ID='Back_window_passenger_3', XB=2.9,3.8,1.8,1.9,1.4,1.5, SURF_ID='Glass', DEVC_ID='Back_window_passenger_3'/
&OBST ID='Back_window_passenger_4', XB=2.9,3.7,1.8,1.9,1.5,1.6, SURF_ID='Glass', DEVC_ID='Back_window_passenger_4'/

&OBST ID='Front_window_2', XB=0.5,0.8,0.1,1.0,1.0,1.1, SURF_ID='Glass', DEVC_ID='Front_window_1'/
&OBST ID='Front_window_2', XB=0.5,0.8,1.0,1.8,1.0,1.1, SURF_ID='Glass', DEVC_ID='Front_window_2'/
&OBST ID='Front_window_3', XB=0.7,1.0,0.1,1.0,1.1,1.2, SURF_ID='Glass', DEVC_ID='Front_window_3'/
&OBST ID='Front_window_4', XB=0.7,1.0,1.0,1.8,1.1,1.2, SURF_ID='Glass', DEVC_ID='Front_window_4'/
&OBST ID='Front_window_5', XB=0.9,1.2,0.1,1.0,1.2,1.3, SURF_ID='Glass', DEVC_ID='Front_window_5'/
&OBST ID='Front_window_6', XB=0.9,1.2,1.0,1.8,1.2,1.3, SURF_ID='Glass', DEVC_ID='Front_window_6'/
&OBST ID='Front_window_7', XB=1.1,1.4,0.1,1.0,1.3,1.4, SURF_ID='Glass', DEVC_ID='Front_window_7'/
&OBST ID='Front_window_8', XB=1.1,1.4,1.0,1.8,1.3,1.4, SURF_ID='Glass', DEVC_ID='Front_window_8'/
&OBST ID='Front_window_9', XB=1.3,1.6,0.1,1.0,1.4,1.5, SURF_ID='Glass', DEVC_ID='Front_window_9'/
&OBST ID='Front_window_10', XB=1.3,1.6,1.0,1.8,1.4,1.5, SURF_ID='Glass', DEVC_ID='Front_window_10'/
&OBST ID='Front_window_11', XB=1.5,1.8,0.1,1.0,1.5,1.6, SURF_ID='Glass', DEVC_ID='Front_window_11'/
&OBST ID='Front_window_12', XB=1.5,1.8,1.0,1.8,1.5,1.6, SURF_ID='Glass', DEVC_ID='Front_window_12'/

&OBST ID='Back_window_1', XB=3.7,3.9,0.1,1.0,1.5,1.6, SURF_ID='Glass', DEVC_ID='Back_window_1'/
&OBST ID='Back_window_2', XB=3.7,3.9,1.0,1.8,1.5,1.6, SURF_ID='Glass', DEVC_ID='Back_window_2'/
&OBST ID='Back_window_3', XB=3.8,4.0,0.1,1.0,1.4,1.5, SURF_ID='Glass', DEVC_ID='Back_window_3'/
&OBST ID='Back_window_4', XB=3.8,4.0,1.0,1.8,1.4,1.5, SURF_ID='Glass', DEVC_ID='Back_window_4'/
&OBST ID='Back_window_5', XB=3.9,4.1,0.1,1.0,1.3,1.4, SURF_ID='Glass', DEVC_ID='Back_window_5'/
&OBST ID='Back_window_6', XB=3.9,4.1,1.0,1.8,1.3,1.4, SURF_ID='Glass', DEVC_ID='Back_window_6'/
&OBST ID='Back_window_7', XB=4.0,4.2,0.1,1.0,1.2,1.3, SURF_ID='Glass', DEVC_ID='Back_window_7'/
&OBST ID='Back_window_8', XB=4.0,4.2,1.0,1.8,1.2,1.3, SURF_ID='Glass', DEVC_ID='Back_window_8'/
&OBST ID='Back_window_9', XB=4.1,4.3,0.2,1.0,1.1,1.2, SURF_ID='Glass', DEVC_ID='Back_window_9'/
&OBST ID='Back_window_10', XB=4.1,4.3,1.0,1.7,1.1,1.2, SURF_ID='Glass', DEVC_ID='Back_window_10'/
/____________________________________________________________________________________________Yellow second car
&OBST ID='Bottom_car', XB=-0.4,-0.1,0.2,0.4,0.2,0.25, COLOR='SILVER', SURF_ID='steel'/

&OBST ID='Bottom_car_car_2', XB=-0.4,-0.1, -2.3,-2.1,    0.2,0.25, COLOR='SILVER', SURF_ID='steel'/
```

```
&OBST ID='Bottom_car_car_2', XB=-0.4,2.6,-2.1,-1.5,0.2,0.25, COLOR='SILVER', SURF_ID='steel'/
&OBST ID='Bottom_car_car_2', XB=-0.3,-0.1,-2.4,-2.3,0.2,0.25, COLOR='SILVER', SURF_ID='steel'/
&OBST ID='Bottom_car_car_2', XB=-0.2,-0.1,-2.5,-2.4,0.2,0.25, COLOR='SILVER', SURF_ID='steel'/
&OBST ID='Bottom_car_car_2', XB=0.7,2.6,-2.5,-2.1,0.2,0.25, COLOR='SILVER', SURF_ID='steel'/
&OBST ID='Bottom_car_car_2', XB=2.6,3.0,-2.5,-2.1,0.2,0.25, COLOR='SILVER', SURF_ID='steel'/
&OBST ID='Bottom_car_car_2', XB=2.6,4.3,-2.1,-1.5,0.2,0.25, COLOR='SILVER', SURF_ID='steel'/
&OBST ID='Bottom_car_car_2', XB=3.8,4.2,-2.5,-2.4,0.2,0.25, COLOR='SILVER', SURF_ID='steel'/
&OBST ID='Bottom_car_car_2', XB=3.8,4.3,-2.4,-2.1,0.2,0.25, COLOR='SILVER', SURF_ID='steel'/
&OBST ID='Bottom_car_car_2', XB=2.6,3.0,-1.0,-0.6,0.2,0.25, COLOR='SILVER', SURF_ID='steel'/
&OBST ID='Bottom_car_car_2', XB=2.6,4.3,-1.5,-1.0,0.2,0.25, COLOR='SILVER', SURF_ID='steel'/
&OBST ID='Bottom_car_car_2', XB=3.8,4.1,-0.7,-0.6,0.2,0.25, COLOR='SILVER', SURF_ID='steel'/
&OBST ID='Bottom_car_car_2', XB=3.8,4.3,-1.0,-0.7,0.2,0.25, COLOR='SILVER', SURF_ID='steel'/
&OBST ID='Bottom_car_car_2', XB=-0.4,-0.1,-1.0,-0.8,0.2,0.25, COLOR='SILVER', SURF_ID='steel'/
&OBST ID='Bottom_car_car_2', XB=-0.4,2.6,-1.5,-1.0,0.2,0.25, COLOR='SILVER', SURF_ID='steel'/
&OBST ID='Bottom_car_car_2', XB=-0.3,-0.1,-0.8,-0.7,0.2,0.25, COLOR='SILVER', SURF_ID='steel'/
&OBST ID='Bottom_car_car_2', XB=-0.2,-0.1,-0.7,-0.6,0.2,0.25, COLOR='SILVER', SURF_ID='steel'/
&OBST ID='Bottom_car_car_2', XB=0.7,2.6,-1.0,-0.6,0.2,0.25, COLOR='SILVER', SURF_ID='steel'/
&OBST ID='Covering_batteries_car_2', XB=0.8,2.3,-2.4,-0.7,0.5,0.6, COLOR='BLUE', SURF_ID='steel'/
&OBST ID='Covering_batteries_back_car_2', XB=2.3,2.9,-2.3,-0.8,0.6,0.7, COLOR='BLUE', SURF_ID='steel'/


&OBST ID='car_body_front_car_2', XB=-0.4,-0.2,-2.3,-1.5,0.8,0.9, COLOR='YELLOW', SURF_ID='steel'/
&OBST ID='car_body_front_car_2', XB=-0.3,-0.2,-2.5,-2.3,0.8,0.9, COLOR='YELLOW', SURF_ID='steel'/
&OBST ID='car_body_front_car_2', XB=-0.4,-0.2,-1.5,-0.8,0.8,0.9, COLOR='YELLOW', SURF_ID='steel'/
&OBST ID='car_body_front_car_2', XB=-0.3,-0.2,-0.8,-0.6,0.8,0.9, COLOR='YELLOW', SURF_ID='steel'/
&OBST ID='car_body_above_wheels:1678653_car_2', XB=-0.2,0.8,-2.5,-2.0,0.8,0.9, COLOR='YELLOW', SURF_ID='steel'/
&OBST ID='car_body_above_wheels:1678732_car_2', XB=-0.2,0.8,-1.1,-0.6,0.8,0.9, COLOR='YELLOW', SURF_ID='steel'/
&OBST ID='car_body_above_wheels:1678748_car_2', XB=2.9,3.9,-1.1,-0.6,0.8,0.9, COLOR='YELLOW', SURF_ID='steel'/
&OBST ID='car_body_above_wheels:1678762_car_2', XB=2.9,3.9,-2.5,-2.0,0.8,0.9, COLOR='YELLOW', SURF_ID='steel'/
&OBST ID='Car_body:1673246_car_2', XB=-0.4,-0.2,-0.9,-0.8,0.3,0.8, COLOR='YELLOW', SURF_ID='steel'/
&OBST ID='Car_body:1673275_car_2', XB=-0.3,-0.2,-0.8,-0.6,0.3,0.8, COLOR='YELLOW', SURF_ID='steel'/
&OBST ID='Car_body:1673381_car_2', XB=-0.2,-0.1,-0.7,-0.6,0.3,0.8, COLOR='YELLOW', SURF_ID='steel'/
&OBST ID='Car_body:1673471_car_2', XB=-0.2,-0.1,-1.1,-0.7,0.3,0.8, COLOR='YELLOW', SURF_ID='steel'/
&OBST ID='Car_body:1673520_car_2', XB=-0.1,0.8,-1.1,-1.0,0.3,0.8, COLOR='YELLOW', SURF_ID='steel'/
&OBST ID='Car_body:1673573_car_2', XB=0.7,0.8,-1.0,-0.6,0.3,0.8, COLOR='YELLOW', SURF_ID='steel'/
```

```
&OBST ID='Car_body:1673628_car_2', XB=2.6,2.9,-0.7,-0.6,0.4,1.0, COLOR='YELLOW', SURF_ID='steel'/
&OBST ID='Car_body:1673628_car_2', XB=0.8,2.6,-0.7,-0.6,0.4,1.0, COLOR='YELLOW', SURF_ID='steel'/
&OBST ID='Car_body:1673732_car_2', XB=2.9,3.9,-1.1,-1.0,0.3,0.8, COLOR='YELLOW', SURF_ID='steel'/
&OBST ID='Car_body:1673763_car_2', XB=3.8,3.9,-1.0,-0.6,0.3,0.8, COLOR='YELLOW', SURF_ID='steel'/
&OBST ID='Car_body:1673788_car_2', XB=3.9,4.2,-0.7,-0.6,0.3,0.9, COLOR='YELLOW', SURF_ID='steel'/
&OBST ID='Car_body:1673830_car_2', XB=4.1,4.2,-0.8,-0.7,0.3,0.9, COLOR='YELLOW', SURF_ID='steel'/
&OBST ID='Car_body:1673916_car_2', XB=4.2,4.3,-2.4,-1.5,0.3,0.9, COLOR='YELLOW', SURF_ID='steel'/
&OBST ID='Car_body:1673916_car_2', XB=4.2,4.3,-1.5,-0.7,0.3,0.9, COLOR='YELLOW', SURF_ID='steel'/
&OBST ID='Car_body:1673967_car_2', XB=4.1,4.2,-2.5,-2.3,0.3,0.9, COLOR='YELLOW', SURF_ID='steel'/
&OBST ID='Car_body:1673995_car_2', XB=4.1,4.2,-2.4,-2.3,0.3,0.9, COLOR='YELLOW', SURF_ID='steel'/
&OBST ID='Car_body:1674064_car_2', XB=3.9,4.1,-2.5,-2.4,0.3,0.9, COLOR='YELLOW', SURF_ID='steel'/
&OBST ID='Car_body:1674105_car_2', XB=3.8,3.9,-2.5,-2.0,0.3,0.8, COLOR='YELLOW', SURF_ID='steel'/
&OBST ID='Car_body:1674245_car_2', XB=0.8,2.6,-2.5,-2.4,0.4,1.0, COLOR='YELLOW', SURF_ID='steel'/
&OBST ID='Car_body:1674245_car_2', XB=2.6,2.9,-2.5,-2.4,0.4,1.0, COLOR='YELLOW', SURF_ID='steel'/
&OBST ID='Car_body:1674536_car_2', XB=0.7,0.8,-2.5,-2.0,0.3,0.8, COLOR='YELLOW', SURF_ID='steel'/
&OBST ID='Car_body:1674582_car_2', XB=-0.2,0.7,-2.1,-2.0,0.3,0.8, COLOR='YELLOW', SURF_ID='steel'/
&OBST ID='Car_body:1674615_car_2', XB=-0.2,-0.1,-2.5,-2.1,0.3,0.8, COLOR='YELLOW', SURF_ID='steel'/
&OBST ID='Car_body:1674733_car_2', XB=-0.3,-0.2,-2.5,-2.2,0.3,0.8, COLOR='YELLOW', SURF_ID='steel'/
&OBST ID='Car_body:1674759_car_2', XB=-0.4,-0.3,-2.3,-2.2,0.3,0.8, COLOR='YELLOW', SURF_ID='steel'/
&OBST ID='Car_body:1674792_car_2', XB=-0.4,-0.3,-2.2,-1.5,0.3,0.8, COLOR='YELLOW', SURF_ID='steel'/
&OBST ID='Car_body:1674792_car_2', XB=-0.4,-0.3,-1.5,-0.9,0.3,0.8, COLOR='YELLOW', SURF_ID='steel'/
&OBST ID='Car_body:1679523_car_2', XB=2.9,3.8,-2.1,-2.0,0.3,0.8, COLOR='YELLOW', SURF_ID='steel'/
&OBST ID='Car_body:1679563_car_2', XB=2.9,3.0,-2.5,-2.1,0.3,0.8, COLOR='YELLOW', SURF_ID='steel'/
&OBST ID='Car_body_roof_car_2', XB=1.7,2.6,-2.5,-1.5,1.6,1.7, COLOR='YELLOW', SURF_ID='steel'/
&OBST ID='Car_body_roof_car_2', XB=2.6,3.8,-2.5,-1.5,1.6,1.7, COLOR='YELLOW', SURF_ID='steel'/
&OBST ID='Car_body_roof_car_2', XB=2.6,3.8,-1.5,-0.6,1.6,1.7, COLOR='YELLOW', SURF_ID='steel'/
&OBST ID='Car_body_roof_car_2', XB=1.7,2.6,-1.5,-0.6,1.6,1.7, COLOR='YELLOW', SURF_ID='steel'/
&OBST ID='engine cover:1685928_car_2', XB=-0.2,0.8,-2.5,-1.5,0.9,1.0, COLOR='YELLOW', SURF_ID='steel'/
&OBST ID='engine cover:1685928_car_2', XB=-0.2,0.8,-1.5,-0.6,0.9,1.0, COLOR='YELLOW', SURF_ID='steel'/
&OBST ID='Car_body:1689403_car_2', XB=2.9,4.1,-0.7,-0.6,0.9,1.1, COLOR='YELLOW', SURF_ID='steel'/
&OBST ID='Car_body:1689425_car_2', XB=4.1,4.2,-0.8,-0.6,0.9,1.1, COLOR='YELLOW', SURF_ID='steel'/
&OBST ID='Car_body:1689461_car_2', XB=4.2,4.3,-0.8,-0.7,0.9,1.1, COLOR='YELLOW', SURF_ID='steel'/
&OBST ID='Car_body:1689516_car_2', XB=4.2,4.3,-2.3,-1.5,0.9,1.1, COLOR='YELLOW', SURF_ID='steel'/
&OBST ID='Car_body:1689516_car_2', XB=4.2,4.3,-1.5,-0.8,0.9,1.1, COLOR='YELLOW', SURF_ID='steel'/
&OBST ID='Car_body:1689545_car_2', XB=4.1,4.3,-2.4,-2.3,0.9,1.1, COLOR='YELLOW', SURF_ID='steel'/
```

```
&OBST ID='Car_body:1689567_car_2', XB=4.1,4.2,-2.5,-2.4,0.9,1.1, COLOR='YELLOW', SURF_ID='steel'/
&OBST ID='Car_body:1689617_car_2', XB=2.9,4.1,-2.5,-2.4,0.9,1.1, COLOR='YELLOW', SURF_ID='steel'/
&OBST ID='Car_body:1680322_car_2', XB=2.9,3.0,-1.0,-0.6,0.3,0.8, COLOR='YELLOW', SURF_ID='steel'/

&OBST ID='Covering_trunk_2', XB=3.7,4.2,-2.0,-1.5,0.3,0.35, SURF_ID='Insulation_car_cabine', BULK_DENSITY=900. /
&OBST ID='Covering_trunk_2', XB=3.9,4.1,-2.4,-2.3,0.3,0.35, SURF_ID='Insulation_car_cabine', BULK_DENSITY=900. /
&OBST ID='Covering_trunk_2', XB=3.9,4.2,-2.3,-2.0,0.3,0.35, SURF_ID='Insulation_car_cabine', BULK_DENSITY=900. /
&OBST ID='Covering_trunk_2', XB=3.7,4.2,-1.5,-1.1,0.3,0.35, SURF_ID='Insulation_car_cabine', BULK_DENSITY=900. /
&OBST ID='Covering_trunk_2', XB=3.9,4.1,-0.8,-0.7,0.3,0.35, SURF_ID='Insulation_car_cabine', BULK_DENSITY=900. /
&OBST ID='Covering_trunk_2', XB=3.9,4.2,-1.1,-0.8,0.3,0.35, SURF_ID='Insulation_car_cabine', BULK_DENSITY=900. /

&OBST ID='Covering_wheels_2', XB=2.9,3.8,2.8,3.3,0.85,0.9, SURF_ID='Insulation_car_cabine', BULK_DENSITY=900. /
&OBST ID='Covering_wheels_2', XB=2.9,3.8,3.3,3.7,0.85,0.9, SURF_ID='Insulation_car_cabine', BULK_DENSITY=900. /
&OBST ID='Cover_befor_transformer:1683732_2', XB=2.9,2.95,-2.0,-1.5,0.3,0.9, SURF_ID='Insulation_car_cabine', BULK_DENSITY=900. /
&OBST ID='Cover_befor_transformer:1683732_2', XB=2.9,2.95,-1.5,-1.1,0.3,0.9, SURF_ID='Insulation_car_cabine', BULK_DENSITY=900. /

&OBST ID='Transformer:1678843_2', XB=3.1,3.7,-2.0,-1.5,0.3,0.8, SURF_ID='transformer'/
&OBST ID='Transformer:1678843_2', XB=3.1,3.7,-1.5,-1.1,0.3,0.8, SURF_ID='transformer'/

&OBST ID='safety cage finishing:1685633_car_2', XB=0.8,2.6,-2.4,-2.3,0.6,1.0,
SURF_ID6='Insulation_car_cabine','Insulation_car_cabine','INERT','Insulation_car_cabine','Insulation_car_cabine','Insulation_car_cabine', BULK_DENSITY=900. /
&OBST ID='safety cage finishing:1685633_car_2', XB=2.6,2.9,-2.4,-2.3,0.6,1.0,
SURF_ID6='Insulation_car_cabine','Insulation_car_cabine','INERT','Insulation_car_cabine','Insulation_car_cabine','Insulation_car_cabine', BULK_DENSITY=900. /
&OBST ID='safety cage finishing:1685910_car_2', XB=2.6,2.9,-0.8,-0.7,0.6,1.0,
SURF_ID6='Insulation_car_cabine','Insulation_car_cabine','Insulation_car_cabine','INERT','Insulation_car_cabine','Insulation_car_cabine', BULK_DENSITY=900. /
&OBST ID='safety cage finishing:1685910_car_2', XB=0.8,2.6,-0.8,-0.7,0.6,1.0,
SURF_ID6='Insulation_car_cabine','Insulation_car_cabine','Insulation_car_cabine','INERT','Insulation_car_cabine','Insulation_car_cabine', BULK_DENSITY=900. /

&OBST ID='Battery_car_2', XB=1.5,2.9,-2.3,-0.8,0.3,0.4, SURF_ID= 'SIMPLE_BATTERY_SURFACE', BULK_DENSITY=900./ [8]
&OBST ID='Battery_rear_car_2', XB=2.3,2.9,-2.3,-0.8,0.4,0.5, SURF_ID='SIMPLE_BATTERY_SURFACE'/ [8]
&OBST ID='Battery:1667225_front_car_2', XB=0.8,1.5,-2.3,-1.9,0.3,0.4, SURF_ID='SIMPLE_BATTERY_SURFACE', BULK_DENSITY=900./ [8]
&OBST ID='Battery:1667226_front_car_2', XB=0.8,1.5,-1.8,-1.3,0.3,0.4, SURF_ID='SIMPLE_BATTERY_SURFACE',  BULK_DENSITY=900./ [8]
&OBST ID='Battery:1667227_front_car_2', XB=0.8,1.5,-1.2,-0.8,0.3,0.4, SURF_ID='SIMPLE_BATTERY_SURFACE', BULK_DENSITY=900./ [8]

&OBST ID='Seating:1684541', XB=1.2,2.0,-1.5,-0.9,0.6,0.8, SURF_ID='Seating', /
```

```
&OBST ID='Seating:1684640', XB=1.2,2.0,-2.2,-1.6,0.6,0.8, SURF_ID='Seating' /
&OBST ID='Seating:1685527', XB=2.3,2.6,-2.2,-1.5,0.7,0.8, SURF_ID='Seating' /
&OBST ID='Seating:1685527', XB=2.6,2.9,-2.2,-1.5,0.7,0.8, SURF_ID='Seating' /
&OBST ID='Seating:1685527', XB=2.6,2.9,-1.5,-0.9,0.7,0.8, SURF_ID='Seating' /
&OBST ID='Seating:1685527', XB=2.3,2.6,-1.5,-0.9,0.7,0.8, SURF_ID='Seating' /

&OBST ID='Dashboard:1686413', XB=0.8,1.1,-2.2,-1.5,0.9,1.1, COLOR='PURPLE', SURF_ID='electronic', BULK_DENSITY=1100. /
&OBST ID='Dashboard:1686413', XB=0.8,1.1,-1.5,-0.9,0.9,1.1, COLOR='PURPLE', SURF_ID='electronic', BULK_DENSITY=1100. /

&OBST ID='Seating_backrest:1684772', XB=1.8,2.0,-2.2,-1.6,0.8,1.4, SURF_ID='Seating' /
&OBST ID='Seating_backrest:1685038', XB=1.8,2.0,-1.5,-0.9,0.8,1.4, SURF_ID='Seating' /
&OBST ID='Seating_backrest:1685444', XB=2.7,2.9,-2.2,-1.5,0.8,1.4, SURF_ID='Seating' /
&OBST ID='Seating_backrest:1685444', XB=2.7,2.9,-1.5,-0.8,0.8,1.4, SURF_ID='Seating'/

&OBST ID='Wheel:1665075_car_2', XB=0.1,0.5,-0.9,-0.6,0.0,0.1, COLOR='BLACK', SURF_ID='Wheel_Assembly', BULK_DENSITY=910. /
&OBST ID='Wheel:1665075_rim_car_2', XB=0.1,0.5,-0.9,-0.6,0.1,0.6, COLOR='SILVER', SURF_ID='steel'/
&OBST ID='Wheel:1665075_car_2', XB=0.1,0.5,-0.9,-0.6,0.6,0.7, COLOR='BLACK', SURF_ID='Wheel_Assembly', BULK_DENSITY=910. /
&OBST ID='Wheel:1665344_car_2', XB=0.5,0.6,-0.9,-0.6,0.1,0.6, COLOR='BLACK', SURF_ID='Wheel_Assembly', BULK_DENSITY=910. /
&OBST ID='Wheel:1666370_car_2', XB=0.0,0.1,-0.9,-0.6,0.1,0.6, COLOR='BLACK', SURF_ID='Wheel_Assembly', BULK_DENSITY=910. /
&OBST ID='Wheel:1666668_car_2', XB=0.1,0.5,-2.5,-2.2,0.0,0.1, COLOR='BLACK', SURF_ID='Wheel_Assembly', BULK_DENSITY=910. /
&OBST ID='Wheel_rim:1666668_car_2', XB=0.1,0.5,-2.5,-2.2,0.1,0.6, COLOR='SILVER', SURF_ID='steel'/
&OBST ID='Wheel:1666668_car_2', XB=0.1,0.5,-2.5,-2.2,0.6,0.7, COLOR='BLACK', SURF_ID='Wheel_Assembly', BULK_DENSITY=910. /
&OBST ID='Wheel:1666669_car_2', XB=0.5,0.6,-2.5,-2.2,0.1,0.6, COLOR='BLACK', SURF_ID='Wheel_Assembly', BULK_DENSITY=910. /
&OBST ID='Wheel:1666670_car_2', XB=0.0,0.1,-2.5,-2.2,0.1,0.6, COLOR='BLACK', SURF_ID='Wheel_Assembly', BULK_DENSITY=910. /
&OBST ID='Wheel:1666678_car_2', XB=3.2,3.6,-2.5,-2.2,0.0,0.1, COLOR='BLACK', SURF_ID='Wheel_Assembly', BULK_DENSITY=910. /
&OBST ID='Wheel:1666678_rim_car_2', XB=3.2,3.6,-2.5,-2.2,0.1,0.6, COLOR='SILVER', SURF_ID='steel'/
&OBST ID='Wheel:1666678_car_2', XB=3.2,3.6,-2.5,-2.2,0.6,0.7, COLOR='BLACK', SURF_ID='Wheel_Assembly', BULK_DENSITY=910. /
&OBST ID='Wheel:1666679_car_2', XB=3.6,3.7,-2.5,-2.2,0.1,0.6, COLOR='BLACK', SURF_ID='Wheel_Assembly', BULK_DENSITY=910. /
&OBST ID='Wheel:1666680_car_2', XB=3.1,3.2,-2.5,-2.2,0.1,0.6, COLOR='BLACK', SURF_ID='Wheel_Assembly', BULK_DENSITY=910. /
&OBST ID='Wheel:1679782_car_2', XB=3.2,3.6,-0.9,-0.6,0.0,0.1, COLOR='BLACK', SURF_ID='Wheel_Assembly', BULK_DENSITY=910. /
&OBST ID='Wheel:1679782_rim_car_2', XB=3.2,3.6,-0.9,-0.6,0.1,0.6, COLOR='SILVER', SURF_ID='steel'/
&OBST ID='Wheel:1679782_car_2', XB=3.2,3.6,-0.9,-0.6,0.6,0.7, COLOR='BLACK', SURF_ID='Wheel_Assembly', BULK_DENSITY=910. /
&OBST ID='Wheel 2:1679783_car_2', XB=3.6,3.7,-0.9,-0.6,0.1,0.6, COLOR='BLACK', SURF_ID='Wheel_Assembly', BULK_DENSITY=910. /
&OBST ID='Wheel 2:1679784_car_2', XB=3.1,3.2,-0.9,-0.6,0.1,0.6, COLOR='BLACK', SURF_ID='Wheel_Assembly', BULK_DENSITY=910. /
&OBST ID=' Frame_front_window:1690476_car_2', XB=0.5,0.8,-2.5,-2.4,1.0,1.1, COLOR='YELLOW', SURF_ID='steel'/
```

```
&OBST ID=' Frame_front_window:1690483_car_2', XB=0.7,1.0,-2.5,-2.4,1.1,1.2, COLOR='YELLOW', SURF_ID='steel'/
&OBST ID=' Frame_front_window:1690490_car_2', XB=0.9,1.2,-2.5,-2.4,1.2,1.3, COLOR='YELLOW', SURF_ID='steel'/
&OBST ID=' Frame_front_window:1690497_car_2', XB=1.1,1.4,-2.5,-2.4,1.3,1.4, COLOR='YELLOW', SURF_ID='steel'/
&OBST ID=' Frame_front_window:1690504_car_2', XB=1.3,1.6,-2.5,-2.4,1.4,1.5, COLOR='YELLOW', SURF_ID='steel'/
&OBST ID=' Frame_front_window:1690511_car_2', XB=1.5,1.8,-2.5,-2.4,1.5,1.6, COLOR='YELLOW', SURF_ID='steel'/
&OBST ID=' Frame_front_window:1690660_car_2', XB=0.5,0.8,-0.7,-0.6,1.0,1.1, COLOR='YELLOW', SURF_ID='steel'/
&OBST ID=' Frame_front_window:1690667_car_2', XB=0.7,1.0,-0.7,-0.6,1.1,1.2, COLOR='YELLOW', SURF_ID='steel'/
&OBST ID=' Frame_front_window:1690674_car_2', XB=0.9,1.2,-0.7,-0.6,1.2,1.3, COLOR='YELLOW', SURF_ID='steel'/
&OBST ID=' Frame_front_window:1690681_car_2', XB=1.1,1.4,-0.7,-0.6,1.3,1.4, COLOR='YELLOW', SURF_ID='steel'/
&OBST ID=' Frame_front_window:1690688_car_2', XB=1.3,1.6,-0.7,-0.6,1.4,1.5, COLOR='YELLOW', SURF_ID='steel'/
&OBST ID=' Frame_front_window:1690695_car_2', XB=1.5,1.8,-0.7,-0.6,1.5,1.6, COLOR='YELLOW', SURF_ID='steel'/
&OBST ID=' Frame_back_window:1690745_car_2', XB=3.7,3.9,-2.5,-2.4,1.5,1.6, COLOR='YELLOW', SURF_ID='steel'/
&OBST ID=' Frame_back_window:1690752_car_2', XB=3.8,4.0,-2.5,-2.4,1.4,1.5, COLOR='YELLOW', SURF_ID='steel'/
&OBST ID=' Frame_back_window:1690759_car_2', XB=3.9,4.1,-2.5,-2.4,1.3,1.4, COLOR='YELLOW', SURF_ID='steel'/
&OBST ID=' Frame_back_window:1690766_car_2', XB=4.0,4.2,-2.5,-2.4,1.2,1.3, COLOR='YELLOW', SURF_ID='steel'/
&OBST ID=' Frame_back_window:1690773_car_2', XB=4.0,4.2,-2.5,-2.4,1.1,1.2, COLOR='YELLOW', SURF_ID='steel'/
&OBST ID=' Frame_back_window:1690773_car_2', XB=4.0,4.3,-2.4,-2.3,1.1,1.2, COLOR='YELLOW', SURF_ID='steel'/
&OBST ID=' Frame_back_window:1691187_car_2', XB=3.7,3.9,-0.7,-0.6,1.5,1.6, COLOR='YELLOW', SURF_ID='steel'/
&OBST ID=' Frame_back_window:1691194_car_2', XB=3.8,4.0,-0.7,-0.6,1.4,1.5, COLOR='YELLOW', SURF_ID='steel'/
&OBST ID=' Frame_back_window:1691201_car_2', XB=3.9,4.1,-0.7,-0.6,1.3,1.4, COLOR='YELLOW', SURF_ID='steel'/
&OBST ID=' Frame_back_window:1691208_car_2', XB=4.0,4.2,-0.7,-0.6,1.2,1.3, COLOR='YELLOW', SURF_ID='steel'/
&OBST ID=' Frame_back_window:1691285_car_2', XB=4.0,4.2,-0.7,-0.6,1.1,1.2, COLOR='YELLOW', SURF_ID='steel'/
&OBST ID=' Frame_back_window:1691285_car_2', XB=4.0,4.3,-0.8,-0.7,1.1,1.2, COLOR='YELLOW', SURF_ID='steel'/
&OBST ID=' Frame_back_window:1691348_car_2', XB=0.8,1.0,-2.55,-2.2,1.0,1.1, COLOR='YELLOW', SURF_ID='steel'/
&OBST ID=' Frame_back_window:1691491_car_2', XB=0.8,1.0,-0.9,-0.5,1.0,1.1, COLOR='YELLOW', SURF_ID='steel'/
&OBST ID=' Window_frame_middle:1687323_car_2', XB=2.0,2.1,-2.5,-2.4,1.0,1.6, COLOR='YELLOW', SURF_ID='steel'/
&OBST ID='Window_frame_middle_safety_cage_finishing:1687719_car_2', XB=2.0,2.1,-2.4,-2.35,1.0,1.6, SURF_ID='Insulation_car_cabine', BULK_DENSITY=900. /
&OBST ID='Window_frame_middle:1687903_car_2', XB=2.8,2.9,-2.5,-2.4,1.0,1.6,COLOR='YELLOW', SURF_ID='steel'/
&OBST ID='Window_frame_middle_safety_cage_finishinge:1687904_car_2', XB=2.8,2.9,-2.4,-2.35,1.0,1.6, SURF_ID='Insulation_car_cabine', BULK_DENSITY=900. /
&OBST ID='Window_frame_middle:1687988_car_2', XB=2.0,2.1,-0.7,-0.6,1.0,1.6, COLOR='YELLOW', SURF_ID='steel'/
&OBST ID='Window_frame_middle_safety_cage_finishing:1687989_car_2', XB=2.0,2.1,-0.75,-0.7,1.0,1.6, SURF_ID='Insulation_car_cabine', BULK_DENSITY=900. /
&OBST ID='Window_frame_middle:1687990_car_2', XB=2.8,2.9,-0.7,-0.6,1.0,1.6, COLOR='YELLOW', SURF_ID='steel'/
&OBST ID='Window_frame_middle_safety_cage_finishing:1687991_car_2', XB=2.8,2.9,-0.75,-0.7,1.0,1.6, SURF_ID='Insulation_car_cabine', BULK_DENSITY=900. /
&OBST ID=' Frame_front_window:1690476_car_2', XB=0.5,0.8,-2.5,-2.4,1.0,1.1, COLOR='YELLOW', SURF_ID='steel'/
&OBST ID=' Frame_front_window:1690483_car_2', XB=0.7,1.0,-2.5,-2.4,1.1,1.2, COLOR='YELLOW', SURF_ID='steel'/
```

```
&OBST ID=' Frame_front_window:1690490_car_2', XB=0.9,1.2,-2.5,-2.4,1.2,1.3, COLOR='YELLOW', SURF_ID='steel'/
&OBST ID=' Frame_front_window:1690497_car_2', XB=1.1,1.4,-2.5,-2.4,1.3,1.4, COLOR='YELLOW', SURF_ID='steel'/
&OBST ID=' Frame_front_window:1690504_car_2', XB=1.3,1.6,-2.5,-2.4,1.4,1.5, COLOR='YELLOW', SURF_ID='steel'/
&OBST ID=' Frame_front_window:1690511_car_2', XB=1.5,1.8,-2.5,-2.4,1.5,1.6, COLOR='YELLOW', SURF_ID='steel'/
&OBST ID=' Frame_front_window:1690660_car_2', XB=0.5,0.8,-0.7,-0.6,1.0,1.1, COLOR='YELLOW', SURF_ID='steel'/
&OBST ID=' Frame_front_window:1690667_car_2', XB=0.7,1.0,-0.7,-0.6,1.1,1.2, COLOR='YELLOW', SURF_ID='steel'/
&OBST ID=' Frame_front_window:1690674_car_2', XB=0.9,1.2,-0.7,-0.6,1.2,1.3, COLOR='YELLOW', SURF_ID='steel'/
&OBST ID=' Frame_front_window:1690681_car_2', XB=1.1,1.4,-0.7,-0.6,1.3,1.4, COLOR='YELLOW', SURF_ID='steel'/
&OBST ID=' Frame_front_window:1690688_car_2', XB=1.3,1.6,-0.7,-0.6,1.4,1.5, COLOR='YELLOW', SURF_ID='steel'/
&OBST ID=' Frame_front_window:1690695_car_2', XB=1.5,1.8,-0.7,-0.6,1.5,1.6, COLOR='YELLOW', SURF_ID='steel'/
&OBST ID=' Frame_back_window:1690745_car_2', XB=3.7,3.9,-2.5,-2.4,1.5,1.6, COLOR='YELLOW', SURF_ID='steel'/
&OBST ID=' Frame_back_window:1690752_car_2', XB=3.8,4.0,-2.5,-2.4,1.4,1.5, COLOR='YELLOW', SURF_ID='steel'/
&OBST ID=' Frame_back_window:1690759_car_2', XB=3.9,4.1,-2.5,-2.4,1.3,1.4, COLOR='YELLOW', SURF_ID='steel'/
&OBST ID=' Frame_back_window:1690766_car_2', XB=4.0,4.2,-2.5,-2.4,1.2,1.3, COLOR='YELLOW', SURF_ID='steel'/
&OBST ID=' Frame_back_window:1690773_car_2', XB=4.0,4.2,-2.5,-2.4,1.1,1.2, COLOR='YELLOW', SURF_ID='steel'/
&OBST ID=' Frame_back_window:1690773_car_2', XB=4.0,4.3,-2.4,-2.3,1.1,1.2, COLOR='YELLOW', SURF_ID='steel'/
&OBST ID=' Frame_back_window:1691187_car_2', XB=3.7,3.9,-0.7,-0.6,1.5,1.6, COLOR='YELLOW', SURF_ID='steel'/
&OBST ID=' Frame_back_window:1691194_car_2', XB=3.8,4.0,-0.7,-0.6,1.4,1.5, COLOR='YELLOW', SURF_ID='steel'/
&OBST ID=' Frame_back_window:1691201_car_2', XB=3.9,4.1,-0.7,-0.6,1.3,1.4, COLOR='YELLOW', SURF_ID='steel'/
&OBST ID=' Frame_back_window:1691208_car_2', XB=4.0,4.2,-0.7,-0.6,1.2,1.3, COLOR='YELLOW', SURF_ID='steel'/
&OBST ID=' Frame_back_window:1691285_car_2', XB=4.0,4.2,-0.7,-0.6,1.1,1.2, COLOR='YELLOW', SURF_ID='steel'/
&OBST ID=' Frame_back_window:1691285_car_2', XB=4.0,4.3,-0.8,-0.7,1.1,1.2, COLOR='YELLOW', SURF_ID='steel'/
&OBST ID=' Frame_back_window:1691348_car_2', XB=0.8,1.0,-2.55,-2.2,1.0,1.1, COLOR='YELLOW', SURF_ID='steel'/
&OBST ID=' Frame_back_window:1691491_car_2', XB=0.8,1.0,-0.9,-0.5,1.0,1.1, COLOR='YELLOW', SURF_ID='steel'/
&OBST ID=' Window_frame_middle:1687323_car_2', XB=2.0,2.1,-2.5,-2.4,1.0,1.6, COLOR='YELLOW', SURF_ID='steel'/
&OBST ID='Window_frame_middle_safety_cage_finishing:1687719_car_2', XB=2.0,2.1,-2.4,-2.35,1.0,1.6, SURF_ID='Insulation_car_cabine', BULK_DENSITY=900. /
&OBST ID='Window_frame_middle:1687903_car_2', XB=2.8,2.9,-2.5,-2.4,1.0,1.6,COLOR='YELLOW', SURF_ID='steel'/
&OBST ID='Window_frame_middle_safety_cage_finishinge:1687904_car_2', XB=2.8,2.9,-2.4,-2.35,1.0,1.6, SURF_ID='Insulation_car_cabine', BULK_DENSITY=900. /
&OBST ID='Window_frame_middle:1687988_car_2', XB=2.0,2.1,-0.7,-0.6,1.0,1.6, COLOR='YELLOW', SURF_ID='steel'/
&OBST ID='Window_frame_middle_safety_cage_finishing:1687989_car_2', XB=2.0,2.1,-0.75,-0.7,1.0,1.6, SURF_ID='Insulation_car_cabine', BULK_DENSITY=900. /
&OBST ID='Window_frame_middle:1687990_car_2', XB=2.8,2.9,-0.7,-0.6,1.0,1.6, COLOR='YELLOW', SURF_ID='steel'/
&OBST ID='Window_frame_middle_safety_cage_finishing:1687991_car_2', XB=2.8,2.9,-0.75,-0.7,1.0,1.6, SURF_ID='Insulation_car_cabine', BULK_DENSITY=900. /
&OBST ID='safety cage finishing:1685633_car_2', XB=0.8,2.6,-2.4,-2.3,0.6,1.0,
SURF_ID6='Insulation_car_cabine','Insulation_car_cabine','INERT','Insulation_car_cabine','Insulation_car_cabine','Insulation_car_cabine', BULK_DENSITY=900. /
```

```
&OBST ID='safety cage finishing:1685633_car_2', XB=2.6,2.9,-2.4,-2.3,0.6,1.0,
SURF_ID6='Insulation_car_cabine','Insulation_car_cabine','INERT','Insulation_car_cabine','Insulation_car_cabine','Insulation_car_cabine', BULK_DENSITY=900. /
&OBST ID='safety cage finishing:1685910_car_2', XB=2.6,2.9,-0.8,-0.7,0.6,1.0,
SURF_ID6='Insulation_car_cabine','Insulation_car_cabine','Insulation_car_cabine','INERT','Insulation_car_cabine','Insulation_car_cabine', BULK_DENSITY=900. /
&OBST ID='safety cage finishing:1685910_car_2', XB=0.8,2.6,-0.8,-0.7,0.6,1.0,
SURF_ID6='Insulation_car_cabine','Insulation_car_cabine','Insulation_car_cabine','INERT','Insulation_car_cabine','Insulation_car_cabine', BULK_DENSITY=900. /
&OBST ID='Battery_car_2', XB=1.5,2.9,-2.3,-0.8,0.3,0.4, SURF_ID= 'SIMPLE_BATTERY_SURFACE', BULK_DENSITY=900./ [8]
&OBST ID='Battery_rear_car_2', XB=2.3,2.9,-2.3,-0.8,0.4,0.5, SURF_ID='SIMPLE_BATTERY_SURFACE'/ [8]
&OBST ID='Battery:1667225_front_car_2', XB=0.8,1.5,-2.3,-1.9,0.3,0.4, SURF_ID='SIMPLE_BATTERY_SURFACE', BULK_DENSITY=900./ [8]
&OBST ID='Battery:1667226_front_car_2', XB=0.8,1.5,-1.8,-1.3,0.3,0.4, SURF_ID='SIMPLE_BATTERY_SURFACE',  BULK_DENSITY=900./ [8]
&OBST ID='Battery:1667227_front_car_2', XB=0.8,1.5,-1.2,-0.8,0.3,0.4, SURF_ID='SIMPLE_BATTERY_SURFACE', BULK_DENSITY=900./ [8]

&OBST ID='Seating:1684541_car_2', XB=1.2,2.0,-1.5,-0.9,0.6,0.8, SURF_ID='Seating', / [12]
&OBST ID='Seating:1684640_car_2', XB=1.2,2.0,-2.2,-1.6,0.6,0.8, SURF_ID='Seating' / [12]
&OBST ID='Dashboard:1686413_car_2', XB=0.8,1.1,-2.2,-1.5,0.9,1.1, COLOR='PURPLE', SURF_ID='electronic', BULK_DENSITY=1100. / [12]
&OBST ID='Dashboard:1686413_car_2', XB=0.8,1.1,-1.5,-0.9,0.9,1.1, COLOR='PURPLE', SURF_ID='electronic', BULK_DENSITY=1100. / [12]
&OBST ID='Seating_backrest:1684772_car_2', XB=1.8,2.0,-2.2,-1.6,0.8,1.4, SURF_ID='Seating' / [12]
&OBST ID='Seating_backrest:1685038_car_2', XB=1.8,2.0,-1.5,-0.9,0.8,1.4, SURF_ID='Seating'/

/__________________________________________________________________________________windows yellow second car

&DEVC ID='Window_driver_1_2', XB=1.0,2.0,-2.5,-2.4,1.0,1.2, QUANTITY='WALL TEMPERATURE', SPATIAL_STATISTIC='MAX', SURF_ID='Glass', SETPOINT=300.,
INITIAL_STATE=T. /
&DEVC ID='Window_driver_2_2', XB=1.2,2.0,-2.5,-2.4,1.2,1.3, QUANTITY='WALL TEMPERATURE', SPATIAL_STATISTIC='MAX', SURF_ID='Glass', SETPOINT=300.,
INITIAL_STATE=T. /
&DEVC ID='Window_driver_3_2', XB=1.4,2.0,-2.5,-2.4,1.3,1.4, QUANTITY='WALL TEMPERATURE', SPATIAL_STATISTIC='MAX', SURF_ID='Glass', SETPOINT=300.,
INITIAL_STATE=T. /
&DEVC ID='Window_driver_4_2', XB=1.6,2.0,-2.5,-2.4,1.4,1.5, QUANTITY='WALL TEMPERATURE', SPATIAL_STATISTIC='MAX', SURF_ID='Glass', SETPOINT=300.,
INITIAL_STATE=T. /
&DEVC ID='Window_driver_5_2', XB=1.8,2.0,-2.5,-2.4,1.5,1.6, QUANTITY='WALL TEMPERATURE', SPATIAL_STATISTIC='MAX', SURF_ID='Glass', SETPOINT=300.,
INITIAL_STATE=T. /
&DEVC ID='Middle_window_driver_Lower_2', XB=2.1,2.8,-2.5,-2.4,1.0,1.3, QUANTITY='WALL TEMPERATURE', SPATIAL_STATISTIC='MAX', SURF_ID='Glass',
SETPOINT=300., INITIAL_STATE=T. /
&DEVC ID='Middle_window_driver_Upper_2', XB=2.1,2.8,-2.5,-2.4,1.3,1.6, QUANTITY='WALL TEMPERATURE', SPATIAL_STATISTIC='MAX', SURF_ID='Glass',
SETPOINT=300., INITIAL_STATE=T. /
```

```
&DEVC ID='Window_passenger_1_2', XB=1.0,2.0,-0.7,-0.6,1.0,1.2, QUANTITY='WALL TEMPERATURE', SPATIAL_STATISTIC='MAX', SURF_ID='Glass', SETPOINT=300., INITIAL_STATE=T. /
&DEVC ID='Window_passenger_2_2', XB=1.2,2.0,-0.7,-0.6,1.2,1.3, QUANTITY='WALL TEMPERATURE', SPATIAL_STATISTIC='MAX', SURF_ID='Glass', SETPOINT=300., INITIAL_STATE=T. /
&DEVC ID='Window_passenger_3_2', XB=1.4,2.0,-0.7,-0.6,1.3,1.4, QUANTITY='WALL TEMPERATURE', SPATIAL_STATISTIC='MAX', SURF_ID='Glass', SETPOINT=300., INITIAL_STATE=T. /
&DEVC ID='Window_passenger_4_2', XB=1.6,2.0,-0.7,-0.6,1.4,1.5, QUANTITY='WALL TEMPERATURE', SPATIAL_STATISTIC='MAX', SURF_ID='Glass', SETPOINT=300., INITIAL_STATE=T. /
&DEVC ID='Window_passenger_5_2', XB=1.8,2.0,-0.7,-0.6,1.5,1.6, QUANTITY='WALL TEMPERATURE', SPATIAL_STATISTIC='MAX', SURF_ID='Glass', SETPOINT=300., INITIAL_STATE=T. /
&DEVC ID='Middle_window_passenger_1_2', XB=2.6,2.8,-0.7,-0.6,1.0,1.6, QUANTITY='WALL TEMPERATURE', SPATIAL_STATISTIC='MAX', SURF_ID='Glass', SETPOINT=300., INITIAL_STATE=T. /
&DEVC ID='Middle_window_passenger_2_2', XB=2.1,2.6,-0.7,-0.6,1.0,1.6, QUANTITY='WALL TEMPERATURE', SPATIAL_STATISTIC='MAX', SURF_ID='Glass', SETPOINT=300., INITIAL_STATE=T. /
&DEVC ID='Back_window_driver_1_2', XB=2.9,4.0,-2.5,-2.4,1.1,1.3, QUANTITY='WALL TEMPERATURE', SPATIAL_STATISTIC='MAX', SURF_ID='Glass', SETPOINT=300., INITIAL_STATE=T. /
&DEVC ID='Back_window_driver_2_2', XB=2.9,3.9,-2.5,-2.4,1.3,1.4, QUANTITY='WALL TEMPERATURE', SPATIAL_STATISTIC='MAX', SURF_ID='Glass', SETPOINT=300., INITIAL_STATE=T. /
&DEVC ID='Back_window_driver_3_2', XB=2.9,3.8,-2.5,-2.4,1.4,1.5, QUANTITY='WALL TEMPERATURE', SPATIAL_STATISTIC='MAX', SURF_ID='Glass', SETPOINT=300., INITIAL_STATE=T. /
&DEVC ID='Back_window_driver_4_2', XB=2.9,3.7,-2.5,-2.4,1.5,1.6, QUANTITY='WALL TEMPERATURE', SPATIAL_STATISTIC='MAX', SURF_ID='Glass', SETPOINT=300., INITIAL_STATE=T. /
&DEVC ID='Back_window_passenger_1_2', XB=2.9,4.0,-0.7,-0.6,1.1,1.3, QUANTITY='WALL TEMPERATURE', SPATIAL_STATISTIC='MAX', SURF_ID='Glass', SETPOINT=300., INITIAL_STATE=T. /
&DEVC ID='Back_window_passenger_2_2', XB=2.9,3.9,-0.7,-0.6,1.3,1.4, QUANTITY='WALL TEMPERATURE', SPATIAL_STATISTIC='MAX', SURF_ID='Glass', SETPOINT=300., INITIAL_STATE=T. /
&DEVC ID='Back_window_passenger_3_2', XB=2.9,3.8,-0.7,-0.6,1.4,1.5, QUANTITY='WALL TEMPERATURE', SPATIAL_STATISTIC='MAX', SURF_ID='Glass', SETPOINT=300., INITIAL_STATE=T. /
&DEVC ID='Back_window_passenger_4_2', XB=2.9,3.7,-0.7,-0.6,1.5,1.6, QUANTITY='WALL TEMPERATURE', SPATIAL_STATISTIC='MAX', SURF_ID='Glass', SETPOINT=300., INITIAL_STATE=T. /
&DEVC ID='Front_window_1_2', XB=0.5,0.8,-2.4,-1.5,1.0,1.1, QUANTITY='WALL TEMPERATURE', SPATIAL_STATISTIC='MAX', SURF_ID='Glass', SETPOINT=300., INITIAL_STATE=T. /
&DEVC ID='Front_window_2_2', XB=0.5,0.8,-1.5,-0.7,1.0,1.1, QUANTITY='WALL TEMPERATURE', SPATIAL_STATISTIC='MAX', SURF_ID='Glass', SETPOINT=300., INITIAL_STATE=T. /
```

```
&DEVC ID='Front_window_3_2', XB=0.7,1.0,-2.4,-1.5,1.1,1.2, QUANTITY='WALL TEMPERATURE', SPATIAL_STATISTIC='MAX', SURF_ID='Glass', SETPOINT=300.,
INITIAL_STATE=T. /
&DEVC ID='Front_window_4_2', XB=0.7,1.0,-1.5,-0.7,1.1,1.2, QUANTITY='WALL TEMPERATURE', SPATIAL_STATISTIC='MAX', SURF_ID='Glass', SETPOINT=300.,
INITIAL_STATE=T. /
&DEVC ID='Front_window_5_2', XB=0.9,1.2,-2.4,-1.5,1.2,1.3, QUANTITY='WALL TEMPERATURE', SPATIAL_STATISTIC='MAX', SURF_ID='Glass', SETPOINT=300.,
INITIAL_STATE=T. /
&DEVC ID='Front_window_6_2', XB=0.9,1.2,-1.5,-0.7,1.2,1.3, QUANTITY='WALL TEMPERATURE', SPATIAL_STATISTIC='MAX', SURF_ID='Glass', SETPOINT=300.,
INITIAL_STATE=T. /
&DEVC ID='Front_window_7_2', XB=1.1,1.4,-2.4,-1.5,1.3,1.4, QUANTITY='WALL TEMPERATURE', SPATIAL_STATISTIC='MAX', SURF_ID='Glass', SETPOINT=300.,
INITIAL_STATE=T. /
&DEVC ID='Front_window_8_2', XB=1.1,1.4,-1.5,-0.7,1.3,1.4, QUANTITY='WALL TEMPERATURE', SPATIAL_STATISTIC='MAX', SURF_ID='Glass', SETPOINT=300.,
INITIAL_STATE=T. /
&DEVC ID='Front_window_9_2', XB=1.3,1.6,-2.4,-1.5,1.4,1.5, QUANTITY='WALL TEMPERATURE', SPATIAL_STATISTIC='MAX', SURF_ID='Glass', SETPOINT=300.,
INITIAL_STATE=T. /
&DEVC ID='Front_window_10_2', XB=1.3,1.6,-1.5,-0.7,1.4,1.5, QUANTITY='WALL TEMPERATURE', SPATIAL_STATISTIC='MAX', SURF_ID='Glass', SETPOINT=300.,
INITIAL_STATE=T. /
&DEVC ID='Front_window_11_2', XB=1.5,1.8,-2.4,-1.5,1.5,1.6, QUANTITY='WALL TEMPERATURE', SPATIAL_STATISTIC='MAX', SURF_ID='Glass', SETPOINT=300.,
INITIAL_STATE=T. /
&DEVC ID='Front_window_12_2', XB=1.5,1.8,-1.5,-0.7,1.5,1.6, QUANTITY='WALL TEMPERATURE', SPATIAL_STATISTIC='MAX', SURF_ID='Glass', SETPOINT=300.,
INITIAL_STATE=T. /
&DEVC ID='Back_window_1_2', XB=3.7,3.9,-2.4,-1.5,1.5,1.6, QUANTITY='WALL TEMPERATURE', SPATIAL_STATISTIC='MAX', SURF_ID='Glass', SETPOINT=300.,
INITIAL_STATE=T. /
&DEVC ID='Back_window_2_2', XB=3.7,3.9,-1.5,-0.7,1.5,1.6, QUANTITY='WALL TEMPERATURE', SPATIAL_STATISTIC='MAX', SURF_ID='Glass', SETPOINT=300.,
INITIAL_STATE=T. /
&DEVC ID='Back_window_3_2', XB=3.8,4.0,-2.4,-1.5,1.4,1.5, QUANTITY='WALL TEMPERATURE', SPATIAL_STATISTIC='MAX', SURF_ID='Glass', SETPOINT=300.,
INITIAL_STATE=T. /
&DEVC ID='Back_window_4_2', XB=3.8,4.0,-1.5,-0.7,1.4,1.5, QUANTITY='WALL TEMPERATURE', SPATIAL_STATISTIC='MAX', SURF_ID='Glass', SETPOINT=300.,
INITIAL_STATE=T. /
&DEVC ID='Back_window_5_2', XB=3.9,4.1,-2.4,-1.5,1.3,1.4, QUANTITY='WALL TEMPERATURE', SPATIAL_STATISTIC='MAX', SURF_ID='Glass', SETPOINT=300.,
INITIAL_STATE=T. /
&DEVC ID='Back_window_6_2', XB=3.9,4.1,-1.5,-0.7,1.3,1.4, QUANTITY='WALL TEMPERATURE', SPATIAL_STATISTIC='MAX', SURF_ID='Glass', SETPOINT=300.,
INITIAL_STATE=T. /
&DEVC ID='Back_window_7_2', XB=4.0,4.2,-2.4,-1.5,1.2,1.3, QUANTITY='WALL TEMPERATURE', SPATIAL_STATISTIC='MAX', SURF_ID='Glass', SETPOINT=300.,
INITIAL_STATE=T. /
```

```
&DEVC ID='Back_window_8_2', XB=4.0,4.2,-1.5,-0.7,1.2,1.3, QUANTITY='WALL TEMPERATURE', SPATIAL_STATISTIC='MAX', SURF_ID='Glass', SETPOINT=300.,
INITIAL_STATE=T. /
&DEVC ID='Back_window_9_2', XB=4.1,4.3,-2.3,-1.5,1.1,1.2, QUANTITY='WALL TEMPERATURE', SPATIAL_STATISTIC='MAX', SURF_ID='Glass', SETPOINT=300.,
INITIAL_STATE=T. /
&DEVC ID='Back_window_10_2', XB=4.1,4.3,-1.5,-0.8,1.1,1.2, QUANTITY='WALL TEMPERATURE', SPATIAL_STATISTIC='MAX', SURF_ID='Glass', SETPOINT=300.,
INITIAL_STATE=T. /
&OBST ID='Window_driver_1_car_2', XB=1.0,2.0,-2.5,-2.4,1.0,1.2, SURF_ID='Glass', DEVC_ID='Window_driver_1_2'/ [3]
&OBST ID='Window_driver_2_car_2', XB=1.2,2.0,-2.5,-2.4,1.2,1.3, SURF_ID='Glass', DEVC_ID='Window_driver_2_2'/ [3]
&OBST ID='Window_driver_3_car_2', XB=1.4,2.0,-2.5,-2.4,1.3,1.4, SURF_ID='Glass', DEVC_ID='Window_driver_3_2'/ [3]
&OBST ID='Window_driver_4_car_2', XB=1.6,2.0,-2.5,-2.4,1.4,1.5, SURF_ID='Glass', DEVC_ID='Window_driver_4_2'/ [3]
&OBST ID='Window_driver_5_car_2', XB=1.8,2.0,-2.5,-2.4,1.5,1.6, SURF_ID='Glass', DEVC_ID='Window_driver_5_2'/ [3]
&OBST ID='Middle_window_driver_Lower_car_2', XB=2.1,2.8,-2.5,-2.4,1.0,1.3, SURF_ID='Glass', DEVC_ID='Middle_window_driver_Lower_2'/ [3]
&OBST ID='Middle_window_driver_Upper_car_2', XB=2.1,2.8,-2.5,-2.4,1.3,1.6, SURF_ID='Glass', DEVC_ID='Middle_window_driver_Upper_2'/ [3]
&OBST ID='Window_passenger_1_car_2', XB=1.0,2.0,-0.7,-0.6,1.0,1.2, SURF_ID='Glass', DEVC_ID='Window_passenger_1_2'/ [4]
&OBST ID='Window_passenger_2_car_2', XB=1.2,2.0,-0.7,-0.6,1.2,1.3, SURF_ID='Glass', DEVC_ID='Window_passenger_2_2'/ [4]
&OBST ID='Window_passenger_3_car_2', XB=1.4,2.0,-0.7,-0.6,1.3,1.4, SURF_ID='Glass', DEVC_ID='Window_passenger_3_2'/ [4]
&OBST ID='Window_passenger_4_car_2', XB=1.6,2.0,-0.7,-0.6,1.4,1.5, SURF_ID='Glass', DEVC_ID='Window_passenger_4_2'/ [4]
&OBST ID='Window_passenger_5_car_2', XB=1.8,2.0,-0.7,-0.6,1.5,1.6, SURF_ID='Glass', DEVC_ID='Window_passenger_5_2'/ [4]
&OBST ID='Middle_window_passenger_car_1_2', XB=2.6,2.8,-0.7,-0.6,1.0,1.6, SURF_ID='Glass', DEVC_ID='Middle_window_passenger_1_2'/ [5]
&OBST ID='Middle_window_passenger_car_2', XB=2.1,2.6,-0.7,-0.6,1.0,1.6, SURF_ID='Glass', DEVC_ID='Middle_window_passenger_2_2'/ [5]
&OBST ID='Back_window_driver_1_car_2', XB=2.9,4.0,-2.5,-2.4,1.1,1.3, SURF_ID='Glass', DEVC_ID='Back_window_driver_1_2'/ [5]
&OBST ID='Back_window_driver_2_car_2', XB=2.9,3.9,-2.5,-2.4,1.3,1.4, SURF_ID='Glass', DEVC_ID='Back_window_driver_2_2'/ [5]
&OBST ID='Back_window_driver_3_car_2', XB=2.9,3.8,-2.5,-2.4,1.4,1.5, SURF_ID='Glass', DEVC_ID='Back_window_driver_3_2'/ [5]
&OBST ID='Back_window_driver_4_car_2', XB=2.9,3.7,-2.5,-2.4,1.5,1.6, SURF_ID='Glass', DEVC_ID='Back_window_driver_4_2'/ [5]
&OBST ID='Back_window_passenger_1_car_2', XB=2.9,4.0,-0.7,-0.6,1.1,1.3, SURF_ID='Glass', DEVC_ID='Back_window_passenger_1_2'/ [6]
&OBST ID='Back_window_passenger_2_car_2', XB=2.9,3.9,-0.7,-0.6,1.3,1.4, SURF_ID='Glass', DEVC_ID='Back_window_passenger_2_2'/ [6]
&OBST ID='Back_window_passenger_3_car_2', XB=2.9,3.8,-0.7,-0.6,1.4,1.5, SURF_ID='Glass', DEVC_ID='Back_window_passenger_3_2'/ [6]
&OBST ID='Back_window_passenger_4_car_2', XB=2.9,3.7,-0.7,-0.6,1.5,1.6, SURF_ID='Glass', DEVC_ID='Back_window_passenger_4_2'/ [6]
&OBST ID='Front_window_1_car_2', XB=0.5,0.8,-2.4,-1.5,1.0,1.1, SURF_ID='Glass', DEVC_ID='Front_window_1_2'/ [6]
&OBST ID='Front_window_2_car_2', XB=0.5,0.8,-1.5,-0.7,1.0,1.1, SURF_ID='Glass', DEVC_ID='Front_window_2_2'/ [6]
&OBST ID='Front_window_3_car_2', XB=0.7,1.0,-2.4,-1.5,1.1,1.2, SURF_ID='Glass', DEVC_ID='Front_window_3_2'/ [6]
&OBST ID='Front_window_4_car_2', XB=0.7,1.0,-1.5,-0.7,1.1,1.2, SURF_ID='Glass', DEVC_ID='Front_window_4_2'/ [6]
&OBST ID='Front_window_5_car_2', XB=0.9,1.2,-2.4,-1.5,1.2,1.3, SURF_ID='Glass', DEVC_ID='Front_window_5_2'/ [6]
&OBST ID='Front_window_6_car_2', XB=0.9,1.2,-1.5,-0.7,1.2,1.3, SURF_ID='Glass', DEVC_ID='Front_window_6_2'/ [6]
&OBST ID='Front_window_7_car_2', XB=1.1,1.4,-2.4,-1.5,1.3,1.4, SURF_ID='Glass', DEVC_ID='Front_window_7_2'/ [6]
```

```
&OBST ID='Front_window_8_car_2', XB=1.1,1.4,-1.5,-0.7,1.3,1.4, SURF_ID='Glass', DEVC_ID='Front_window_8_2'/ [6]
&OBST ID='Front_window_9_car_2', XB=1.3,1.6,-2.4,-1.5,1.4,1.5, SURF_ID='Glass', DEVC_ID='Front_window_9_2'/ [6]
&OBST ID='Front_window_10_car_2', XB=1.3,1.6,-1.5,-0.7,1.4,1.5, SURF_ID='Glass', DEVC_ID='Front_window_10_2'/ [6]
&OBST ID='Front_window_11_car_2', XB=1.5,1.8,-2.4,-1.5,1.5,1.6, SURF_ID='Glass', DEVC_ID='Front_window_11_2'/ [6]
&OBST ID='Front_window_12_car_2', XB=1.5,1.8,-1.5,-0.7,1.5,1.6, SURF_ID='Glass', DEVC_ID='Front_window_12_2'/ [6]
&OBST ID='Back_window_1_car_2', XB=3.7,3.9,-2.4,-1.5,1.5,1.6, SURF_ID='Glass', DEVC_ID='Back_window_1_2'/ [7]
&OBST ID='Back_window_2_car_2', XB=3.7,3.9,-1.5,-0.7,1.5,1.6, SURF_ID='Glass', DEVC_ID='Back_window_2_2'/ [7]
&OBST ID='Back_window_3_car_2', XB=3.8,4.0,-2.4,-1.5,1.4,1.5, SURF_ID='Glass', DEVC_ID='Back_window_3_2'/ [7]
&OBST ID='Back_window_4_car_2', XB=3.8,4.0,-1.5,-0.7,1.4,1.5, SURF_ID='Glass', DEVC_ID='Back_window_4_2'/ [7]
&OBST ID='Back_window_5_car_2', XB=3.9,4.1,-2.4,-1.5,1.3,1.4, SURF_ID='Glass', DEVC_ID='Back_window_5_2'/ [7]
&OBST ID='Back_window_6_car_2', XB=3.9,4.1,-1.5,-0.7,1.3,1.4, SURF_ID='Glass', DEVC_ID='Back_window_6_2'/ [7]
&OBST ID='Back_window_7_car_2', XB=4.0,4.2,-2.4,-1.5,1.2,1.3, SURF_ID='Glass', DEVC_ID='Back_window_7_2'/ [7]
&OBST ID='Back_window_8_car_2', XB=4.0,4.2,-1.5,-0.7,1.2,1.3, SURF_ID='Glass', DEVC_ID='Back_window_8_2'/ [7]
&OBST ID='Back_window_9_car_2', XB=4.1,4.3,-2.3,-1.5,1.1,1.2, SURF_ID='Glass', DEVC_ID='Back_window_9_2'/ [7]
&OBST ID='Back_window_10_car_2', XB=4.1,4.3,-1.5,-0.8,1.1,1.2, SURF_ID='Glass', DEVC_ID='Back_window_10_2'/ [7]

/__________________________ ____________________________________________________________________Orange third car
&OBST ID='Battery_car_3', XB=1.5,2.9,2.5,4.0,0.3,0.4, SURF_ID='SIMPLE_BATTERY_SURFACE', BULK_DENSITY=900./ [8]
&OBST ID='Battery_rear_car_3', XB=2.3,2.9,2.5,4.0,0.4,0.5, SURF_ID='SIMPLE_BATTERY_SURFACE'/ [8]
&OBST ID='Battery:1667225_front_car_3', XB=0.8,1.5,2.5,2.9,0.3,0.4, SURF_ID='SIMPLE_BATTERY_SURFACE', BULK_DENSITY=900./ [8]
&OBST ID='Battery:1667226_front_car_3', XB=0.8,1.5,3.0,3.5,0.3,0.4, SURF_ID='SIMPLE_BATTERY_SURFACE',  BULK_DENSITY=900./ [8]
&OBST ID='Battery:1667227_front_car_3', XB=0.8,1.5,3.6,4.0,0.3,0.4, SURF_ID='SIMPLE_BATTERY_SURFACE', BULK_DENSITY=900./ [8]

&OBST ID='Bottom_car_3', XB=-0.4,-0.1,2.7,2.9,0.2,0.25,COLOR='SILVER', SURF_ID='steel'/ Current: floor with space in between
&OBST ID='Bottom_car_3', XB=-0.4,2.6,2.9,3.5,0.2,0.25,COLOR='SILVER', SURF_ID='steel'/
&OBST ID='Bottom_car_3', XB=-0.3,-0.1,2.6,2.7,0.2,0.25,COLOR='SILVER', SURF_ID='steel'/
&OBST ID='Bottom_car_3', XB=-0.2,-0.1,2.5,2.6,0.2,0.25,COLOR='SILVER', SURF_ID='steel'/
&OBST ID='Bottom_car_3', XB=0.7,2.6,2.5,2.9,0.2,0.25,COLOR='SILVER', SURF_ID='steel'/
&OBST ID='Bottom_car_3', XB=2.6,3.0,2.5,2.9,0.2,0.25,COLOR='SILVER', SURF_ID='steel'/
&OBST ID='Bottom_car_3', XB=2.6,4.3,2.9,3.5,0.2,0.25,COLOR='SILVER', SURF_ID='steel'/
&OBST ID='Bottom_car_3', XB=3.8,4.2,2.5,2.6,0.2,0.25,COLOR='SILVER', SURF_ID='steel'/
&OBST ID='Bottom_car_3', XB=3.8,4.3,2.6,2.9,0.2,0.25,COLOR='SILVER', SURF_ID='steel'/
&OBST ID='Bottom_car_3', XB=2.6,3.0,4.0,4.4,0.2,0.25,COLOR='SILVER', SURF_ID='steel'/
&OBST ID='Bottom_car_3', XB=2.6,4.3,3.5,4.0,0.2,0.25,COLOR='SILVER', SURF_ID='steel'/
&OBST ID='Bottom_car_3', XB=3.8,4.1,4.3,4.4,0.2,0.25,COLOR='SILVER', SURF_ID='steel'/
```

```
&OBST ID='Bottom_car_3', XB=3.8,4.3,4.0,4.3,0.2,0.25,COLOR='SILVER', SURF_ID='steel'/
&OBST ID='Bottom_car_3', XB=-0.4,-0.1,4.0,4.2,0.2,0.25,COLOR='SILVER', SURF_ID='steel'/
&OBST ID='Bottom_car_3', XB=-0.4,2.6,3.5,4.0,0.2,0.25,COLOR='SILVER', SURF_ID='steel'/
&OBST ID='Bottom_car_3', XB=-0.3,-0.1,4.2,4.3,0.2,0.25,COLOR='SILVER', SURF_ID='steel'/
&OBST ID='Bottom_car_3', XB=-0.2,-0.1,4.3,4.4,0.2,0.25,COLOR='SILVER', SURF_ID='steel'/
&OBST ID='Bottom_car_3', XB=0.7,2.6,4.0,4.4,0.2,0.25,COLOR='SILVER', SURF_ID='steel'/

&OBST ID='Covering_batteries_3', XB=0.8,2.3,2.6,4.3,0.5,0.6,COLOR='BLUE', SURF_ID='steel'/  seperation between seating and batteries for oxygen
&OBST ID='Covering_batteries_back_3', XB=2.3,2.9,2.7,4.2,0.6,0.7,COLOR='BLUE', SURF_ID='steel'/  seperation between seating and batteries for oxygen

/______________________________________________________________________________________Orange car frame /

&OBST ID='car_body_front_3', XB=-0.4,-0.2,2.7,3.5,0.8,0.9,COLOR='ORANGE', SURF_ID='steel'/
&OBST ID='car_body_front_3', XB=-0.3,-0.2,2.5,2.7,0.8,0.9,COLOR='ORANGE', SURF_ID='steel'/
&OBST ID='car_body_front_3', XB=-0.4,-0.2,3.5,4.2,0.8,0.9,COLOR='ORANGE', SURF_ID='steel'/
&OBST ID='car_body_front_3', XB=-0.3,-0.2,4.2,4.4,0.8,0.9,COLOR='ORANGE', SURF_ID='steel'/
&OBST ID='car_body_above_wheels:1678653_3', XB=-0.2,0.8,2.5,3.0,0.8,0.9,COLOR='ORANGE', SURF_ID='steel'/
&OBST ID='car_body_above_wheels:1678732_3', XB=-0.2,0.8,3.9,4.4,0.8,0.9,COLOR='ORANGE', SURF_ID='steel'/
&OBST ID='car_body_above_wheels:1678748_3', XB=2.9,3.9,3.9,4.4,0.8,0.9,COLOR='ORANGE', SURF_ID='steel'/
&OBST ID='car_body_above_wheels:1678762_3', XB=2.9,3.9,2.5,3.0,0.8,0.9,COLOR='ORANGE', SURF_ID='steel'/
&OBST ID='Car_body:1673246_3', XB=-0.4,-0.2,4.1,4.2,0.3,0.8,COLOR='ORANGE', SURF_ID='steel'/
&OBST ID='Car_body:1673275_3', XB=-0.3,-0.2,4.2,4.4,0.3,0.8,COLOR='ORANGE', SURF_ID='steel'/
&OBST ID='Car_body:1673381_3', XB=-0.2,-0.1,4.3,4.4,0.3,0.8,COLOR='ORANGE', SURF_ID='steel'/
&OBST ID='Car_body:1673471_3', XB=-0.2,-0.1,3.9,4.3,0.3,0.8,COLOR='ORANGE', SURF_ID='steel'/
&OBST ID='Car_body:1673520_3', XB=-0.1,0.8,3.9,4.0,0.3,0.8,COLOR='ORANGE', SURF_ID='steel'/
&OBST ID='Car_body:1673573_3', XB=0.7,0.8,4.0,4.4,0.3,0.8,COLOR='ORANGE', SURF_ID='steel'/
&OBST ID='Car_body:1673628_3', XB=2.6,2.9,4.3,4.4,0.4,1.0,COLOR='ORANGE', SURF_ID='steel'/
&OBST ID='Car_body:1673628_3', XB=0.8,2.6,4.3,4.4,0.4,1.0,COLOR='ORANGE', SURF_ID='steel'/
&OBST ID='Car_body:1673732_3', XB=2.9,3.9,3.9,4.0,0.3,0.8,COLOR='ORANGE', SURF_ID='steel'/
&OBST ID='Car_body:1673763_3', XB=3.8,3.9,4.0,4.4,0.3,0.8,COLOR='ORANGE', SURF_ID='steel'/
&OBST ID='Car_body:1673788_3', XB=3.9,4.2,4.3,4.4,0.3,0.9,COLOR='ORANGE', SURF_ID='steel'/
&OBST ID='Car_body:1673830_3', XB=4.1,4.2,4.2,4.3,0.3,0.9,COLOR='ORANGE', SURF_ID='steel'/
&OBST ID='Car_body:1673916_3', XB=4.2,4.3,2.6,3.5,0.3,0.9,COLOR='ORANGE', SURF_ID='steel'/
&OBST ID='Car_body:1673916_3', XB=4.2,4.3,3.5,4.3,0.3,0.9,COLOR='ORANGE', SURF_ID='steel'/
&OBST ID='Car_body:1673967_3', XB=4.1,4.2,2.5,2.7,0.3,0.9,COLOR='ORANGE', SURF_ID='steel'/
```

```
&OBST ID='Car_body:1673995_3', XB=4.1,4.2,2.6,2.7,0.3,0.9,COLOR='ORANGE', SURF_ID='steel'/
&OBST ID='Car_body:1674064_3', XB=3.9,4.1,2.5,2.6,0.3,0.9,COLOR='ORANGE', SURF_ID='steel'/
&OBST ID='Car_body:1674105_3', XB=3.8,3.9,2.5,3.0,0.3,0.8,COLOR='ORANGE', SURF_ID='steel'/
&OBST ID='Car_body:1674245_3', XB=0.8,2.6,2.5,2.6,0.4,1.0,COLOR='ORANGE', SURF_ID='steel'/
&OBST ID='Car_body:1674245_3', XB=2.6,2.9,2.5,2.6,0.4,1.0,COLOR='ORANGE', SURF_ID='steel'/
&OBST ID='Car_body:1674536_3', XB=0.7,0.8,2.5,3.0,0.3,0.8,COLOR='ORANGE', SURF_ID='steel'/
&OBST ID='Car_body:1674582_3', XB=-0.2,0.7,2.9,3.0,0.3,0.8,COLOR='ORANGE', SURF_ID='steel'/
&OBST ID='Car_body:1674615_3', XB=-0.2,-0.1,2.5,2.9,0.3,0.8,COLOR='ORANGE', SURF_ID='steel'/
&OBST ID='Car_body:1674733_3', XB=-0.3,-0.2,2.5,2.8,0.3,0.8,COLOR='ORANGE', SURF_ID='steel'/
&OBST ID='Car_body:1674759_3', XB=-0.4,-0.3,2.7,2.8,0.3,0.8,COLOR='ORANGE', SURF_ID='steel'/
&OBST ID='Car_body:1674792_3', XB=-0.4,-0.3,2.8,3.5,0.3,0.8,COLOR='ORANGE', SURF_ID='steel'/
&OBST ID='Car_body:1674792_3', XB=-0.4,-0.3,3.5,4.1,0.3,0.8,COLOR='ORANGE', SURF_ID='steel'/
&OBST ID='Car_body:1679523_3', XB=2.9,3.8,2.9,3.0,0.3,0.8,COLOR='ORANGE', SURF_ID='steel'/
&OBST ID='Car_body:1679563_3', XB=2.9,3.0,2.5,2.9,0.3,0.8,COLOR='ORANGE', SURF_ID='steel'/
&OBST ID='Car_body_roof_3', XB=1.7,2.6,2.5,3.5,1.6,1.7,COLOR='ORANGE', SURF_ID='steel'/
&OBST ID='Car_body_roof_3', XB=2.6,3.8,2.5,3.5,1.6,1.7,COLOR='ORANGE', SURF_ID='steel'/
&OBST ID='Car_body_roof_3', XB=2.6,3.8,3.5,4.4,1.6,1.7,COLOR='ORANGE', SURF_ID='steel'/
&OBST ID='Car_body_roof_3', XB=1.7,2.6,3.5,4.4,1.6,1.7,COLOR='ORANGE', SURF_ID='steel'/
&OBST ID='engine cover:1685928_3', XB=-0.2,0.8,2.5,3.5,0.9,1.0,COLOR='ORANGE', SURF_ID='steel'/
&OBST ID='engine cover:1685928_3', XB=-0.2,0.8,3.5,4.4,0.9,1.0,COLOR='ORANGE', SURF_ID='steel'/
&OBST ID=' Frame_front_window:1690476_3', XB=0.5,0.8,2.5,2.6,1.0,1.1,COLOR='ORANGE', SURF_ID='steel'/
&OBST ID=' Frame_front_window:1690483_3', XB=0.7,1.0,2.5,2.6,1.1,1.2,COLOR='ORANGE', SURF_ID='steel'/
&OBST ID=' Frame_front_window:1690490_3', XB=0.9,1.2,2.5,2.6,1.2,1.3,COLOR='ORANGE', SURF_ID='steel'/
&OBST ID=' Frame_front_window:1690497_3', XB=1.1,1.4,2.5,2.6,1.3,1.4,COLOR='ORANGE', SURF_ID='steel'/
&OBST ID=' Frame_front_window:1690504_3', XB=1.3,1.6,2.5,2.6,1.4,1.5,COLOR='ORANGE', SURF_ID='steel'/
&OBST ID=' Frame_front_window:1690511_3', XB=1.5,1.8,2.5,2.6,1.5,1.6,COLOR='ORANGE', SURF_ID='steel'/
&OBST ID=' Frame_front_window:1690660_3', XB=0.5,0.8,4.3,4.4,1.0,1.1,COLOR='ORANGE', SURF_ID='steel'/
&OBST ID=' Frame_front_window:1690667_3', XB=0.7,1.0,4.3,4.4,1.1,1.2,COLOR='ORANGE', SURF_ID='steel'/
&OBST ID=' Frame_front_window:1690674_3', XB=0.9,1.2,4.3,4.4,1.2,1.3,COLOR='ORANGE', SURF_ID='steel'/
&OBST ID=' Frame_front_window:1690681_3', XB=1.1,1.4,4.3,4.4,1.3,1.4,COLOR='ORANGE', SURF_ID='steel'/
&OBST ID=' Frame_front_window:1690688_3', XB=1.3,1.6,4.3,4.4,1.4,1.5,COLOR='ORANGE', SURF_ID='steel'/
&OBST ID=' Frame_front_window:1690695_3', XB=1.5,1.8,4.3,4.4,1.5,1.6,COLOR='ORANGE', SURF_ID='steel'/
&OBST ID=' Frame_back_window:1690745_3', XB=3.7,3.9,2.5,2.6,1.5,1.6,COLOR='ORANGE', SURF_ID='steel'/
&OBST ID=' Frame_back_window:1690752_3', XB=3.8,4.0,2.5,2.6,1.4,1.5,COLOR='ORANGE', SURF_ID='steel'/
&OBST ID=' Frame_back_window:1690759_3', XB=3.9,4.1,2.5,2.6,1.3,1.4,COLOR='ORANGE', SURF_ID='steel'/
```

```
&OBST ID=' Frame_back_window:1690766_3', XB=4.0,4.2,2.5,2.6,1.2,1.3,COLOR='ORANGE', SURF_ID='steel'/
&OBST ID=' Frame_back_window:1690773_3', XB=4.0,4.2,2.5,2.6,1.1,1.2,COLOR='ORANGE', SURF_ID='steel'/
&OBST ID=' Frame_back_window:1690773_3', XB=4.0,4.3,2.6,2.7,1.1,1.2,COLOR='ORANGE', SURF_ID='steel'/
&OBST ID=' Frame_back_window:1691187_3', XB=3.7,3.9,4.3,4.4,1.5,1.6,COLOR='ORANGE', SURF_ID='steel'/
&OBST ID=' Frame_back_window:1691194_3', XB=3.8,4.0,4.3,4.4,1.4,1.5,COLOR='ORANGE', SURF_ID='steel'/
&OBST ID=' Frame_back_window:1691201_3', XB=3.9,4.1,4.3,4.4,1.3,1.4,COLOR='ORANGE', SURF_ID='steel'/
&OBST ID=' Frame_back_window:1691208_3', XB=4.0,4.2,4.3,4.4,1.2,1.3,COLOR='ORANGE', SURF_ID='steel'/
&OBST ID=' Frame_back_window:1691285_3', XB=4.0,4.2,4.3,4.4,1.1,1.2,COLOR='ORANGE', SURF_ID='steel'/
&OBST ID=' Frame_back_window:1691285_3', XB=4.0,4.3,4.2,4.3,1.1,1.2,COLOR='ORANGE', SURF_ID='steel'/
&OBST ID=' Frame_back_window:1691348_3', XB=0.8,1.0,2.4,2.8,1.0,1.1,COLOR='ORANGE', SURF_ID='steel'/
&OBST ID=' Frame_back_window:1691491_3', XB=0.8,1.0,4.1,4.5,1.0,1.1,COLOR='ORANGE', SURF_ID='steel'/
&OBST ID='Car_body:1689403_3', XB=2.9,4.1,4.3,4.4,0.9,1.1,COLOR='ORANGE', SURF_ID='steel'/
&OBST ID='Car_body:1689425_3', XB=4.1,4.2,4.2,4.4,0.9,1.1,COLOR='ORANGE', SURF_ID='steel'/
&OBST ID='Car_body:1689461_3', XB=4.2,4.3,4.2,4.3,0.9,1.1,COLOR='ORANGE', SURF_ID='steel'/
&OBST ID='Car_body:1689516_3', XB=4.2,4.3,2.7,3.5,0.9,1.1,COLOR='ORANGE', SURF_ID='steel'/
&OBST ID='Car_body:1689516_3', XB=4.2,4.3,3.5,4.2,0.9,1.1,COLOR='ORANGE', SURF_ID='steel'/
&OBST ID='Car_body:1689545_3', XB=4.1,4.3,2.6,2.7,0.9,1.1,COLOR='ORANGE', SURF_ID='steel'/
&OBST ID='Car_body:1689567_3', XB=4.1,4.2,2.5,2.6,0.9,1.1,COLOR='ORANGE', SURF_ID='steel'/
&OBST ID='Car_body:1689617_3', XB=2.9,4.1,2.5,2.6,0.9,1.1,COLOR='ORANGE', SURF_ID='steel'/
&OBST ID='Car_body:1680322_3', XB=2.9,3.0,4.0,4.4,0.3,0.8,COLOR='ORANGE', SURF_ID='steel'/


&OBST ID='Covering_trunk_3', XB=3.7,4.2,3.0,3.5,0.3,0.35,SURF_ID='Insulation_car_cabine', BULK_DENSITY=900. /
&OBST ID='Covering_trunk_3', XB=3.9,4.1,2.6,2.7,0.3,0.35,SURF_ID='Insulation_car_cabine', BULK_DENSITY=900. /
&OBST ID='Covering_trunk_3', XB=3.9,4.2,2.7,3.0,0.3,0.35,SURF_ID='Insulation_car_cabine', BULK_DENSITY=900. /
&OBST ID='Covering_trunk_3', XB=3.7,4.2,3.5,3.9,0.3,0.35,SURF_ID='Insulation_car_cabine', BULK_DENSITY=900. /
&OBST ID='Covering_trunk_3', XB=3.9,4.1,4.2,4.3,0.3,0.35,SURF_ID='Insulation_car_cabine', BULK_DENSITY=900. /
&OBST ID='Covering_trunk_3', XB=3.9,4.2,3.9,4.2,0.3,0.35,SURF_ID='Insulation_car_cabine', BULK_DENSITY=900. /
&OBST ID='Covering_wheels_3', XB=2.9,3.8,3.0,3.5,0.85,0.9,SURF_ID='Insulation_car_cabine', BULK_DENSITY=900. /
&OBST ID='Covering_wheels_3', XB=2.9,3.8,3.5,3.9,0.85,0.9,SURF_ID='Insulation_car_cabine', BULK_DENSITY=900. /

&OBST ID='Covering_wheels_3', XB=2.9,3.8,-2.0,-1.5,0.85,0.9, SURF_ID='Insulation_car_cabine', BULK_DENSITY=900. /
&OBST ID='Covering_wheels_3', XB=2.9,3.8,-1.5,-1.1,0.85,0.9, SURF_ID='Insulation_car_cabine', BULK_DENSITY=900. /

&OBST ID='Wheel:1665075_3', XB=0.1,0.5,4.1,4.4,0.0,0.1,COLOR='BLACK', SURF_ID='Wheel_Assembly', BULK_DENSITY=910. /
```

```
&OBST ID='Wheel:1665075_rim_3', XB=0.1,0.5,4.1,4.4,0.1,0.6,COLOR='SILVER', SURF_ID='steel'/
&OBST ID='Wheel:1665075_3', XB=0.1,0.5,4.1,4.4,0.6,0.7,COLOR='BLACK', SURF_ID='Wheel_Assembly', BULK_DENSITY=910. /
&OBST ID='Wheel:1665344_3', XB=0.5,0.6,4.1,4.4,0.1,0.6,COLOR='BLACK', SURF_ID='Wheel_Assembly', BULK_DENSITY=910. /
&OBST ID=' Wheel:1666370_3', XB=0.0,0.1,4.1,4.4,0.1,0.6,COLOR='BLACK', SURF_ID='Wheel_Assembly', BULK_DENSITY=910. /
&OBST ID='Wheel:1666668_3', XB=0.1,0.5,2.5,2.8,0.0,0.1,COLOR='BLACK', SURF_ID='Wheel_Assembly', BULK_DENSITY=910. /
&OBST ID='Wheel_rim:1666668_3', XB=0.1,0.5,2.5,2.8,0.1,0.6,COLOR='SILVER', SURF_ID='steel'/
&OBST ID='Wheel:1666668_3', XB=0.1,0.5,2.5,2.8,0.6,0.7,COLOR='BLACK', SURF_ID='Wheel_Assembly', BULK_DENSITY=910. /
&OBST ID=' Wheel:1666669_3', XB=0.5,0.6,2.5,2.8,0.1,0.6,COLOR='BLACK', SURF_ID='Wheel_Assembly', BULK_DENSITY=910. /
&OBST ID=' Wheel:1666670_3', XB=0.0,0.1,2.5,2.8,0.1,0.6,COLOR='BLACK', SURF_ID='Wheel_Assembly', BULK_DENSITY=910. /
&OBST ID='Wheel:1666678_3', XB=3.2,3.6,2.5,2.8,0.0,0.1,COLOR='BLACK', SURF_ID='Wheel_Assembly', BULK_DENSITY=910. /
&OBST ID='Wheel:1666678_rim_3', XB=3.2,3.6,2.5,2.8,0.1,0.6,COLOR='SILVER', SURF_ID='steel'/
&OBST ID='Wheel:1666678_3', XB=3.2,3.6,2.5,2.8,0.6,0.7,COLOR='BLACK', SURF_ID='Wheel_Assembly', BULK_DENSITY=910. /
&OBST ID=' Wheel:1666679_3', XB=3.6,3.7,2.5,2.8,0.1,0.6,COLOR='BLACK', SURF_ID='Wheel_Assembly', BULK_DENSITY=910. /
&OBST ID=' Wheel:1666680_3', XB=3.1,3.2,2.5,2.8,0.1,0.6,COLOR='BLACK', SURF_ID='Wheel_Assembly', BULK_DENSITY=910. /
&OBST ID='Wheel:1679782_3', XB=3.2,3.6,4.1,4.4,0.0,0.1,COLOR='BLACK', SURF_ID='Wheel_Assembly', BULK_DENSITY=910. /
&OBST ID='Wheel:1679782_rim_3', XB=3.2,3.6,4.1,4.4,0.1,0.6,COLOR='SILVER', SURF_ID='steel'/
&OBST ID='Wheel:1679782_3', XB=3.2,3.6,4.1,4.4,0.6,0.7,COLOR='BLACK', SURF_ID='Wheel_Assembly', BULK_DENSITY=910. /
&OBST ID='Wheel 2:1679783_3', XB=3.6,3.7,4.1,4.4,0.1,0.6,COLOR='BLACK', SURF_ID='Wheel_Assembly', BULK_DENSITY=910. /
&OBST ID='Wheel 2:1679784_3', XB=3.1,3.2,4.1,4.4,0.1,0.6,COLOR='BLACK', SURF_ID='Wheel_Assembly', BULK_DENSITY=910. /
/&OBST ID='Division_insulation_battery_rows_3', XB=0.8,2.6,3.4,3.5,0.3,0.5,SURF_ID='Insulation_batteries'/
/&OBST ID='Division_insulation_battery_rows_3', XB=2.6,2.9,3.4,3.5,0.3,0.5,SURF_ID='Insulation_batteries'/
/&OBST ID='Insulation_battery_rows:1671243_3', XB=2.6,2.9,4.2,4.3,0.3,0.5,SURF_ID='Insulation_batteries'/
/&OBST ID='Insulation_battery_rows:1671243_3', XB=0.8,2.6,4.2,4.3,0.3,0.5,SURF_ID='Insulation_batteries'/
/&OBST ID='Insulation_battery_rows:1672588_3', XB=0.8,2.6,2.6,2.7,0.3,0.5,SURF_ID='Insulation_batteries'/
/&OBST ID='Insulation_battery_rows:1672588_3', XB=2.6,2.9,2.6,2.7,0.3,0.5,SURF_ID='Insulation_batteries'/
&OBST ID='Technical_stuff_front:1676605_3', XB=-0.2,0.2,3.0,3.5,0.3,0.8,COLOR='GRAY 47', SURF_ID='electronic', BULK_DENSITY=1100. /
&OBST ID='Technical_stuff_front:1676605_3', XB=-0.2,0.2,3.5,3.9,0.3,0.8,COLOR='GRAY 47', SURF_ID='electronic', BULK_DENSITY=1100. /
&OBST ID='Cylinders:1677342_3', XB=0.3,0.6,3.0,3.5,0.3,0.8,RGB=244,245,246, SURF_ID='Cylinders'/
&OBST ID='Cylinders:1677342_3', XB=0.3,0.6,3.5,3.9,0.3,0.8,RGB=244,245,246, SURF_ID='Cylinders'/
&OBST ID='Buffer_behind_engine:1677885_3', XB=0.6,0.65,3.0,3.5,0.3,0.9,SURF_ID='Insulation_car_cabine', BULK_DENSITY=900. /
&OBST ID='Buffer_behind_engine:1677885_3', XB=0.6,0.65,3.5,3.9,0.3,0.9,SURF_ID='Insulation_car_cabine', BULK_DENSITY=900. /
&OBST ID='Buffer_behind_Transformer:1683239_3', XB=3.7,3.75,3.0,3.5,0.3,0.9,SURF_ID='Insulation_car_cabine', BULK_DENSITY=900. /
&OBST ID='Buffer_behind_Transformer:1683239_3', XB=3.7,3.75,3.5,3.9,0.3,0.9,SURF_ID='Insulation_car_cabine', BULK_DENSITY=900. /
&OBST ID='Cover_befor_transformer:1683732_3', XB=2.9,2.95,3.0,3.5,0.3,0.9,SURF_ID='Insulation_car_cabine', BULK_DENSITY=900. /
&OBST ID='Cover_befor_transformer:1683732_3', XB=2.9,2.95,3.5,3.9,0.3,0.9,SURF_ID='Insulation_car_cabine', BULK_DENSITY=900. /
```

```
&OBST ID='Transformer:1678843_3', XB=3.1,3.7,3.0,3.5,0.3,0.8,SURF_ID='transformer'/
&OBST ID='Transformer:1678843_3', XB=3.1,3.7,3.5,3.9,0.3,0.8,SURF_ID='transformer'/
&OBST ID='Seating:1684541_3', XB=1.2,2.0,3.5,4.1,0.6,0.8,SURF_ID='Seating', /
&OBST ID='Seating:1684640_3', XB=1.2,2.0,2.8,3.4,0.6,0.8,SURF_ID='Seating' /
&OBST ID='Seating:1685527_3', XB=2.3,2.6,2.8,3.5,0.7,0.8,SURF_ID='Seating' /
&OBST ID='Seating:1685527_3', XB=2.6,2.9,2.8,3.5,0.7,0.8,SURF_ID='Seating' /
&OBST ID='Seating:1685527_3', XB=2.6,2.9,3.5,4.1,0.7,0.8,SURF_ID='Seating' /
&OBST ID='Seating:1685527_3', XB=2.3,2.6,3.5,4.1,0.7,0.8,SURF_ID='Seating' /
&OBST ID='Dashboard:1686413_3', XB=0.8,1.1,2.8,3.5,0.9,1.1,COLOR='PURPLE', SURF_ID='electronic', BULK_DENSITY=1100. /
&OBST ID='Dashboard:1686413_3', XB=0.8,1.1,3.5,4.1,0.9,1.1,COLOR='PURPLE', SURF_ID='electronic', BULK_DENSITY=1100. /
&OBST ID='Seating_backrest:1684772_3', XB=1.8,2.0,2.8,3.4,0.8,1.4,SURF_ID='Seating' /
&OBST ID='Seating_backrest:1685038_3', XB=1.8,2.0,3.5,4.1,0.8,1.4,SURF_ID='Seating' /
&OBST ID='Seating_backrest:1685444_3', XB=2.7,2.9,2.8,3.5,0.8,1.4,SURF_ID='Seating' /
&OBST ID='Seating_backrest:1685444_3', XB=2.7,2.9,3.5,4.2,0.8,1.4,SURF_ID='Seating' /


/xmin, xmax, ymin, ymax, zmin, zmax
&OBST ID='safety cage finishing:1685633_3',
XB=0.8,2.6,2.6,2.7,0.6,1.0,SURF_ID6='Insulation_car_cabine','Insulation_car_cabine','INERT','Insulation_car_cabine','Insulation_car_cabine','Insulation_car_cabine',
BULK_DENSITY=900. /
&OBST ID='safety cage finishing:1685633_3',
XB=2.6,2.9,2.6,2.7,0.6,1.0,SURF_ID6='Insulation_car_cabine','Insulation_car_cabine','INERT','Insulation_car_cabine','Insulation_car_cabine','Insulation_car_cabine',
BULK_DENSITY=900. /
&OBST ID='safety cage finishing:1685910_3',
XB=2.6,2.9,4.2,4.3,0.6,1.0,SURF_ID6='Insulation_car_cabine','Insulation_car_cabine','Insulation_car_cabine','INERT','Insulation_car_cabine','Insulation_car_cabine',
BULK_DENSITY=900. /
&OBST ID='safety cage finishing:1685910_3',
XB=0.8,2.6,4.2,4.3,0.6,1.0,SURF_ID6='Insulation_car_cabine','Insulation_car_cabine','Insulation_car_cabine','INERT','Insulation_car_cabine','Insulation_car_cabine',
BULK_DENSITY=900. /

&OBST ID=' Window_frame_middle:1687323_3', XB=2.0,2.1,2.5,2.6,1.0,1.6,COLOR='ORANGE', SURF_ID='steel'/
&OBST ID='Window_frame_middle_safety_cage_finishing:1687719_3', XB=2.0,2.1,2.6,2.65,1.0,1.6,SURF_ID='Insulation_car_cabine', BULK_DENSITY=900. /
&OBST ID='Window_frame_middle:1687903_3', XB=2.8,2.9,2.5,2.6,1.0,1.6,COLOR='ORANGE', SURF_ID='steel'/
&OBST ID='Window_frame_middle_safety_cage_finishinge:1687904_3', XB=2.8,2.9,2.6,2.65,1.0,1.6,SURF_ID='Insulation_car_cabine', BULK_DENSITY=900. /
&OBST ID='Window_frame_middle:1687988_3', XB=2.0,2.1,4.3,4.4,1.0,1.6,COLOR='ORANGE', SURF_ID='steel'/
```

&OBST ID='Window_frame_middle_safety_cage_finishing:1687989_3', XB=2.0,2.1,4.25,4.3,1.0,1.6,SURF_ID='Insulation_car_cabine', BULK_DENSITY=900. /
&OBST ID='Window_frame_middle:1687990_3', XB=2.8,2.9,4.3,4.4,1.0,1.6,COLOR='ORANGE', SURF_ID='steel'/
&OBST ID='Window_frame_middle_safety_cage_finishing:1687991_3', XB=2.8,2.9,4.25,4.3,1.0,1.6,SURF_ID='Insulation_car_cabine', BULK_DENSITY=900. /

/____windows orange car 3

&DEVC ID='Window_driver_1_3', XB=1.0,2.0,2.5,2.6,1.0,1.2,QUANTITY='WALL TEMPERATURE', SPATIAL_STATISTIC='MAX', SETPOINT=300., SURF_ID='Glass', INITIAL_STATE=T./
&DEVC ID='Window_driver_2_3', XB=1.2,2.0,2.5,2.6,1.2,1.3,QUANTITY='WALL TEMPERATURE', SPATIAL_STATISTIC='MAX', SETPOINT=300., SURF_ID='Glass', INITIAL_STATE=T./
&DEVC ID='Window_driver_3_3', XB=1.4,2.0,2.5,2.6,1.3,1.4,QUANTITY='WALL TEMPERATURE', SPATIAL_STATISTIC='MAX', SETPOINT=300., SURF_ID='Glass', INITIAL_STATE=T./
&DEVC ID='Window_driver_4_3', XB=1.6,2.0,2.5,2.6,1.4,1.5,QUANTITY='WALL TEMPERATURE', SPATIAL_STATISTIC='MAX', SETPOINT=300., SURF_ID='Glass', INITIAL_STATE=T./
&DEVC ID='Window_driver_5_3', XB=1.8,2.0,2.5,2.6,1.5,1.6,QUANTITY='WALL TEMPERATURE', SPATIAL_STATISTIC='MAX', SETPOINT=300., SURF_ID='Glass', INITIAL_STATE=T./
&DEVC ID='Middle_window_driver_Lower_3', XB=2.1,2.8,2.5,2.6,1.0,1.3,QUANTITY='WALL TEMPERATURE', SPATIAL_STATISTIC='MAX', SETPOINT=300., SURF_ID='Glass', INITIAL_STATE=T./
&DEVC ID='Middle_window_driver_Upper_3', XB=2.1,2.8,2.5,2.6,1.3,1.6,QUANTITY='WALL TEMPERATURE', SPATIAL_STATISTIC='MAX', SETPOINT=300., SURF_ID='Glass', INITIAL_STATE=T./
&DEVC ID='Window_passenger_1_3', XB=1,2.0,4.3,4.4,1.0,1.2,QUANTITY='WALL TEMPERATURE', SPATIAL_STATISTIC='MAX', SETPOINT=300., SURF_ID='Glass', INITIAL_STATE=T./
&DEVC ID='Window_passenger_2_3', XB=1.2,2.0,4.3,4.4,1.2,1.3,QUANTITY='WALL TEMPERATURE', SPATIAL_STATISTIC='MAX', SETPOINT=300., SURF_ID='Glass', INITIAL_STATE=T./
&DEVC ID='Window_passenger_3_3', XB=1.4,2.0,4.3,4.4,1.3,1.4,QUANTITY='WALL TEMPERATURE', SPATIAL_STATISTIC='MAX', SETPOINT=300., SURF_ID='Glass', INITIAL_STATE=T./
&DEVC ID='Window_passenger_4_3', XB=1.6,2.0,4.3,4.4,1.4,1.5,QUANTITY='WALL TEMPERATURE', SPATIAL_STATISTIC='MAX', SETPOINT=300., SURF_ID='Glass', INITIAL_STATE=T./
&DEVC ID='Window_passenger_5_3', XB=1.8,2.0,4.3,4.4,1.5,1.6,QUANTITY='WALL TEMPERATURE', SPATIAL_STATISTIC='MAX', SETPOINT=300., SURF_ID='Glass', INITIAL_STATE=T./
&DEVC ID='Middle_window_passenger_1_3', XB=2.6,2.8,4.3,4.4,1.0,1.6,QUANTITY='WALL TEMPERATURE', SPATIAL_STATISTIC='MAX', SETPOINT=300., SURF_ID='Glass', INITIAL_STATE=T./
&DEVC ID='Middle_window_passenger_2_3', XB=2.1,2.6,4.3,4.4,1.0,1.6,QUANTITY='WALL TEMPERATURE', SPATIAL_STATISTIC='MAX', SETPOINT=300., SURF_ID='Glass', INITIAL_STATE=T./

&DEVC ID='Back_window_driver_1_3', XB=2.9,4.0,2.5,2.6,1.1,1.3,QUANTITY='WALL TEMPERATURE', SPATIAL_STATISTIC='MAX', SETPOINT=300., SURF_ID='Glass', INITIAL_STATE=T./
&DEVC ID='Back_window_driver_2_3', XB=2.9,3.9,2.5,2.6,1.3,1.4,QUANTITY='WALL TEMPERATURE', SPATIAL_STATISTIC='MAX', SETPOINT=300., SURF_ID='Glass', INITIAL_STATE=T./
&DEVC ID='Back_window_driver_3_3', XB=2.9,3.8,2.5,2.6,1.4,1.5,QUANTITY='WALL TEMPERATURE', SPATIAL_STATISTIC='MAX', SETPOINT=300., SURF_ID='Glass', INITIAL_STATE=T./
&DEVC ID='Back_window_driver_4_3', XB=2.9,3.7,2.5,2.6,1.5,1.6,QUANTITY='WALL TEMPERATURE', SPATIAL_STATISTIC='MAX', SETPOINT=300., SURF_ID='Glass', INITIAL_STATE=T./
&DEVC ID='Back_window_passenger_1_3', XB=2.9,4.0,4.3,4.4,1.1,1.3,QUANTITY='WALL TEMPERATURE', SPATIAL_STATISTIC='MAX', SETPOINT=300., SURF_ID='Glass', INITIAL_STATE=T./
&DEVC ID='Back_window_passenger_2_3', XB=2.9,3.9,4.3,4.4,1.3,1.4,QUANTITY='WALL TEMPERATURE', SPATIAL_STATISTIC='MAX', SETPOINT=300., SURF_ID='Glass', INITIAL_STATE=T./
&DEVC ID='Back_window_passenger_3_3', XB=2.9,3.8,4.3,4.4,1.4,1.5,QUANTITY='WALL TEMPERATURE', SPATIAL_STATISTIC='MAX', SETPOINT=300., SURF_ID='Glass', INITIAL_STATE=T./
&DEVC ID='Back_window_passenger_4_3', XB=2.9,3.7,4.3,4.4,1.5,1.6,QUANTITY='WALL TEMPERATURE', SPATIAL_STATISTIC='MAX', SETPOINT=300., SURF_ID='Glass', INITIAL_STATE=T./
&DEVC ID='Front_window_1_3', XB=0.5,0.8,2.6,3.5,1.0,1.1,QUANTITY='WALL TEMPERATURE', SPATIAL_STATISTIC='MAX', SETPOINT=300., SURF_ID='Glass', INITIAL_STATE=T./
&DEVC ID='Front_window_2_3', XB=0.5,0.8,3.5,4.3,1.0,1.1,QUANTITY='WALL TEMPERATURE', SPATIAL_STATISTIC='MAX', SETPOINT=300., SURF_ID='Glass', INITIAL_STATE=T./
&DEVC ID='Front_window_3_3', XB=0.7,1.0,2.6,3.5,1.1,1.2,QUANTITY='WALL TEMPERATURE', SPATIAL_STATISTIC='MAX', SETPOINT=300., SURF_ID='Glass', INITIAL_STATE=T./
&DEVC ID='Front_window_4_3', XB=0.7,1.0,3.5,4.3,1.1,1.2,QUANTITY='WALL TEMPERATURE', SPATIAL_STATISTIC='MAX', SETPOINT=300., SURF_ID='Glass', INITIAL_STATE=T./
&DEVC ID='Front_window_5_3', XB=0.9,1.2,2.6,3.5,1.2,1.3,QUANTITY='WALL TEMPERATURE', SPATIAL_STATISTIC='MAX', SETPOINT=300., SURF_ID='Glass', INITIAL_STATE=T./
&DEVC ID='Front_window_6_3', XB=0.9,1.2,3.5,4.3,1.2,1.3,QUANTITY='WALL TEMPERATURE', SPATIAL_STATISTIC='MAX', SETPOINT=300., SURF_ID='Glass', INITIAL_STATE=T./
&DEVC ID='Front_window_7_3', XB=1.1,1.4,2.6,3.5,1.3,1.4,QUANTITY='WALL TEMPERATURE', SPATIAL_STATISTIC='MAX', SETPOINT=300., SURF_ID='Glass', INITIAL_STATE=T./
&DEVC ID='Front_window_8_3', XB=1.1,1.4,3.5,4.3,1.3,1.4,QUANTITY='WALL TEMPERATURE', SPATIAL_STATISTIC='MAX', SETPOINT=300., SURF_ID='Glass', INITIAL_STATE=T./
&DEVC ID='Front_window_9_3', XB=1.3,1.6,2.6,3.5,1.4,1.5,QUANTITY='WALL TEMPERATURE', SPATIAL_STATISTIC='MAX', SETPOINT=300., SURF_ID='Glass', INITIAL_STATE=T./

```
&DEVC ID='Front_window_10_3', XB=1.3,1.6,3.5,4.3,1.4,1.5,QUANTITY='WALL TEMPERATURE', SPATIAL_STATISTIC='MAX', SETPOINT=300., SURF_ID='Glass', INITIAL_STATE=T./
&DEVC ID='Front_window_11_3', XB=1.5,1.8,2.6,3.5,1.5,1.6,QUANTITY='WALL TEMPERATURE', SPATIAL_STATISTIC='MAX', SETPOINT=300., SURF_ID='Glass', INITIAL_STATE=T./
&DEVC ID='Front_window_12_3', XB=1.5,1.8,3.5,4.3,1.5,1.6,QUANTITY='WALL TEMPERATURE', SPATIAL_STATISTIC='MAX', SETPOINT=300., SURF_ID='Glass', INITIAL_STATE=T./
&DEVC ID='Back_window_1_3', XB=3.7,3.9,2.6,3.5,1.5,1.6,QUANTITY='WALL TEMPERATURE', SPATIAL_STATISTIC='MAX', SETPOINT=300., SURF_ID='Glass', INITIAL_STATE=T./
&DEVC ID='Back_window_2_3', XB=3.7,3.9,3.5,4.3,1.5,1.6,QUANTITY='WALL TEMPERATURE', SPATIAL_STATISTIC='MAX', SETPOINT=300., SURF_ID='Glass', INITIAL_STATE=T./
&DEVC ID='Back_window_3_3', XB=3.8,4.0,2.6,3.5,1.4,1.5,QUANTITY='WALL TEMPERATURE', SPATIAL_STATISTIC='MAX', SETPOINT=300., SURF_ID='Glass', INITIAL_STATE=T./
&DEVC ID='Back_window_4_3', XB=3.8,4.0,3.5,4.3,1.4,1.5,QUANTITY='WALL TEMPERATURE', SPATIAL_STATISTIC='MAX', SETPOINT=300., SURF_ID='Glass', INITIAL_STATE=T./
&DEVC ID='Back_window_5_3', XB=3.9,4.1,2.6,3.5,1.3,1.4,QUANTITY='WALL TEMPERATURE', SPATIAL_STATISTIC='MAX', SETPOINT=300., SURF_ID='Glass', INITIAL_STATE=T./
&DEVC ID='Back_window_6_3', XB=3.9,4.1,3.5,4.3,1.3,1.4,QUANTITY='WALL TEMPERATURE', SPATIAL_STATISTIC='MAX', SETPOINT=300., SURF_ID='Glass', INITIAL_STATE=T./
&DEVC ID='Back_window_7_3', XB=4.0,4.2,2.6,3.5,1.2,1.3,QUANTITY='WALL TEMPERATURE', SPATIAL_STATISTIC='MAX', SETPOINT=300., SURF_ID='Glass', INITIAL_STATE=T./
&DEVC ID='Back_window_8_3', XB=4.0,4.2,3.5,4.3,1.2,1.3,QUANTITY='WALL TEMPERATURE', SPATIAL_STATISTIC='MAX', SETPOINT=300., SURF_ID='Glass', INITIAL_STATE=T./
&DEVC ID='Back_window_9_3', XB=4.1,4.3,2.7,3.5,1.1,1.2,QUANTITY='WALL TEMPERATURE', SPATIAL_STATISTIC='MAX', SETPOINT=300., SURF_ID='Glass', INITIAL_STATE=T./
&DEVC ID='Back_window_10_3', XB=4.1,4.3,3.5,4.2,1.1,1.2,QUANTITY='WALL TEMPERATURE', SPATIAL_STATISTIC='MAX', SETPOINT=300., SURF_ID='Glass', INITIAL_STATE=T./

&OBST ID='Window_driver_1_3', XB=1.0,2.0,2.5,2.6,1.0,1.2,SURF_ID='Glass', DEVC_ID='Window_driver_1_3'/
&OBST ID='Window_driver_2_3', XB=1.2,2.0,2.5,2.6,1.2,1.3,SURF_ID='Glass', DEVC_ID='Window_driver_2_3'/
&OBST ID='Window_driver_3_3', XB=1.4,2.0,2.5,2.6,1.3,1.4,SURF_ID='Glass', DEVC_ID='Window_driver_3_3'/
&OBST ID='Window_driver_4_3', XB=1.6,2.0,2.5,2.6,1.4,1.5,SURF_ID='Glass', DEVC_ID='Window_driver_4_3'/
&OBST ID='Window_driver_5_3', XB=1.8,2.0,2.5,2.6,1.5,1.6,SURF_ID='Glass', DEVC_ID='Window_driver_5_3'/
&OBST ID='Middle_window_driver_Lower_3', XB=2.1,2.8,2.5,2.6,1.0,1.3,SURF_ID='Glass', DEVC_ID='Middle_window_driver_Lower_3'/
&OBST ID='Middle_window_driver_Upper_3', XB=2.1,2.8,2.5,2.6,1.3,1.6,SURF_ID='Glass', DEVC_ID='Middle_window_driver_Upper_3'/
&OBST ID='Window_passenger_1_3', XB=1.0,2.0,4.3,4.4,1.0,1.2,SURF_ID='Glass', DEVC_ID='Window_passenger_1_3'/
```

```
&OBST ID='Window_passenger_2_3', XB=1.2,2.0,4.3,4.4,1.2,1.3,SURF_ID='Glass', DEVC_ID='Window_passenger_2_3'/
&OBST ID='Window_passenger_3_3', XB=1.4,2.0,4.3,4.4,1.3,1.4,SURF_ID='Glass', DEVC_ID='Window_passenger_3_3'/
&OBST ID='Window_passenger_4_3', XB=1.6,2.0,4.3,4.4,1.4,1.5,SURF_ID='Glass', DEVC_ID='Window_passenger_4_3'/
&OBST ID='Window_passenger_5_3', XB=1.8,2.0,4.3,4.4,1.5,1.6,SURF_ID='Glass', DEVC_ID='Window_passenger_5_3'/
 &OBST ID='Middle_window_passenger_3', XB=2.6,2.8,4.3,4.4,1.0,1.6,SURF_ID='Glass', DEVC_ID='Middle_window_passenger_1_3'/
&OBST ID='Middle_window_passenger_3', XB=2.1,2.6,4.3,4.4,1.0,1.6,SURF_ID='Glass', DEVC_ID='Middle_window_passenger_2_3'/
&OBST ID='Back_window_driver_1_3', XB=2.9,4.0,2.5,2.6,1.1,1.3,SURF_ID='Glass', DEVC_ID='Back_window_driver_1_3'/
&OBST ID='Back_window_driver_2_3', XB=2.9,3.9,2.5,2.6,1.3,1.4,SURF_ID='Glass', DEVC_ID='Back_window_driver_2_3'/
&OBST ID='Back_window_driver_3_3', XB=2.9,3.8,2.5,2.6,1.4,1.5,SURF_ID='Glass', DEVC_ID='Back_window_driver_3_3'/
&OBST ID='Back_window_driver_4_3', XB=2.9,3.7,2.5,2.6,1.5,1.6,SURF_ID='Glass', DEVC_ID='Back_window_driver_4_3'/
&OBST ID='Back_window_passenger_1_3', XB=2.9,4.0,4.3,4.4,1.1,1.3,SURF_ID='Glass', DEVC_ID='Back_window_passenger_1_3'/
&OBST ID='Back_window_passenger_2_3', XB=2.9,3.9,4.3,4.4,1.3,1.4,SURF_ID='Glass', DEVC_ID='Back_window_passenger_2_3'/
&OBST ID='Back_window_passenger_3_3', XB=2.9,3.8,4.3,4.4,1.4,1.5,SURF_ID='Glass', DEVC_ID='Back_window_passenger_3_3'/
&OBST ID='Back_window_passenger_4_3', XB=2.9,3.7,4.3,4.4,1.5,1.6,SURF_ID='Glass', DEVC_ID='Back_window_passenger_4_3'/
&OBST ID='Front_window_2_3', XB=0.5,0.8,2.6,3.5,1.0,1.1,SURF_ID='Glass', DEVC_ID='Front_window_1_3'/
&OBST ID='Front_window_2_3', XB=0.5,0.8,3.5,4.3,1.0,1.1,SURF_ID='Glass', DEVC_ID='Front_window_2_3'/
&OBST ID='Front_window_3_3', XB=0.7,1.0,2.6,3.5,1.1,1.2,SURF_ID='Glass', DEVC_ID='Front_window_3_3'/
&OBST ID='Front_window_4_3', XB=0.7,1.0,3.5,4.3,1.1,1.2,SURF_ID='Glass', DEVC_ID='Front_window_4_3'/
&OBST ID='Front_window_5_3', XB=0.9,1.2,2.6,3.5,1.2,1.3,SURF_ID='Glass', DEVC_ID='Front_window_5_3'/
&OBST ID='Front_window_6_3', XB=0.9,1.2,3.5,4.3,1.2,1.3,SURF_ID='Glass', DEVC_ID='Front_window_6_3'/
&OBST ID='Front_window_7_3', XB=1.1,1.4,2.6,3.5,1.3,1.4,SURF_ID='Glass', DEVC_ID='Front_window_7_3'/
&OBST ID='Front_window_8_3', XB=1.1,1.4,3.5,4.3,1.3,1.4,SURF_ID='Glass', DEVC_ID='Front_window_8_3'/
&OBST ID='Front_window_9_3', XB=1.3,1.6,2.6,3.5,1.4,1.5,SURF_ID='Glass', DEVC_ID='Front_window_9_3'/
&OBST ID='Front_window_10_3', XB=1.3,1.6,3.5,4.3,1.4,1.5,SURF_ID='Glass', DEVC_ID='Front_window_10_3'/
&OBST ID='Front_window_11_3', XB=1.5,1.8,2.6,3.5,1.5,1.6,SURF_ID='Glass', DEVC_ID='Front_window_11_3'/
&OBST ID='Front_window_12_3', XB=1.5,1.8,3.5,4.3,1.5,1.6,SURF_ID='Glass', DEVC_ID='Front_window_12_3'/
&OBST ID='Back_window_1_3', XB=3.7,3.9,2.6,3.5,1.5,1.6,SURF_ID='Glass', DEVC_ID='Back_window_1_3'/
&OBST ID='Back_window_2_3', XB=3.7,3.9,3.5,4.3,1.5,1.6,SURF_ID='Glass', DEVC_ID='Back_window_2_3'/
&OBST ID='Back_window_3_3', XB=3.8,4.0,2.6,3.5,1.4,1.5,SURF_ID='Glass', DEVC_ID='Back_window_3_3'/
&OBST ID='Back_window_4_3', XB=3.8,4.0,3.5,4.3,1.4,1.5,SURF_ID='Glass', DEVC_ID='Back_window_4_3'/
&OBST ID='Back_window_5_3', XB=3.9,4.1,2.6,3.5,1.3,1.4,SURF_ID='Glass', DEVC_ID='Back_window_5_3'/
&OBST ID='Back_window_6_3', XB=3.9,4.1,3.5,4.3,1.3,1.4,SURF_ID='Glass', DEVC_ID='Back_window_6_3'/
&OBST ID='Back_window_7_3', XB=4.0,4.2,2.6,3.5,1.2,1.3,SURF_ID='Glass', DEVC_ID='Back_window_7_3'/
&OBST ID='Back_window_8_3', XB=4.0,4.2,3.5,4.3,1.2,1.3,SURF_ID='Glass', DEVC_ID='Back_window_8_3'/
&OBST ID='Back_window_9_3', XB=4.1,4.3,2.7,3.5,1.1,1.2,SURF_ID='Glass', DEVC_ID='Back_window_9_3'/
```

```
&OBST ID='Back_window_10_3', XB=4.1,4.3,3.5,4.2,1.1,1.2,SURF_ID='Glass', DEVC_ID='Back_window_10_3'/
/________________________________________________________________________________________________boundaries
&VENT DB='XMIN', SURF_ID='OPEN' /
&VENT DB='XMAX', SURF_ID='OPEN' /
&VENT DB='YMIN', SURF_ID='OPEN' /
&VENT DB='YMAX', SURF_ID='OPEN' /
&VENT DB='ZMIN', SURF_ID='OPEN' /
&VENT DB='ZMAX', SURF_ID='OPEN' /
/_________________________________________________________________________________sprinklers
&SPEC ID='WATER VAPOR' /

&PART ID='waterdrops_FM',
    SPEC_ID='WATER VAPOR',
    DIAMETER=1000.0,
    SAMPLING_FACTOR=10 /

&PROP ID='FM_Global_QR_ESS',
    QUANTITY='SPRINKLER LINK TEMPERATURE',
    RTI=100,
    ACTIVATION_TEMPERATURE=68.0,
    K_FACTOR=80.0,
    PARTICLE_VELOCITY = 10,
    OPERATING_PRESSURE=1.0,
    PART_ID='waterdrops_FM',
    OFFSET=0.10,
    SPRAY_ANGLE=30.0,90.0,
    SMOKEVIEW_ID='sprinkler_pendent' /

/ --- Column A (Y = -6.0) --- /
&DEVC ID='Spr_A1', XYZ= 0.3, -6.0, 2.3, PROP_ID='FM_Global_QR_ESS' /
&DEVC ID='Spr_A2', XYZ= 3.8, -6.0, 2.3, PROP_ID='FM_Global_QR_ESS' /
&DEVC ID='Spr_A3', XYZ= 7.3, -6.0, 2.3, PROP_ID='FM_Global_QR_ESS' /

/ --- Column B (Y = -2.6) -/
&DEVC ID='Spr_B1', XYZ= 0.3, -2.6, 2.3, PROP_ID='FM_Global_QR_ESS' /
```

```
&DEVC ID='Spr_B2', XYZ= 3.8, -2.6, 2.3, PROP_ID='FM_Global_QR_ESS' /
&DEVC ID='Spr_B2', XYZ= 7.3, -2.6, 2.3, PROP_ID='FM_Global_QR_ESS' /

/ --- Column C (Y = 0.8) --- /
&DEVC ID='Spr_C1', XYZ= 0.3,  0.8, 2.3, PROP_ID='FM_Global_QR_ESS' /
&DEVC ID='Spr_C2', XYZ= 3.8,  0.8, 2.3, PROP_ID='FM_Global_QR_ESS' /
&DEVC ID='Spr_C3', XYZ= 7.3,  0.8, 2.3, PROP_ID='FM_Global_QR_ESS' /

/ --- Column D(Y = 4.2) -/
&DEVC ID='Spr_D1', XYZ= 0.3,  4.2, 2.3, PROP_ID='FM_Global_QR_ESS' /
&DEVC ID='Spr_D2', XYZ= 3.8,  4.2, 2.3, PROP_ID='FM_Global_QR_ESS' /
&DEVC ID='Spr_D2', XYZ= 7.3,  4.2, 2.3, PROP_ID='FM_Global_QR_ESS' /

/ ---  Column E (Y = 7.6) --- /
&DEVC ID='Spr_E1', XYZ= 0.3,  7.6, 2.3, PROP_ID='FM_Global_QR_ESS' /
&DEVC ID='Spr_E2', XYZ= 3.8,  7.6, 2.3, PROP_ID='FM_Global_QR_ESS' /
&DEVC ID='Spr_E3', XYZ= 7.3,  7.6, 2.3, PROP_ID='FM_Global_QR_ESS' /

/ --- Controle spray pattern z =  1,6 m/
&SLCF PBZ=1.6, QUANTITY='PARTICLE FLUX Z', PART_ID='waterdrops_FM' /
/________________________________________________________________________________________________Thermocouples

/Tree 1 Middle battery pack
&DEVC ID='T1-1',XYZ= 1.8, 0.9, 0.5, QUANTITY= 'TEMPERATURE'/
&DEVC ID='T1-2', XYZ=  1.8, 0.9, 1.0, QUANTITY= 'TEMPERATURE'/
&DEVC ID='T1-3', XYZ= 1.8, 0.9, 1.4, QUANTITY= 'TEMPERATURE'/
&DEVC ID='T1-4', XYZ= 1.8, 0.9, 2.0, QUANTITY= 'TEMPERATURE'/


/Tree 2 door third car
&DEVC ID='T2-1',XYZ= 1.8, 2.5, 0.5, QUANTITY= 'TEMPERATURE'/
&DEVC ID='T2-2', XYZ=  1.8, 2.5, 1.0, QUANTITY= 'TEMPERATURE'/
&DEVC ID='T2-3', XYZ= 1.8, 2.5, 1.4, QUANTITY= 'TEMPERATURE'/
&DEVC ID='T2-4', XYZ= 1.8, 2.5, 2.0, QUANTITY= 'TEMPERATURE'/
```

```
/Tree 4 middle third car
&DEVC ID='T4-1',XYZ= 1.8, 3.5, 0.5, QUANTITY= 'TEMPERATURE'/
&DEVC ID='T4-2', XYZ=  1.8, 3.5, 1.0, QUANTITY= 'TEMPERATURE'/
&DEVC ID='T4-3', XYZ= 1.8, 3.5, 1.4, QUANTITY= 'TEMPERATURE'/
&DEVC ID='T4-4', XYZ= 1.8, 3.5, 2.0, QUANTITY= 'TEMPERATURE'/

/Tree 3 door second car
&DEVC ID='T3-1',XYZ= 1.8, -0.6, 0.5, QUANTITY= 'TEMPERATURE'/
&DEVC ID='T3-2', XYZ=  1.8, -0.6, 1.0, QUANTITY= 'TEMPERATURE'/
&DEVC ID='T3-3', XYZ= 1.8, -0.6, 1.4, QUANTITY= 'TEMPERATURE'/
&DEVC ID='T3-4', XYZ= 1.8, -0.6, 2.0, QUANTITY= 'TEMPERATURE'/

/Tree 5 middle second car
&DEVC ID='T5-1',XYZ= 1.8, -1.6, 0.5, QUANTITY= 'TEMPERATURE'/
&DEVC ID='T5-2', XYZ=  1.8, -1.6, 1.0, QUANTITY= 'TEMPERATURE'/
&DEVC ID='T5-3', XYZ= 1.8, -1.6, 1.4, QUANTITY= 'TEMPERATURE'/
&DEVC ID='T5-4', XYZ= 1.8, -1.6, 2.0, QUANTITY= 'TEMPERATURE'/

/middel above the car
&DEVC ID='TC_GCRW',XYZ= 3.6, 0.9, 2.3, QUANTITY= 'TEMPERATURE'/
&DEVC ID='TC_GR', XYZ=  2.4, 0.9, 2.3, QUANTITY= 'TEMPERATURE'/
&DEVC ID='TC_GW', XYZ= 1.2, 0.9, 2.3, QUANTITY= 'TEMPERATURE'/
&DEVC ID='TC_GB', XYZ= 0.4, 0.9, 2.3, QUANTITY= 'TEMPERATURE'/

/More to the side
&DEVC ID='TC_CRW', XYZ= 2.6, 0.2, 2.3, QUANTITY= 'TEMPERATURE'/
&DEVC ID='TC_GFW', XYZ= 1.8, 0.2, 2.3, QUANTITY= 'TEMPERATURE'/

&DEVC ID='TC_FW', XYZ= 2.6, 0.2, 1.3, QUANTITY= 'TEMPERATURE'/
&DEVC ID='TC_RW', XYZ= 1.8, 0.2, 1.3, QUANTITY= 'TEMPERATURE'/

/in the car estimated locations
&DEVC ID='TC_WF',XYZ= 0.4, 1.8, 0.8, QUANTITY= 'TEMPERATURE'/
&DEVC ID='TC_WR', XYZ= 3.4, 1.8, 0.8, QUANTITY= 'TEMPERATURE'/
&DEVC ID='TC_M', XYZ=  0.2, 0.9, 0.8, QUANTITY= 'TEMPERATURE'/
```

```
&DEVC ID='TC_CD', XYZ= 0.8, 0.9, 0.8, QUANTITY= 'TEMPERATURE'/
&DEVC ID='TC_CFF', XYZ= 0.8, 0.9, 0.6, QUANTITY= 'TEMPERATURE'/
&DEVC ID='TC_CFS',XYZ= 2.0, 0.9, 0.8, QUANTITY= 'TEMPERATURE'/
&DEVC ID='TC_CRF', XYZ= 2.0, 0.9, 0.6, QUANTITY= 'TEMPERATURE'/
&DEVC ID='TC_CRS', XYZ= 2.5, 0.9, 0.8, QUANTITY= 'TEMPERATURE'/
&DEVC ID='TC_T', XYZ= 3.5, 0.9, 0.8, QUANTITY= 'TEMPERATURE'/

&DEVC ID='Flux_1.6m', XB=-0.7, 8.3, -7.0, 8.9, 1.6, 1.6, QUANTITY='PARTICLE FLUX Z', SPATIAL_STATISTIC='AREA INTEGRAL', PART_ID='waterdrops_FM' /
&DEVC ID='Total_Water_kg',PART_ID ='waterdrops_FM', XB=0.0,3.0, 0.0,3.0, 0.0,0.1,QUANTITY='AMPUA',SPATIAL_STATISTIC='SURFACE INTEGRAL' /
/________________________________________________________________________________

&SLCF ID='Temp at Head Height', QUANTITY='TEMPERATURE', PBZ=1.8/
&SLCF ID='Temp at battery Height', QUANTITY='TEMPERATURE', PBZ=0.35/

&SLCF ID='Temp y-axis', QUANTITY='TEMPERATURE', PBY=0.9/
&SLCF ID='Temp_y_driver', QUANTITY='TEMPERATURE', PBY=-0.5/
&SLCF ID='Temp_y_passenger', QUANTITY='TEMPERATURE', PBY=2.8/
&SLCF ID='Temp x-axis', QUANTITY='TEMPERATURE', PBX=1.95/

&SLCF PBZ=1.8, QUANTITY='DENSITY', SPEC_ID='WATER VAPOR' /
&SLCF PBZ=1.0, QUANTITY='VISIBILITY' /
&SLCF PBZ=0.5, QUANTITY='PARTICLE FLUX Z', PART_ID='waterdrops_FM' /

&DEVC ID='HRR_Total_Side',
    XB=0.8, 2.6, -0.7, -0.6, 0.4, 1.0,
    QUANTITY='HRRPUV',
    SPATIAL_STATISTIC='VOLUME INTEGRAL' /

&DEVC ID='HRR_Total_Side',
    XB=2.9,3.0,4.0,4.4,0.3,0.8,
    QUANTITY='HRRPUV',
    SPATIAL_STATISTIC='VOLUME INTEGRAL' /

&DEVC ID='Ignition_Risk',
    XB=0.8, 2.6, -0.7, -0.6, 0.4, 1.0,
```

```
    QUANTITY='INCIDENT HEAT FLUX',
    SPATIAL_STATISTIC='MAX',
    SURF_ID='steel' /

&DEVC ID='Ignition_Risk',
    XB=2.9,3.0,4.0,4.4,0.3,0.8,
    QUANTITY='INCIDENT HEAT FLUX',
    SPATIAL_STATISTIC='MAX',
    SURF_ID='steel' /

&DEVC ID='Rad_Flux_Auto',
    SURF_ID='steel',
    XB=0.8, 2.6, -0.6, -0.7, 0.4, 0.8,
    QUANTITY='RADIATIVE HEAT FLUX',
    SPATIAL_STATISTIC='MAX' /

&BNDF QUANTITY='NET HEAT FLUX' /
&BNDF QUANTITY='WALL TEMPERATURE' /
&BNDF QUANTITY='AMPUA', PART_ID='waterdrops_FM' /
&BNDF QUANTITY='RADIATIVE HEAT FLUX' /

&DEVC ID='Spray_Density_T2_1', XYZ=0.6, 0.0, 0.5, QUANTITY='MPUV', PART_ID='waterdrops_FM'/
&DEVC ID='Gas_Vel_X_T2_1', XYZ=0.6, 0.0, 0.5, QUANTITY='U-VELOCITY' /
&DEVC ID='Rad_Flux_T2_1', XYZ=1.8, 2.4, 0.5, QUANTITY='RADIATIVE HEAT FLUX GAS', ORIENTATION=-1,0,0 /

&SLCF ID='Force_Vertical_Plane', PBY=0.2, QUANTITY='F_X', VECTOR=T /
&SLCF ID='Force_Vertical_Plane', PBY=0.2, QUANTITY='F_Y' /
&SLCF ID='Force_Vertical_Plane', PBY=0.2, QUANTITY='F_Z' /

&SLCF ID='Spray_Flux', PBY=0.2, QUANTITY='PARTICLE FLUX X', PART_ID='waterdrops_FM' /

&TAIL /
```

6.2.5) Annex E: Most sold EV cars 2025

Most sold EV cars 2025

Number	Name EV	Length (mm)	Width (mm)	Height (mm)	Width with mirrors (mm)	Nota's
1	Volkswagen ID.4	4584	1852	1640		
2	Chevrolet Blazer EV	4883	1982	1651		
3	Ford F-150 Lighting	5911	2032	1988		No city car, eliminated => to high
4	Honda Prologue	4877	1989	1650		
5	Hyundai Ioniq 5	4655	1890	1605		
6	Ford Mustang March-E	4730	1883	1620		
7	Chervolet Equinox EV	4840	1954	1646	2155	
8	Tesla Model 3	4722	1850	1440	2089	
9	Tesla Model Y	4750	1921	1624	2129	
10	Skoda Elroq	4488	1884	1650	2148	
	Tesla Cybertruck	-	-	-	-	Not allowed in Europe
	Average	4725	1912	1614	2130	0
	Average in metres	4,73	1,91	1,61	2,13	
	FDS	4,70	1,90	1,60	2,10	
	Average length EV	4,30-4,80 m				
	Average length Combustible V	4,4-				